

THE NATURE OF ANORTHOSITE - COUNTRY ROCK INTERACTION
DURING GRANULITE FACIES METAMORPHISM

If you want to know what happens when you throw a stone into a pond, it is infinitely better to make a trial and film it than to attempt to theorize about it; the best specialists (in fluid dynamics) would certainly be unable to tell you more about it.

Rene Thom

THE NATURE OF ANORTHOSITE - COUNTRY ROCK INTERACTION
DURING GRANULITE FACIES METAMORPHISM: AN
EXAMPLE FROM THE WHITESTONE ANORTHOSITE

by

DANNY LEE THOMPSON, B.Sc. (HONOURS)

A Thesis

Submitted to the School of Graduate Studies
in Partial Fulfilment of the Requirements
for the Degree
Master of Science

McMaster University

June 1983

MASTER OF SCIENCE (1983)
(Geology)

McMASTER UNIVERSITY
Hamilton, Ontario

TITLE: The Nature of Anorthosite - Country Rock Interaction
 During Granulite Facies Metamorphism: An Example From
 the Whitestone Anorthosite

AUTHOR: Danny Lee Thompson, B.Sc. (McMaster University)

SUPERVISOR: Professor H. D. Grundy

NUMBER OF PAGES: xviii, 312

ABSTRACT

The Whitestone Anorthosite is a relatively small anorthosite body (160 km²) located within the Parry Sound structural domain, Western Grenville Province, Ontario. Both the anorthosite and the surrounding gneisses have been affected by a granulite grade metamorphic event which predates the Grenville Orogeny. The outer margin of the anorthosite body has been strongly deformed and recrystallized and is characterized by a pervasive metasomatic alteration consisting of garnet, scapolite, hornblende, apatite, biotite, sphene, carbonate and opaques. The country rock gneisses exhibit a corresponding discontinuous, and highly variable, reaction aureole. Pre-existing mafic gneisses are particularly affected, being characterized by the breakdown of orthopyroxene and hornblende, an increase in garnet, clinopyroxene, apatite and opaques, and enrichment in Fe, Ti and P.

The metasomatic alteration exhibited by the Whitestone Anorthosite is thought to be due to a combination of two processes: 1. Mechanical mixing at the anorthosite/country rock contact during intense deformation (tectonic assimilation), and 2. Widespread absorption of mobile components (predominantly volatiles) from both included material and the surrounding gneisses.

The formation of the country rock reaction aureole is a continuous solid state metamorphic process, whereby mobile components are preferentially leached from the rock leaving a mafic restite. Post-

deformation cooling of the anorthosite, combined with an increased volatile flux, has imparted a polygonal mosaic texture suggestive of contact metamorphism. The typical garnet-clinopyroxene assemblage exhibited by mafic gneisses within the reaction aureole, is a consequence of the increased Fe/Mg ratio which stabilizes this assemblage at lower P, T conditions. The temperature of final equilibration and recrystallization is estimated to be 750 ± 70 °C, based on clinopyroxene-garnet geothermometry.

A similar metasomatic interaction, to the one outlined in this thesis, is to be expected at all anorthosite/country rock contacts which have been overprinted by granulite metamorphism.

Acknowledgements

First and foremost I wish to thank my supervisor, Dr. H. D. Grundy, for suggesting the thesis problem, arranging for use of the Mossbauer spectrometer and microprobe, helping with numerous computing problems, critically reading the manuscript and above all for being a friend. His patience and perpetual good humour are truly praiseworthy.

Discussions with Drs. A. Davidson and R. Emslie of the Geological Survey contributed to the author's knowledge of Grenville geology and anorthosite evolution, respectively. Drs. R. H. McNutt and B. J. Burley read early drafts of chapters one and five, respectively, and suggested improvements. Their efforts are greatly appreciated.

I thank J. Cekr, O. Mudroch, J. Whorwood, and L. Zwicker for their expert technical support, advice, and friendship, and B. Barnett (Univ. of Western Ontario) for instructing me in the "art" of microbeam analysis. His commitment to excellence and ability to remain calm in the face of disaster are especially noted.

Drs. T. Birchall and G. Dienes (McMaster Chemistry Dept.) assisted with the Mossbauer experiments and deconvolution of the spectra. Their help is appreciated.

I wish to thank the I.S.S.G. (Informal Sedimentology Seminar Group) for increasing my appreciation of cheap wine and to a lesser extent my knowledge of sediments - behold "The Armchair Sedimentologist Lives"!

I especially thank Patty, for accurately typing the manuscript, in spite of my help!

To my comrades in the Geology Dept., who provided helpful advice, critical discussion, and above all, friendship and good times, I offer my sincere thanks. I will remember each of you dearly.

Finally, I thank my wife, Wendy, for her love and support, without which this study could not have been completed.

TABLE OF CONTENTS

CHAPTER		Page
1	Introduction	1
	1-I Introduction to Study	1
	1-II Previous Work on the Whitestone Anorthosite	3
	(i) Introduction	3
	(ii) Mason's Synthesis of Whitestone Geology	3
	1-III Regional Geology and Tectonic Framework of the Parry Sound Region, Western Grenville Province	11
	1-IV General Approach to Problem	16
	1-V Note on Terminology	18
2	Field Relations and General Mineralogy of Study Area	19
	2-I Introduction	19
	2-II Anorthosite-Gneiss Contact Relations	20
	2-III Distribution of Garnet Bearing Rocks	26
	2-IV Retrograde Metamorphism	44
	2-V Mineral and Whole Rock Chemistry	49
	2-VI Discussion	57
3	Mossbauer Spectroscopy	61
	3-I Introduction	61
	3-II Precision of Least Squares Fitting Procedure	62
	3-III Mineral Spectra: Peak Assignments and Results	65

CHAPTER		Page
	(i) Pyroxene	65
	(ii) Amphibole	72
	(iii) Garnet	77
3-IV	Quantitative Estimation of Site Occupancy	81
	(i) Introduction	81
	(ii) Chemical and Structural Inhomogeneities	82
	(iii) Next-Nearest-Neighbour and Intervalence Charge Transfer Effects	83
	(iv) Temperature Dependence of Site Populations (Order - Disorder Phenomenon)	85
	(v) Summary and Conclusions	87
4	Oxidation State of Iron in Granulite Facies Gneisses and Co-existing Minerals	91
4-I	Determination of the Oxidation State of Iron in Minerals	91
	(i) Introduction	91
	(ii) Wet Chemical Analyses	91
	(iii) Indirect Instrumental Analyses	93
	(iv) Calculation Methods	94
	(v) Results of F* Measurement Using Mossbauer Spectroscopy and Comparison with F* Determined by Charge Balancing Calculations	95
4-II	Determination of the Oxidation State of Fe in Whole Rock Samples	100
4-III	Discussion	100
4-IV	Conclusions	107
5	Estimation of the Physical Conditions of Metamorphism	109

CHAPTER		Page
5-I	Introduction	109
5-II	Garnet-Clinopyroxene Geothermometry	110
	(i) Thermodynamic Basis of Geothermometer	110
	(ii) Accuracy of Calibration	115
5-III	Orthopyroxene-Clinopyroxene Geothermometry	121
	(i) Thermodynamic Basis of Geothermometer	121
	(ii) Accuracy of Calibration	122
5-IV	Significance of Calculated Temperatures: Discussion	125
5-V	Summary	148
6	Reaction Rim Study	149
6-I	Introduction	149
6-II	Observations Made in Slab Study	153
6-III	Discussion	170
7	The Association of Garnet-Clinopyroxene and Apatite- Oxide Assemblages with Anorthosite Massifs	173
7-I	Review of Field Relations	173
	(i) The Marcy Massif	173
	(ii) Allard Lake	180
	(iii) The Morin Anorthosite	180
7-II	Fe-Ti-P Concentrations and Their Relationships to Liquid Immiscibility	182
7-III	Discussion	186
7-IV	Summary and Conclusions	195
8	Controls on the Development of Garnet-Clinopyroxene Assemblages	196

CHAPTER		Page
8-I	Temperature - Pressure Boundary Conditions of the Granulite Facies and the Significance of Garnet Granulites	196
8-II	Composition Paragenesis Diagrams	201
8-III	Significance of Hydrous Minerals	208
8-IV	Conclusions	211
9	Summary and Conclusions	212
9-I	General Statement	212
9-II	Final Word	214
REFERENCES		217
APPENDIX		
A		233
A-I	General Theory of Mossbauer Spectroscopy	233
	(i) Introduction	233
	(ii) Hyperfine Parameters	236
A-II	Precision of Mossbauer Parameters	240
A-III	Mossbauer Sample Preparation	247
A-IV	Key to Constraints Used in Fitting	249
A-V	Mossbauer Calibration Values	250
A-VI	Listing of Mossbauer Parameters	251
A-VII	Listing of Individual Spectra	257
B		276
B-I	Accuracy and Precision of Chemical Analyses	276

APPENDIX		Page
	(i) XRF	276
	(ii) Microprobe	288
C		
C-I	Mineral Oxidation State Calculated by Charge Balancing	310
D		
D-I	Sample Locations	312

LIST OF FIGURES

FIGURE		Page
1-I	Distribution of Secondary Alteration: Marginal Facies of the Whitestone Anorthosite	8
1-II	Structural Trend Map Showing the Distribution of Tectonite Gneiss Zones in the Parry Sound Region	13
2-I	Mineral Assemblage Map	21
2-II	Composition of Whitestone Metamorphic Pyroxenes	53
2-III	Amphibole Classification, Leake 1978	54
2-IV	Composition of Whitestone Garnets	55
2-V	Plot of Chemical Variation Across Anorthosite Contact	58
2-VI	Fe/Mg Ratio of Granulite Facies Gneisses	60
3-I	Mossbauer Spectra of Clinopyroxene	68
3-II	Mossbauer Spectra of Orthopyroxene	70
3-III	Mossbauer Spectra of Amphibole	75
3-IV	Mossbauer Spectra of Garnet	78
3-V	Fe ²⁺ Distribution in Orthopyroxene as a Function of Heating	86
3-VI	Fe-Mg Disorder as a Function of Temperature	86
3-VII	Ideal Equilibrium Isotherms for Fe ²⁺ in Orthopyroxene	88
4-I	Comparison of F* Determined by Wet Chemistry and Mossbauer	92
4-II	Oxidation State of Fe in Granulite Facies Mafic Minerals	96
4-III	Comparison of Fe Oxidation State (F*) Determined by Mossbauer Spectroscopy and Charge Balancing	97

FIGURE		Page
4-IV	Distribution of Whole Rock F*	101
4-V	Plot of $\text{Fe}^{2+}/(\text{Fe}^{2+} + \text{Mg})$ vs. F* (Whole Rock)	103
4-VI	Whole Rock Fe_2O_3 (Fe total) vs. F* (Whole Rock)	104
4-VII	Plot of F* (Mineral) Against F* (Whole Rock)	105
5-I	Dahl Isotherm (CPX-GT)	116
5-II	Fe-Mg Distribution Between Co-existing Garnet and Hornblende	118
5-III	Comparison of Known vs. Calculated Temperature: Wells Geothermometer	124
5-IV	Clinopyroxene-Garnet and Orthopyroxene-Clinopyroxene Temperatures from Granulite Facies Gneisses in the Whitestone Area	126
5-V	Location of Samples Used in Temperature Determinations	128
5-VI	Distribution of Calculated Temperatures	129
5-VII	Mineral-Mineral Element Distributions	135
5-VIII	Whole Rock-Mineral Fe/Mg Distribution	146
6-I	Modal Mineralogy Across A Melt/Inclusion Reaction Rim	159
6-II	Mineral Analyses Across A Melt/Inclusion Reaction Rim	161
6-III	Plot of Major Element Variation Across Melt/Inclusion Reaction Rim	164
7-I	Simplified Geology of the Marcy Massif	178
7-II	Comparison of Al_2O_3 Concentration in Known Immiscible Liquids, Mafic Gneisses, Jotunites and Ferrodiorites Associated with Anorthosite Massifs	188
7-III	Distribution of TiO_2 and P_2O_5 in Granulite Facies Gneisses	190
7-IV	Plot of TiO_2 vs. P_2O_5	191

FIGURE		Page
7-V	Variation of TiO_2 and P_2O_5 in Granulites, Ferrodiorite Jotunite, and Anorthosite Border Facies	192
8-I	Pressure - Temperature Boundary Conditions of the Granulite Facies	197
8-II	Subdivisions of the Granulite Facies	199
8-III	Composition Paragenesis Diagrams: Diagrammatic Representation of the Relation Between Bulk Chemistry and Mineral Composition	203
8-IV	Replacement of Hornblende by Garnet in Granulite Facies Assemblages	209
A-I	Characteristics of a Typical Mossbauer Spectra	234
A-II	Mossbauer Spectra of Silicate Glass	255
D-I	Sample Locations	312

LIST OF TABLES

TABLE		Page
1-I	Average Chemical Composition and Modal Mineralogy of Rocks from the Whitestone Anorthosite	5
2-I	Whole Rock Composition and CIPW Norm of Selected Samples	50
2-II	Modal Composition of Selected Samples	51
3-I	Precision of Mossbauer Areas from Least Squares Fit	66
3-II	Relative Peak Areas for Clinopyroxenes	69
3-III	Relative Peak Areas for Orthopyroxenes	71
3-IV	Relative Peak Areas for Amphiboles	76
3-V	Mossbauer Parameters and Relative Peak Areas for Garnets	80
3-VI	Distribution of Fe ²⁺ and Mg Over the M1 and M2 Sites in Orthopyroxene	89
5-I	Compositional Data Used in the Calculation of CPX-GT Temperatures	113
5-II	CPX-GT Temperatures Calculated from Dahl (1980) and Compositional Effects on k_D	114
5-III	OPX-CPX Temperatures Calculated Using the Wood and Banno (1973), and Wells (1977) Calibrations and Compositional Data	123
6-I	Calculation of Melt Composition by Removal of Restite Phase	169
7-I	Average Chemical Analyses and Modal Mineralogy of Marcy and Whiteface Facies Anorthosite Rocks	177
A-I	Precision of Mossbauer Parameters	242

TABLE	Page
A-II Mossbauer Parameters for Clinopyroxenes	252
A-III Mossbauer Parameters for Orthopyroxenes	253
A-IV Mossbauer Parameters for Amphiboles	254
A-V Mossbauer Parameters and Relative Peak Areas for Glasses	256
B-I Listing of Whole Rock Analyses	277
B-II Precision of XRF Whole Rock Analyses	284
B-III Whole Rock Iron Oxidation State	286
B-IV Mean Composition and Structural Formula of Clinopyroxenes	290
B-V Mean Composition and Structural Formula of Orthopyroxenes	291
B-VI Mean Composition and Structural Formula of Amphiboles	292
B-VII Mean Composition and Structural Formula of Garnets	293
B-VIII Mean Composition and Structural Formula of Biotites	294
B-IX Listing of Microprobe Analyses, Calculated Average and Precision (1σ)	295
C-I Mineral Oxidation States Calculated by Charge Balancing	310

LIST OF PLATES

PLATE	Page
2-I Metasomatic Border Zone of the Whitestone Anorthosite	22
2-II Detail of Central Region of Plate 2-I	22
2-III Photomicrograph: Metasomatic Border Zone	24
2-IV Pyroxene-Garnet-Oxide Rich Border Gneiss	27
2-V Pyroxene-Plagioclase Veinlet in Border Gneiss	27
2-VI Photomicrograph: Pyroxene-Garnet-Oxide Rich Border Gneiss	30
2-VII Photomicrograph: Mafic Granulite Gneiss	32
2-VIII Photomicrograph: Mafic Granulite Gneiss	34
2-IX Banded Tectonite Gneiss	36
2-X Folded Mafic Gneiss in Marble	36
2-XI Photomicrograph: Tectonite Gneiss	38
2-XII Photomicrograph: Tectonite Gneiss	40
2-XIII Photomicrograph: Mafic Tectonite Gneiss	42
2-XIV Pyroxene-Garnet Granulite Gneiss	45
2-XV Detail of Plate 2-XIV	45
2-XVI Mafic Granulite Gneiss Cut by Late Veins	47
2-XVII Detail of Plate 2-XVI	47
6-I Mafic Granulite Exhibiting Felsic Segregations	151
6-II Detail of Plate 6-I	152
6-III Detail of Plate 6-I	152

PLATE		Page
6-IV	Detail of Slab Section	154
6-V	Field Location of Slab Section	155
6-VI	Photomicrograph: Detail of Slab Section	156
6-VII	Photomicrograph: Detail of Slab Section	156

CHAPTER I
INTRODUCTION

1-I Introduction to Study

This thesis is concerned with the mineralogy and chemistry of granulite facies gneisses bordering the Whitestone Anorthosite. The Whitestone is one of a number of anorthosite bodies which occur within the Parry Sound Structural Domain. Davidson (1980, 1982) interprets this domain as a thrust slice of high grade metamorphic rocks which have moved upwards in the crust.

During his study of the Whitestone Anorthosite, Mason (1969) noted the development of a strong metasomatic alteration within the outer margin of the body and a corresponding discontinuous metamorphic aureole within the country rocks, characterized by rusty weathering gneisses rich in pyroxene, garnet, and opaques. He concluded that both the alteration within the anorthosite and the country rocks was due to the influx of an Fe, Ti, P, volatile rich fluid, thought to represent the last stage of differentiation of the anorthosite.

Fe, Ti, P, rich mafic rocks, similar to those described above, are a volumetrically minor, but consistent component of most anorthosite massifs (see reviews by Emslie 1980 and Morse 1982). In undeformed bodies (such as the Harp Lake complex, Emslie 1980), small dykes or pod-shaped intrusions of ferrodiorite postdate the main anorthosite emplacement. In deformed bodies (such as the Marcy Massif, Buddington 1939,

and the Morin Anorthosite, Martignole and Schrijver 1970), jotunite gneisses (pyroxene, garnet granulite) are common and locally grade into ore grade concentrations of titanium. Both of these rock types have similar chemistries and typically occur at the periphery of the main anorthosite body. Their origin is of considerable importance in the overall scheme of anorthosite evolution, because they may represent an advanced stage of differentiation of the anorthosite primary magma (Emslie 1980). Alternatively, it has been suggested that they represent an immiscible fraction of the anorthosite parental magma (Phillipotts 1981). Evaluation of the merits of these various models is complicated by the fact that the processes which occur during high grade metamorphism tend to merge with magmatic processes (with respect to textures and mineralogy), so that it is difficult to untangle the physiochemical events which occurred during emplacement from those associated with a later deformation and metamorphism. Consequently, considerable confusion exists in the literature because observations from both unmetamorphosed and metamorphosed massifs have been combined in attempts at a general synthesis. It is for this reason that the study of anorthosite contact relations is of interest.

In this thesis, anorthosite/gneiss contact relations are examined with the objective of determining, firstly, what role high grade metamorphism plays in the formation of "jotunite-like" gneisses, and secondly, if the altered marginal facies of the anorthosite is related to this process. In other words, it attempts to recognize features attributable to the granulite overprint, features which should not be considered in models of anorthosite genesis.

1-II Previous Work on the Whitestone Anorthosite

(i) Introduction

The geology of the study area was first described by Lacy (1960), who recognized a number of bulbous plutonic bodies surrounded by strongly deformed and metamorphosed layered gneisses of diverse composition and mineralogy. One of these plutons, the "Whitestone Anorthosite," has been mapped in detail by Mason (1969). Further studies of the Whitestone Anorthosite (Kretchmar 1968, Barker 1972, and Mummery 1972) have generally been interpreted in terms of Mason's original synthesis, therefore it is appropriate to review his observations and conclusions briefly.

(ii) Mason's Synthesis of Whitestone Geology

The Whitestone Anorthosite is composed predominantly of anorthosite to gabbroic anorthosite intrusive rocks.¹ In the field these rocks occur as massive rounded outcrops, typically light grey in colour, with a somewhat speckled appearance due to the presence of scattered dark pyroxene crystals. In the central region of the intrusion, the main phase is plagioclase (An_{57}) with lesser amounts of pale green clinopyroxene.² The pyroxene occurs in two distinct habits:

1. Anorthosite = 0 to 10% mafic minerals. Gabbroic anorthosite = 10 to 22.5% mafic minerals (Buddington 1939).

2. The plagioclase becomes more calcic near the margin of the intrusion, however, the difference is probably associated with the overprinted alteration to be discussed below.

1. Glomeropoikilitic - dark pyroxenes occur in blotchy subspherical patches surrounded by plagioclase giving the rock a polkadot appearance.
2. Porphyritic - a more homogeneous distribution and slightly higher average modal value of pyroxene.

Individual outcrops exhibit mineral banding, graded beds and block structures. These features are indicative of gravitational settling of crystals during slow cooling, with contemporaneous disruption of the layering by unsolidified liquid. Similar observations have been made in most anorthosite massifs.

The outer margin of the Whitestone Anorthosite has been strongly deformed and altered to a volatile rich mineral assemblage. The development of gneissosity and degree of alteration are most intense at the anorthosite/country rock contact and decrease rapidly inward toward the core of the pluton. Mason has subdivided the alteration into two distinct types based on the occurrence of garnet and epidote. Epidote occurs along the western margin of the pluton both as separate grains and as coronas on pyroxene (myrmekitic intergrowth of epidote and plagioclase). Garnet is subordinate, generally being restricted to rocks close to the country rock contact. In contrast, garnet and opaques are abundant along the eastern margin while epidote is absent. The average mineralogy and chemistry of the anorthosite core and the foliated marginal facies is given in table 1-I.

The development of scapolite and hornblende (secondary after feldspar and pyroxene respectively) is clearly controlled by the

TABLE 1-I

Average Chemical Composition and Modal Mineralogy
of Rocks from the Whitestone Anorthosite

The average chemical composition of the various facies has been calculated from the analytical data given in Mason (1969, p. 281) using the following samples:

central core: samples 30, 105, 134, 144, 181, 213, 214, 261;

eastern margin: samples 2, 13, 17, 20, 90, 222, 248, 250;

western margin: samples 79, 140, 206, 241.

The coefficient of variation is 2%-10% for most major elements and 20%-80% for minor elements.

The average modal mineralogy is based on consideration of selected modal data from Mason, Mason's mineral distribution maps and to a lesser extent modal data from this study. Due to the inhomogeneous character of these rocks (e.g., the widely varying degree of alteration and the presence of magmatic banding) these average values must be considered crude approximations only.

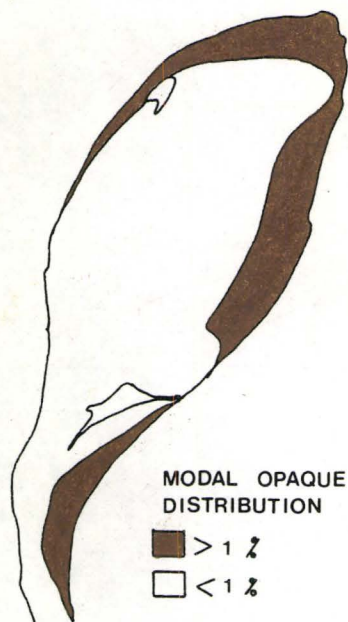
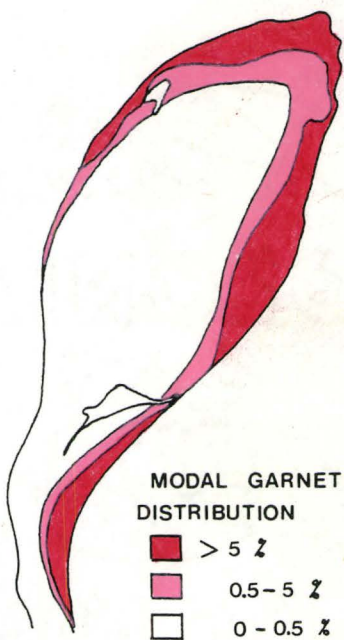
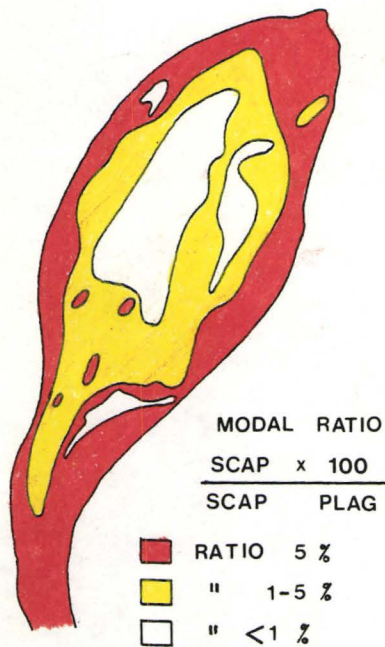
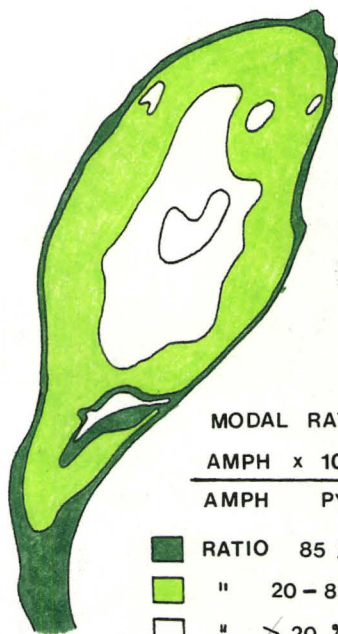
	Central core	Eastern margin	Western margin
SiO ₂	52.49	51.78	51.34
TiO ₂	0.19	1.14	0.49
Al ₂ O ₃	27.66	22.24	24.01
Fe ₂ O ₃	0.63	1.52	1.14
FeO	1.03	5.02	3.12
MnO	0.02	0.12	0.07
MgO	0.93	2.17	2.24
CaO	12.08	10.69	11.73
Na ₂ O	3.96	3.60	3.93
K ₂ O	0.47	0.62	0.52
P ₂ O ₅	0.02	0.11	0.04
H ₂ O	0.46	0.49	0.76
CO ₂	0.21	0.56	0.32
S	0.01	0.04	0.02
Cl	0.01	0.01	0.02
SrO	0.08	0.08	0.09
Total	100.25	100.19	99.84
Plag	91.8	60.3	60.5
Pyx	4.2	5.5	2.9
Amph	2.4	11.4	14.6
Scap	1.6	12.8	15.6
Gt	tr	6.3	1.0
Ep	—	—	3.9
Opaq	tr	1.5	0.2
Other ¹	tr	2.2	1.3

1. Other: refers to apatite, quartz, carbonate, biotite, sphene, serpentine, muscovite and/or orthopyroxene.

FIGURE 1-I

Distribution of Secondary Alteration:
Marginal Facies of the Whitestone Anorthosite

Mineral distributions are based on modal analyses of 340 thin sections. Taken directly from Mason (1969).



0 5 10 km.

Because the mineralogy and chemical characteristics of the contact gneiss are similar, in some respects, to the foliated border phase of the anorthosite (i.e., the presence of garnet and opaques and the enrichment of Fe, Ti and P), Mason considers them to have been affected by the same general metamorphic process. This process is thought to be a type of auto-metasomatism whereby late stage fluids, resulting from differentiation of the anorthositic magma, are concentrated along the intrusive/country rock contact during the final stages of crystallization.

The inferred metasomatism is restricted to rocks juxtaposed to the garnet-bearing foliated facies and is inhomogeneously developed in any one outcrop. Rocks already rich in ferromagnesian minerals appear to have been affected to a greater degree than the more felsic rocks; for example, thin mafic bands have well developed "metasomatic assemblages" while the enclosing felsic gneisses appear to be unaffected. Mason (1969, p. 110) explains:

I believe this polygonal texture to be the result of thorough-going recrystallization which has affected the mafic amphibolites more completely than the acid rocks. The reason for this is presumed to be the greater 'porosity' of the amphibolites to the metasomatizing fluids due to their original richness in the inherently reactive hydrous mafic minerals and that these hot fluids have greatly enhanced the efficiency of the recrystallization.

1. Although Mason does give several analyses of the contact gneisses having relatively high values of Fe, Ti and P, he does not provide analyses of more typical gneisses for comparison.

Mason states that the regional metamorphic grade throughout the map area is upper amphibolite (he estimates $T = 700\text{ }^{\circ}\text{C}$, $P = 4\text{-}5\text{ kb}$), but that it has been raised to the high pressure gt-cpx granulite facies in the vicinity of the pluton. He reviews other occurrences of gt-cpx assemblages associated with anorthosites and concludes that rather than high pressure, the low $\text{Mg}/(\text{Mg} + \text{Fe})$ imposed by the metasomatism is responsible for the development of this assemblage.

1-III Regional Geology and Tectonic Framework of the Parry Sound Region, Western Grenville Province

The Grenville structural province is interpreted by Wynne Edwards (1972) as a deep crustal section through an orogenic belt, in which the exposed rocks are predominantly reworked sialic basement. Recent investigators (Davidson 1982a, and Whitney 1982) conclude that the Grenvillian orogeny represents a major period of crustal shortening (and therefore thickening) through the formation of large scale nappe and thrust structures. Although the exact timing of specific events is only known locally, it now appears fairly clear that considerable activity occurred at $1100\pm 50\text{ Ma}$ (Heaman 1982, Whitney 1982). The peak of deformation and metamorphism associated with the Grevillian orogeny proper is thought to fall in this range. This thesis is concerned with the metamorphic and tectonic history of the rocks east of Georgian Bay, in the vicinity of Parry Sound (the Ontario Gneiss segment of Wynne Edwards 1972). At present, this region is the subject of a G.S.C. reconnaissance mapping project at a scale of 1:250,000 (Davidson 1980,

1982a, 1982b).

Davidson's most important contribution, is his recognition of the "style" of tectonism prevalent in this region during the Grenville orogeny. A number of continuous tectonite gneiss zones have been recognized, which outline subdomains of distinctive lithology and metamorphic grade (see figure 1-III). The general sense of movement on these tectonite zones indicates that a number of allochthonous crustal segments have been "stacked" by northwest-directed thrusting.¹ The most northerly Britt Domain is overlain by the Parry Sound Domain, which in turn is overlain by the Moon River and Sequin Domains to the southwest. The Rosseau segment is overlain by all three of the latter domains. The tectonite zones are well layered gneisses containing continuous small scale layering, sheath folds and a variety of other complex bulbous shaped structures, all indicative of ductile deformation. At various locations, they could properly be termed tectonic breccias,² containing numerous, partially assimilated blocks of local country rock, as well as lesser exotic blocks of anorthosite gneiss and possibly eclogite. Granulite grade assemblages occur throughout the Parry Sound and parts of the Go Home and Rosseau Domains. Partial to complete retrogradation to amphibolite assemblages is common. The Britt, Moon River and Sequin Domains are predominantly middle to upper amphibolite grade. The

1. The sense of movement is determined by sigmoidal (rotated) feldspar augen and by the character of truncation along the tectonite-subdomain contact.

2. Or tectonic melange.

FIGURE 1-II

Structural Trend Map Showing the Distribution of Tectonite
Gneiss Zones and Structural Subdivisions in
the Parry Sound Region

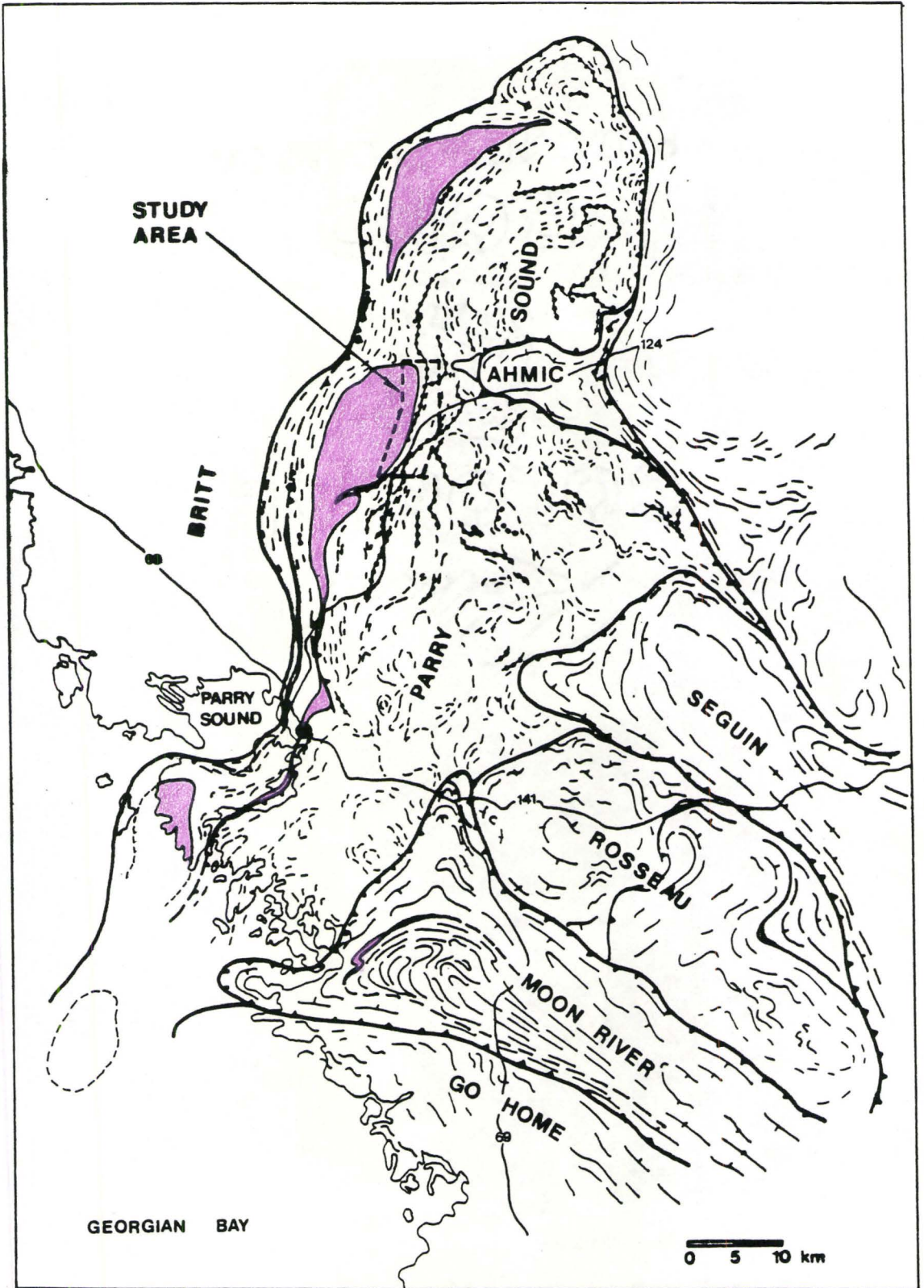
Main tectonite zones are shown as heavy lines with direction
of dip indicated. Modified from Davidson (1982a).

 Marble location.

 Structural boundary.

 Structural trend.

 Anorthosite.



juxtaposition of these medium to high grade terrains separated by tectonite zones exhibiting ductile flow, suggests that the movement took place deep in the crust.

The Parry Sound Domain is underlain by severely deformed mafic gneisses, marble, quartzite, quartzofeldspathic gneiss and granitoid rocks. The strong deformation complicates mapping considerably. Davidson (1982a, p. 177) elaborates, ". . . the mafic gneisses are particularly confusing to map, as they change insensibly from uniform rocks of probable plutonic parentage to well layered though commonly highly contorted gneiss. . . . Narrow marble layers were found in many places, and can be used to trace out the regional structure. They are almost invariably breccias of tectonic type, containing fragments, some highly contorted, of disaggregated silicate layers. . . . A large proportion of the rocks in this whole region are, in fact, tectonites, to the extent that most of their textural and structural features are the effects of tectonism. For example, primary internal features in metasedimentary gneisses are almost entirely lacking. Compositional layering nearly everywhere can be shown to have been severely transposed, locally so much so that enveloping surfaces cannot be traced; even if they can, it is not certain whether they represent bedding or an earlier transposed layering. . . ."

The Whitestone anorthosite is an elongate body located along the western margin of the Parry Sound Domain. Although the exact details of its involvement in the tectonism are only vaguely known at present, Davidson (personal communication 1982) envisions it as one of a number

of large boudin type structures contained within an isoclinally folded sequence. Thin, but persistent units of anorthosite gneiss to the west, may represent the continuation of a large-scale fold structure, in which an originally much larger anorthosite body has been drawn out and disrupted.

1-IV General Approach to Problem

Because a number of topics are discussed in this thesis, which at first appear to be unrelated to the central problem, it is advantageous to provide some sort of unifying theme at the beginning. The thesis problem, as it was initially posed, consisted of two different but related parts:

1. To determine the origin of the garnet-clinopyroxene-oxide rich contact aureole which partially surrounds the Whitestone Anorthosite.
2. To evaluate the use of Mossbauer spectroscopy as an aid in understanding the metamorphic processes which have occurred in these rocks.

Mason (1969) concluded that the Whitestone Anorthosite was emplaced during the waning stages of the Grenvillian Orogeny; the contact aureole being attributed to a combination of very slow cooling and associated late stage metasomatism. It is now known that these conclusions were incorrect. Davidson (1982) interprets the Whitestone Anorthosite as an immense tectonic fragment which has been severely deformed and

recrystallized under high grade metamorphic conditions. The salient observation which led Mason to conclude that the contact aureole post-dated the deformation, was the clear textural evidence that near the anorthosite contact, granulite gneisses have been overprinted by an apparently static recrystallization. Massive garnet rich gneisses exhibiting similar characteristics have been noted at the contact of a number of anorthosite massifs, particularly those which have been involved in a granulite metamorphic event (see Ch. 7). If, as this author believes, the contact effect is an expected consequence of high grade metamorphism, then the garnet rich border zone should not be viewed as a contact aureole in the classic sense. A more appropriate term would be reaction aureole.

This theme, the concept of a reaction aureole, is followed throughout the thesis. Emphasis is placed not so much on the Whitestone Anorthosite, as on understanding the general processes which affect all anorthosite massifs during granulite metamorphism. In chapter 6 (Reaction Rim Study), evidence is reviewed which demonstrates that the Fe, Ti, P rich mafic rocks can be formed by metamorphic processes and in chapter 5, chemical analyses of co-existing minerals, augmented by Mossbauer spectrographic studies, are used to estimate the temperature at which the metamorphic processes of interest occur: In chapter 7, the phenomenon of liquid immiscibility is discussed, because it has been suggested as an alternative differentiation mechanism responsible for the formation of the Fe, Ti, P rich rocks.

1-V Note on Terminology

Unfortunately, there is no universal consensus as to the definition of the term "granulite" (see Behr 1971, Winkler 1979). As used in this thesis, the term will denote rocks which are within the granulite metamorphic facies, as indicated by the occurrence of metamorphic orthopyroxene. No reference to whole rock composition, degree of deformation or type of microtexture is intended. While it is recognized by the author that this definition is not necessarily desirable, it is very convenient and is broadly consistent with use of the term by Canadian field geologists.

The term "hornblende" is used as a field term to denote the dark brown, Ca rich amphibole common in the study area. Specific amphibole names (according to the classification of Leake 1978) are given in the text where determined.

In discussion of magma evolution, the following convention is used (Brown 1979):

- Primary magma: the initial melted material.
- Parental magma: the molten material which makes its way to the predominant crystallization site.
- Derivative magma: magmas formed during cooling and differentiation of the parental magma.

This classification provides a simple division of magma evolution in space and time which is quite useful for discussion purposes.

CHAPTER 2

FIELD RELATIONS AND GENERAL MINERALOGY OF STUDY AREA

2-I Introduction

Field work was conducted during the summer and fall of 1979, and the spring of 1980. The area chosen for detailed study is a small zone (approximately 30 km²) straddling the Anorthosite contact in the vicinity of Whitestone Lake. The E-W trending arms of Whitestone Lake and several cottage roads provide good access and excellent cross-sections of the contact. In addition, Mason (1969) indicates that the contact effect is best developed in this area. Emphasis was placed on careful observation and sample collection at each outcrop, using the geological map of Mason (1969) as a guide. Limited structural information was collected, and no attempt has been made to produce a "geological map" outlining the extent and geometry of the various rock units. The style of deformation in this region would make such an endeavour very difficult, as has been emphasized by Davidson (1982).

The study area is underlain by:

1. Dark grey to light grey (or pinkish-grey) weathering, massive, fine to medium grained, granoblastic gneisses. Mafic compositions predominate.
2. Light grey weathering marble breccia, containing numerous extremely deformed mafic fragments.¹

3. Light grey anorthosite gneiss (border phase).

For the most part, mineral assemblages are consistent with the granulite facies of metamorphism (see Figure 2-I). Outcrops exhibit a transposed layering characterized by very tight fold-like structures and extreme boudinage (see Plates 2-I, 2-II, 2-K, 2-X). These features may be attributed to flow of a layered sequence comprised of units having widely varying competency. No evidence has been observed in outcrop (e.g., bedding, clasts, cobbles, phenocrysts, pillows, flow structures, etc.), which might indicate the protolith for these units. The abundant marble in the vicinity of Whitestone Lake is considered to be of sedimentary origin.

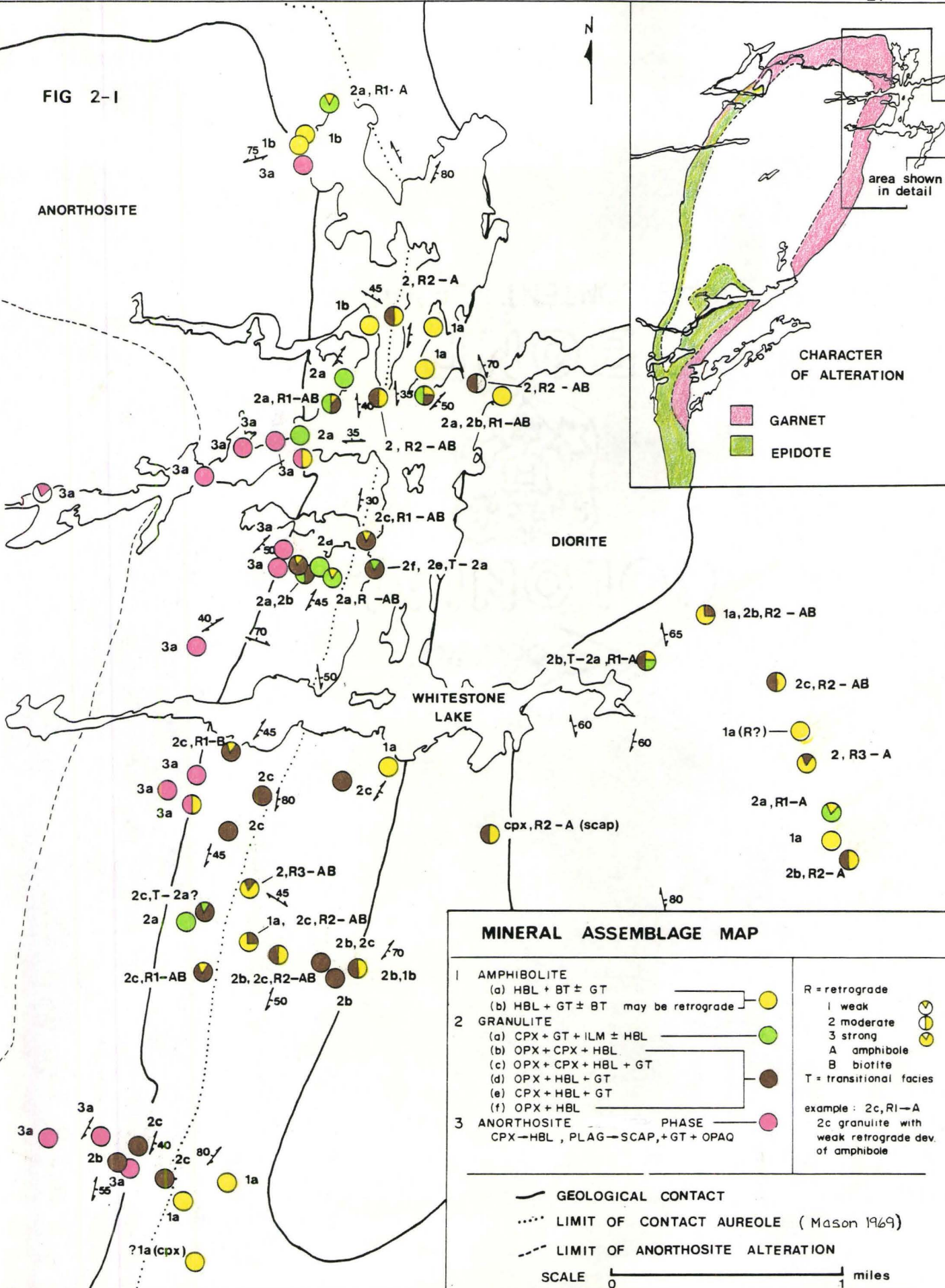
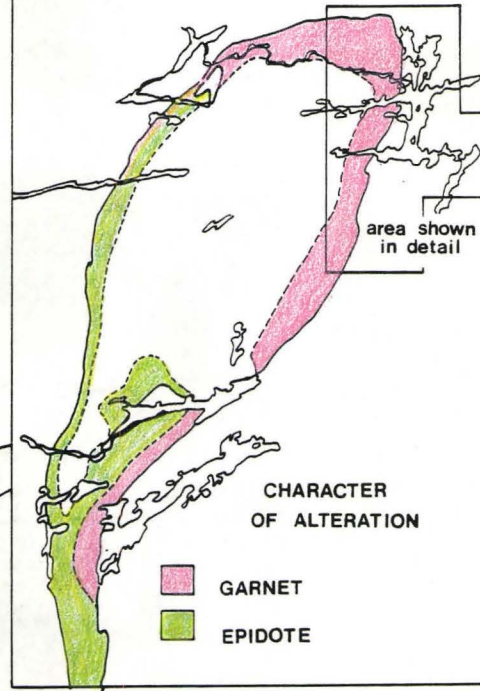
2-II Anorthosite - Gneiss Contact Relations

The anorthosite/granulite gneiss boundary is typically defined by a deep gully and a slight topographic high toward the anorthosite. The actual contact is rarely observable in outcrop. The anorthosite (or tectonite) gneiss which borders the contact is extremely deformed and inhomogeneous (see Plates 2-I, 2-II). Inclusions of foreign material are common, and although in many cases, it is not possible to recognize the protolith due to strong deformation, the increased mafic character of the border facies (as shown by mineralogy and chemistry) supports the concept of tectonic mixing.

1. Little is known about the marble units beyond brief examination in the field.

FIG 2-1

ANORTHOSITE



MINERAL ASSEMBLAGE MAP

1	AMPHIBOLITE		
	(a) HBL + BT ± GT	●	
	(b) HBL + GT ± BT may be retrograde	●	
2	GRANULITE		
	(a) CPX + GT + ILM ± HBL	●	
	(b) OPX + CPX + HBL	●	
	(c) OPX + CPX + HBL + GT	●	
	(d) OPX + HBL + GT	●	
	(e) CPX + HBL + GT	●	
	(f) OPX + HBL	●	
3	ANORTHOSITE	●	
	PHASE	●	
	CPX → HBL, PLAG → SCAP, +GT + OPAQ	●	

R = retrograde
 1 weak
 2 moderate
 3 strong
 A amphibole
 B biotite
 T = transitional facies

example: 2c,R1-A
 2c granulite with weak retrograde dev. of amphibole

— GEOLOGICAL CONTACT
 LIMIT OF CONTACT AUREOLE (Mason 1969)
 - - - - - LIMIT OF ANORTHOSITE ALTERATION

SCALE 0 1 miles

Plate 2-I

(OTC-020, Sample DT-31)

Metasomatic border zone of the Whitestone Anorthosite, approximately 20 meters from the anorthosite/gneiss contact.

Plate 2-II

Detail of central region of Plate I (the hammer and notebook are in the same location in both Plates). The border gneiss exhibits local compositional inhomogeneities and intense deformation, indicating a complex history of tectonic mixing. While the modal concentration of any one mineral is extremely variable, the overall mineralogy is remarkably constant. Mafic pods are defined by local concentrations of hornblende, garnet and/or magnetite and ilmenite.



Plate I



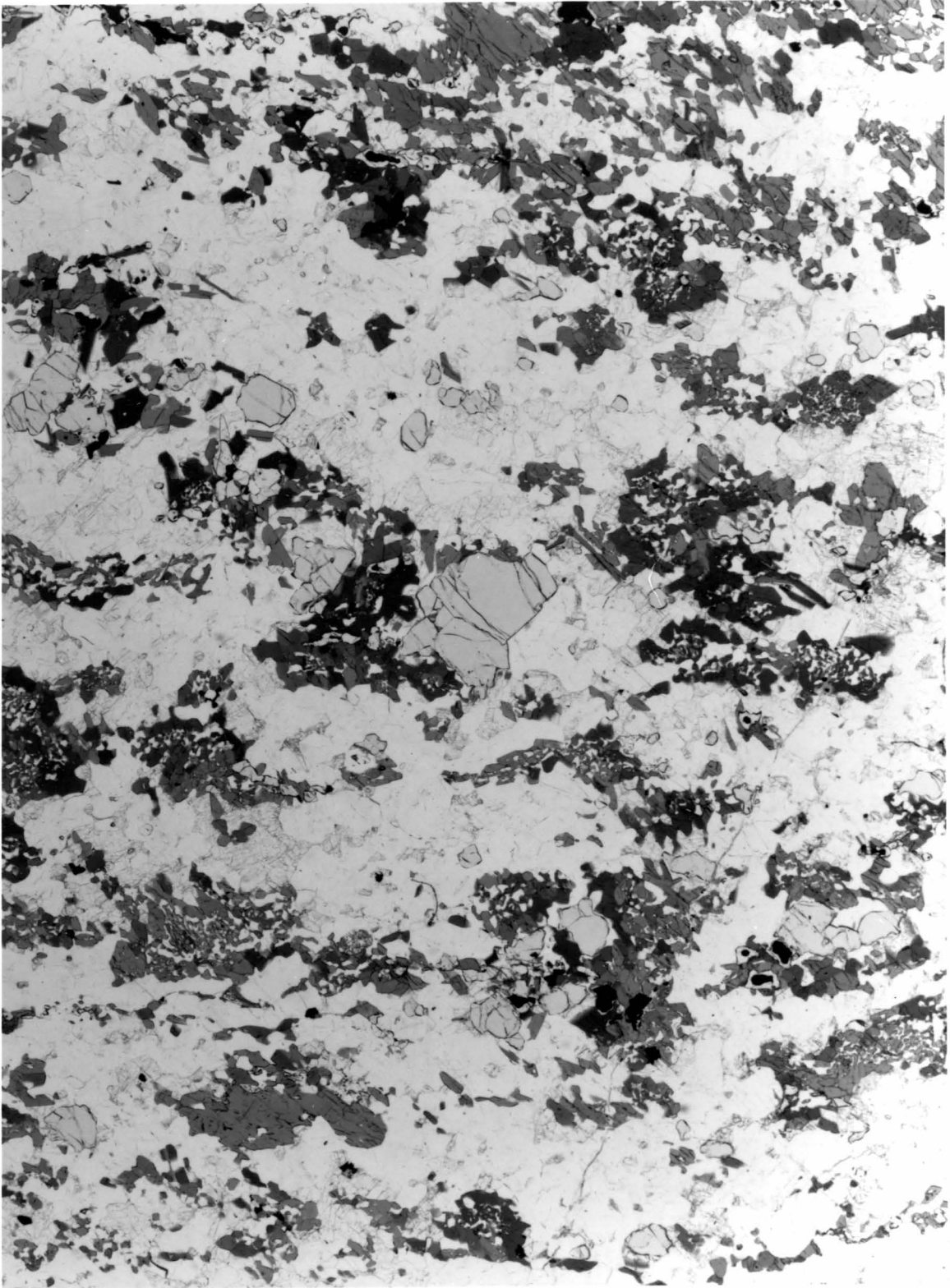
Plate II

Plate 2-III

(Photomicrograph OTC-020, Sample DT-031)

Metasomatic border zone of Whitestone Anorthosite, Eastern margin. Scapolite (very light grey mineral with fine cleavage traces) occurs as strings and beads along feldspar grain boundaries and as large patches normally surrounded or in close contact with plagioclase. Plagioclase exhibits a granoblastic polygonal texture (very smooth grain boundaries and 120° junctions) indicative of complete recrystallization. Deformation features are generally not observable in any of the constituent minerals, except for minor undulatory extinction and/or subgrain development in quartz, and to a lesser extent in plagioclase. Hornblende poikiloblasts most commonly contain inclusions of quartz and feldspar, but may contain any mineral present in the section. Pleochroism is green to blue-green to yellow-green. This colour scheme contrasts with the dark green to brown hornblende typically found in granulites and is generally considered indicative of lower grade metamorphism (Miyashiro 1973). Calcite is ubiquitous, occurring predominantly in very small irregular patches, but also in larger, approximately planar veins with biotite. The veins have fuzzy, indistinct borders and adjacent feldspar appears cloudy and altered. Sphene occurs as discrete grains and as a thick mantle on opaque grains.

Composition of Sample DT-031			
% Modal Mineralogy		Whole Rock Chemistry	
scapolite	7.6	SiO ₂	52.77
garnet	10.9	TiO ₂	1.34
amphibole	21.1	Al ₂ O ₃	20.50
plagioclase	47.6	Fe ₂ O ₃	2.80
quartz	2.7	FeO	5.17
biotite	2.1	MnO	0.11
sphene	2.4	MgO	2.73
opaque	2.2	CaO	10.47
apatite	1.9	Na ₂ O	3.46
calcite	1.4	K ₂ O	0.70
orthopyroxene	tr	P ₂ O ₅	0.28
		CO ₂	0.93
		Tot	101.26



mm

The contact aureole (or reaction aureole), as defined by Mason (1969), is quite variable. At certain locations (see Plate 2-IV) the contact is characterized by:

1. Rust-coloured, sugary textured gneisses. The foliation may be quite weak and gives the impression of having been overprinted by a static recrystallization.
2. An increase in garnet, clinopyroxene and opaques and a decrease in hornblende and orthopyroxene, as compared with the majority of mafic gneisses in the study area. The high concentration and homogeneous distribution of small euhedral garnets is particularly noticeable in outcrop.

However, at other locations (e.g., southern part of the study area), garnet rich rocks are only sporadically developed and in many instances, the only effect observed at the contact is a subtle reduction in grain size. The rocks which exhibit the most extensive changes are clearly the mafic units and in general, it would seem that the variability of the reaction aureole is compositionally controlled.

2-III Distribution of Garnet Bearing Rocks

Garnet occurs throughout the study area in a wide variety of rock types, however, it is only in certain mafic compositions where the modal concentrations becomes great enough to be conspicuous in the field. It was primarily on the occurrence of small euhedral garnets that Mason defined his "contact aureole." The field and petrographic

Plate 2-IV

(OTC-037, Sample DT-057)

Pyroxene-garnet-oxide rich border gneiss. The contact with the anorthosite is to the extreme upper left of the photo (near the diving board). This outcrop is one of the few locations where the anorthosite/gneiss contact can be closely defined and represents the best example of altered mafic gneisses observed in the study area. Most of the outcrop appears approximately homogeneous in composition and exhibits a fine to medium grained texture. That this texture overprints an earlier foliation can be demonstrated by tracing the altered rocks into more typical, weakly foliated, hornblende bearing (garnet poor) mafic gneisses. The rusty nature of the weathered surface is due to the breakdown of garnet and oxide minerals.

Composition of Sample DT-057

% Modal Mineralogy		Whole Rock Chemistry	
orthopyroxene	2.9	SiO ₂	45.83
clinopyroxene	25.7	TiO ₂	4.39
garnet	19.9	Al ₂ O ₃	11.80
amphibole	2.6	Fe ₂ O ₃	4.66
plagioclase	37.4	FeO	13.00
opaques	7.4	MnO	0.23
apatite	2.0	MgO	2.93
sphene	2.0	CaO	11.96
biotite	0.1	Na ₂ O	2.23
quartz	tr	K ₂ O	0.61
carbonate	tr	P ₂ O ₅	1.02
		CO ₂	0.08
		Tot	98.74

Plate 2-V

Pyroxene-plagioclase ± garnet ± hornblende veinlet. Small, very planar veins (approximately 2 cm wide) commonly cross-cut the border gneiss perpendicular to the anorthosite contact (detail of Plate above).



Plate IV



Plate V

characteristics of these rocks are shown in Plates 2-III, 2-IV, 2-V, 2-VI, 2-VII, and 2-VIII. Other occurrences of garnet in the study area may be summarized as follows:

1. Fine to medium grained fragmented crystals in fine grained mafic and felsic gneisses. The modal concentration of garnet is typically low (< 5%, see Plate 2-XIII).
2. Extremely irregular, poikilitic crystals in felsic gneisses, sometimes rimming opaque grains. The modal concentration is usually very low (< 1-2%).
3. Relatively large patches (2.0 - 10.0 cm) and isolated crystals of very coarse grained garnet (1.0 - 3.0 cm dia.) in rocks otherwise poor in garnet.
4. Reaction rims bordering veins (see Plate 2-XVI) and mafic/felsic interfaces (see Reaction Rim Study, Ch. 6). Also in linear patches and small shear zones in mafic rocks.

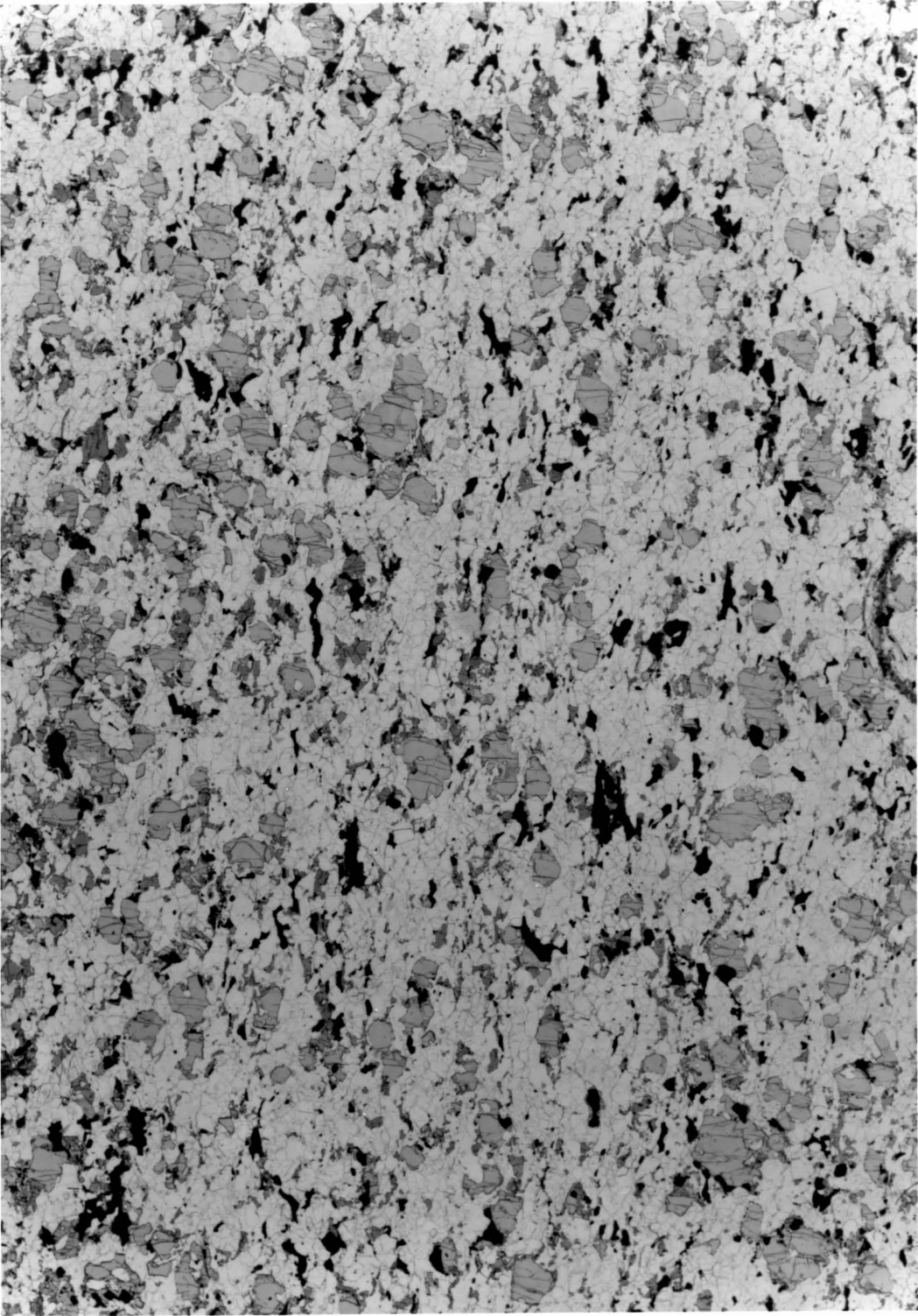
Some of the garnet bearing rocks of category (4) are very similar in texture and mineralogy to the garnet rich gneisses present in the reaction aureole. In each case they appear to be associated with zones of progressive dehydration.

Pyroxene-garnet-oxide rich border gneiss. See previous plate for description of outcrop characteristics. The predominant mafic minerals are garnet and clinopyroxene. Orthopyroxene is absent and amphibole occurs as very small pod shaped crystals associated with opaques and clinopyroxene. The amphibole is considered to be prograde and, is very similar in morphology to the remnant amphibole fragments present in sample DT-98-2 (Reaction Rim Study, see Ch. 6) resulting from progressive dehydration. The garnets are generally subhedral in outline, however, on a smaller scale, they have very irregular boundaries and are heavily fractured. Some contain numerous inclusions of quartz (?) (not positively identified).

Composition of Sample DT-028

% Modal Mineralogy		Whole Rock Chemistry	
orthopyroxene	tr	SiO ₂	56.04
clinopyroxene	14.2	TiO ₂	2.13
garnet	28.6	Al ₂ O ₃	11.58
amphibole	0.2	Fe ₂ O ₃	5.86
plagioclase	42.8	FeO	10.99
quartz	tr	MnO	0.36
opaque	9.4	MgO	1.56
biotite	tr	CaO	6.75
apatite	1.9	Na ₂ O	1.89
sphene	2.9	K ₂ O	0.81
hematite ¹	tr	P ₂ O ₅	0.50
		Tot	98.47

1. Identification not certain.



mm

Plate 2-VII

(Photomicrograph OTC-023, Sample DT-035)

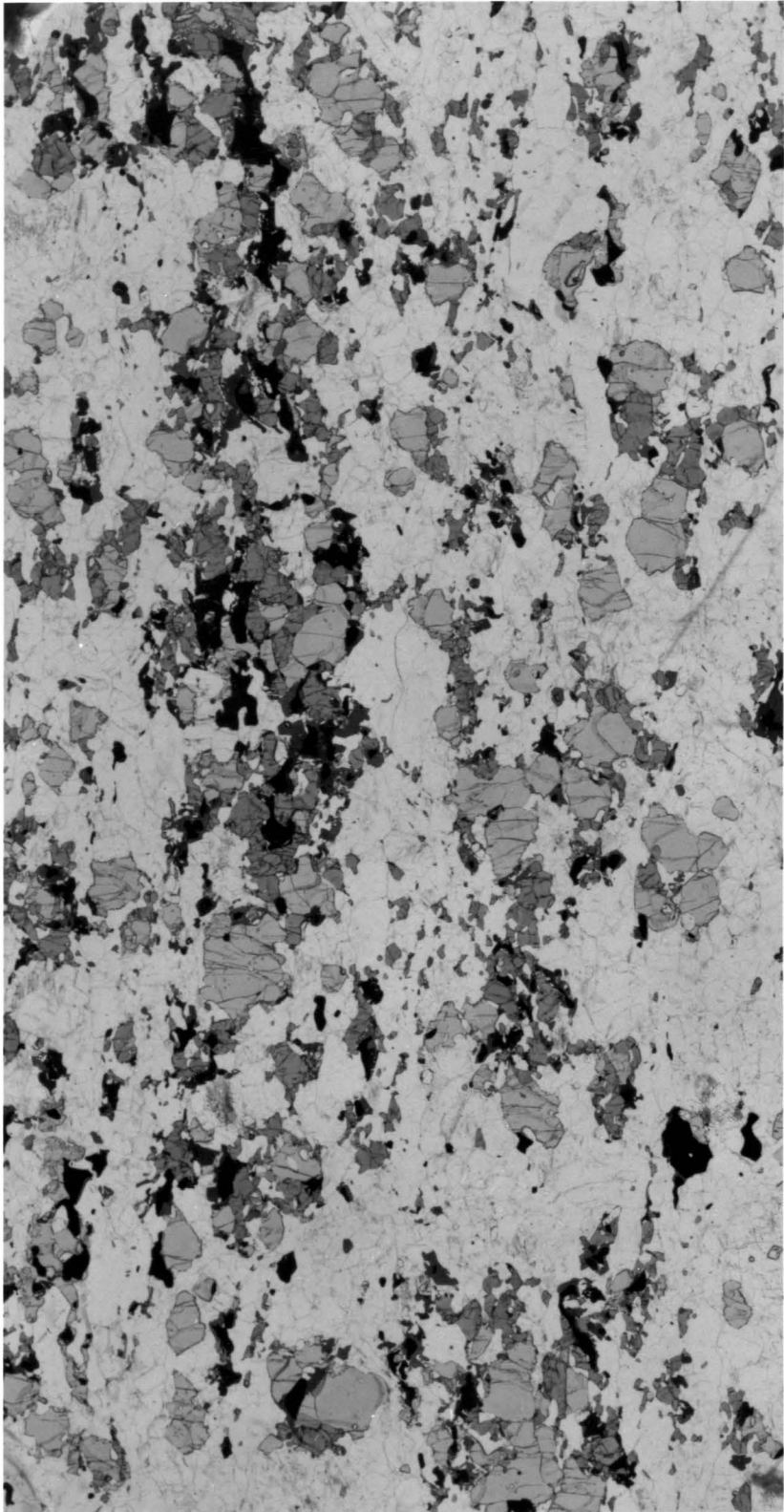
Mafic granulite gneiss. OTC-023 is approximately 300 meters from the anorthosite contact and is on strike with OTC-075 (shown in Plates 6-I, 6-II, and 6-III). Both outcrops contain irregular felsic segregations. Sample DT-035 has many characteristics in common with the mafic border gneiss (two previous plates, samples DT-028 and DT-057), as well as sample DT-098-2 (Reaction Rim Study) discussed in Chapter 6. The nebulous leucocratic patches are enriched in plagioclase, quartz, clinopyroxene, garnet, and opaques, while amphibole and orthopyroxene are depleted. In the photomicrograph (opposite), amphibole occurs in two forms:

1. optically continuous crystals
2. skeletal (or poikilolitic) crystals

Amphibole (2) is exactly similar in morphology to the amphibole shown in Plate 2-III (sample DT-031) and typically occurs as a corona on clinopyroxene and amphibole (1). Amphibole (2) has a light bluish-green colour--distinct from amphibole (1), which is pleochroic dark green to straw yellow. Rare biotite blades are associated with opaques and amphibole. Sphene occurs as a thick mantle on some (but not all) opaque grains and less commonly as discrete grains. Carbonate occurs as small "amoeboid-like" patches, having very irregular arcuate boundaries and thin vein-like apophyses.

Composition of Sample DT-035

% Modal Mineralogy		Whole Rock Chemistry	
orthopyroxene	tr	SiO ₂	57.91
clinopyroxene	13.3	TiO ₂	0.99
garnet	24.0	Al ₂ O ₃	19.13
amphibole	6.6	Fe ₂ O ₃	1.56
plagioclase	37.8	FeO	4.81
quartz	7.4	MnO	0.10
opaque	6.2	MgO	1.91
biotite	0.5	CaO	7.45
apatite	1.1	Na ₂ O	4.82
sphene	2.6	K ₂ O	0.96
carbonate	0.5	P ₂ O ₅	0.23
		Tot	99.87



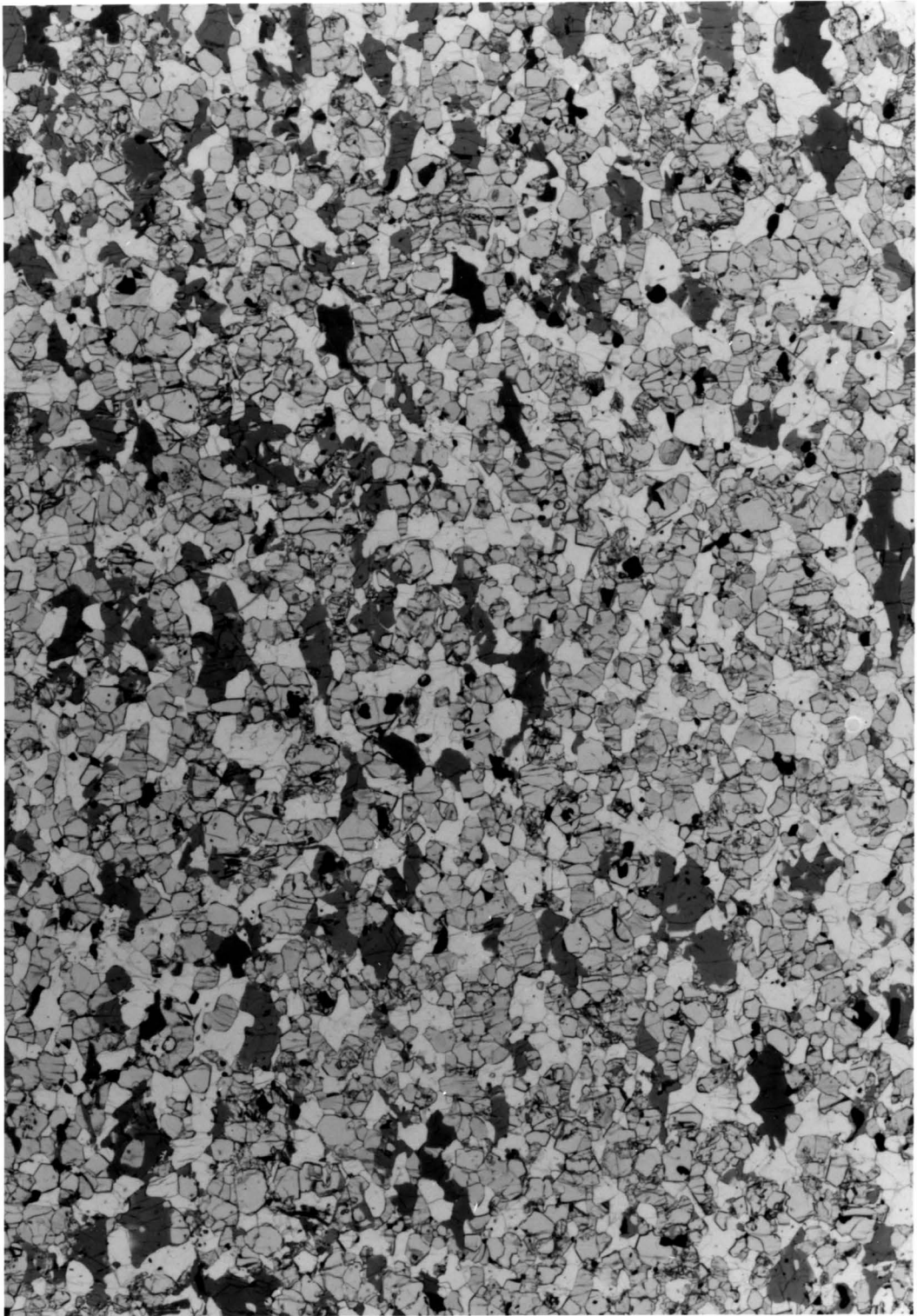
mm

Mafic granulite gneiss (approximately 200 meters from the anorthosite contact). Rounded irregular pyroxene and euhedral garnet grains in a granoblastic polygonal plagioclase matrix. No indication of deformation is present, with the exception of minor undulatory extinction and subgrain development in plagioclase. Rutile occurs as small, glassy, orange-brown grains. Biotite occurs as small blades in contact with hornblende, orthopyroxene or opaque minerals, and as discrete radiating patches or rosettes.

Composition of Sample DT-030

% Modal Mineralogy		Whole Rock Chemistry	
orthopyroxene	10.6	SiO ₂	49.22
clinopyroxene	20.0	TiO ₂	1.38
garnet	18.4	Al ₂ O ₃	13.61
amphibole	13.0	Fe ₂ O ₃	2.79
plagioclase	34.8	FeO	8.32
opaque	1.4	MnO	0.17
biotite	0.9	MgO	9.69
rutile	0.9	CaO	11.99
apatite ¹	tr	Na ₂ O	1.77
		K ₂ O	0.40
		P ₂ O ₅	0.04
		CO ₂	0.06
		Tot	99.44

1. Identification not certain.



mm

Plate 2-IX

(OTC-014, Samples DT-024, DT-025)

Banded tectonite (or mylonite) gneiss, located approximately 1.0 Km from the anorthosite contact. No evidence of dehydration or recrystallization, typical of the contact gneisses is evident in this outcrop. The transposed layering is defined by alternating layers of resinous, grey-green, medium grained felsic granulite (plagioclase - K-spar - quartz - pyroxene gneiss) and very dark grey to black, medium to fine grained mafic granulite (pyroxene - garnet - hornblende - plagioclase ± quartz gneiss). Note: the weathered surface tends to be much lighter in colour than the fresh surface.

Plate 2-X

(OTC-024)

Tightly folded and disrupted garnet rich mafic gneiss in an impure marble matrix. Western shore of Whitestone Lake.



Plate IX



Plate X

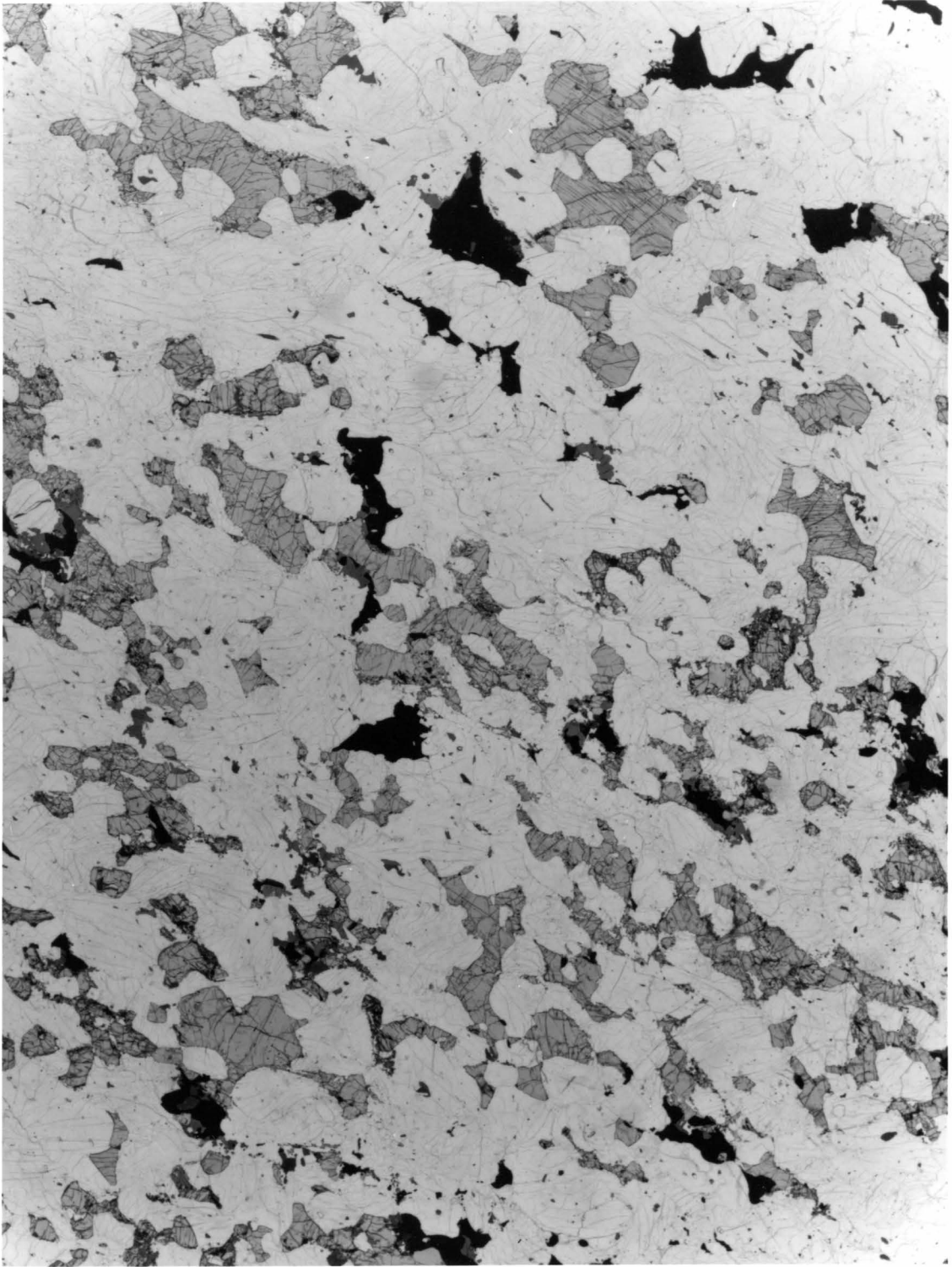
Plate 2-XI

(Photomicrograph OTC-014, Sample DT-24)

Tectonite (or mylonite) gneiss (see Plate 2-XI). Irregular-shaped, rounded pyroxene crystals in a mylonitic quartzofeldspathic matrix. Pale green clinopyroxene exhibits exsolution of Ca poor pyroxene (as fine continuous bands and very small lenses), and an opaque mineral (as fine bands and blocky patches of oriented needles). Orthopyroxene (pleochroic pale green to pink) occurs as fractured and fragmented crystals commonly altered to biotite (and less commonly amphibole) along cleavage planes and fractures. Hornblende (pleochroic dark green to straw yellow-green) exhibits arcuate, irregular crystal outlines. It occurs in two distinct forms: as medium-sized optically continuous patches, almost always in close association with pyroxene or opaques, and as a very fine grained symplectitic border on clinopyroxene. Biotite, in addition to occurring as a common alteration product of orthopyroxene, occurs as small, rusty brown patches, usually touching, but not encompassing, an opaque grain.

Composition of Sample DT-24

% Modal Mineralogy		Whole Rock Chemistry	
orthopyroxene	8.3	SiO ₂	58.21
clinopyroxene	12.9	TiO ₂	0.66
amphibole	5.8	Al ₂ O ₃	16.23
plagioclase	46.4	Fe ₂ O ₃	2.88
k-spar	10.2	FeO	4.86
quartz	10.1	MnO	0.15
opaque	5.4	MgO	3.46
apatite	0.8	CaO	6.36
biotite	0.1	Na ₂ O	3.88
carbonate	tr	K ₂ O	1.63
		P ₂ O ₅	0.18
		Tot	98.50

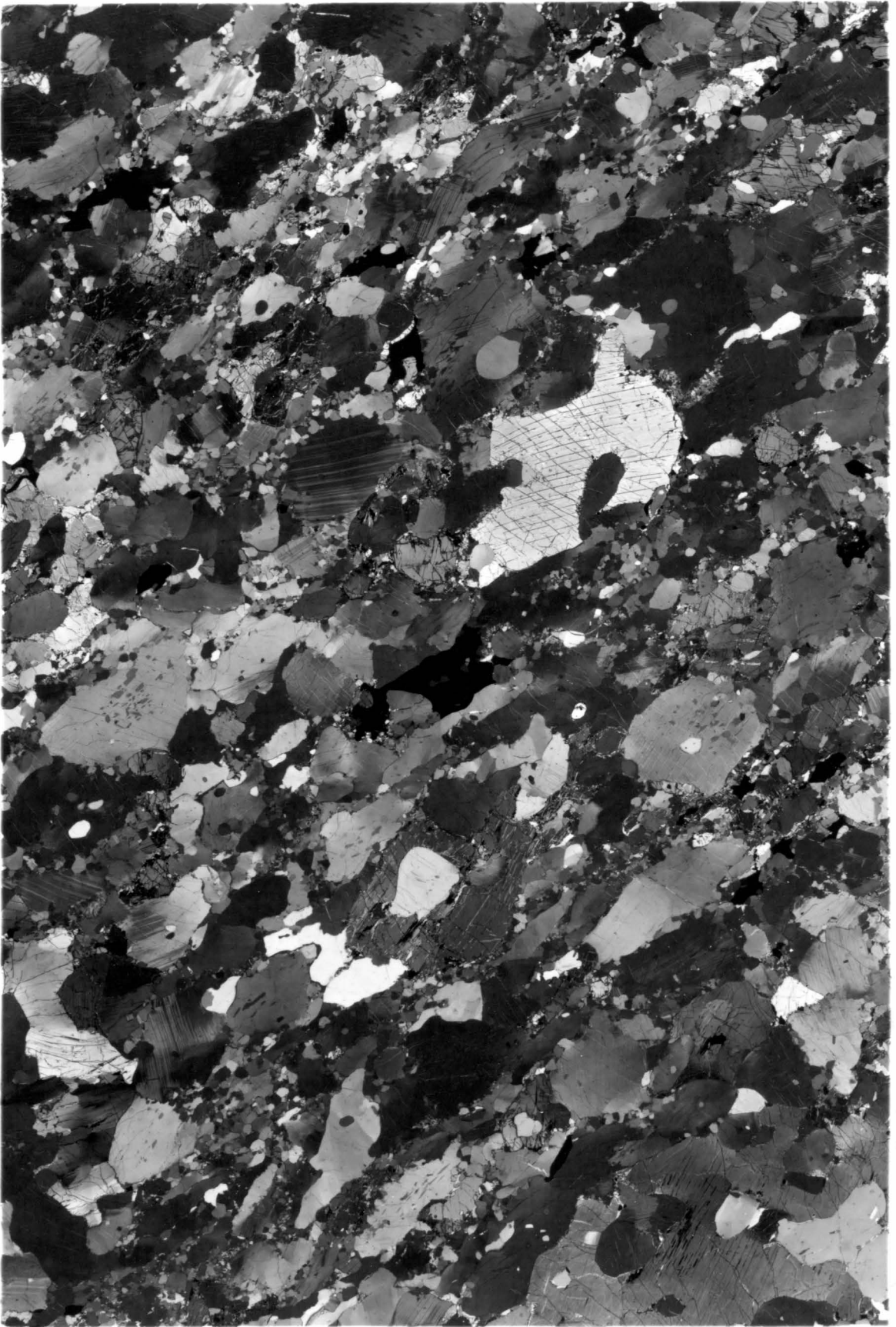


mm

Plate 2-XII

(Photomicrograph OTC-014, Sample DT-24)

Tectonite (or mylonite) gneiss. Same slide as Plate 2-XI in polarized light. Chemical and modal analyses given in Plate 2-XI. The presence of undulose extinction and deformation bands within the new-grains (and subgrains) indicates that dynamic recovery and recrystallization occurred simultaneously (see White 1977, and Bell and Etheridge 1973). This deformation is thought to postdate the major granulite metamorphism and most likely, did not result in re-equilibration of all minerals. Myrmekite is common along grain boundaries and within the narrow bands of new grains.



mm

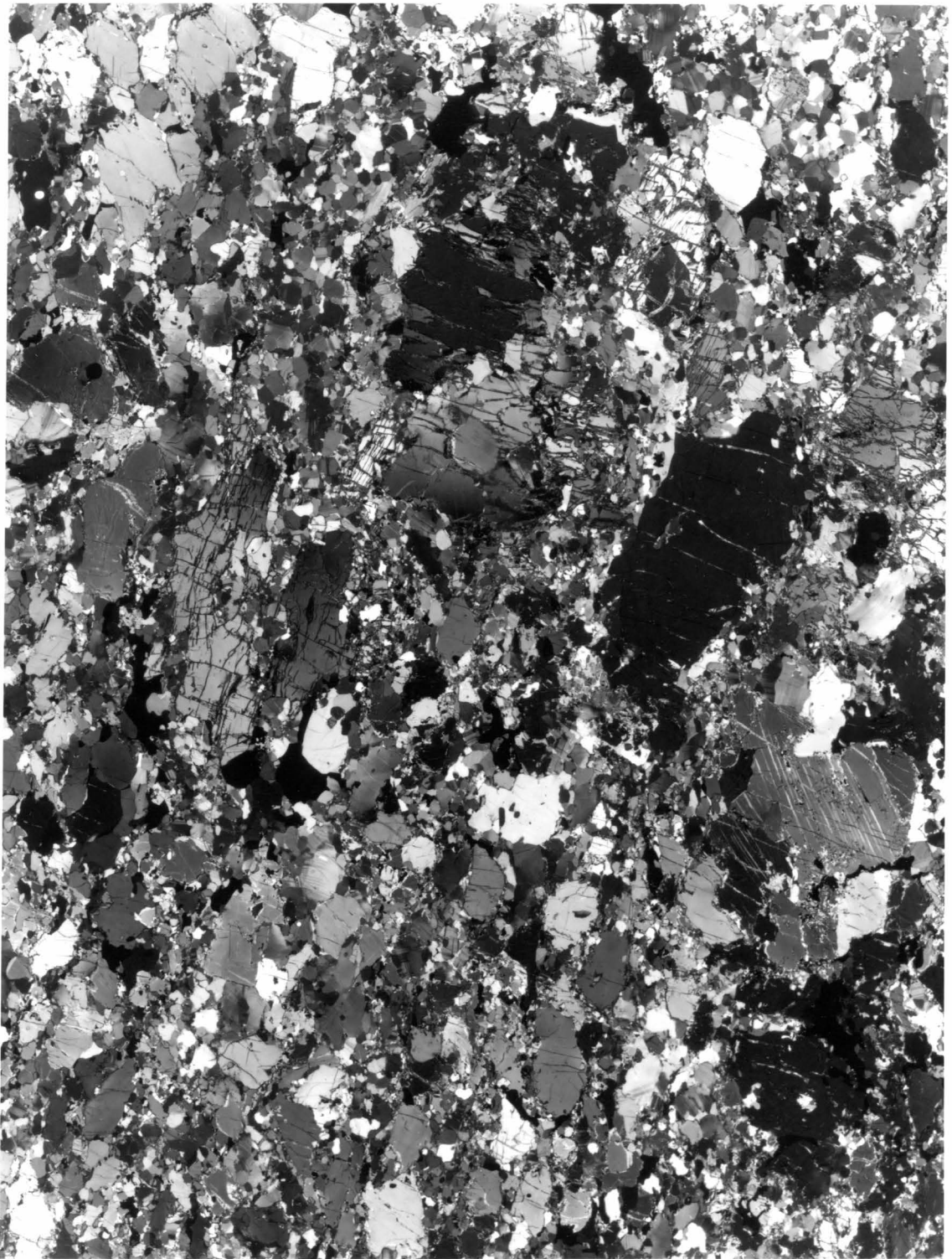
Plate 2-XIII

(Photomicrograph OTC-014, Sample DT-25)

Mafic tectonite (or mylonite) gneiss. Note: sample DT-25 and DT-24 (two previous plates) are from the same outcrop. Quartz, feldspar and hornblende show extensive plastic deformation and recrystallization. Garnet and pyroxene (particularly orthopyroxene) are commonly fractured and in general, do not show the same degree of plastic deformation as quartz and feldspar.

Composition of Sample DT-25

% Modal Mineralogy		Whole Rock Chemistry	
orthopyroxene	2.3	SiO ₂	49.03
clinopyroxene	15.7	TiO ₂	1.69
amphibole	41.1	Al ₂ O ₃	12.07
plagioclase	31.8	Fe ₂ O ₃	5.17
garnet	2.8	FeO	8.35
quartz	0.9	MnO	0.23
apatite	0.8	MgO	7.55
biotite	0.5	CaO	11.80
opaque	6.5	Na ₂ O	2.72
		K ₂ O	1.07
		P ₂ O ₅	0.18
		Tot	99.86



mm

2-IV Retrograde Metamorphism

Retrograde development of amphibole and biotite is widespread throughout the study area. The eastern and northern regions (in the vicinity of Whitestone Lake) show moderate to complete retrogression. In thin section, one observes large irregular or ragged, poikilitic amphibole crystals with indistinct cores of a highly birefringent mineral--probably pyroxene.

The south central region and the zone along the anorthosite contact show the least retrograde effects. Most of the samples selected for detailed study come from this area. In the less altered rocks, amphibole occurs as fine symplectic (?) coronas on clinopyroxene. Attempts to probe these "halos" gave non-stoichiometric, confusing results, which suggests the alteration may be taking place by selective replacement of the pyroxene lattice. Biotite occurs as small blades and rosettes, typically in contact with an opaque grain and as an alteration of orthopyroxene (along cleavage traces). Biotite is less commonly associated with amphibole and clinopyroxene. In general, orthopyroxene crystals tend to be more fragmented and altered than clinopyroxene.

Several distinct groups of small pegmatites, veins and healed fractures postdate the major deformation and metamorphism. The most common group is thin (1.0 mm to 5.0 cm, 2.0 - 3.0 cm most common) light-coloured feldspar-quartz \pm garnet \pm pyroxene \pm hornblende veins (see Plates 2-XVI, 2-XVII). Several generations are present in most outcrops, as shown by cross-cutting relationships and minor changes in

Pyroxene-garnet granulite gneiss located 250 meters from the anorthosite contact. The outcrop is a uniform, granoblastic, dark grey to pinkish-grey, fine grained gneiss. In thin section, rounded irregular-shaped crystals of pyroxene and garnet are surrounded by a matrix of granoblastic, polygonal to decussate plagioclase and quartz showing only minor undulatory extinction. Amphibole is rare, occurring as large patchy crystals with irregular arcuate outlines. This texture is thought to represent the last vestige of hydrous minerals in the process of breakdown. Orthopyroxene is strongly altered to biotite, appearing as small irregular brown patches.

	estimated mode DT-087
clinopyroxene	21
garnet	18
plagioclase	35
quartz	7
orthopyroxene	3
amphibole	5
opaques	8
apatite	3
biotite	tr
carbonate	tr

Detail of above plate showing late (post-granulite metamorphism) plagioclase-quartz vein with hornblende hydration halo. The geometry of the vein cross-linking and the distribution and density of hydration are controlled by the radial stress field surrounding the nose of the advancing dyke (or vein) (Johnson and Pollard 1973).



Plate XIV

detail shown below



Plate XV

Plate 2-XVI

(OTC-068)

Mafic granulite gneiss (hornblende - pyroxene - garnet - plagioclase gneiss) cut by late (post-deformation) veins. The earliest formed pyroxene - plagioclase veins (planar dark units with light grey borders) exhibit a hornblende depleted margin or dehydration halo, indicating a reduced $a_{\text{H}_2\text{O}}$ in the vicinity of the vein and possibly, transport of H_2O out of the system along this pathway. Later, irregular, leucocratic, plagioclase - quartz - garnet (\pm magnetite, ilmenite, pyroxene, and hornblende) veins, exhibit garnet concentrations along their margins suggesting possible interaction with the parent gneiss but no dehydration halo.

Plate 2-XVII

Detail of plate above.



Plate XVI



Plate XVII

mineralogy. The earliest formed set often exhibits dehydration halos, followed by plagioclase - quartz - garnet \pm hornblende veins with garnet borders and no dehydration halo. Other (rare) plagioclase - quartz \pm hornblende \pm biotite veins exhibit sharp outlines and greater planar continuity than the garnet rich veins, and often have wide hornblende hydration halos (see Plate 2-XV). The later set have not been observed cross-cutting the garnet rich veins, however, taken together, the various sets seem to suggest increasingly lower temperatures and a more hydrous mineralogy with time. This trend in veining is possibly related to the upthrusting and partial hydration of the entire Parry Sound block.

2-V Mineral and Whole Rock Chemistry

The whole rock chemistry and modal mineralogy of selected samples is given in Tables 2-I and 2-II, respectively. The composition of mafic minerals is given in Figures 2-II (Pyroxene), 2-III (Amphibole), and 2-IV (Garnet).¹ The mineral assemblages present in the study area may be divided into four groups which reflect, in part, their whole rock chemistry, and in part, their metamorphic history. These are:

1. Whole Rock analysis by XRF. Fe oxidation state by titration. Modal composition based on 1200 points. Mineral analysis by WD microprobe (Material Analysis Co. instrument). Fe oxidation state in minerals by Mossbauer spectroscopy.

TABLE 2-I

Whole Rock composition and CIPW Norm of selected samples

Sample No	DT-24	DT-25	DT-27	DT-28	DT-30	DT-31	DT-32	DT-33	DT-34	DT-35	DT-36	DT-37	DT-57	DT-98-1	DT-98-2	DT-98-3	DT-174	DT-176	DT-177	DT-178
SiO ₂	58.21	49.03	56.58	56.04	49.22	52.77	54.33	5.58	55.02	57.91	47.95	63.95	45.83	49.76	47.29	47.14	51.19	50.02	58.45	54.32
TiO ₂	0.66	1.69	0.79	2.13	1.38	1.34	0.59	0.92	1.81	0.99	2.53	0.46	4.39	3.24	3.34	1.87	1.31	1.14	0.68	0.75
Al ₂ O ₃	16.23	12.07	18.74	11.58	13.61	20.50	12.20	13.01	12.07	19.13	11.91	15.51	11.80	15.57	15.22	12.73	14.89	17.70	17.46	18.21
Fe ₂ O ₃	2.88	5.17	2.43	5.86	2.79	2.80	2.31	2.31	3.08	1.56	3.49	0.86	4.66	5.43	4.07	3.26	4.59	3.40	2.41	4.15
FeO	4.86	8.35	5.65	10.99	8.32	5.17	12.24	6.94	11.90	4.81	12.55	3.52	13.00	11.54	14.49	11.54	8.79	7.13	4.13	5.12
MnO	0.15	0.23	0.13	0.36	0.17	0.11	0.45	0.19	0.32	0.10	0.28	0.06	0.23	0.27	0.40	0.27	0.21	0.15	0.10	0.19
MgO	3.46	7.55	3.49	1.56	9.69	2.73	5.30	6.18	1.47	1.91	5.40	1.82	2.93	0.87	2.34	6.42	5.38	5.09	2.80	3.74
CaO	6.36	11.80	7.45	6.75	11.99	10.47	9.03	8.49	6.98	7.45	9.26	4.18	11.73	5.78	6.36	10.17	6.60	8.83	6.49	7.35
Na ₂ O	3.88	2.72	3.93	1.89	1.77	3.46	1.69	3.22	2.92	4.82	2.36	4.69	2.23	2.75	2.68	2.62	4.83	4.05	4.87	4.55
K ₂ O	1.63	1.07	0.65	0.81	0.40	0.70	0.81	1.06	0.86	0.96	0.90	2.29	0.61	0.64	0.49	0.61	0.72	0.50	0.78	0.82
P ₂ O ₅	0.18	0.18	0.18	0.50	0.04	0.28	0.17	0.22	0.45	0.23	0.26	0.08	1.02	0.41	0.47	0.13	0.26	0.20	0.17	0.23
CO ₂					0.06	0.93	0.46	0.25			0.15		0.08	0.16	0.16	0.19		0.14		0.79
Total	98.50	99.86	100.02	98.47	99.44	101.26	99.58	100.37	96.88	99.87	97.04	97.42	98.74	96.42	97.31	96.95	98.77	98.35	98.34	100.22
Calcite	na	na	na	na	0.14	2.12	1.05	0.57	na	na	0.34	na	0.18	0.36	0.36	0.43	na	0.32	na	1.80
Apatite	0.42	0.42	0.42	1.16	0.09	0.65	0.39	0.51	1.04	0.53	0.60	0.19	2.36	0.95	1.09	0.30	0.60	0.46	0.39	0.53
Ilmenite	1.25	3.21	1.50	4.05	2.62	2.55	1.12	1.75	3.44	1.88	4.81	0.87	8.34	6.15	6.34	3.55	2.49	2.17	1.29	1.42
Magnetite	4.18	7.50	3.52	8.50	4.05	4.06	3.35	3.35	4.47	2.26	5.06	1.25	6.76	7.87	5.90	4.73	6.66	4.93	3.49	6.02
Albite	32.83	23.02	33.26	15.99	14.98	29.28	14.30	27.25	24.71	40.79	19.97	39.69	18.87	23.27	22.68	22.17	40.87	34.27	41.21	38.50
Anorthite	22.06	17.57	31.58	20.72	28.01	38.34	23.31	17.92	17.29	27.73	19.25	14.51	20.39	24.99	27.47	21.17	16.82	28.64	23.48	26.84
Orthoclase	9.63	6.32	3.84	4.79	2.36	4.14	4.79	6.26	5.08	5.67	5.32	13.53	3.61	3.78	2.90	3.61	4.26	2.96	4.61	4.45
Quartz	10.32	0.0	8.16	22.93	0.0	5.71	10.35	8.86	14.27	6.93	1.71	15.37	4.47	13.82	6.06	0.0	0.0	0.0	9.06	4.55
Diopside _T	6.80	32.16	3.46	8.16	24.90	4.84	14.67	17.27	12.48	6.45	20.04	4.74	26.83	0.0	0.0	22.53	11.68	10.60	6.21	2.54
Wo	3.48	16.62	1.76	3.97	12.87	2.46	7.29	8.85	6.01	3.23	10.14	2.38	13.27	0.0	0.0	11.37	5.94	5.42	3.18	1.31
En	1.99	10.63	0.93	1.00	8.26	1.35	2.90	5.17	1.15	1.41	4.49	1.11	4.83	0.0	0.0	5.59	3.21	3.08	1.82	0.80
Fs	1.33	4.92	0.78	3.20	3.77	1.03	4.48	3.25	5.32	1.81	5.51	1.25	8.73	0.0	0.0	5.57	2.53	2.11	1.22	0.44
Hypersthene _T	11.03	3.70	14.29	12.18	20.15	9.60	26.25	16.64	14.11	7.63	19.96	7.28	6.94	14.02	24.30	12.10	7.65	8.15	8.59	13.17
En	6.62	2.53	7.77	2.89	13.83	5.45	10.30	10.22	1.15	3.34	8.96	3.42	2.47	2.17	5.83	6.07	4.27	4.84	5.15	8.52
Fs	4.41	1.17	6.53	9.29	6.32	4.15	15.95	6.42	5.32	4.29	11.00	3.86	4.47	11.86	18.47	6.04	3.37	3.31	3.44	4.65
Olivine _T	0.0	5.98	0.0	0.0	2.15	0.0	0.0	0.0	0.0	0.0	0.0	0.0	0.0	0.0	0.0	6.36	7.76	5.85	0.0	0.0
Fo	0.0	3.96	0.0	0.0	1.43	0.0	0.0	0.0	0.0	0.0	0.0	0.0	0.0	0.0	0.0	3.04	4.15	3.33	0.0	0.0
Fa	0.0	2.02	0.0	0.0	0.72	0.0	0.0	0.0	0.0	0.0	0.0	0.0	0.0	0.0	0.0	3.33	3.61	2.52	0.0	0.0
Corundum														1.20	0.21					

TABLE 2-II

Modal Mineralogy

	DT-024	DT-025	DT-027	DT-028	DT-030	DT-031	DT-032	DT-033	DT-034	DT-035	DT-036	DT-037
Orthopyroxene	8.3	2.3	11.4	tr	10.6	tr	3.0	9.7	—	tr	5.2	—
Clinopyroxene	12.9	15.7	3.0	14.2	20.0	tr	19.9	17.0	10.4	13.3	22.8	3.4
Garnet	—	2.8	1.1	28.6	18.4	10.9	23.7	—	17.1	24.0	20.7	0.2
Amphibole	5.8	38.7	7.1	0.2	13.0	21.1	12.1	29.1	7.1	6.6	8.3	10.0
Opaque	5.4	6.5	2.6	9.4	1.4	2.2	2.3	0.9	3.1	6.2	7.3	1.4
Plagioclase	46.4	31.8	72.3	42.8	34.8	47.6	34.8	41.6	61.9	37.8	31.1	71.3
Quartz	10.1	0.9	—	tr	—	2.7	tr	—	—	7.4	1.0	—
K-spar	10.2	—	—	—	—	—	—	—	—	—	—	12.1
Scapolite	—	—	—	—	—	7.6	—	—	—	—	—	—
Apatite	0.8	0.8	0.5	1.9	tr	1.9	1.6	0.2	0.7	1.1	2.1	0.2
Biotite	0.1	0.5	1.0	tr	0.9	2.1	1.2	1.6	tr	0.5	1.6	1.6
Sphene	—	—	—	2.9	—	2.4	—	—	—	2.6	—	—
Rutile	—	—	—	—	0.9	—	—	—	—	—	—	—
Carbonate	tr	tr	1.1	—	—	1.4	1.4	—	—	0.5	—	—

TABLE 2-II (Cont'd)

Modal Mineralogy

	DT-057	DT-98-1	DT-98-2	DT-98-3	DT-174	DT-176	DT-177	DT-178
Orthopyroxene	2.9	tr	tr	9.8	9.3	9.7	7.5	—
Clinopyroxene	25.7	tr	30.4	21.1	21.2	27.3	8.5	—
Garnet	19.9	19.8	20.2	9.3	2.3	8.6	0.5	6.5
Amphibole	2.6	—	tr	20.9	7.6	4.9	4.5	18.6
Opaque	7.4	8.1	3.1	2.2	5.2	6.0	5.1	5.2
Plagioclase	37.4	60.1	39.7	34.1	53.5		66.3	38.6
Quartz	tr	10.7	5.0	tr	tr	43.3	5.2	20.1
K-spar	—	—	—	—	—	—	—	—
Scapolite	—	—	—	—	—	—	—	—
Apatite	2.0	1.2	1.5	0.5	0.9	0.2	0.6	2.0
Biotite	0.1	tr	tr	2.0	tr	tr	1.0	8.0
Sphene	2.0	—	—	—	—	—	—	—
Rutile	—	—	—	—	—	—	—	—
Carbonate	tr	tr	tr	tr	—	—	0.8	1.0

FIG 2-II COMPOSITION OF WHITESTONE METAMORPHIC PYROXENES

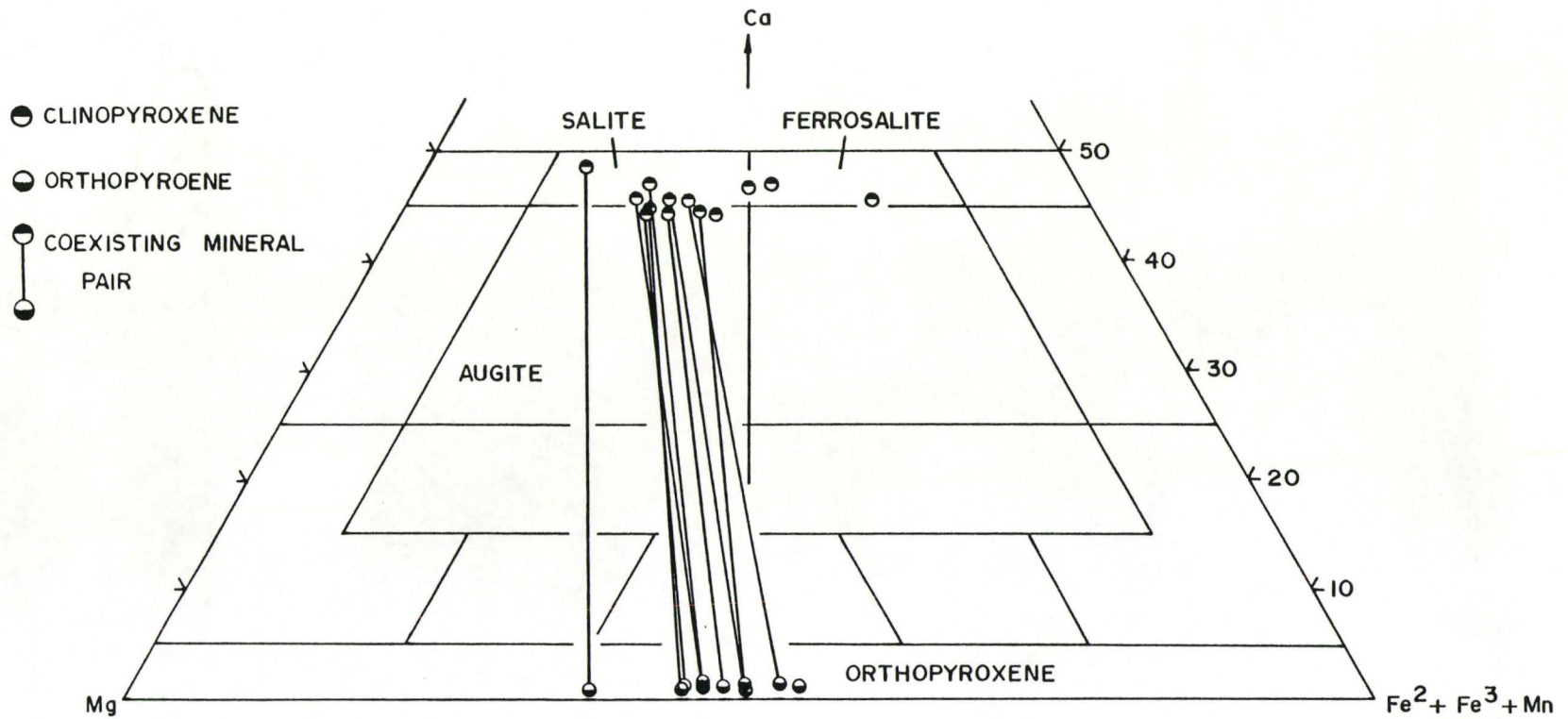


FIG 2-III Amphibole Classification , Leake 1978

Detail of Calcic Amphiboles = $(Ca + Na)_B \geq 1.34$, $Na_B < 0.67$

Section = $(Na + K)_A \geq 0.50$, $Tl < 0.50$, $Fe^{3+} > Al^{VI}$

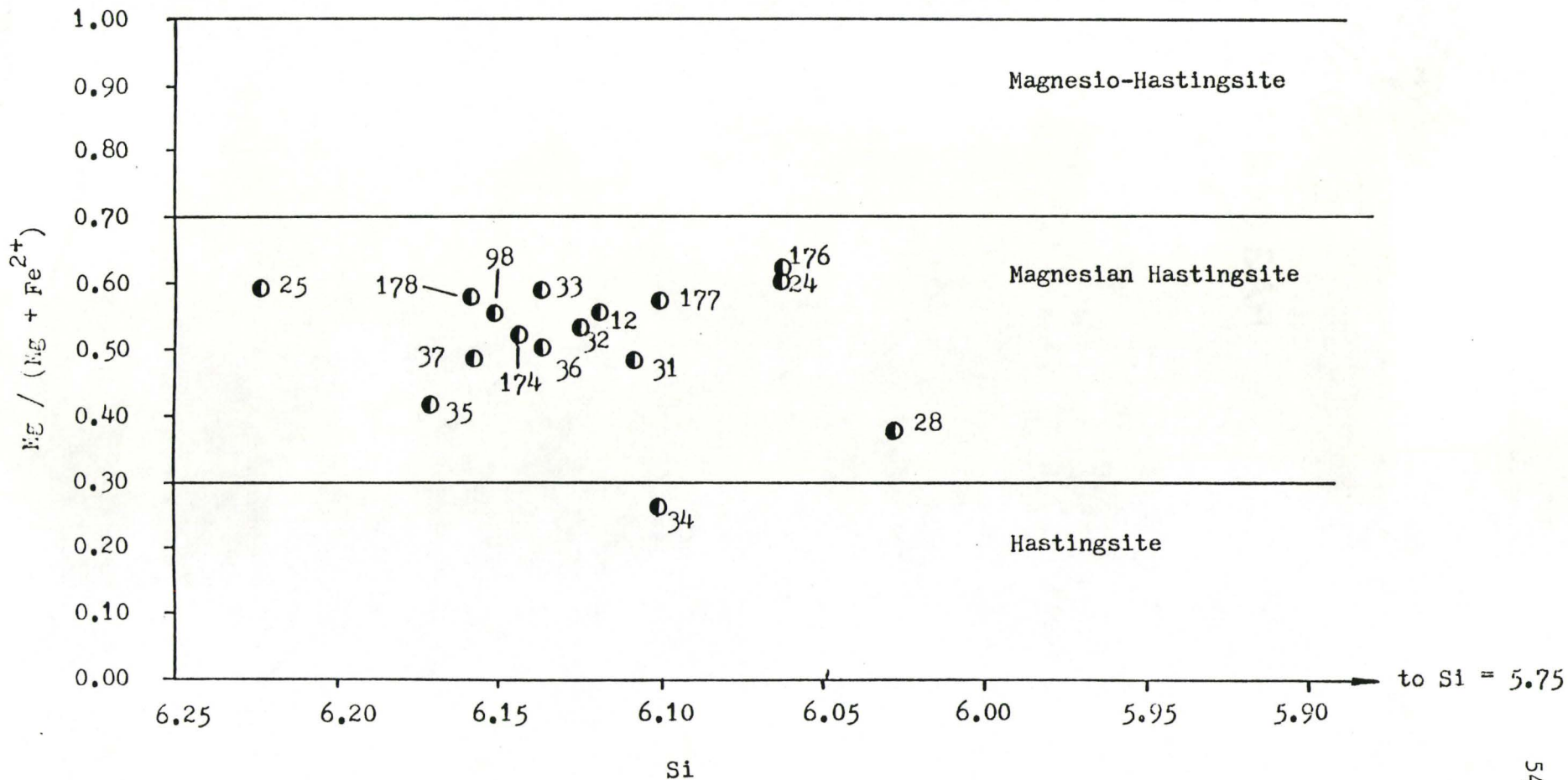
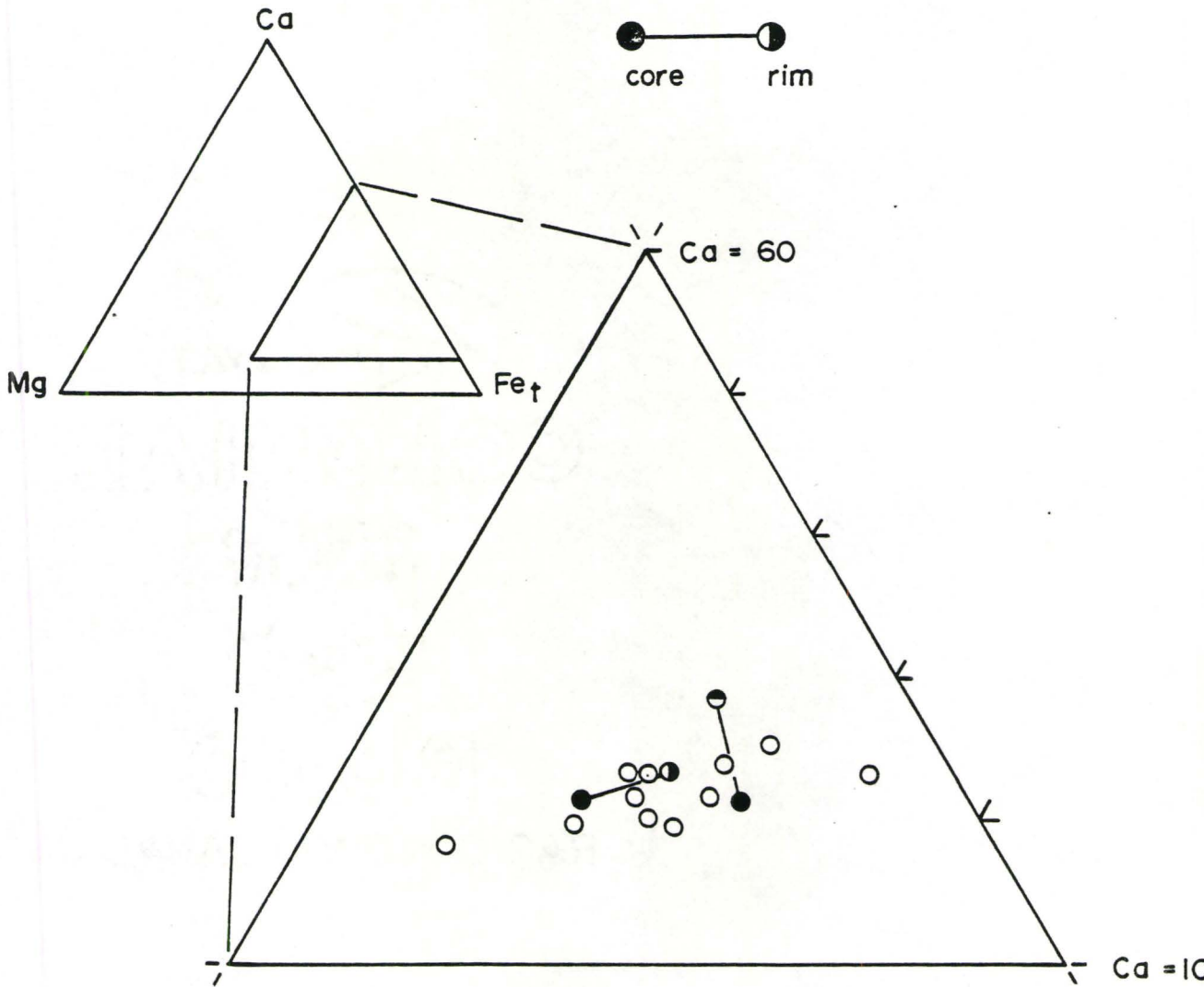


FIG 2-IV

COMPOSITION OF WHITESTONE GARNETS
 (Fe - Mg - Ca), $Fe = Fe^{2+} + Fe^{3+}$



	Major Minerals	Minor Minerals
1. Garnet Poor Mafic Gneisses	OPX, CPX, HBL, GT, PLAG	AP, OPAQ, CARB, BT, ± QT
2. Garnet Rich Mafic Gneisses	CPX, GT, PLAG, OPAQ	AP, SPH, CARB, BT, ± OPX, ± HBL, ± QT
3. Felsic Gneisses	PLAG, K-SPAR, QT, OPX, CPX, HBL	OPAQ, AP, BT, ZIRCON
4. Altered Anorthosite	PLAG, HBL, SCAP, GT, OPAQ	SPH, CARB, AP, QT, ± CPX, ± OPX

The mineralogy of the study area is both surprising simple and consistent, and mineral compositions are fairly constant with the exception of the Fe/Mg ratio, which can be shown to be directly related to the whole rock Fe/Mg ratio (see Ch. 5, Figure 5-VIII). Microprobe analyses of mafic minerals indicates the following compositions:

- Clinopyroxene - predominantly Salite-Augite, with minor Ferrosalite
- Orthopyroxene - Hypersthene
- Garnet - Pyrope₁₅, Almandine₆₀, Grossular₂₅
- Amphibole - Potassian magnesian Hastingsite (samples 24, 25, 28, 31, 32, 35, 37, 176, 177, 98, and 12)
- Titanian potassian magnesian Hastingsite (samples 33, 36)
- Potassian Hastingsite (sample 34)
- Magnesian Hastingsite (sample 179)
- Titanian Pargasite (sample 30)

- Biotite
- Mg rich biotite $Fe/Fe + Mg = 0.45$
 - $Al^{VI} = 0.38 - 0.60$
 - DT-30 is on the phlogopite-biotite join, $Fe/Fe + Mg = 0.29$

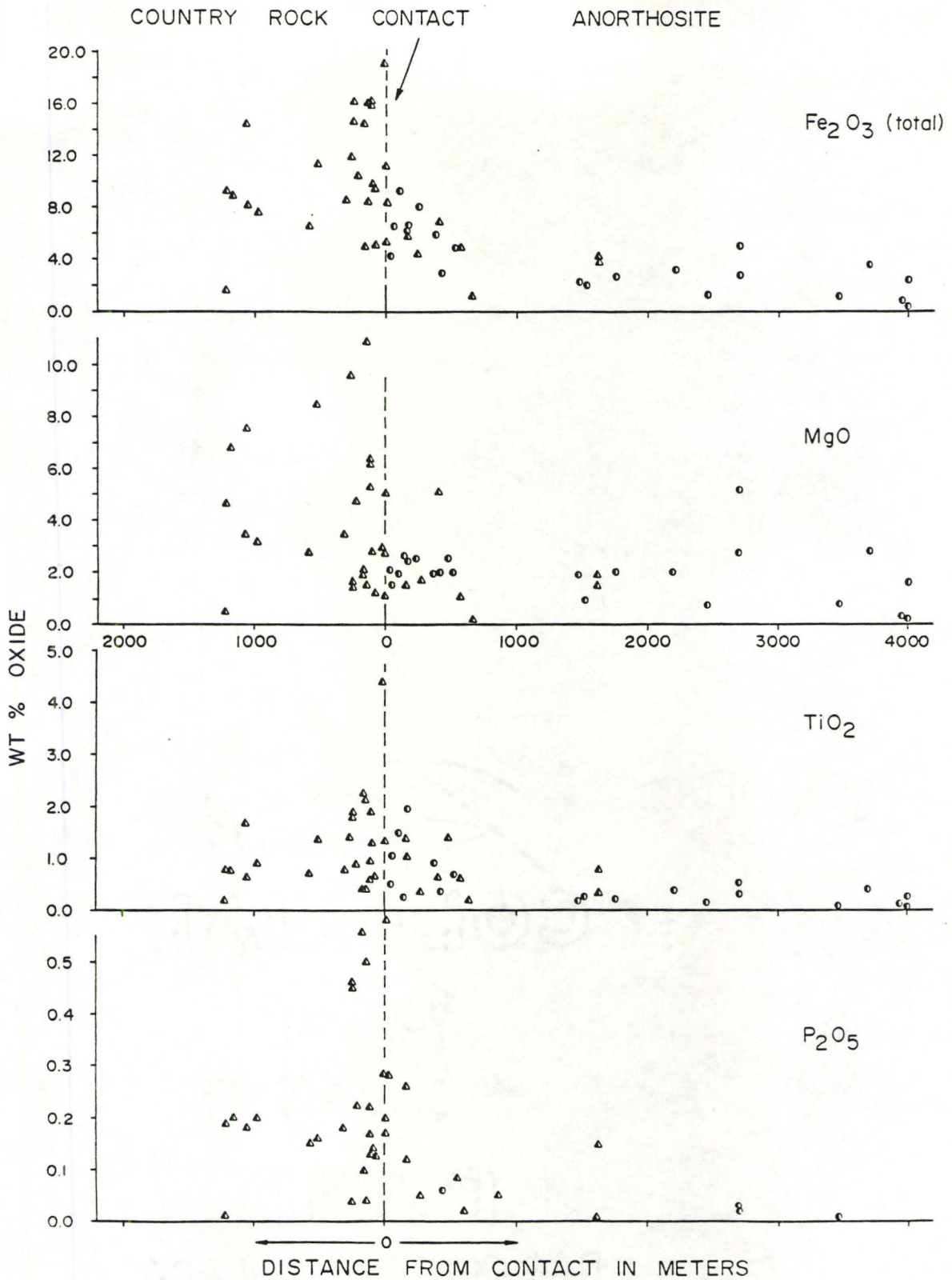
Other minerals examined include plagioclase feldspar, rutile, ilmenite, magnetite, and quartz. The purpose of these analyses was to determine the approximate composition of unknown or very small mineral grains. The results are only qualitative due to improper calibration.

2-VI Discussion

The observations made by Mason (1969) have been verified and expanded by the present field work. Figure 2-V shows the concentration of Fe, Mg, Ti, and P, as a function of distance from the anorthosite/granulite gneiss interface. The anorthosite shows an exponential increase in mafic components toward the contact, coincident with the concentric distribution of secondary alteration shown in Figure 1-I. The country rock gneisses show a more scattered pattern reflecting the variable lithology, however, the extremely high concentration of Fe, Ti, and P, present in several of the contact mafic gneisses, is greatly in excess of that found in the "normal" mafic gneisses of the study area.

These observations support the following tentative conclusions:

1. The anorthosite border phase is a contaminated zone formed by a combination of tectonic mixing and metasomatism. The widespread distribution of secondary amphibole and scapolite is thought to result from the greater mobility of volatile components.



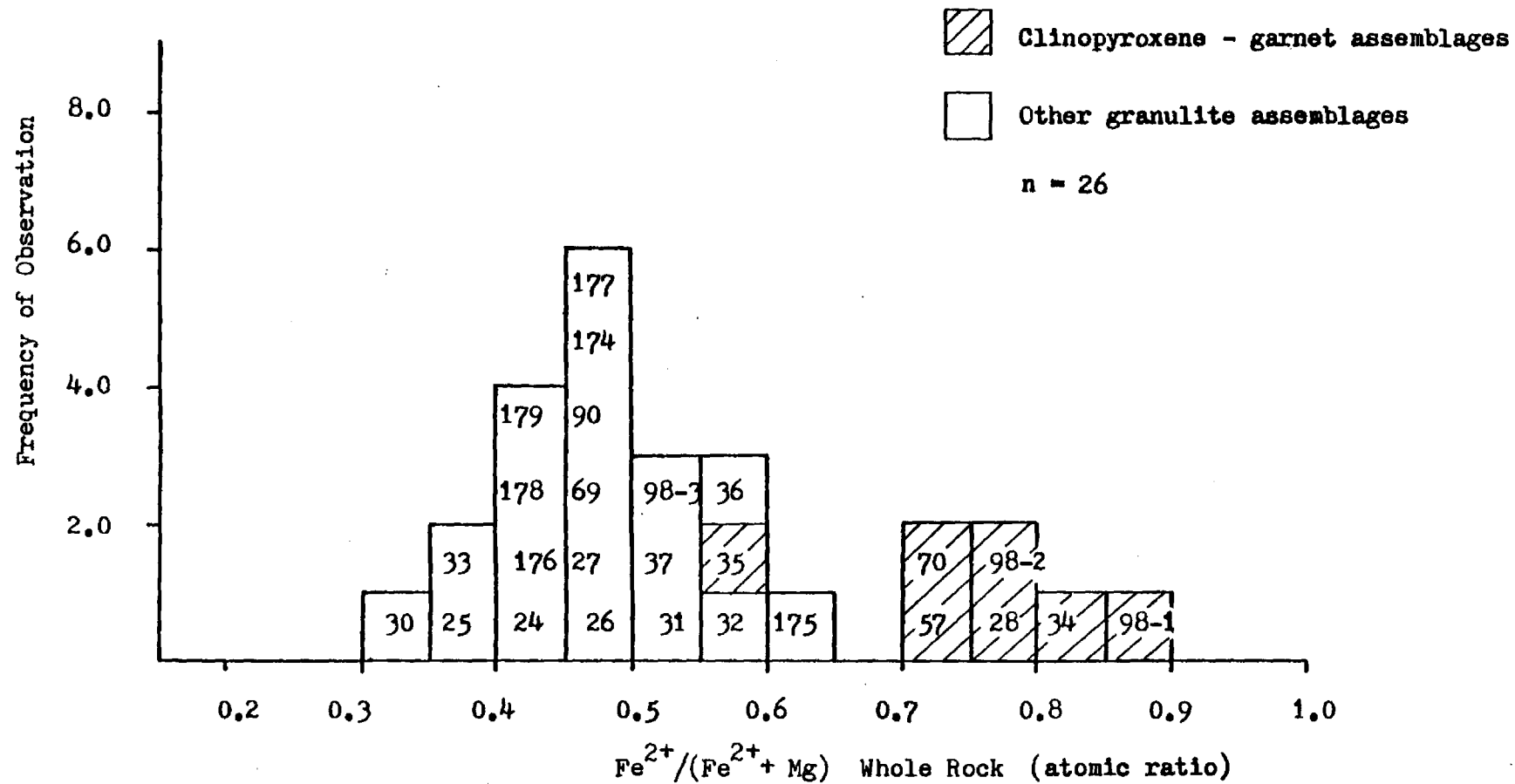
- ▲ Data from this thesis
- Data from Mason (1969)

2. The unusual chemistry and mineralogy exhibited by the mafic contact gneisses is due to metasomatic interaction with the anorthosite. They represent (at least in part) the source of the volatiles introduced into the anorthosite.

Mason (1969) noted that one of the unusual characteristics of the altered gneisses is their high Fe/Mg ratio, and speculated that the Fe enrichment stabilizes the garnet rich mineral assemblages. Figure 2-VI shows the value of $Fe^{2+}/(Fe^{2+} + Mg)$ for a variety of units within the study area. It is clear that the occurrence of the garnet-clinopyroxene assemblage is related to the Fe/Mg ratio, however, the occurrence of garnet alone is not. Sample DT-030 (see Plate 2-VIII) has the lowest Fe/Mg ratio of all the samples studied, but contains 18.4% (modal) garnet. This sample is very interesting because in the field, it exhibits all the characteristics of the altered gneisses, however, the mineralogy is quite different. Further discussion of the Fe/Mg ratio and sample DT-030 is deferred to Chapter 7.

FIG 2-VI

Fe/Mg Ratio of Granulite Facies Gneisses



CHAPTER 3
MOSSBAUER SPECTROSCOPY

3-I Introduction

Mossbauer spectroscopy (Recoil Free Nuclear Gamma Resonance) is a spectrographic method which may be used to characterize both the valence state and coordination number of Fe in minerals (Bancroft 1973).¹ It is employed in this study to measure the crystallographic site occupancy and oxidation state of Fe in the mafic minerals, pyroxene, hornblende, and garnet. This information is of interest because:

1. It was thought that there might be a measurable gradient in mineral F^* across the Whitestone Anorthosite contact aureole.²
2. Accurate determination of mineral F^* is required for geothermometry and structural formula calculations.
3. Accurate site occupancies are required for calculations of mineral component mole fractions.

The granulite gneisses in the Whitestone area are ideal for such a study, because Fe rich minerals give very good Mossbauer spectra with a minimum of sample. In addition, the well crystallized, relatively inclusion

-
1. See appendix for details of Mossbauer theory.
 2. F^* is defined as: $F^* = \text{Fe}^{2+} / (\text{Fe}^{2+} + \text{Fe}^{3+})$, atomic ratio.

free, homogeneous nature of the mineral phases facilitates mechanical separation.

Mossbauer spectra were recorded with an Elscint (electromechanical) Drive system (Model MDF-N-5, Mossbauer Function Gen.) in conjunction with an Elscint Promeda multichannel analyser operating in the auto-folding mode. The velocity waveform was a constant acceleration, symmetric sawtooth with source velocity varying between $\pm 4.5 \text{ mm sec}^{-1}$ for most experiments. The velocity scale was calibrated using the four inner lines of Fe foil. The source was ^{57}Co in a palladium matrix. Source-sample-counter geometry were arranged to minimize the cosine effect, while at the same time obtaining an optimum count rate. Counts in excess of 1×10^6 per channel were collected for each spectrum.

3-II Precision of Least Squares Fitting Procedure

Under ideal experimental conditions Mossbauer absorption peaks are Lorentzian. The line shape, $Y(X)$, of the envelope for a Lorentzian line is given by:

$$Y(X) = b - \frac{Y(0)}{1 + \left[\frac{X - X(0)}{\Gamma/2} \right]^2}$$

where $Y(0)$ = the intensity at the resonance energy, $X(0)$.

Γ = the full-width at half maximum, generally referred to as the half-width.

b = the baseline intensity.

For most minerals, the observed spectra consists of a number of superimposed Lorentzian lines. Deconvolution of the observed spectra into its component peaks is accomplished using least squares refinement techniques.¹ This is a non-trivial process requiring a certain degree of judgement on the part of the programmer. Problems associated with the fitting procedure are discussed by Bancroft (1973) and Hawthorne (1981).

The general fitting procedure used in this thesis is as follows:

1. The number of peaks in the spectra to be fit is estimated by a combination of visual inspection of the raw data, and a knowledge of the mineral crystal chemistry.
2. Starting parameters are then calculated from the raw data and the area and width of component peaks is constrained to be equal. For complex spectra (with a number of overlapping peaks), the Q.S. and I.S. may also be constrained to have a specific value.
3. In succeeding runs, the Q.S. and I.S. constraints, and some of the area constraints are removed, with the provision that the fit remains "acceptable" from a crystal-chemical point of view. For complex spectra, it is commonly necessary to retain the area and width constraints in the final refinement.

1. Spectra were fit using the program of Stone (1969) on a CDC 6400 computer.

The least squares method is chosen over other fitting techniques because the peaks are fit to a known function. This is absolutely necessary in spectra where the observed absorption envelope consists of a number of overlapping peaks. A second advantage, is the ability to obtain a statistical measure of the "goodness of fit". Unfortunately, for complex spectra, the equations for close spaced lines may be so similar that the iterative process tends to oscillate about a local minimum, and convergence to a unique answer is not possible. The error estimates given by the fitting program must therefore be considered minimum errors. A further problem is that Mossbauer absorption peaks are not truly Lorentzian, but have a Gaussian component. This is particularly noticeable in spectra with a number of lines, in which there appears to be "too much area" under the tail of the calculated envelope. Programs which fit spectra to a combination of peak functions have been used by some workers, but were not available for use in this study.

Law (1973) discusses the theoretical basis for use of the statistical parameter, X^2 (chi squared), as a criteria of "best fit" and points out some of the experimental conditions which lead to an increase in its value. He concludes that for a fit with R_o below the 1% point (R_o = the observed residual, see Law, 1973, p. 128), crystal chemical considerations should be used to distinguish between various possible "fits" instead of the X^2 test. The precision of uniqueness of Mossbauer parameters, determined using the least squares technique, has been discussed by Dollase (1975) and Hawthorne (1973). The semi-empirical error treatment described by Dollase, represents the only quantitative

method available for the calculation of M.S. parameter precision, and is employed in this thesis.¹ Calculated errors (precision) are given in Table 3-I. In general, it is very difficult to give an accurate estimate of the true error. The precision of Mossbauer areas given in Table 3-I must be considered minimum errors, however it is possible that the true precision is considerably better than shown. No attempt has been made to determine the accuracy of Mossbauer parameters. The accuracy and precision of mineral F* determined by Mossbauer is discussed in Chapter 4.

3-III Mineral Spectra: Peak Assignments and Results

(i) Pyroxenes

The crystal structure and chemistry of pyroxenes has been reviewed by Deer et al. (1978), and Cameron and Papike (1980). The general formula for pyroxenes can be expressed as:



where A = M(2): Mg, Fe²⁺, Mn, Li, Ca, Na.

B = M(1): Al, Fe²⁺, Fe³⁺, Cr, Ti⁴⁺, Mn.

T = Si, Al (also Fe³⁺ under certain conditions).

The M(1) site is coordinated to six oxygen in a very regular octahedron.

1. The error treatment of Dollase (1975) is described in appendix A-II. The precision of the area, width, and position of all peaks is given for each mineral in table A-I.

TABLE 3-I

Precision of Mossbauer Areas from Least Squares Fit

Mineral	Peak	$\bar{\Sigma}$ (least squares) ¹	$\bar{\Sigma}$ (Dollase) ²	$\bar{\Sigma} F^*$ ³
Clinopyroxene	AA'	2.94	13.55	2.34
	BB'	1.48	4.58	
	CC'	2.35	4.48	
Orthopyroxene	AA'	2.53	6.06	1.60
	BB'	0.86	1.26	
	CC'	7.59	12.74	
Hornblende	AA'	2.45	4.68	2.54
	BB'	2.45	5.11	
	CC'	4.58	15.38	
	DD'	1.31	1.95	
Garnet	AA'	0.40	0.41	0.95
	BB'	4.21	8.89	

1. The % error given by the fitting program (Stone 1969) which represents the standard error of the least squares method.
2. The % error calculated using the method of Dollase (1975) using the program RPQ written by the author. This value represents the minimum standard error of the technique in general, taking into consideration peak overlap.
3. The minimum error in F* based on a weighted average according to the % area contributed by each peak to the total area.

The larger M(2) site is very distorted and has a variable coordination: six for hypersthene, eight for diopside. X-ray structure studies indicate that Fe^{2+} prefers M(2) over M(1) (Bancroft 1973), therefore, assuming Fe^{2+} is present in both sites, the M(2) peak should be more intense. In addition, because the M(2) site is more distorted than M(1), it can be expected to have a smaller Q.S.

The six peak computer fits shown in Figure 3-I (clinopyroxene) and Figure 3-II (orthopyroxene) correspond to the following peak assignments:

AA' Fe^{2+} in M(1)
 BB' Fe^{2+} in M(2)
 CC' Fe^{3+} in M(1) and M(2)

The partitioning (or average site preference) of Fe^{2+} may now be calculated by normalizing the area ratios of the M(1) and M(2) sites to 1.0. This gives:

		Clinopyroxene				
Peak	Partitioning		σ_1	σ_2	Precision σ_3	σ_3 in %
AA'	Fe^{2+} in M(1)	0.228	0.030	0.007	0.031	13.6
BB'	Fe^{2+} in M(2)	0.772	0.037	0.011	0.035	4.6

FIG 3-I
MOSSBAUER SPECTRA OF CLINOPYROXENE

Plot shows 6 peak (3 doublet) computer fit. Bars above spectra indicate the approximate position of each peak and the Quadrupole Splitting for each doublet.

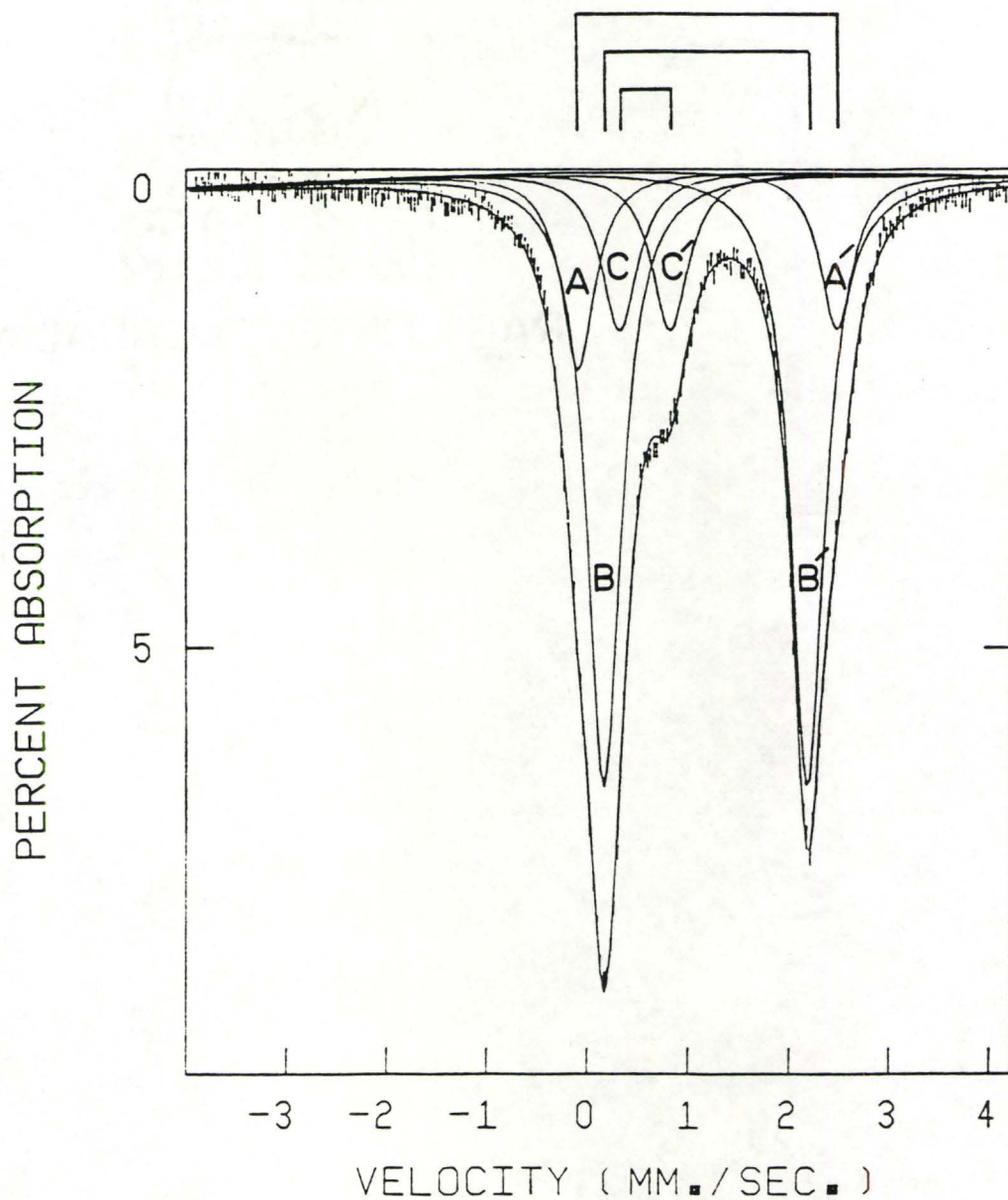


TABLE 3-II

Relative Peak Areas for Clinopyroxenes

Sample	Code	Fe ²⁺		Fe ³⁺	Fe ²⁺	Fe ³⁺
		% Area AA'	% Area BB'	% Area CC'		
DT-24	BOH	.161	.640	.199	.801	.199
		.154	.645	.201	.799	.201
DT-24	ECQ	.162	.628	.211	.790	.211
		.161	.630	.209	.791	.209
DT-24	DUD	.163	.625	.212	.788	.212
		.131	.658	.211	.789	.211
DT-25	BPZ	.193	.593	.214	.786	.214
		.174	.607	.219	.781	.219
DT-28	ANI	.164	.622	.214	.786	.214
		.134	.644	.222	.778	.222
DT-30	CUG	.169	.662	.169	.832	.169
		.130	.693	.176	.824	.176
DT-33	BQO	.181	.649	.170	.830	.170
		.174	.654	.172	.829	.172
DT-35	CDA	.255	.545	.200	.800	.200
		.257	.543	.199	.801	.199
DT-36	BQF	.190	.624	.186	.815	.186
		.182	.631	.187	.813	.187
DT-174	CUN	.184	.634	.182	.818	.182
		.167	.648	.185	.815	.185
DT-174	BHQ	.181	.645	.174	.826	.174
		.162	.660	.178	.822	.178
DT-176	CFC	.177	.591	.232	.768	.232
		.148	.612	.240	.760	.240
DT-177	BPG	.184	.623	.194	.807	.194
		.144	.653	.203	.797	.203
DT-003	BPB	.196	.606	.197	.803	.197
		.172	.625	.203	.797	.203
All Peaks	\bar{X}	.183	.621	.197	.804	.197
	S	.024	.030	.019	.019	.019
High Vel.	\bar{X} only	.164	.636	.200	.800	.200
	S	.032	.034	.019	.020	.019

FIG 3-II

MOSSBAUER SPECTRA OF ORTHOPYROXENE

Plot shows 6 peak (3 doublet) computer fit. Bars above spectra indicate the approximate position of each peak and the Quadrupole Splitting for each doublet.

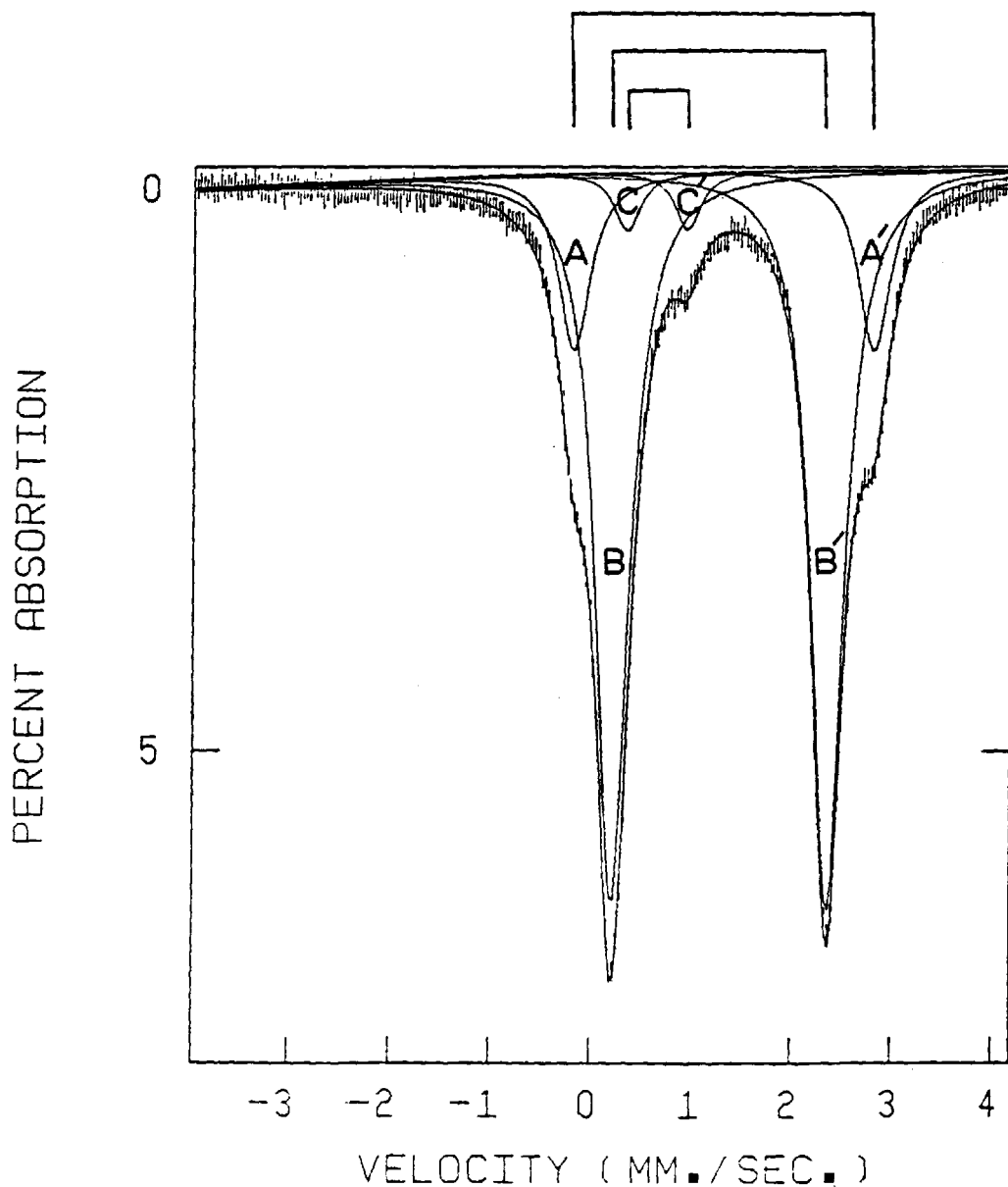


TABLE 3-III

Relative Peak Areas for Orthopyroxenes

Sample	Code	Fe ²⁺		Fe ³⁺		Constraints used in fitting	
		% Area AA'	% Area BB'	% Area CC'	Fe ²⁺		Fe ³⁺
DT-24	CBG	.162	.796	.042	.958	.042	1,2,3(C),6(C)
DT-25	DWO	.205	.732	.063	.937	.063	1(A,C),3(C),5(C)
DT-30	BPF	.096	.875	.029	.971	.029	1,2,3(C)
DT-32	DIK	.177	.799	.024	.976	.024	1,2,3(C),6(A,C)
DT-32	BOH	N/F	.972	.028	.972	.028	1,2(C),5(C),7(C)
DT-33	BBT	.163	.831	.006	.994	.006	1(C),3(C),5(C)
DT-37	AXF	.188	.767	.045	.955	.045	1,2,3(C),5(C)
DT-37	BAZ	.188	.766	.046	.954	.046	1,2,3(C),5(C)
DT-174	DZP	.186	.764	.050	.950	.050	1,2,3(C)
DT-176	BZP	.122	.833	.045	.955	.045	1,2,3(C)
DT-177	BGZ	.126	.823	.051	.949	.051	1,3(C)
DT-177	BGW	.138	.809	.052	.948	.052	1,2,3(C)
DT-177	DZW	.271	.662	.066	.934	.066	1,2,3(C),6(C)
DT-177	ECT	.240	.699	.061	.939	.061	1,2,3(A,C),6(C)
All Data	\bar{X}	.174	.781	.043	.957	.043	
	S	.048	.059	.017	.017	.017	
Low Temp	\bar{X} Data	.159	.800	.040	.960	.040	
	S	.036	.043	.016	.016	.016	

Orthopyroxene

Peak	Partitioning		Precision			
			σ_1	σ_2	σ_3	σ_3 in %
AA'	Fe ²⁺ in M(1)	0.166	0.038	0.004	0.010	6.1
BB'	Fe ²⁺ in M(2)	0.834	0.045	0.007	0.011	1.3

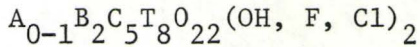
σ_1 = 1 sigma of measured distribution.

σ_2 = 1 sigma, error given by least squares fitting program.

σ_3 = 1 sigma, error calculated using the method of Dollase (1975).

(ii) Amphibole

The crystal structure and chemistry of amphiboles has been reviewed by Hawthorne (1981). A generalized amphibole formula may be written:



where: A = A site; Na, K

B = M(4); Na, Li, Ca, Mn, Fe²⁺, Mg

C = M(1), M(2), and M(3); Mg, Fe²⁺, Mn, Al, Fe³⁺, Ti

T = T(1), T(2); Si, Al

In monoclinic amphiboles (C2/m), the M(1), M(2), and M(3) sites have pseudo-octahedral symmetry. Both the M(1) and M(2) sites are coordinated by four oxygens and two O(3) anions (OH⁻, F⁻, Cl⁻, or O²⁻). The M(2) site is coordinated by six oxygens and is somewhat distorted from octahedral symmetry (Bancroft 1973). All three sites differ significantly

in next-nearest neighbour configuration and are therefore, subject to differing cation occupancy. The M(4) site is larger than M(1), M(2), or M(3); the anions are arranged in a distorted square antiprism and the coordination number (6 or 8) may vary with cation occupancy (Hawthorne 1981).

The eight peak computer fit shown in Figure 3-III, corresponds to the following peak assignments:

AA' Fe²⁺ in M(1)
 BB' Fe²⁺ in M(3)
 CC' Fe²⁺ in M(2)
 DD' Fe³⁺ in M(1), M(2), and M(3).

The assignment of individual absorption peaks to specific crystallographic sites is not without some controversy, however, certain basic constraints do exist which support the fitting procedure used above.

The four major cation sites are present in the ratio:

$$M(1): M(2): M(3): M(4) = 2:2:1:2$$

The M(1) and M(3) sites are crystallographically similar, therefore, the Q.S. and C.S. should be similar, and because there are twice as many M(1) sites as M(3) sites, the M(1) peak should be more intense (all other things being equal). The M(2) site, is distorted from octahedral symmetry and should therefore, have a smaller Q.S. than M(1) or M(3). In addition, because Fe³⁺ is known to strongly order at the M(2) site (Hawthorne 1981), the intensity of the Fe²⁺M(2) peak will be reduced.

In this way, doublets AA', BB', and CC' are assigned to Fe²⁺ in M(1), M(3), and M(2), respectively. Doublet DD' is assigned to Fe³⁺; predominantly in M(2), with minor amounts in M(1) and M(3). It is commonly accepted that the typically greater peak half-width (for Fe³⁺ peaks) is due to a number of unresolved, superimposed doublets, however, Hawthorne (1981) suggests that the larger half-width could be an artifact of the fitting procedure.

Previous Mossbauer studies of the calcic amphiboles by Bancroft et al. (1967), Haggstrom et al. (1969), Burns and Greaves (1971), and Bancroft and Brown (1975), have assumed that Ca, Na and K completely fill the M(4) site, hence peak assignments have been made only for Fe²⁺ in the M(1), M(2) and M(3) sites, as has been done in this thesis. However, according to Goldman and Rossman (1977), electronic absorption spectra indicate that Fe²⁺ is likely to be present in the M(4) site in all calcic amphiboles; in many cases in amounts too small to be resolved in complex spectra. While this supposition remains somewhat controversial (see Goldman 1982, and Aldridge et al. 1982), it is clear that it may not be possible to distinguish between Fe²⁺ in M(2) and M(4) when both are present; consequently, the assignment of doublet CC' to Fe²⁺ in M(2) may be subject to some error. The amount of Fe²⁺ present in M(4) is expected to be approximately 5% or less of the total Fe for the amphiboles under study (magnesian hastings site).

The partitioning (or average site preference) of Fe²⁺ may now be calculated by dividing the areas of M(1) and M(2) by two, and normalizing the area ratios to 1.0. This gives:

Plot shows 10 peak (5 doublet) computer fit. Bars above spectra indicate the approximate position of each peak and the Quadrupole Splitting for each doublet. The central doublet marked ILM is an impurity which has been "fit out" of the spectra, and is not included in calculation of M.S. parameters or areas.

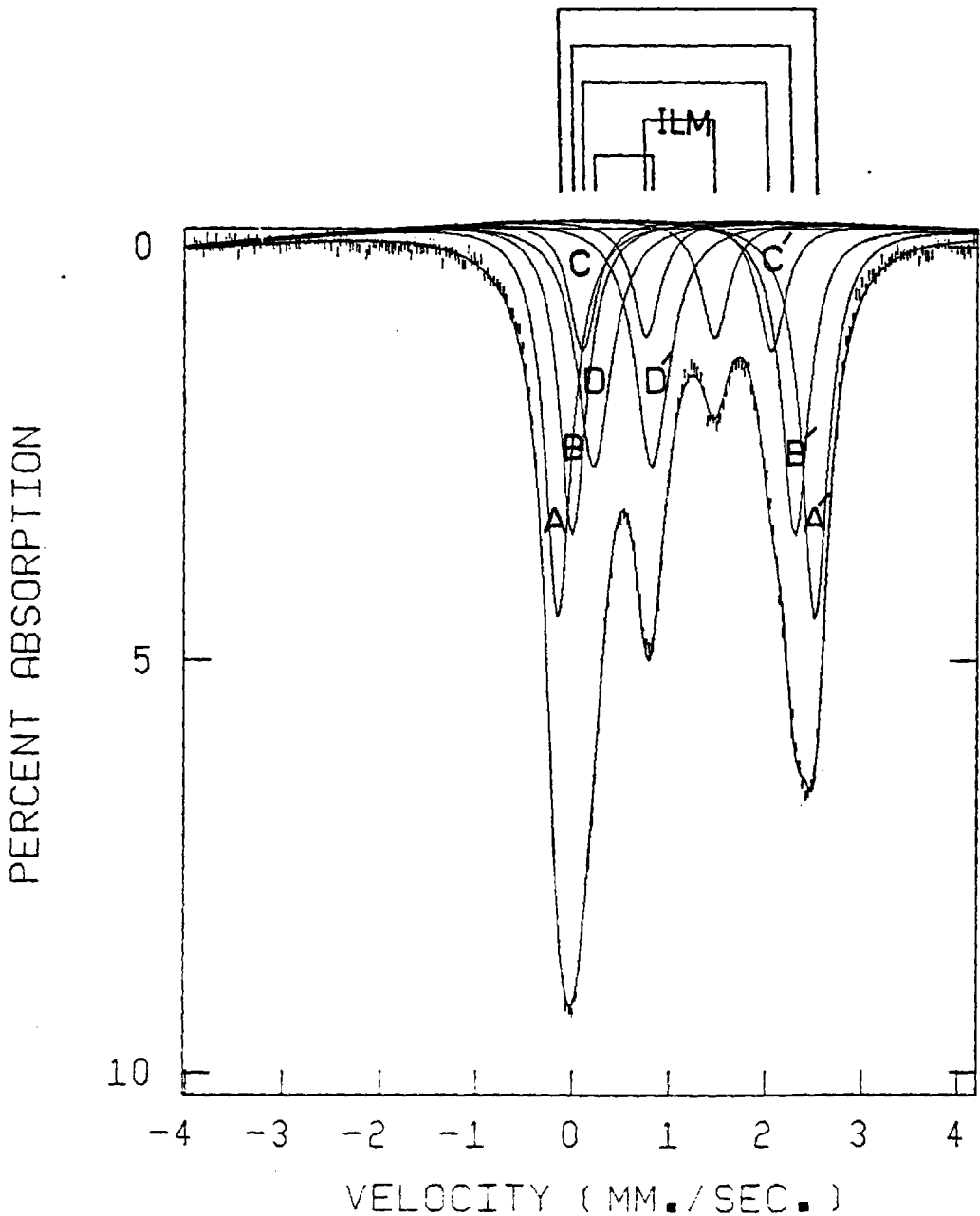


TABLE 3-IV RELATIVE PEAK AREAS FOR AMPHIBOLES

SAMPLE	CODE	Fe ²⁺			Fe ³⁺		Constraints used in fitting	
		% AREA AA'	% AREA BB'	% AREA CC'	% AREA DD'	Fe ²⁺		Fe ³⁺
DT-12	DWC	.345	.240	.100	.314	.686	.314	1,2,3
DT-25	DVD	.342	.272	.113	.273	.727	.273	1,2,3
DT-30	DRT	.355	.261	.106	.278	.722	.278	1,2,3
DT-31	DDH	.358	.249	.103	.290	.710	.290	1,2,3,6(C,D)
DT-32	BHI	.381	.250	.092	.277	.723	.277	1,2,3
DT-33	BHF	.338	.264	.128	.270	.730	.270	1,2,3
DT-35	BVX	.338	.261	.123	.279	.721	.279	1,2,3
DT-36	BGM	.183	.378	.169	.270	.730	.270	1,3,6(B,C,D)
DT-37	DHL	.367	.277	.108	.248	.752	.248	1,2,3
DT-176	DXL	.361	.268	.081	.290	.710	.290	1,2,3
DT-004	DQT	.340	.250	.128	.283	.717	.283	1,2,3
	\bar{x}	.353	.259	.108	.280	.720	.280	
	S	.014	.012	.015	.017	.017	.017	

Peak	Partitioning			Precision			σ3 in %
				σ1	σ2	σ3	
AA'	Fe ²⁺	M(1)	0.361	0.014	0.009	0.017	4.7
CC'	Fe ²⁺	M(2)	0.110	0.015	0.005	0.017	15.5
BB'	Fe ²⁺	M(3)	0.529	0.025	0.013	0.027	5.1

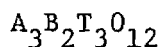
σ1 = 1 sigma of measured distribution.

σ2 = 1 sigma, error given by least squares fitting program.

σ3 = 1 sigma, error calculated using the method of Dollase (1975).

(iii) Garnet

The crystal structure and chemistry of garnets has been reviewed by Meagher (1980). The general formula for the collective garnet group is:



where: A = Ca, Mn, Fe²⁺, Mg, (minor Na)

B = Al, Cr, Fe³⁺, (minor Ti^{3+,4+}, V³⁺, Fe²⁺)

T = Si, (minor Al, Ti, Fe³⁺, Fe²⁺)

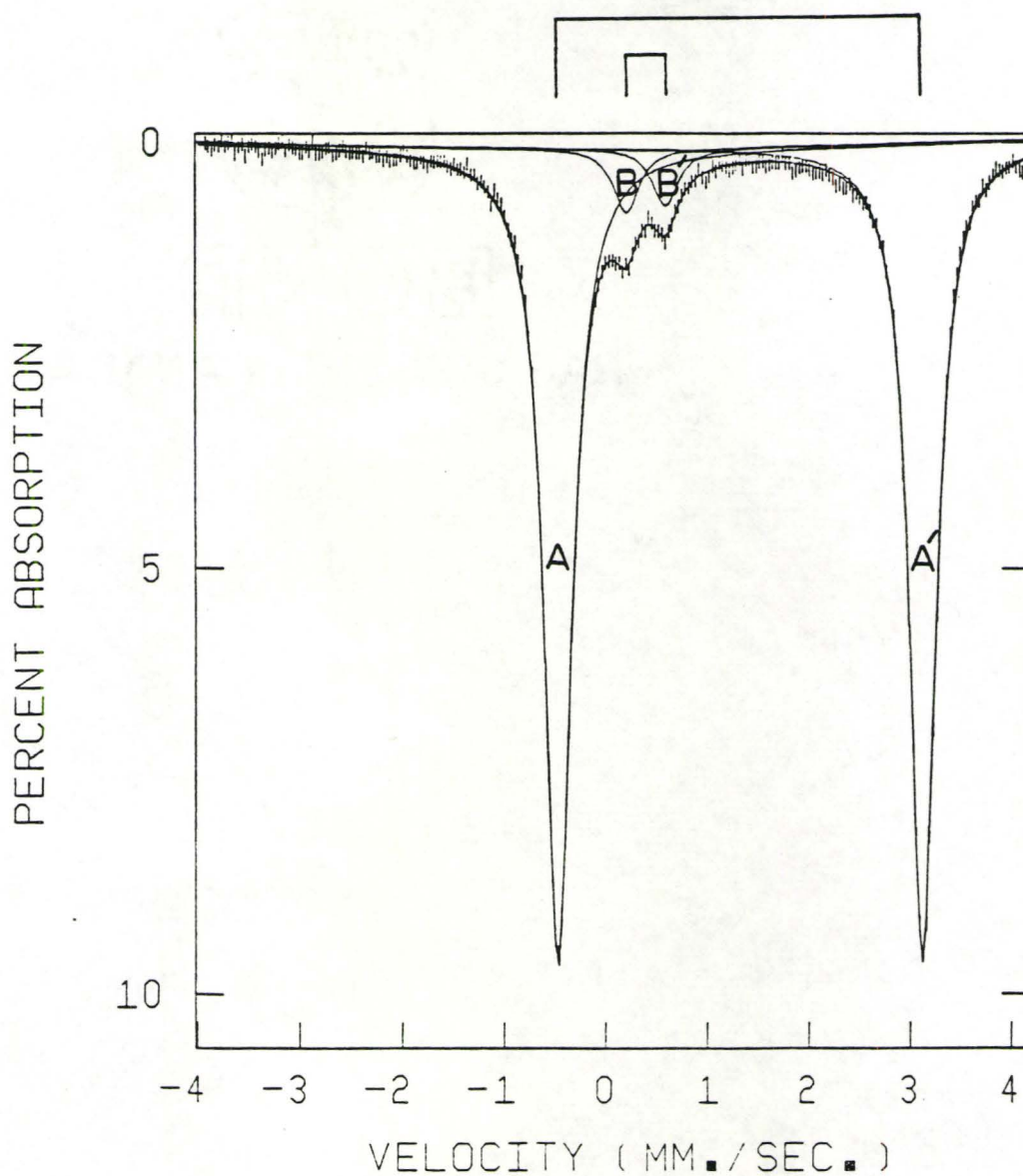
The garnet structure consists of independent SiO₄ tetrahedra linked by trivalent ions in octahedral coordination (the B site) and divalent ions in eightfold coordination (the A site).

The four peak computer fit shown in Figure 3-IV corresponds to the following peak assignments:

FIG 3-IV

MOSSBAUER SPECTRA OF GARNET

Plot shows 4 peak (2 doublet) computer fit. Bars above spectra indicate the approximate position of each peak and the Quaarupole Splitting for each doublet.



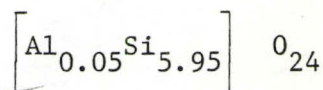
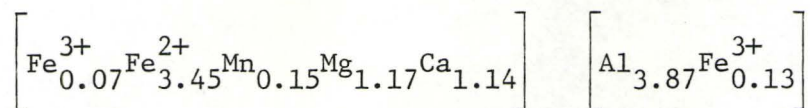
AA' Fe²⁺ in the A site

BB' Fe³⁺ in the B site

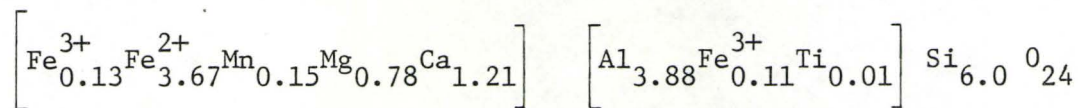
The very large Q.S. exhibited by Fe²⁺ results from the increased q_{val} contribution to the field gradient, due to the almost regular nature of the A site (Bancroft et al. 1967, Bancroft 1973). Attempts to fit the most intense peaks (AA') to two doublets results in unacceptably narrow line widths (see spectra GT DT-32 BEM, Appendix A).

One further observation is worthy of mention. Two representative garnet analysis are given below:

DT-32



DT-35 (core)



In both examples, excess Fe³⁺ is present which cannot be accounted for in the T site. This suggests that a minor amount of Fe³⁺ is present in the A site.

TABLE 3-V

Mossbauer Parameters (mm sec^{-1}) and Relative Peak Areas for Garnets

Sample	Code	X^2	Peaks AA'			Peaks BB'			Constraints used in fitting	Fe ²⁺	Fe ³⁺
			C.S.	Q.S.	H.W.	C.S.	Q.S.	H.W.		% Area AA'	% Area BB'
DT-25	CJF	238	1.29	3.52	.31	.35	.38	.27	0	.941	.059
DT-28	BAH	346	1.29	3.53	.32	.37	.40	.31	1(B)	.924	.076
DT-30	AGV	503	1.27	3.55	.33	.41	.47	.48	1(B)	.943	.057
DT-31	BAK	533	1.29	3.54	.33	.37	.37	.31	1(B)	.941	.059
DT-32	BJH	490	1.29	3.55	.34	.37	.36	.33	1(B)	.946	.054
DT-34	CZH	202	1.29	3.59	.32	.36	.39	.31	1(B)	.930	.070
DT-35	BEN	437	1.29	3.54	.34	.37	.39	.31	1(B)	.939	.061
DT-36	CJH	238	1.30	3.52	.34	.36	.45	.38	0	.919	.081
DT-176	BMV	522	1.28	3.55	.33	.38	.40	.40	1(B)	.941	.059
DT-176	BMU	562	1.28	3.55	.32	.37	.40	.40	1(B),3(B)	.942	.058
DT-178	BGJ	513	1.28	3.55	.36	.37	.38	.36	1(B)	.928	.072
DT-002	BFK	274	1.28	3.55	.35	.37	.39	.35	1(B)	.930	.070
DT-002	BGL	427	1.28	3.55	.35	.38	.39	.35	1(B)	.929	.071
		\bar{X}	1.29	3.55	.33	.37	.40	.35		.935	.065
		S	.01	.02	.01	.01	.03	.05		.008	.008

3-IV Quantitative Estimation of Site Occupancy

(i) Introduction

In this section, the theoretical basis (and the assumptions required) for the use of Mossbauer area ratios to estimate site populations will be briefly described. Also, several selected experimental studies will be examined which document important limitations of the technique.

For spectra containing r quadrupole doublets, the area of the j th doublet is related to the number of atoms giving rise to the absorption by (Bancroft 1967):

$$A_j / \sum_{i=1}^r A_i = n_j / \sum_{i=1}^r c_i n_i$$

where:
$$c_i = \frac{f_i \Gamma_i G_i}{f_j \Gamma_j G_j}$$

f_i = the recoil free fraction of absorber atom i

Γ_i = the half-width of peak i

$G_i(n_i, f_i, \sigma_o)$ = the saturation correction

n_i = the number of atoms (i) per formula unit

σ_o = the maximum resonance absorption cross-section

In most studies (as in this thesis), c_i is assumed to be unity, thus the site populations are given by the simple relation:

$$\text{Area (doublet } i) \propto \text{Number of atoms (site } i)$$

The validity of this assumption is discussed by Bancroft (1967, 1969, 1973) and Hawthorne (1981). Several studies have derived values of c different from unity (Bancroft 1967, 1975, and Sawatzky 1969; for f_A/f_B in garnet), but such measurements are difficult and subject to large errors. In general, the value of c and in particular, the ratio of recoil free fractions (f_A/f_B) for each site, remain unknown for most silicate minerals.

Given that the assumptions discussed above are approximately valid, or at least that the value of c may eventually be determined, there remain a number of problems which may limit the application of Mossbauer spectroscopy in determining site occupancy. These are:

1. Chemical and structural inhomogeneities.
2. Next-nearest-neighbour (NNN) and intervalence charge transfer interaction (IVCT) effects.
3. Temperature dependence of site populations.

A brief discussion of these phenomenon is given below. Pyroxenes have been used as examples in most cases because it is for this group of minerals that the effects are best understood.

(ii) Chemical and Structural Inhomogeneities

Mineral separates are commonly contaminated with inclusions or alteration products. For example, retrograde clinopyroxene-amphibole and orthopyroxene-biotite intergrowths are common in granulite facies

gneisses. The small quantities of secondary minerals present are difficult to detect and almost impossible to remove.

Of far more importance, is the vast array of subsolidous phenomenon exhibited by pyroxenes. During heating or cooling, pyroxenes undergo structural and chemical changes, however, kinetic factors often inhibit equilibrium. As a consequence, many pyroxene crystals consist of intimately intergrown regions of pre- and post-reaction material, of transitional and/or intermediate types of material, or of ordered or disordered combinations of the above (Buseck, Nord and Veblen, 1980).

Because pyroxene, amphibole and biotite have similar Mossbauer parameters, the spectra of mixed samples consists of a number of superimposed, unresolved doublets having slightly different Q.S. and I.S. This results in apparent line broadening and non-lorenzian line shapes. Site populations derived from such spectra are subject to large errors.

(iii) Next-Nearest-Neighbour and Intervalence Charge Transfer Interaction Effects

Next-nearest-neighbour (NNN) effects refer to the variation in electronic environment experienced by an ion (in a specific site), surrounded by differing ligand configurations (Bancroft 1979). For example, in their study of the pyroxene series, hedenbergite-ferrosilite,¹ Dowty and Lindsley (1973) concluded that four basically different NNN configurations may be distinguished for the M(1) site, according to whether the

1. Synthetic minerals were used in the study.

three adjacent sites are occupied by:

1. three Fe atoms
2. two Fe atoms and one Ca atom
3. one Fe atom and two Ca atoms
4. three Ca atoms.

They fit their spectra to four doublets¹ and, by assuming a random distribution of cations over the M(2) site, were able to achieve good agreement between calculated and observed areas.

In natural pyroxenes, which are chemically complex and partially ordered, it is difficult to predict the NNN configurations, consequently most are fit to one doublet due to Fe^{2+} in M(1). According to Dowty and Lindsley, this procedure will overestimate the area of the M(2) doublet, because it is partially overlapping with one or more of the M(1) doublets. They conclude that "it is questionable whether very accurate site distributions for high-calcium clinopyroxenes can be obtained from Mossbauer spectra" (Dowty and Lindsley 1973, p.).

Intervalence charge transfer interaction (IVCT) arises from the exchange of electrons from Fe^{2+} to adjacent Fe^{3+} , stimulated by the incident radiation (Rossman, 1980). This results in an extra broad

1. Three doublets were fit to Fe^{2+} in the M(1) site (the fourth M(1) configuration accounts for less than 10% of the area so it was not considered resolvable) and one to Fe^{2+} in M(2). Fe^{3+} was not present. The relative areas of the doublets were predetermined by calculation and constrained during the fitting procedure. A combination of Lorentzian and Gaussian functions were used to approximate the line shapes.

absorption pattern of intermediate Q.S. in addition to the Fe^{2+} and Fe^{3+} doublets (Bancroft 1979). In some cases, this doublet is resolvable (for example, in the Ti rich garnet-schorlite, see Burns, 1972), but often it is not, and simply results in a subtle smearing of the spectra, indistinguishable from NNN effects.

(iv) Temperature Dependence of Site Populations (Order-Disorder Phenomenon)

The temperature dependence of the Fe^{2+} -Mg distribution over the octahedrally coordinated sites M(1) and M(2) in orthopyroxene has been studied by Virgo and Hafner (1968, 1969, 1970). Natural samples having compositions close to $\text{Fe}_x\text{Mg}_{1-x}\text{SiO}_2$, were equilibrated at temperatures of 1000, 800, 700, 600, and 500 °C, and the Fe-Mg distribution determined by Mossbauer spectroscopy at liquid nitrogen temperatures. The Fe-Mg distribution for sample 3209, as a function of time of heating, is shown in Figure 3-V. The Fe-Mg distribution (or degree of Fe-Mg order-disorder) for sample 3209, as a function of temperature, is shown in Figure 3-VI. For sample 3209 ($\text{Fe}/\text{Fe} + \text{Mg} = 0.574$), Virgo and Hafner estimate the average activation energy for disordering is about 20 kcal/mole and for ordering 15-16 kcal/mole. They conclude that, "Fe, Mg exchange between the octahedral sites is a rapid process characterized by small energy barriers" (Virgo and Hafner 1969, p. 67). The distribution reaches a steady state value at approximately 1000 °C, beyond which further disordering does not occur. This is thought to reflect the strong preference of Fe^{2+} for the M(2) site which is maintained with increasing temperature, thereby providing a limit to the maximum degree

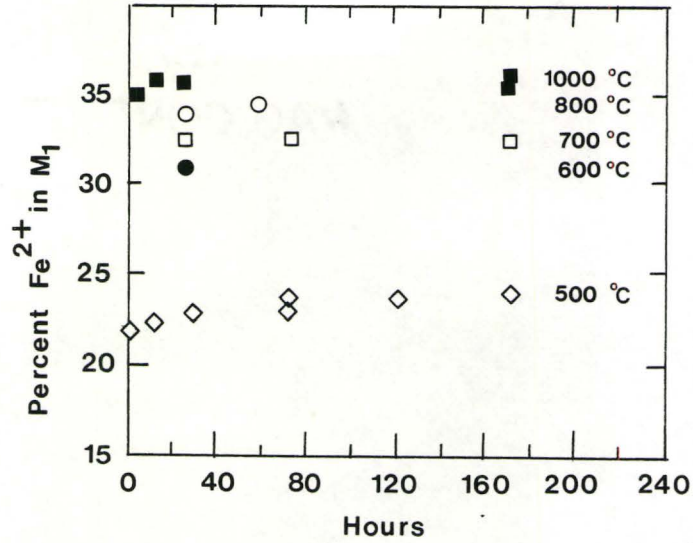


Figure 3-V. Fe^{2+} distribution in orthopyroxene (sample 3209, $\text{Fe}/\text{Fe} + \text{Mg} = 0.574$) as a function of time of heating. The fraction of Fe^{2+} in M(1) of the unheated sample is 22 percent (From Virgo and Hafner 1969).

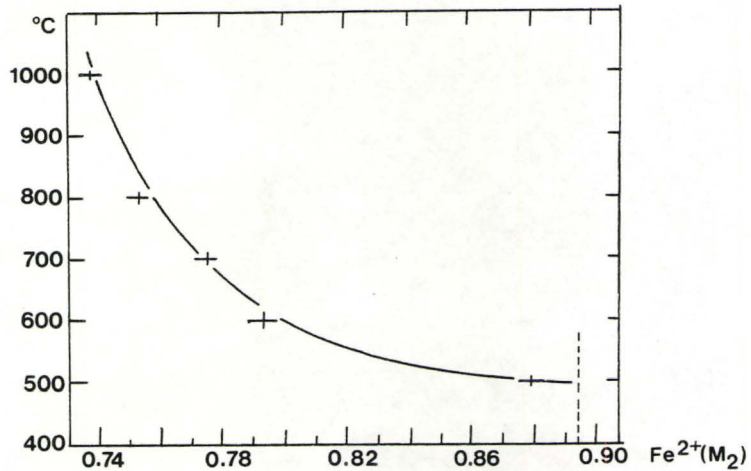


Figure 3-VI. Fe-Mg order-disorder as a function of temperature for the sample 3209. Vertical dashed line refers to the site occupancy number (X_2) for the natural sample (From Virgo and Hafner 1969). Note: $X_2 = \text{Fe}/\text{Fe} + \text{Mg}, \text{M}(2)$.

of disorder. The lower temperature limit of Fe-Mg exchange is estimated to be approximately 480 °C, based on comparison of distributions in natural (unheated) metamorphic orthopyroxenes with the ideal distribution isotherms measured experimentally. This temperature is interpreted as the critical temperature, below which diffusion between sites is not possible even within geological times.

The Fe-Mg distributions for the orthopyroxenes studied in this thesis are shown in Figure 3-VII (see Table 3-VI for calculated values). They indicate an average final equilibration temperature of 480-550 °C, in good agreement with the lower limit suggested by Virgo and Hafner (1970).

(v) Summary and Conclusions

Fortunately, granulite minerals tend to be inclusion free, therefore, it is possible to obtain a relatively pure mineral separate. Even so, in several cases it has been necessary to "fit out" the absorption area due to ilmenite contamination. Minor contamination by other minerals is far more difficult to resolve and has probably not been recognized. In addition, some of the minerals studied exhibit exsolution textures in thin section, and this remains a problem. In most cases, the fitted doublets have acceptably narrow line widths, and while this is normally taken as an indication that the spectra has been fit to the correct number of peaks (Bancroft 1973), it is clear from the studies of Dowty and Lindsley (1973), and Dollase (1975), that true peak configurations and areas may not be resolvable in certain complex spectra.

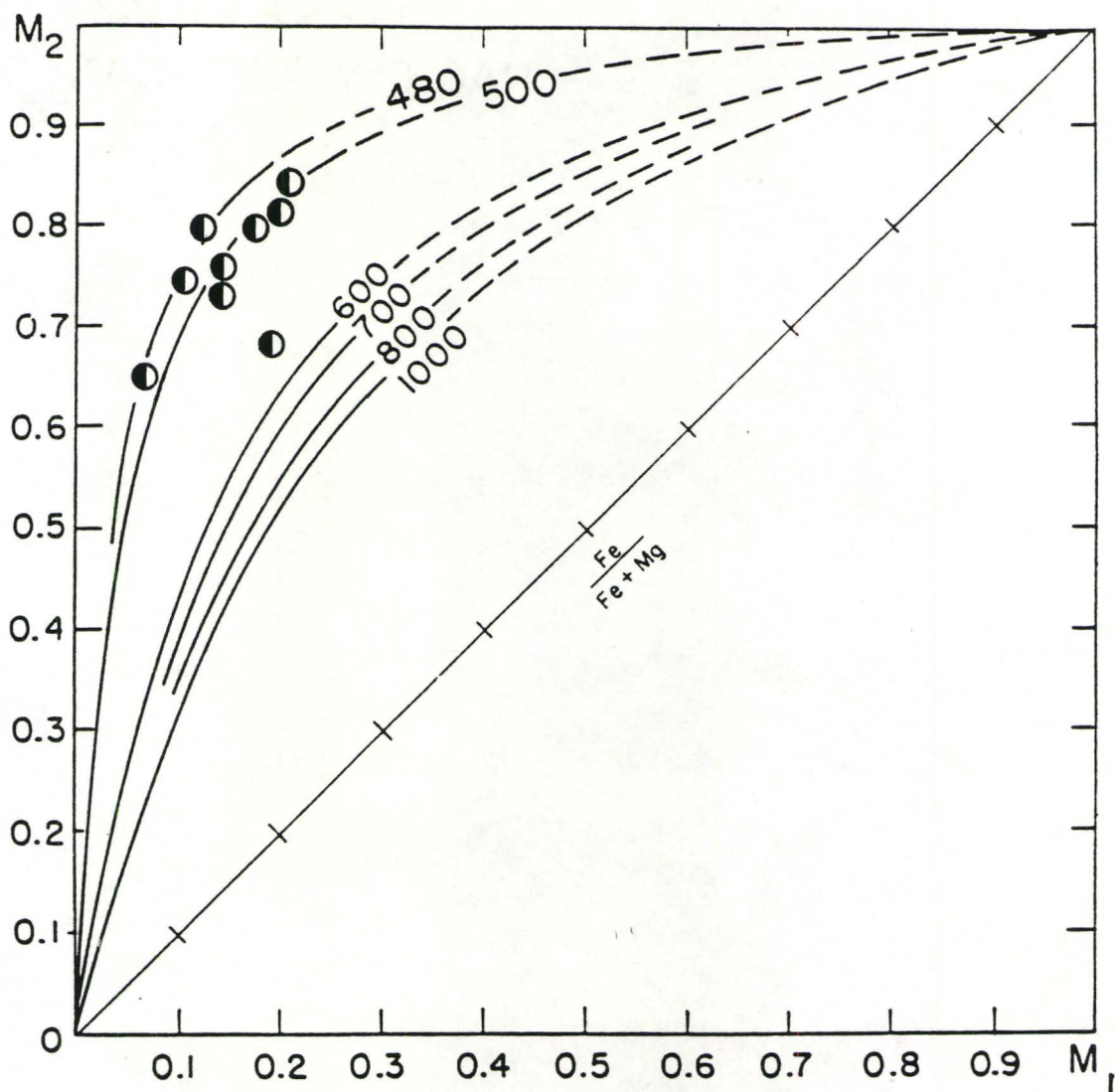


Fig.3-VII Ideal equilibrium isotherms for Fe^{2+} in orthopyroxene. Determined by Virgo and Hafner (1969). Data points represent the Fe-Mg distribution measured for orthopyroxenes studied in this thesis. See Table 3-VI for calculated values. Spectra were measured at liquid nitrogen temperatures.

TABLE 3-VI

Distribution of Fe²⁺ and Mg over the M1 and M2 Sites in Orthopyroxene

Sample	Fe ²⁺	Mg	(Fe+Mg)	Fe/(Fe+Mg)	% Fe(M1) ¹	% Fe(M2)	Fe/Mg(M1) ²	Fe/Mg(M2)
DT-24	.826	1.080	1.906	.432	.169	.831	.146	.719
DT-25	.800	1.028	1.828	.438	.219	.781	.192	.684
DT-30	.693	1.220	1.913	.362	.099	.901	.072	.653
DT-32	.945	.988	1.933	.489	.181	.819	.177	.801
DT-33	.898	1.077	1.975	.455	.164	.836	.149	.760
DT-37	.986	.889	1.875	.526	.197	.803	.207	.845
DT-174	.941	.922	1.863	.505	.196	.804	.199	.811
DT-176	.825	1.094	1.863	.430	.129	.871	.111	.749
DT-177	.858	1.006	1.864	.460	.133	.867	.122	.798

1. % Fe(M1) + % Fe(M2) = 1.0, normalized from Mossbauer area ratios.

2. Fe/Mg(M1) = Fe/(Fe+Mg) (M1) as atoms,

$$\text{where: } \text{Fe}/(\text{Fe}+\text{Mg})_{\text{M1}} = 2 \text{ Fe}/(\text{Fe}+\text{Mg})_{\text{MIN}}^3 * \text{Fe}_{\text{M1}} / (\text{Fe}_{\text{M1}} + \text{Fe}_{\text{M2}})^4$$

3. - from chem anal.

4. - from Mossbauer fractions (normalized to 1.0).

One of the central reasons for determining cation site occupancies is for the estimation of component mole fractions and formulation of an equation of state for silicate minerals. This is necessary in all thermodynamic calculations related to mineral equilibria and inter-crystalline exchange reactions (Grover 1980). Virgo and Hafner (1969) have demonstrated that site occupancies measured from slowly cooled (natural) orthopyroxenes cannot be expected to bear any relation to those prevailing during granulite metamorphism. Inter-site cation exchange occurs more readily in orthopyroxene than in many other silicate minerals, therefore, without further experimental studies, it is difficult to know what physical-chemical event(s) the measured site occupancies correspond to. For example, the rather consistent Fe^{2+} ordering exhibited by the amphiboles may be due to:

1. A systematic error in the fitting procedure.
2. A low temperature, partially ordered state--
controlled by the kinetics of the ordering process.
3. An optimum ordering distribution, structurally controlled during high temperature growth and retained at lower temperature.
4. Some combination of these three.

In conclusion, it would seem that a complete understanding of the site occupancies measured in natural samples must await further experimental studies. These should be careful, temperature controlled experiments, using synthetic minerals, which have been well characterized through X-ray and TEM studies to alleviate the problem of exsolution phenomenon.

CHAPTER 4

OXIDATION STATE OF IRON IN GRANULITE FACIES GNEISSES AND CO-EXISTING MINERALS

4-I Determination of the Oxidation State of Iron in Minerals

(i) Introduction

The use of the electron microprobe for determination of mineral chemistry has replaced the much slower, traditional method of wet chemical analyses of a mineral separate. A common problem, inherent in microprobe analysis, is the inability of the technique to distinguish between variable oxidation states; in particular, many geochemical problems require a knowledge of the oxidation state of iron. The various methods available for determination of Fe oxidation state may be subdivided into three categories:

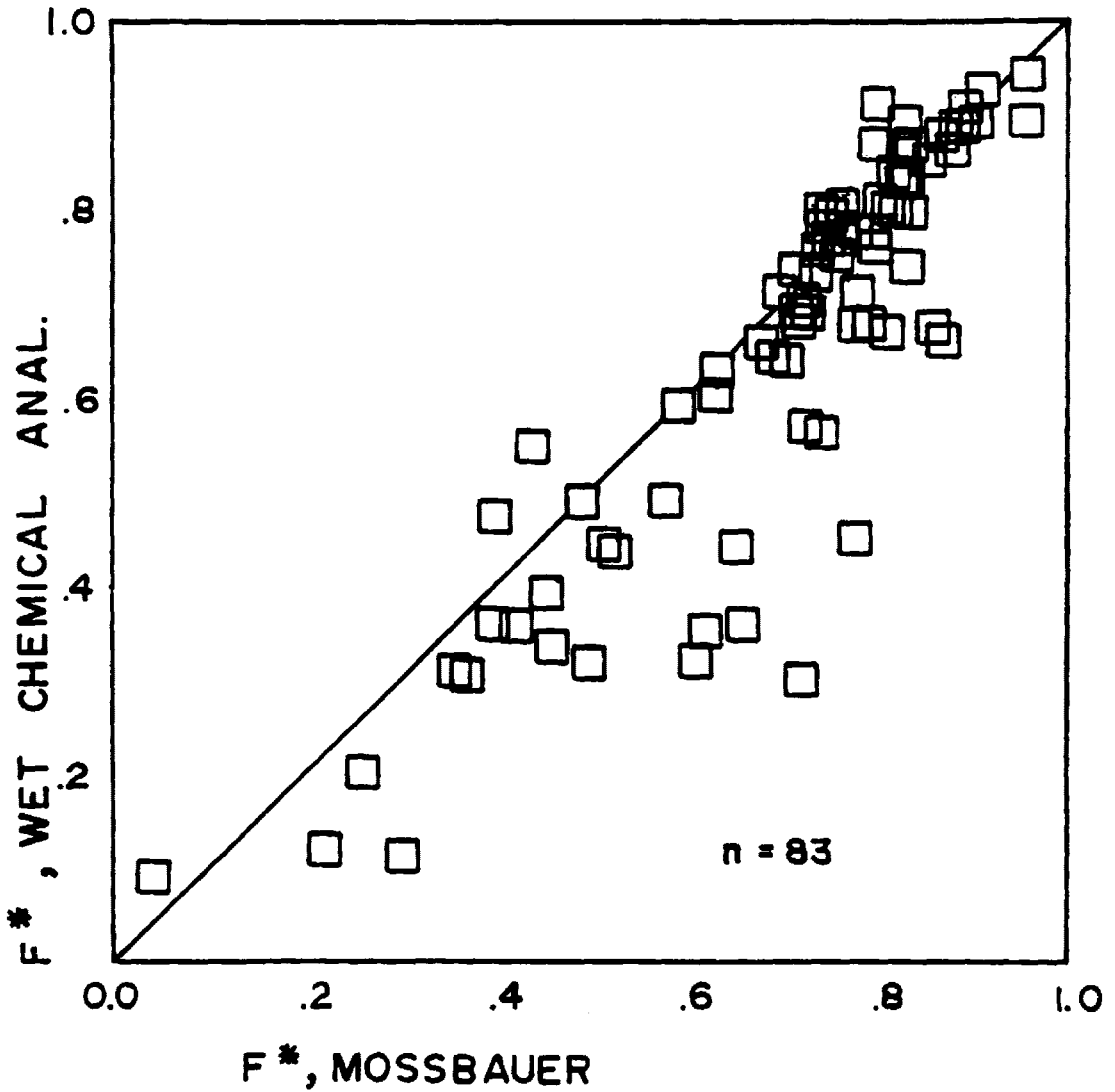
1. Wet chemical analysis.
2. Indirect instrumental methods.
3. Calculation methods.

(ii) Wet Chemical Analysis

Apart from the fact that this method is time consuming, it is plagued by the problems of incomplete phase separation (especially due to small inclusions) and oxidation during acid digestion. Figure 4-I is a comparison of Fe oxidation state determined by wet chemical techniques and Mossbauer spectroscopy. If we assume the Mossbauer values to be approximately correct, then it would appear that a certain amount of

FIG 4-1

COMPARISON OF F^* , DETERMINED
BY WET CHEM. AND MOSSBAUER



Note : Data taken from the literature. Sources available from the author upon request.

oxidation has occurred during wet chemical analyses, as shown by the points which fall below the line.

(iii) Indirect Instrumental Methods

Three fundamental different instrumental methods have been used in the determination of Fe oxidation state in minerals:

1. Spectrophotometric methods.
2. Thermogravimetry.
3. Mossbauer spectroscopy.

The spectrophotometric method (Halenius and Langer 1980) is based on correlation of spectral band intensities (arising from specific electronic transitions) in mineral spectra with concentrations of 3d ions. Knowledge of mineral absorption coefficients, sample thickness, and the influence of elements other than Fe is required for quantitative work.

The thermogravimetric method (Angeletos 1975) is based on the change in weight accompanying oxidation under controlled conditions. This technique is potentially capable of providing very accurate measurements of Fe oxidation state in minerals, providing the influence of volatiles and additional transition elements can be understood or eliminated.

Of the three methods listed above, Mossbauer spectroscopy is the only one which is sufficiently well developed to be used routinely for the determination of Fe oxidation state on a wide variety of minerals.

(iv) Calculation Methods

Most calculation methods involve estimation of Fe^{3+} by assuming mineral stoichiometry and then charge balancing the crystal. Neumann (1976) discusses several approaches (Essene and Fyfe 1967, and Hamm and Vietan 1971) and concludes that the most widely applicable one is the cation basis method. The cation basis method is employed in this thesis and the results are compared with those measured by Mossbauer.

The procedure followed is to calculate the mineral structural formula on the basis of the number of cations, instead of the usual way on the basis of oxygen. Ferric iron is calculated as the difference between the observed total charge (calculated from the amounts and valencies of the cations), and the theoretical total charge (number of oxygens multiplied by two). The equation used is as follows:

$$\text{Fe}^{3+} = \text{Tc} - \sum (\text{C}_i^{\text{N}} \delta_i)$$

$$\text{C}_i^{\text{N}} = \text{C}_i [(\sum \text{C}_i) / \text{CB}]$$

C_i = concentration of component i in moles

CB = cation basis = \sum cations in structural formula

δ_i = charge of component i

TC = total theoretical charge

Application of the cation basis method is dependent on the following assumptions:

1. The mineral is stoichiometric.
2. The valence state of all other ions is known.
3. The chemical analysis is correct.

In practice, the first two assumptions are closely approached for most minerals, so that the most significant factor determining the accuracy of this technique is the quality of the chemical analysis. For example, relatively small errors in SiO_2 result in large errors in the estimation of Fe^{3+} .

(v) Results of F^* Measurement Using Mossbauer Spectroscopy and Comparison with F^* Determined by Charge Balancing Calculations

The distribution of Fe oxidation states determined by M.S. for the minerals, clinopyroxene, orthopyroxene, hornblende, and garnet is shown in Figure 4-II. The average values are:

Mineral	F^*	$\pm 1\sigma$	ϵ_1	ϵ_2
Clinopyroxene	.804	.020	2.49	2.34
Orthopyroxene	.960	.016	1.67	1.60
Hornblende	.720	.017	2.36	2.54
Garnet	.935	.008	0.86	0.90

where: $F^* = \text{Fe}^{2+} / (\text{Fe}^{2+} + \text{Fe}^{3+})$, mean value shown

1σ = suggested uncertainty in the mean (one standard deviation)

ϵ_1 = relative error ($1\sigma/F^* \times 100$)

ϵ_2 = the calculated 1σ error (given in % relative error) in the Mossbauer technique (see Table 3-I).

FIG 4-II OXIDATION STATE OF IRON IN GRANULITE FACIES

MAFIC MINERALS
 $F^* = Fe^{2+} / Fe^{2+} + Fe^{3+}$

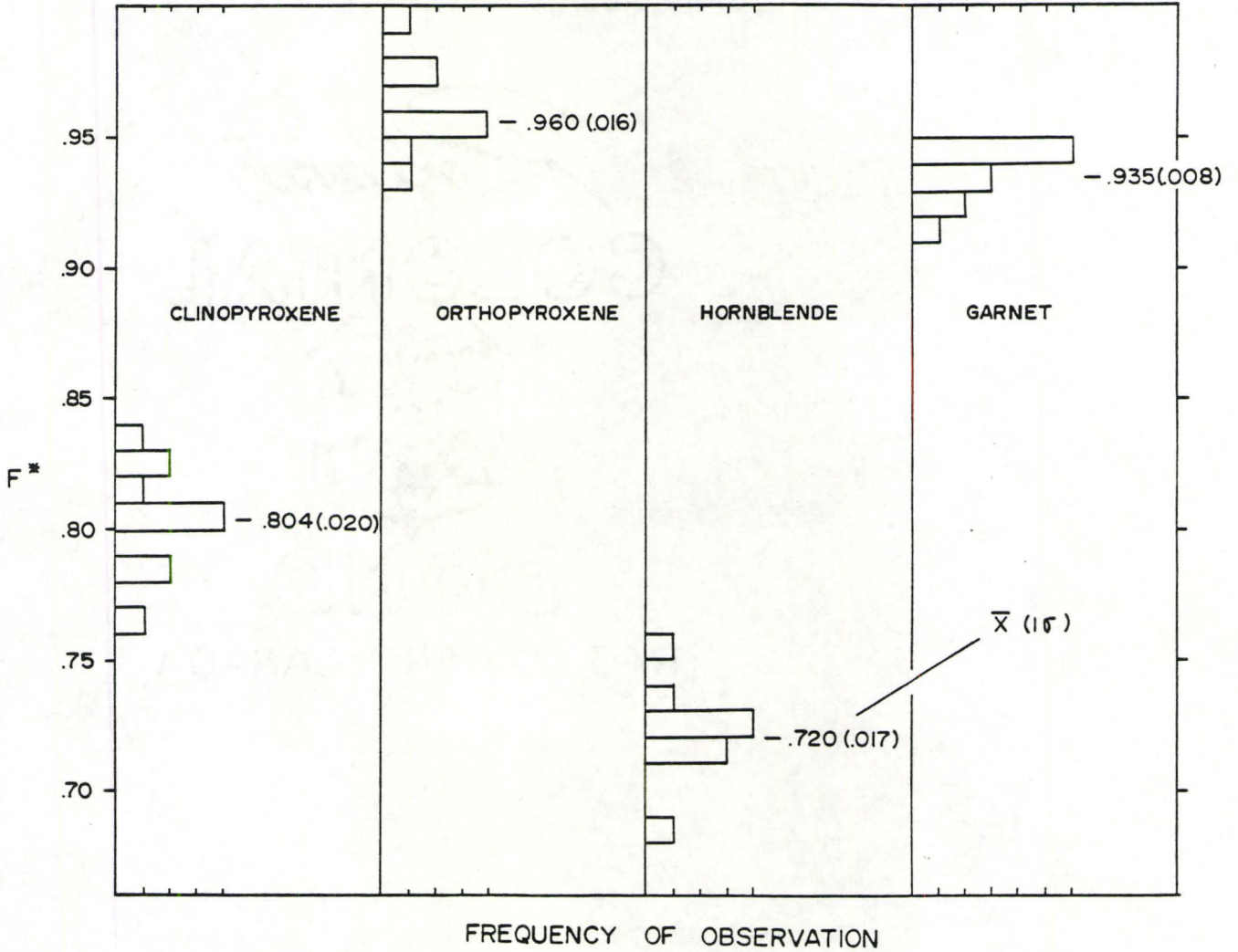


Fig 4-III(a) Comparison of Iron Oxidation State (F*) Determined by Mossbauer Spectroscopy and Charge Balancing

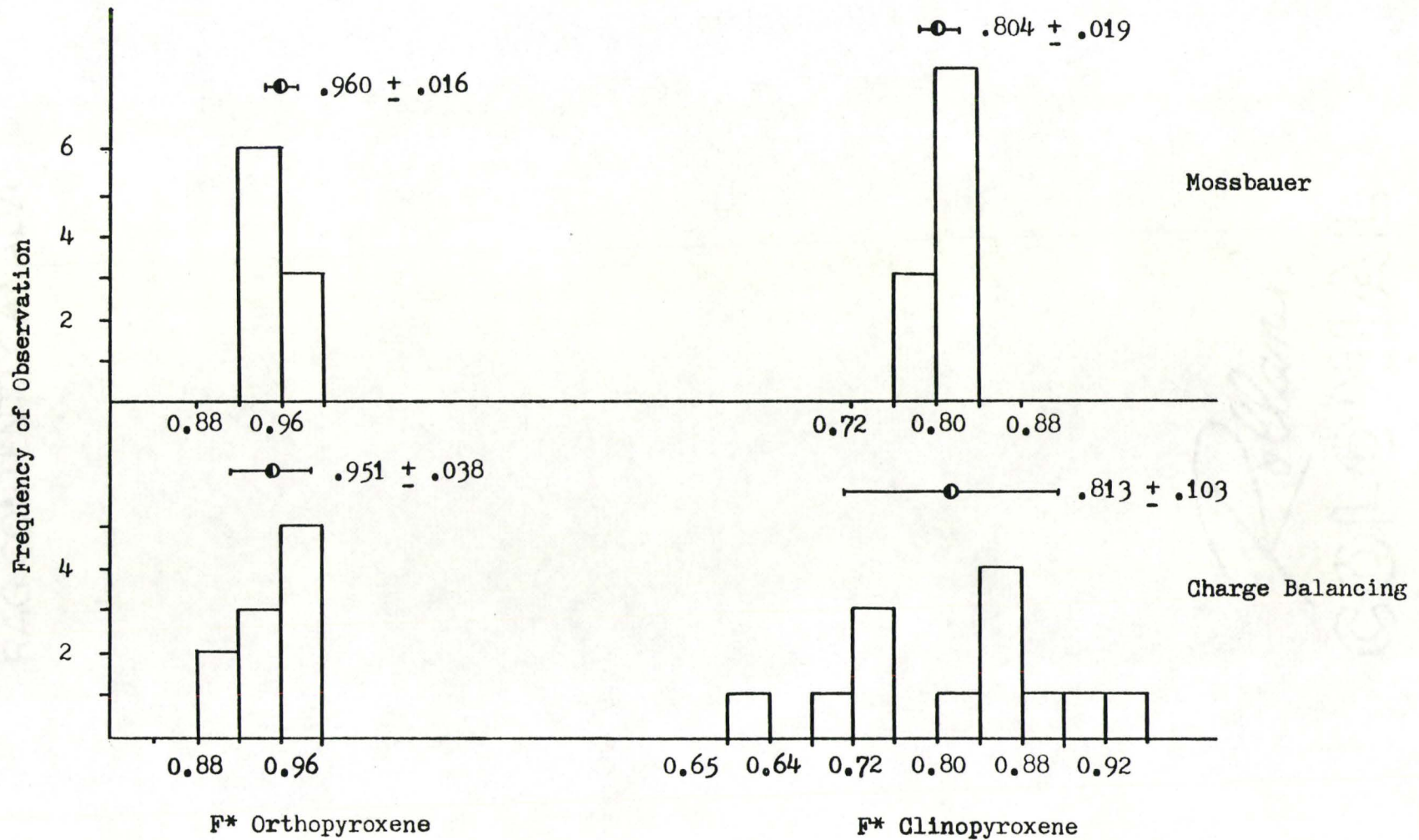
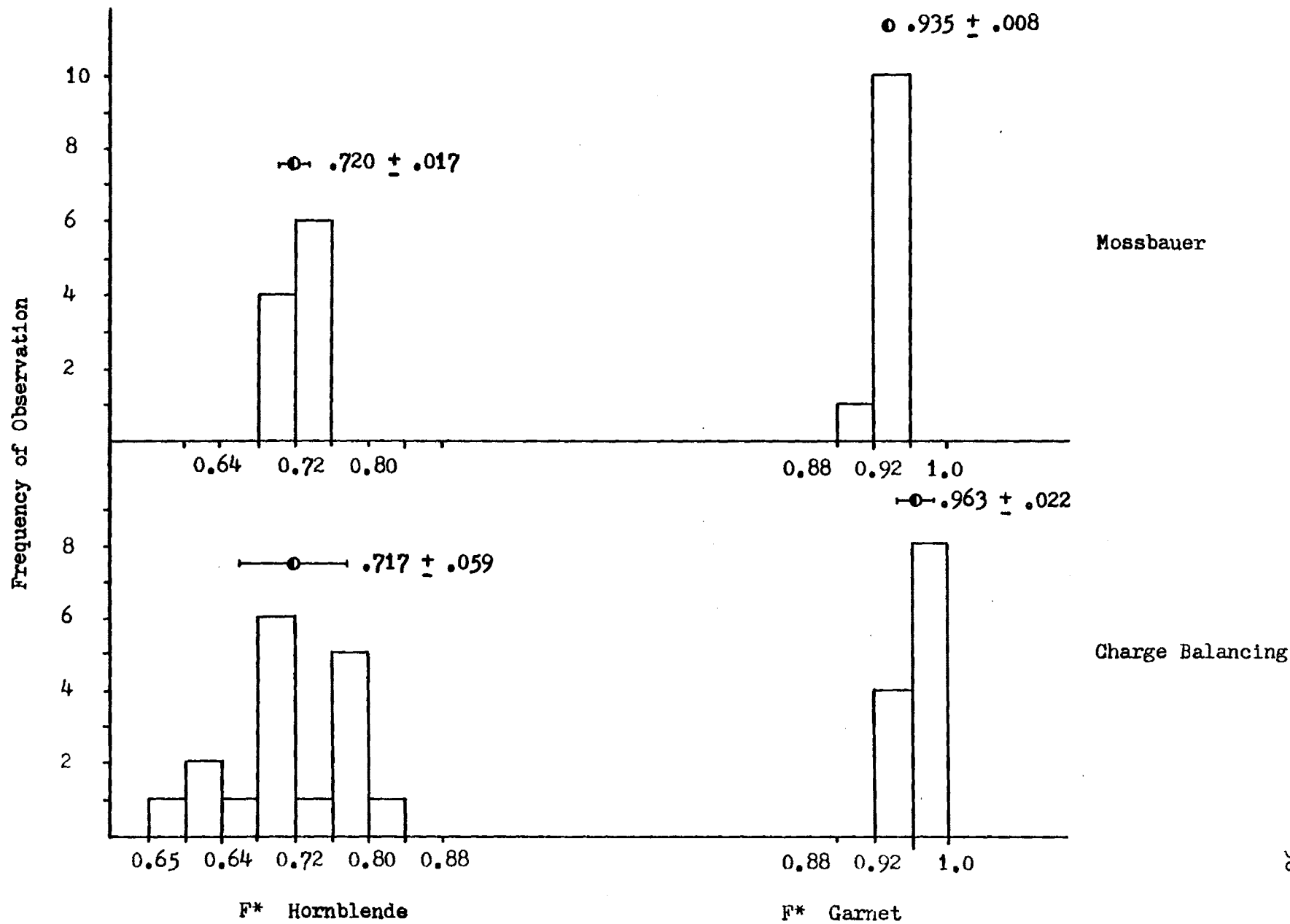


Fig 4-III(b) Comparison of Iron Oxidation State (F*) Determined by Mossbauer Spectroscopy and Charge Balancing



It is significant to note that the estimated error in the mean (one standard deviation) of each distribution is of approximately the same magnitude as the estimated error in each individual Mossbauer determination. One may conclude therefore, that for each mineral species, the Fe oxidation state is approximately constant within the resolution of the measurement technique. The normal distribution exhibited by each mineral is interpreted as an error function.¹

Figures 4-III(a) and 4-III(b) compare Fe oxidation state, calculated using the charge balance method, with that measured by M.S. Although the charge balance method shows a much wider spread of values than the rather tight cluster measured by M.S., the calculated mean of both methods is almost identical. Charge balancing is therefore a very useful method for calculating the approximate Fe oxidation state of a single mineral, or an average F^* from a group of mineral data. The average value is significant only when it can be assumed that F^* is approximately constant and that the analytical errors are symmetrically distributed.

1. The garnet distribution is unique in that ferric iron appears to have a clearly defined upper limit. It is possible that this "cutoff" is due to some systematic error in the Mossbauer fitting procedure, however, examination of the garnet spectra indicates that the peaks arising from ferric iron, although small in size, are fairly well defined so that there is no obvious support for this supposition.

4-II Determination of the Oxidation State of Fe in Whole Rock Samples

The oxidation state of Fe in 27 of the whole rock samples studied in this thesis is given in Figure 4-IV. The bimodal nature of the F* distribution is not considered significant, being merely due to sample selection. FeO was determined by titration (see Appendix B-I for method), and Fe₂O₃ by difference. In all cases, analyses were repeated until three similar values were obtained. This procedure is deemed necessary due to the common problem of minor oxidation during acid digestion. Repeated analyses of unknowns and standards indicate a very high accuracy and precision (approx. ± 1.0%). However, because many of the samples analysed are inhomogeneous gneisses, a minimum relative error of ± 5% is suggested as a reasonable estimate of the true accuracy.

4-III Discussion

The relationship between mineral and whole rock Fe oxidation state and metamorphism has been discussed by Chinner (1960) and Eugster (1959) (see additional references in these papers). Systematic changes in whole rock F* during progressive metamorphism (normally reduction) have been described by Schwarcz (1966), and Engel and Engel (1958). Chinner (1960) studied a sequence of sillimanite bearing metapelites and found a good correlation between mineral F* and mineral chemistry, mineral F* and whole rock F*, and whole rock F* and whole rock Fe (total). He concluded that the rocks behaved as closed systems and that the failure of adjacent layers to reach equilibrium with each other, is a result of the relatively low "oxidizing" or "reducing" capacity of the

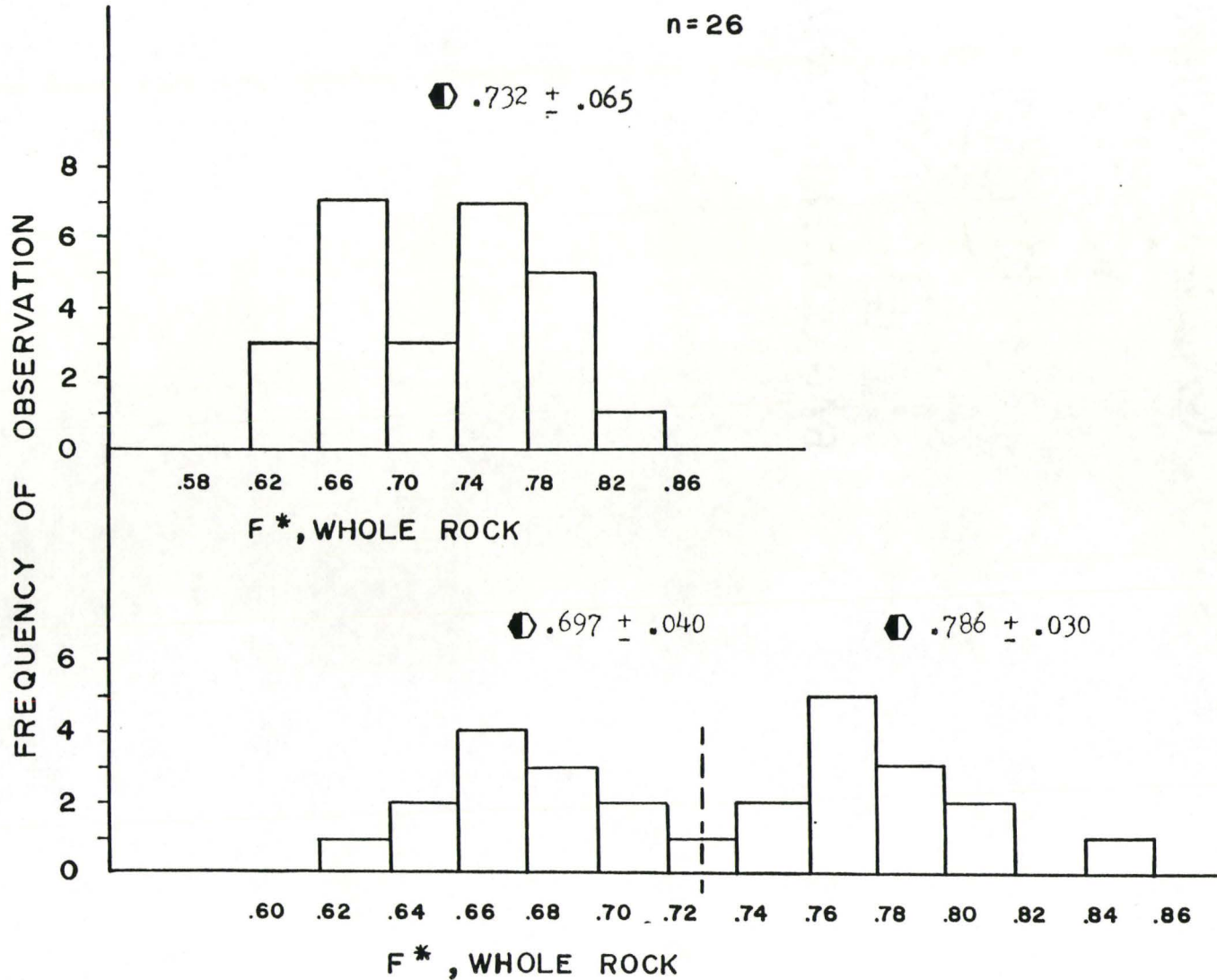
FIG 4-IV

DISTRIBUTION OF WHOLE ROCK F*

TWO CLASS INTERVALS ARE SHOWN:

CI = .04 and .02

n = 26

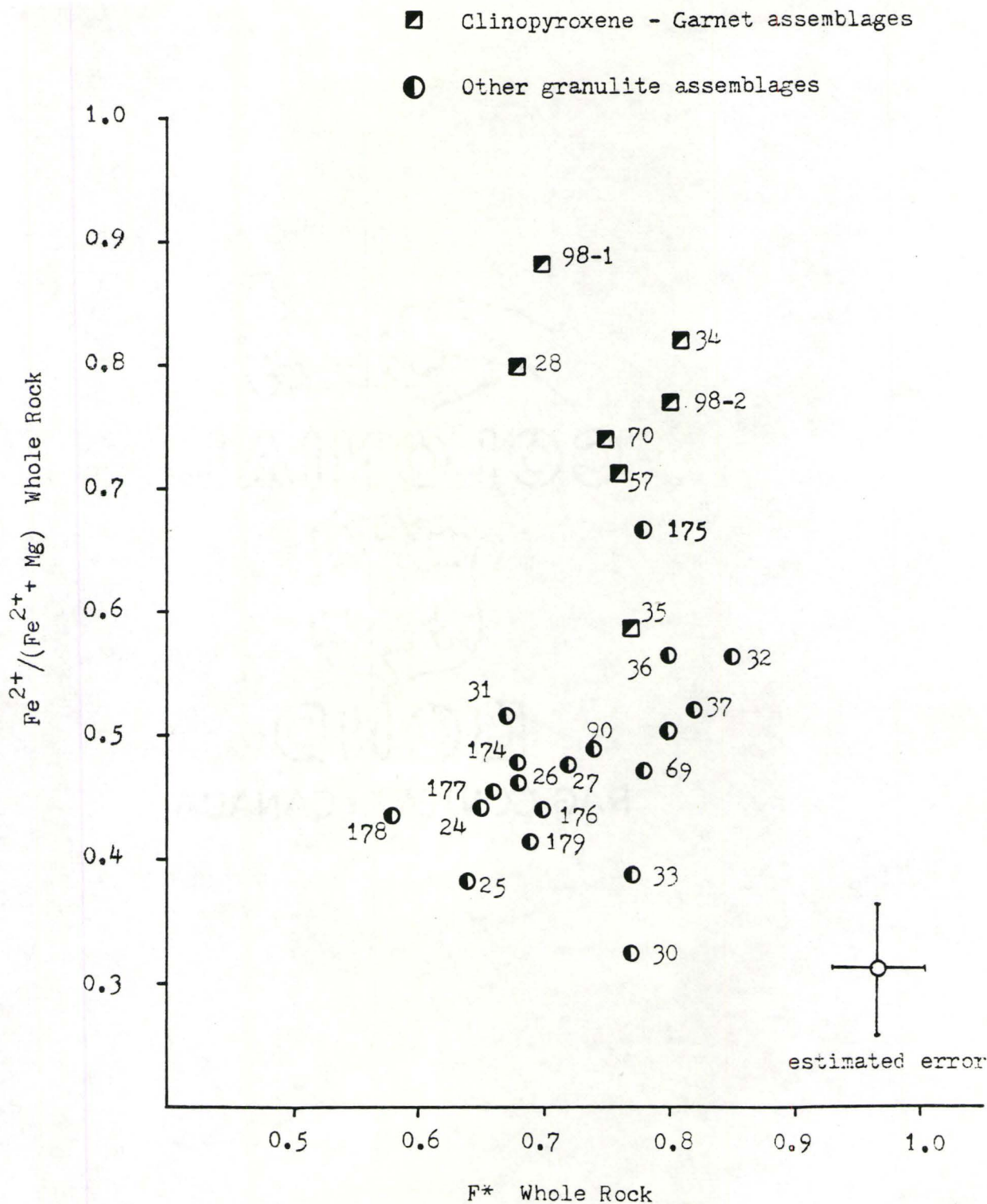


vapour phase, due to the mass of the solids far exceeding that of the vapour present. Further, he suggests that in general, contact metamorphism is more likely to result in widespread homogenization of oxidation state and reduction of ferric iron, due to the steep thermal gradients and increased mobility of H_2O .

Plots of whole rock F^* vs. $Fe/(Fe + Mg)$, F^* vs. $Fe(\text{total})$ and whole rock F^* vs. mineral F^* are given in Figures 4-V, 4-VI and 4-VII, respectively. The whole rock F^* vs. $Fe/(Fe + Mg)$ and F^* vs. $Fe(\text{total})$ show no discernible correlation, in marked contrast to the good correlations found by Chinner (1960). The whole rock F^* vs. mineral F^* plot shows a weak positive correlation for the three minerals, hornblende, clinopyroxene and orthopyroxene. The variation in F^* for garnet is so slight that no trend is seen. Unfortunately, because the variation in mineral F^* values can be explained wholly in terms of analytical error, the significance of the correlation remains uncertain.

Rocks containing both the reduced and oxidized members of a redox reaction have a fixed $P(O_2)$ at any given temperature (buffered system). Additions or subtractions of hydrogen do not change $P(O_2)$ as long as the masses of the solids prevail (Euster 1959). Reflected light microscopy and a limited number of microprobe analyses indicates that all of the samples under study contain co-existing magnetite and ilmenite. The simplest interpretation would be that, within this relatively small study area, all of the samples studied have been buffered to approximately the same $P(O_2)$, resulting in the observed consistency of F^* for each group of silicate minerals. However, there are

Plot of $Fe^{2+}/(Fe^{2+} + Mg)$ VS F^*_{WR} (Whole Rock Oxidation State)



$F^* = Fe^{2+}/(Fe^{2+} + Fe^{3+})$, atomic ratio

Fig 4-VI Whole Rock Fe_2O_3 (Total) VS Whole Rock F* (Whole Rock Iron Oxidation State)

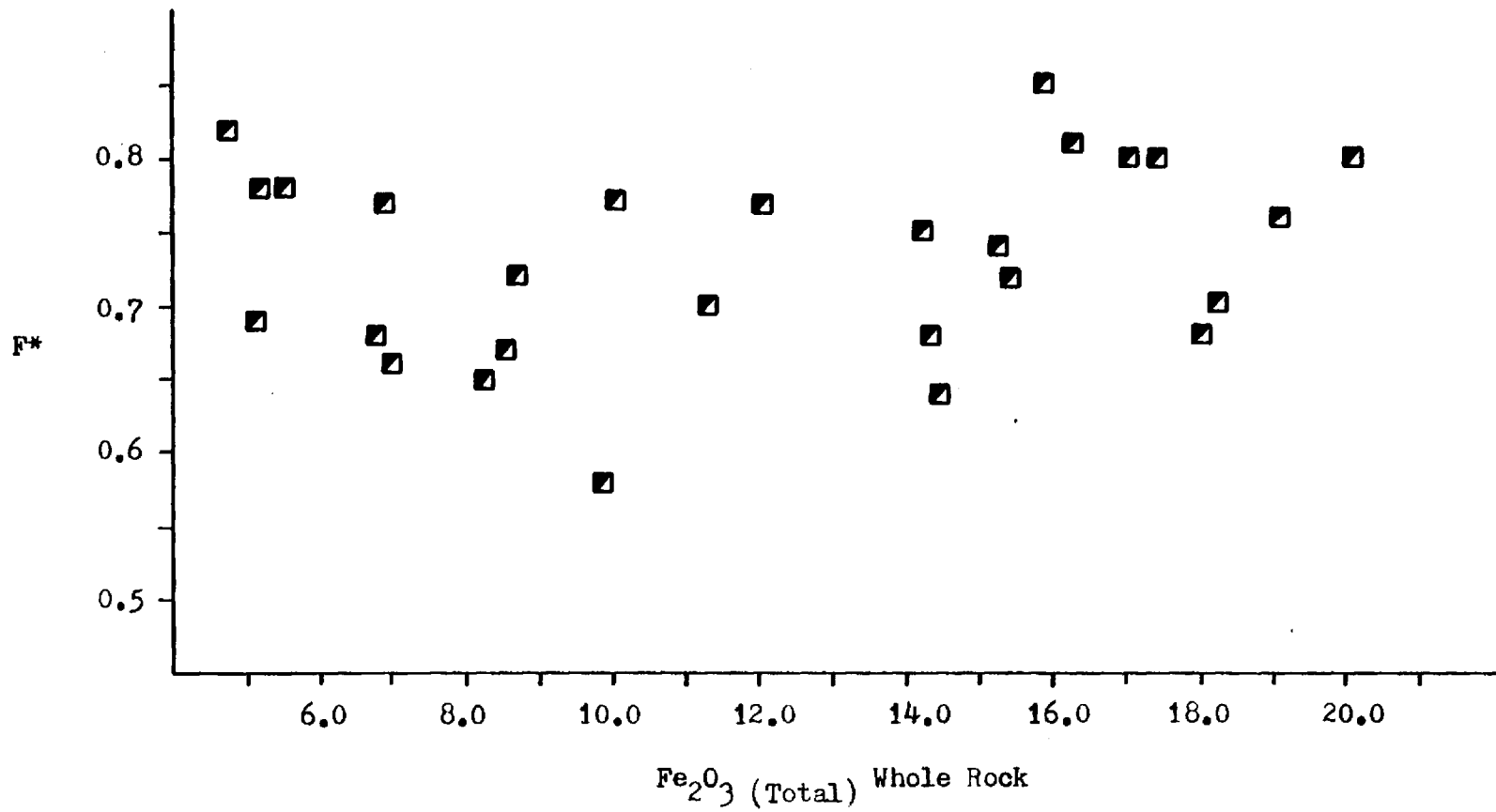


FIGURE 4-VII

Plot of Mineral F* Against Whole Rock F*

Uncertainties shown are minimum errors as follows:

whole rock $\pm 5.0\%$

mineral (see Appendix B)

Straight lines have been fit using the reduced major axis method (RMA) (see below). The abscissa is offset to increase clarity.

hornblende	$y = 4.065x - 2.174$	$r = .41$
clinopyroxene	$y = 3.964x - 2.441$	$r = .45$
orthopyroxene	$y = 4.588x - 3.678$	$r = .67$

Reduced Major Axis Method (RMA)

The RMA method (Middleton 1963) fits a straight line to X - Y data allowing for error in both parameters. It is particularly useful for widely scattered data points.

The line $y = mx + b$ is fit to the data points using:

$$b = \bar{Y} - (\sigma_y / \sigma_x) \bar{X} \quad m = (\sigma_y / \sigma_x)$$

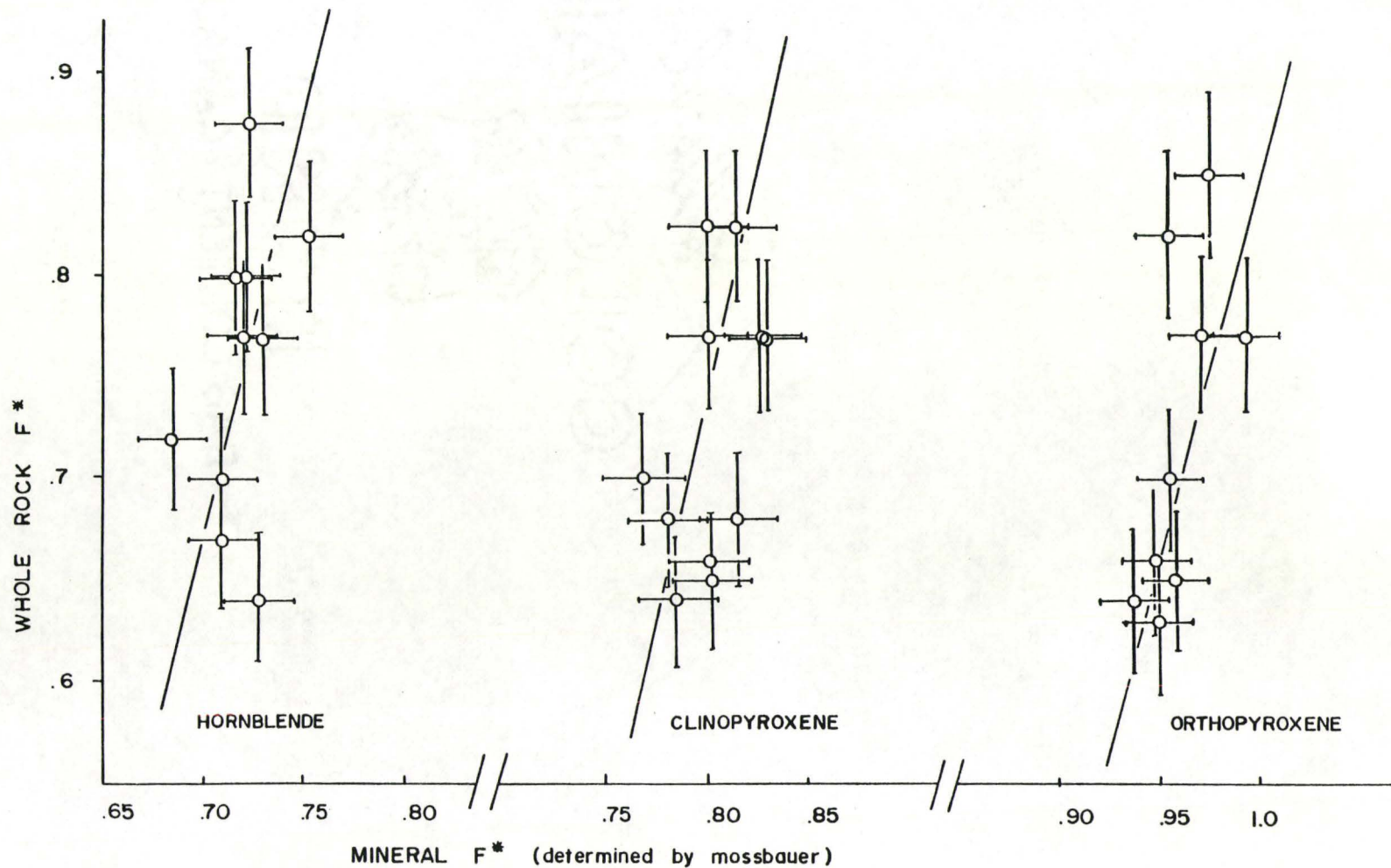
where: \bar{X} = mean of X

\bar{Y} = mean of Y

σ_x = std. dev. of X

σ_y = std. dev. of Y

PLOT OF MINERAL F* AGAINST WHOLE ROCK F*



some problems with this interpretation. During cooling, secondary ilmenite-magnetite assemblages are formed by oxidation of the magnetite-ulvospinel solid solution (Buddington and Lindsley 1964). Magnetite-ilmenite microintergrowths and external "granule" exsolution can both occur. In many rocks, it is not clear from the microfabric how much of the ilmenite is due to contemporaneous crystallization, and how much is due to external exsolution. Bohlen and Essene (1977) have demonstrated that it is possible to distinguish between the two generations of ilmenite based on minor element composition. This has not been done in this thesis. Sample DT-030 contains the assemblage rutile-ilmenite-magnetite. Buddington and Lindsley (1964) note that the assemblage magnetite-rutile is occasionally found instead of the usual ilmenite-hematite (solid solution), or its exsolved equivalent, and that a number of assemblages are clearly non-equilibrium indicating a very complex history.

4-IV Conclusions

The variations in mineral assemblage within the study area, in particular the extreme contrast between the volatile rich nature of the anorthosite border phase and the volatile depleted garnet rich contact gneisses, argues against consistency of $P(O_2)$. In addition, it is not known what the true equilibrium oxide mineral assemblages were during granulite metamorphism. Geothermometry calculations (see Chapter 5) indicate that it is unlikely that all of the rocks in the study area have experienced the same temperature history, consequently, it is hard to see how the $P(O_2)$ could have remained fixed, even if each sample did

contain an equilibrated assemblage of co-existing magnetite-ulvospinel and hematite-ilmenite solid solutions.

At present, the observations of mineral Fe oxidation state made in this thesis have not been adequately explained.

CHAPTER 5

ESTIMATION OF THE PHYSICAL CONDITIONS OF METAMORPHISM

5-I Introduction

Comparison of the mineral assemblages and textures observed in thin section with the existing petrogenetic grid allows approximate determination of the physio-chemical conditions of metamorphism. For example, many granulite terrains have mineral assemblages which suggest the following broad ranges:

Temperature	-	650-900 °C
Pressure	-	4.5-10 kbs
P_{H_2O}	-	$< P_T$ (0.10-0.50) ?
P_{CO_2}	-	may be increased in comparison to lower grade facies

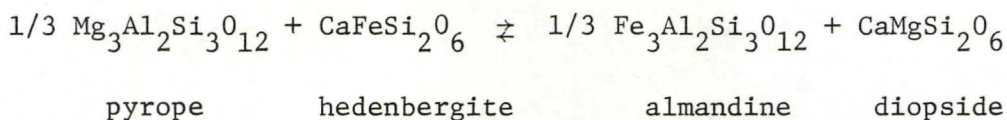
In addition, for selected whole rock compositions, the occurrence of specific minerals (e.g., cordierite or kyanite) allows further refinement. More quantitative estimation of conditions is possible through the use of established geothermometers and geobarometers. These techniques are based on the concept that for any rock containing several phases, it is generally possible to write a number of mass balanced reactions involving components of the phases present in the rock. In theory, these may be used to evaluate various intensive variables of interest, providing one knows the phase compositions and the

equilibrium constants of the reactions. In practice, the only useful equilibria are those for which thermochemical data are available and for which, some understanding of the relationship between activities of the relevant components in complex phases and the composition of the phases exists. At present, these two constraints restrict application of the technique to a small number of oversimplified systems.

5-II Garnet - Clinopyroxene Geothermometry

(i) Thermodynamic Basis of Geothermometer

Consider the Fe-Mg exchange reaction between coexisting garnet and clinopyroxene (Ellis and Green 1979). The reaction may be expressed as:



If the solid solutions can be assumed to be ideal then $a_i^j = X_i^j$ ($\delta_i^j = 1$), and:

$$k = \frac{X_{\text{Fe}}^{\text{GT}}/X_{\text{Mg}}^{\text{GT}}}{X_{\text{Fe}}^{\text{CPX}}/X_{\text{Mg}}^{\text{CPX}}} = k_D; \text{ the distribution coefficient}$$

If deviations from ideal solid solution exist, then this model is inadequate to explain the variations in the measured k_D with P, T, and X_i^j . A more rigorous treatment requires knowledge of the activity coefficients

(δ_i^j) of the various solid solutions. It is possible, in theory, to derive activity-composition relationships for different solid solutions by evaluating the non-ideal contributions in terms of regular solution model interaction parameters.

A much simpler (and therefore less rigorous) approach taken by Ellis and Green (1979), is to allocate all the non-ideal effects in k_D to Ca substitution in garnet. They argue that this approach is justified, because variations in Di and CaTs contents of clinopyroxene, is in the same sense as that of Ca in the co-existing garnet with variations in P, T, and rock composition. They derive the following expression:

$$T \text{ } ^\circ\text{K} = \frac{3104 X_{\text{Ca}}^{\text{GT}} + 3030 + 10.86 P \text{ (kbars)}}{\ln k_D + 1.9034} \quad (5-1)$$

It is significant to note that the correction term, $X_{\text{Ca}}^{\text{GT}}$, represents the net effect of all the non-ideal behaviour in both garnet and clinopyroxene solid solutions and is strictly empirical in nature.

A more rigorous evaluation of the compositional dependence on k_D is discussed by Ganguly and Kennedy (1974), Ganguly (1979), and Dahl (1980). Ganguly (using the simple mixture model of Guggenheim 1952, 1967) derives an expression for the activity coefficients in terms of binary solution interaction parameters. Dahl (1979, 1980) has evaluated the above coefficients using garnet-clinopyroxene pairs from the Ruby Range (S. W. Montana), for which the temperature and pressure are known from independent methods. This leads to the expression:

$$T = \frac{2324 + 0.022 P \text{ (bars)} + 1509 (X_{\text{Fe}}^{\text{GT}} - X_{\text{Mg}}^{\text{GT}}) + 2810 (X_{\text{Ca}}^{\text{GT}}) + 2855 (X_{\text{Mn}}^{\text{GT}})}{1.987 \ln k_D} \quad (5-2)$$

The garnet-clinopyroxene temperatures calculated using the Ellis and Green (equation 1) and Dahl (equation 2) calibrations, and the relevant compositional data, are given in Tables 5-I and 5-II, respectively.¹ Both of these equations require knowledge of the pressure (which is generally not available), therefore temperatures have been calculated by assuming reasonable pressures. It can be seen from the calculated values that these calibrations are only weakly pressure dependent, so that the accuracy of the pressure guess is not critical. Temperatures were also calculated assuming $\text{Fe} = \text{Fe}_T$ (Dahl's calibration). This results in an average increase in temperature of 100.4 °C (for nine samples), which clearly demonstrates the importance of considering the oxidation state of Fe when using geothermometers based on Fe-Mg exchange equilibria.

A second method of determining garnet-clinopyroxene temperatures has been devised by Dahl (1980) by considering the compositional dependence of $\ln k_D$. Equation 5-2 may be rearranged as follows:

$$\ln k_D = \frac{\text{Sum } X}{RT} + \frac{2482}{RT} \quad (5-3)$$

$$\text{where: Sum } X = 1509 (X_{\text{Fe}}^{\text{GT}} - X_{\text{Mg}}^{\text{GT}}) + 2810 (X_{\text{Ca}}^{\text{GT}}) + 2855 (X_{\text{Mn}}^{\text{GT}}) \quad (5-4)$$

1. Pyroxene end members have been calculated using the method of Cawthorn and Collerson (1974).

TABLE 5-I

Compositional data used in the calculation of CPX-GT Temperatures Ellis and Green (1979)

SAMPLE No.	K _D	Garnet				FS	EN	WO	Pyroxene			Ac	JD	T °C	T °C
		X _{Fe}	X _{Mg}	X _{Ca}	X _{Mn}				CaTs	CaTiTs	CaFeTs			P= 7 kb	P= 9 kb
DT-25	6.395	.555	.202	.222	.022	.144	.335	.389	.017	.007	.040	.000	.070	735.3	742.1
DT-28	7.238	.623	.097	.245	.036	.203	.228	.397	.007	.007	.057	.000	.102	722.4	727.95
DT-30	5.529	.482	.325	.180	.014	.095	.356	.403	.047	.016	.020	.000	.064	740.7	746.7
DT-32	5.941	.584	.198	.193	.025	.155	.313	.398	.006	.005	.040	.000	.083	732.4	738.2
DT-34	8.000	.693	.050	.226	.030	.276	.159	.369	.037	.005	.066	.005	.084	683.2	688.6
DT-35(C)	5.348	.632	.134	.209	.025	.217	.245	.390	.024	.005	.049	.000	.070	775.4	781.4
DT-35(R)	5.736	.586	.116	.278	.020	.217	.245	.390	.024	.005	.049	.000	.070	813.9	819.9
DT-36	6.099	.605	.148	.211	.036	.191	.286	.381	.010	.005	.044	.000	.084	740.1	746.0
DT-98	6.262	.602	.184	.193	.021	.160	.305	.401	.016	.005	.041	.000	.073	718.3	724.1
DT-176	5.548	.545	.238	.195	.023	.133	.322	.400	.031	.007	.041	.000	.066	752.5	758.5
C-34*	8.496	.483	.149	.334	.034	.122	.338	.393	.028	.009	.023	.011	.075	738.2	743.5
C-23*	8.496	.517	.140	.304	.040	.130	.300	.422	.027	.010	.033	.011	.067	728.2	733.6
C-28*	9.006	.523	.160	.294	.023	.136	.372	.392	.015	.010	.035	.011	.030	706.9	712.2
C-48*	9.208	.555	.172	.254	.020	.119	.337	.417	.014	.009	.028	.010	.066	671.1	676.3

* Values from Mummery (1972)

TABLE 5-II

CPX-GT Temperatures calculated from Dahl (1980) and compositional effects on K_D

Sample No.	$\ln K_D$	$1509(X_{Fe} - X_{Mg})^{GT} + 2810(X_{Ca}^{GT}) + 2855(X_{Mn}^{GT}) - \text{SUM}(X)$	T °C P = 7.2 kb	T °C P = 10.0 kb			
DT-25	1.897*	533.1	623.3	61.9	1218.4	708.5	724.8
	1.710**				1228.1	819.1	837.2
DT-28	1.991	793.9	504.6	101.9	1583.4	754.4	769.9
	1.822				1579.8	849.1	866.1
DT-30	1.723	235.9	504.6	38.5	779.1	679.6	697.6
	1.595				799.7	762.4	781.8
DT-32	1.791	582.9	542.8	70.0	1195.7	760.2	777.5
	1.625				1206.0	869.3	888.4
DT-34	2.095	970.8	636.3	86.5	1693.6	730.2	745.0
	1.944				1684.5	805.8	821.8
DT-35 (CORE)	1.787	751.9	586.5	71.7	1410.1	822.8	840.2
	1.627				1413.9	932.1	951.1
DT-35 (RIM)	1.857	709.8	780.3	58.0	1548.2	818.9	835.7
DT-36	1.835	689.3	592.8	101.6	1383.8	787.1	804.0
	1.709				1390.1	867.4	885.6
DT-98	1.851	630.5	543.1	60.2	1233.8	737.0	753.8
	1.701				1245.7	830.0	848.3
DT-176	1.741	462.8	546.5	65.4	1074.7	754.9	772.8
	1.527				1089.1	903.6	923.9
C-34***	2.232	503.8	938.2	95.8	1537.9	633.3	647.2
C-23***	2.151	567.7	853.2	113.1	1534.0	666.6	681.0
C-28***	2.209	548.5	827.1	65.8	1441.3	620.9	604.7
C-48***	2.232	578.3	712.8	57.3	1348.3	590.8	604.7

* Fe = Fe⁺² , ** Fe = Fe_{total} , *** Fe = Fe⁺² samples from Nummery 1972

At a fixed temperature, a plot of $\ln k_D$ vs. Sum X gives a straight line.¹

A plot of the Dahl (1980) isotherm ($\ln k_D$ vs. Sum X) using the compositional data from this thesis is shown in Figure 5-I. The broken lines are Dahl's approximate isotherms based on independently determined temperatures (of garnet-clinopyroxene assemblages) taken from the literature. The solid lines are linear fits to the data from this thesis (using the Reduced Major Axis Method). The calculated line for $\text{Fe} = \text{Fe}^{2+}$ is almost exactly parallel to the isotherms previously determined by Dahl and gives a temperature of $T = 750 \pm 70$ °C, in good agreement with the temperature of $T = 750 \pm 45$ °C, calculated using equation 13 for $P = 7.2$ kbs. The line calculated for $\text{Fe} = \text{Fe}_T$ is steeper and gives a higher temperature of $T = 792 \pm 70$ °C. Also shown are four samples taken from Mummery (1972). Unfortunately, there are not enough data points to define a line, however a temperature of < 675 °C is indicated. A parallel isotherm drawn through the average value (mathematically equivalent to determining the RMA best fit line) gives an approximate temperature of 668 ± 70 °C.

(ii) Accuracy of Calibration

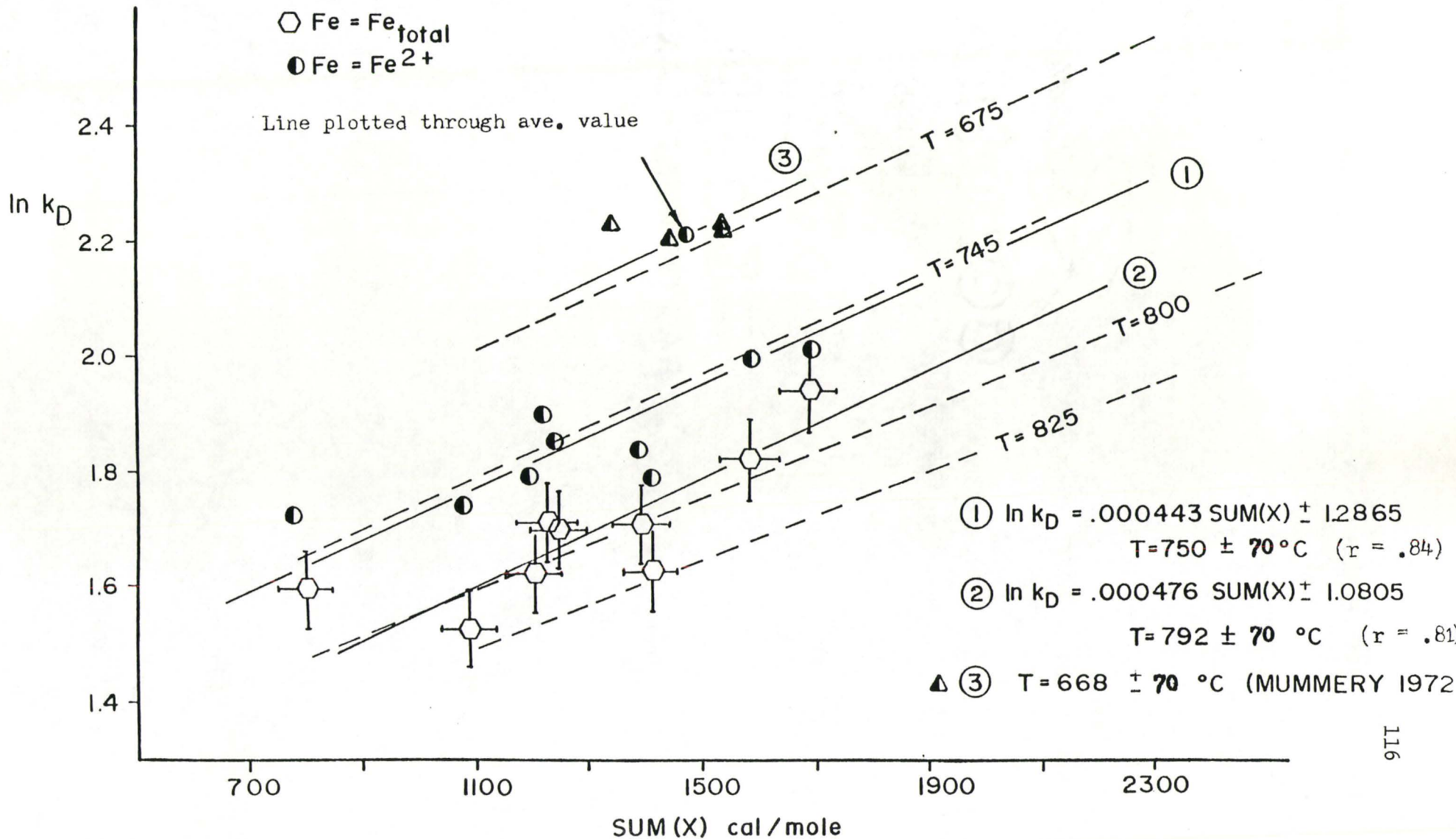
Equation 5-10 (Ellis and Green 1979) has been calibrated using experimental data covering the range $T = 750$ - 1300 °C and $P = 24$ - 30 kbs. The accuracy of this method is estimated to be $\pm 5\%$ based on comparison

1. The isotherm is also pressure dependent, however, because the effect is so small, Dahl (1980) considers it unimportant in the isotherm calibration.

FIG 5-1

DAHL ISOTHERM (CPX - GT)

(Broken lines are approximate isotherms from Dahl 1980)



of calculated and known (experimental) temperatures.

Dahl (1980) determined the thermal-compositional dependence of k_D^{Gt-Cpx} , by comparison of garnet-clinopyroxene compositional data with independently determined temperature estimates. The accuracy of the calibration is critically dependent on the quality of these estimates.

Temperatures were calculated using the following methods:

Mineral Pair	Calibration	Accuracy suggested by author °C
Opx-Cpx	Wood and Banno (1973)	± 70
	Wells (1977)	± 70
	Ross and Huebner (1975)	± 100
Cpx-Gt	Raheim and Green (1974)	?
	Mysen and Heier (1972)	± 60
2-feldspar	Whitney and Stormer (1977)	± 80
Gt-Bt	Thompson (1976)	± 50
Gt-Hbl	Saxena (1968) Turner (1968)	± 80 (Dahl)

According to Dahl (1980), these methods yield average peak metamorphic temperatures of $T = 745 \pm 50$ °C for the Kelly area and $T = 675 \pm 45$ °C for the Carter Creek area (southwestern Montana). Unfortunately, these estimates may not be as accurate as stated. The Gt-Hbl temperatures are based on Saxena's (1968) empirically determined k_D^{Gt-Hbl} 's for the epidote-amphibolite ($k_D = 9.0$) and granulite ($k_D = 4.7$) facies. Figure 5-II(b) shows Saxena's original data which, as he notes, "is rather scattered." Dahl uses the very approximate temperature estimates of Turner (1968) for these two facies to calibrate the curves. A further problem is the unknown influence of Fe oxidation

FIGURE 5-II

Fe-Mg Distribution Between Coexisting
Garnet and Hornblende

Sample	$\text{Fe}^{2+}/(\text{Fe}^{2+} + \text{Mg}) \text{ Gt}$	$\text{Fe}^{2+}/\text{Sum Hbl}$	k_D
25	.733	.305	6.26
28	.866	.445	8.06
30	.597	.209	5.61
31	.759	.374	5.27
34*	.933	.532	12.25
35	.825	.414	6.67
36	.803	.368	7.00
98	.766	.334	6.53
176	.696	.288	5.66
178	.717	.312	5.59
			6.397 \pm .894 (14.0%)

Sample	$\text{Fe}_T/(\text{Fe}_T + \text{Mg}) \text{ Gt}$	$\text{Fe}_T/\text{Sum Hbl}$	k_D
25	.745	.420	4.04
28	.875	.617	4.35
30	.611	.290	3.85
31	.770	.523	3.05
34*	.937	.738	5.28
35	.834	.574	3.73
36	.816	.510	4.26
37	.833	.512	4.75
98	.779	.466	4.04
176	.709	.406	3.57
178	.732	.446	3.39
			3.902 \pm .496 (12.7%)

*Sample DT-34 not included in the calculation of average k_D .

Dotted line in Figure 5-II(a) is for $k_D = 3.9$, line for $k_D = 6.4$ not shown. The other two lines are replotted from Saxena (1968) using the data shown in Figure 5-II(b). Sum refers to the sum of all other ions which may substitute for Fe^{2+} on the crystallographic site or sites of interest.

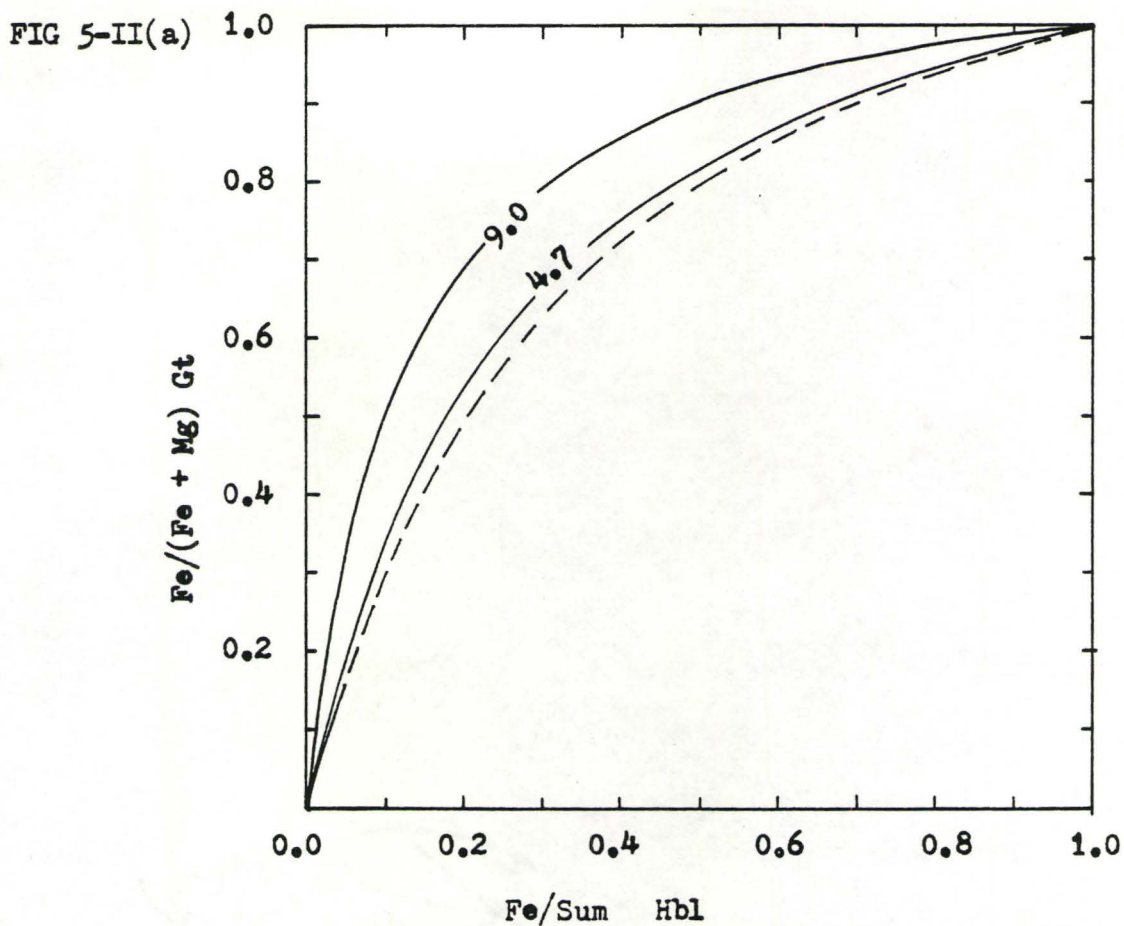
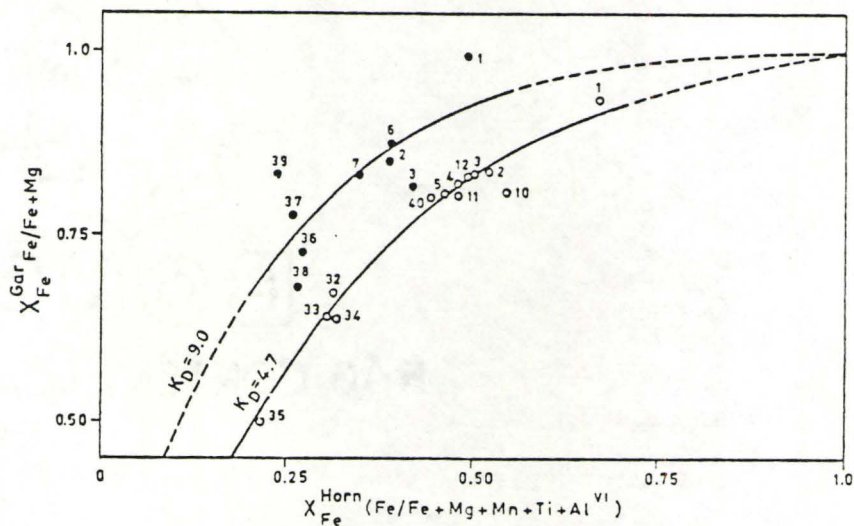


FIG 5-II(b)



Distribution of Fe and Mg between co-existing Gt-Hbl in rocks of the Epidote-amphibolite and Granulite facies (Saxena 1968).

state. Figure 5-II(a) shows k_D^{Gt-Hbl} 's calculated using the data from this thesis for $Fe = Fe^{2+}$ ($k_D = 6.4$) and $Fe = Fe_T$ ($k_D = 3.9$). These calculations indicate that the value of k_D is strongly dependent on a knowledge of Fe^{2+}/Fe^{3+} , however, this problem is dismissed by Dahl as being of minor significance. It is concluded that the thermal dependence of k_D^{Gt-Hbl} is insufficiently calibrated to allow accurate estimation of temperatures.

The other geothermometry methods employed by Dahl are considered to be more accurately calibrated, however the exact significance of the results remains controversial. Recent work (to be discussed later in this chapter) indicates that geothermometers cannot be expected to record peak metamorphic temperatures, nor can they be expected to record a unique temperature, due to differing blocking temperatures and varying response to kinetic factors. Therefore, the temperature estimates used by Dahl (1980) in the calibration of the Gt-Cpx geothermometer are considered poorly constrained.

Two further assumptions (inferred by Dahl) may also be criticised:

1. the temperature history is the same over the area from which the various samples were obtained;
2. each rock type can be expected to give the same temperature, i.e., the kinetic influence on blocking temperature is independent of the character of the system, specifically, whole rock chemistry and crystallinity.

While neither of these assumptions is likely to be valid, quantitative estimation of their importance is limited at present, due to the generally poor understanding of kinetic mechanisms in natural materials. Similar problems exist with the calibration of the Dahl isotherm. For example, the $T = 800\text{ }^{\circ}\text{C}$ isotherm is based on Opx-Cpx temperatures from charnockites (Varberg, Sweden, Saxena 1968).

In summary, the accuracy of the Dahl geothermometer and isotherm is probably at least as poor as the methods used to calibrate it. This value is estimated to be $\pm 70\text{ }^{\circ}\text{C}$ (minimum uncertainty).

5-III Orthopyroxene - Clinopyroxene Geothermometry

(i) Thermodynamic Basis of Geothermometer

Wood and Banno (1973), using experimental data on the diopside-enstatite miscibility gap (investigated at 30 kbs by Davis and Boyd 1966), derive an expression for the temperature dependence of the pyroxene compositions by considering the difference in chemical potential between the Mg components. For the exchange reaction:

$$\text{Mg}_2\text{Si}_2\text{O}_6^{\text{OPX}} + \text{Ca}_2\text{Si}_2\text{O}_6^{\text{Cpx}} = \text{Ca}_2\text{Si}_2\text{O}_6^{\text{Opx}} + \text{Mg}_2\text{Si}_2\text{O}_6^{\text{Cpx}}$$

$$T = \frac{-10202}{\ln k - 7.65 X_{\text{Fe}}^{\text{OPX}} + 3.88 (X_{\text{Fe}}^{\text{OPX}})^2 - 4.6} \quad (5-5)$$

Assuming that both orthopyroxene and clinopyroxene behave as ideal two site solutions of En and Di components, the activity of the Mg components may be calculated from:

$$a_{En}^{Cpx} = (X_{Mg}^{M2} \cdot X_{Mg}^{M1})_{Cpx}$$

$$a_{En}^{Opx} = (X_{Mg}^{M2} \cdot X_{Mg}^{M1})_{Opx}$$

Wood and Banno note that these "idealized" activities cannot be the true activities, but that they should bear some systematic relationship to the latter.

Using more recent experimental data, Wells (1977) has recalibrated the opx-cpx geothermometer as follows:

$$T = \frac{7341}{3.355 + 2.44 X_{Fe}^{OPX} - \ln k} \quad (5-6)$$

Temperatures calculated using both methods and compositional data are given in Table 5-III.

(ii) Accuracy of Calibration

Figure 5-III compares temperatures calculated using Wells (1977) with the known experimental temperatures used in the calibration of the Opx-Cpx geothermometer. The mean deviation of the calculated temperatures is ± 40 °C, with 90% lying within ± 70 °C of the known temperature. According to Wells, some of the discrepancy could be due to disequilibrium in experiments or difficulty in analyzing fine run products. A value of ± 70 °C is suggested as an estimate of the expected accuracy over the calibration range 875-1500 °C. The error associated with extrapolation to lower temperatures is generally unknown.

TABLE 5-III

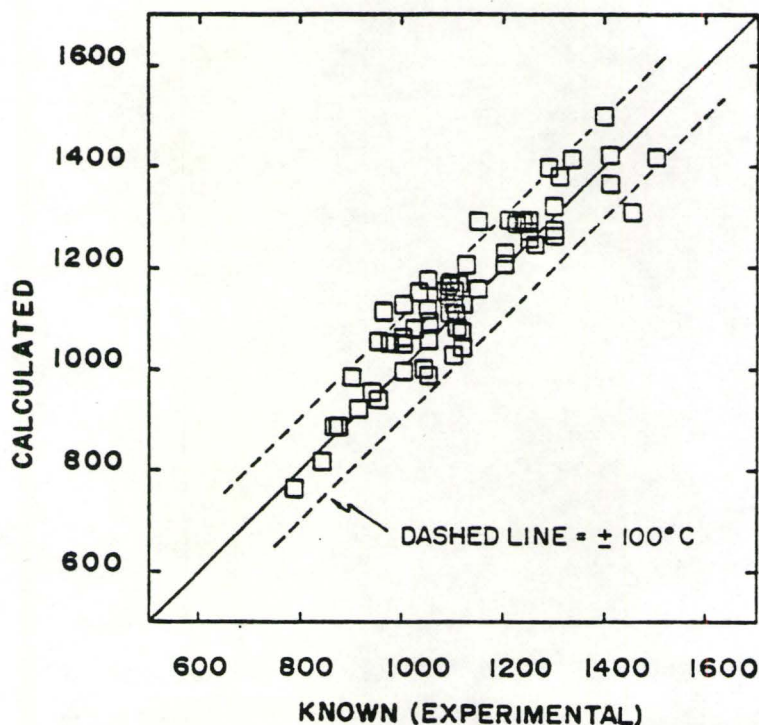
Orthopyroxene-Clinopyroxene Temperatures Calculated Using the Wood and Banno (1973) and Wells (1977) Calibrations and Compositional Data

Sample	$X_{\text{Mg}_2\text{Si}_2\text{O}_6}^{\text{Cpx}}$	$X_{\text{Mg}_2\text{Si}_2\text{O}_6}^{\text{Opx}}$	$X_{\text{Fe}}^{\text{Opx}}$	$X^{\text{Cpx}}/X^{\text{Opx}}$	T_{WB}^1	T_{W}	T_{Ave}
DT-24	0.0355	0.2739	0.4332	0.130	832.3	864.1	848.2
DT-25	0.0320	0.2529	0.4376	0.127	827.2	857.9	842.6
DT-30	0.0223	0.3443	0.3623	0.065	789.6	779.2	784.4
DT-32	0.0223	0.2342	0.4891	0.095	771.6	790.8	781.2
DT-33	0.0283	0.2710	0.4548	0.104	796.7	818.6	807.7
DT-98	0.0207	0.2354	0.4879	0.088	763.6	779.1	771.4
DT-174	0.0204	0.2044	0.5053	0.100	770.1	791.9	781.0
DT-176	0.0187	0.2750	0.4301	0.068	761.5	761.9	761.7
DT-177	0.0327	0.2382	0.4604	0.137	825.6	862.5	844.1
L2-199 ²	0.0376	0.2123	0.4965	0.177	839.6	892.5	865.8

1. Temperatures in °C.

2. Sample from Mummery (1972).

COMPARISON OF KNOWN VS
CALCULATED TEMPERATURE:
WELLS GEOTHERMOMETER



According to Lindsley (1981, personal communication 1981), Wood and Banno's assumption of ideality is not justified. Recent experiments in the system $\text{CaSiO}_3 - \text{MgSiO}_3 - \text{FeSiO}_3$ (Turnock and Lindsley 1981) indicate that for Mg rich compositions, the Wells calibration gives temperatures which are 187-258 C° too high, while the Wood and Banno calibration gives temperatures which are 130-223 C° too high. For Fe rich compositions, the Wood and Banno temperatures are too low and the Wells temperatures are too high.

The pyroxenes studied in this thesis are predominantly Fe rich, therefore the two methods are expected to bracket the true temperature.

5-IV Significance of Calculated Temperatures: Discussion

The distribution of garnet-clinopyroxene and orthopyroxene-clinopyroxene temperatures, calculated using the methods outlined above, is shown in Figure 5-IV. Sample locations are shown in Figure 5-V and Figure 5-VI. The Ellis and Green (1979) and Dahl (1980) values show good agreement, indicating an average final equilibration temperature of 750 °C (precision = ± 45 °C, accuracy = ± 70 °C). The garnet-clinopyroxene data from Mummery (1972) give more varied results. Garnets along the western margin of the anorthosite (see Table 5-I) have increased X_{Ca}^{Gt} and decreased X_{Fe}^{Gt} , therefore, the Dahl geothermometer should give the best temperature estimation, on the basis that the Sum X parameter is more sensitive to compositional variation than the single X_{Ca}^{Gt} correction term present in the Ellis and Green calibration. The Dahl geothermometer gives an average value of 628 °C (precision = ± 30 °C), while the Dahl isotherm gives $T = 668$ °C (estimated accuracy = ± 70 °C). Due to this discrepancy, in addition to the calibration problems with the Dahl geothermometer discussed above, the preferred value for the western margin is 670 °C (estimated precision = ± 45 °C, accuracy = ± 70 °C), which covers the range in values obtained from Ellis and Green, and Dahl.¹ The lower temperature for the western margin indicates a decrease in temperature of 80 °C (estimated precision = ± 90 °C) from

1. The temperatures calculated using the data from Mummery should be considered tentative estimates, because it was necessary to alter most of the analyses to give reasonable totals and structural formulas. These changes were made completely at the author's discretion, consequently, the resultant chemical analyses are approximations only.

FIGURE 5-IV

Clinopyroxene-Garnet and Orthopyroxene-Clinopyroxene
Temperatures from Granulite Facies Gneisses
in the Whitestone Area

- (a) Temperatures for Western margin of Whitestone Anorthosite using data from Mummery (1972). DI = Dahl isotherm, uncertainty is estimated. Dahl = calibration from Dahl (1980), uncertainty given is 1 sigma. E & G = calibration from Ellis and Green (1979), uncertainty given is 1 sigma.
- (b) Temperatures for Eastern margin of Whitestone Anorthosite, values calculated using calibration of Dahl (1980), uncertainty given is 1 sigma. Uncertainty in Dahl isotherm is estimated. Pressure in kbs.
- (c) Temperatures calculated using the calibration of Ellis and Green (1979), Eastern margin, uncertainty given in 1 sigma.
- (d) Average temperature calculated using calibration of Wood and Banno (1973), and Wells (1977), Eastern margin, uncertainty given is 1 sigma.

Frequency of Observation

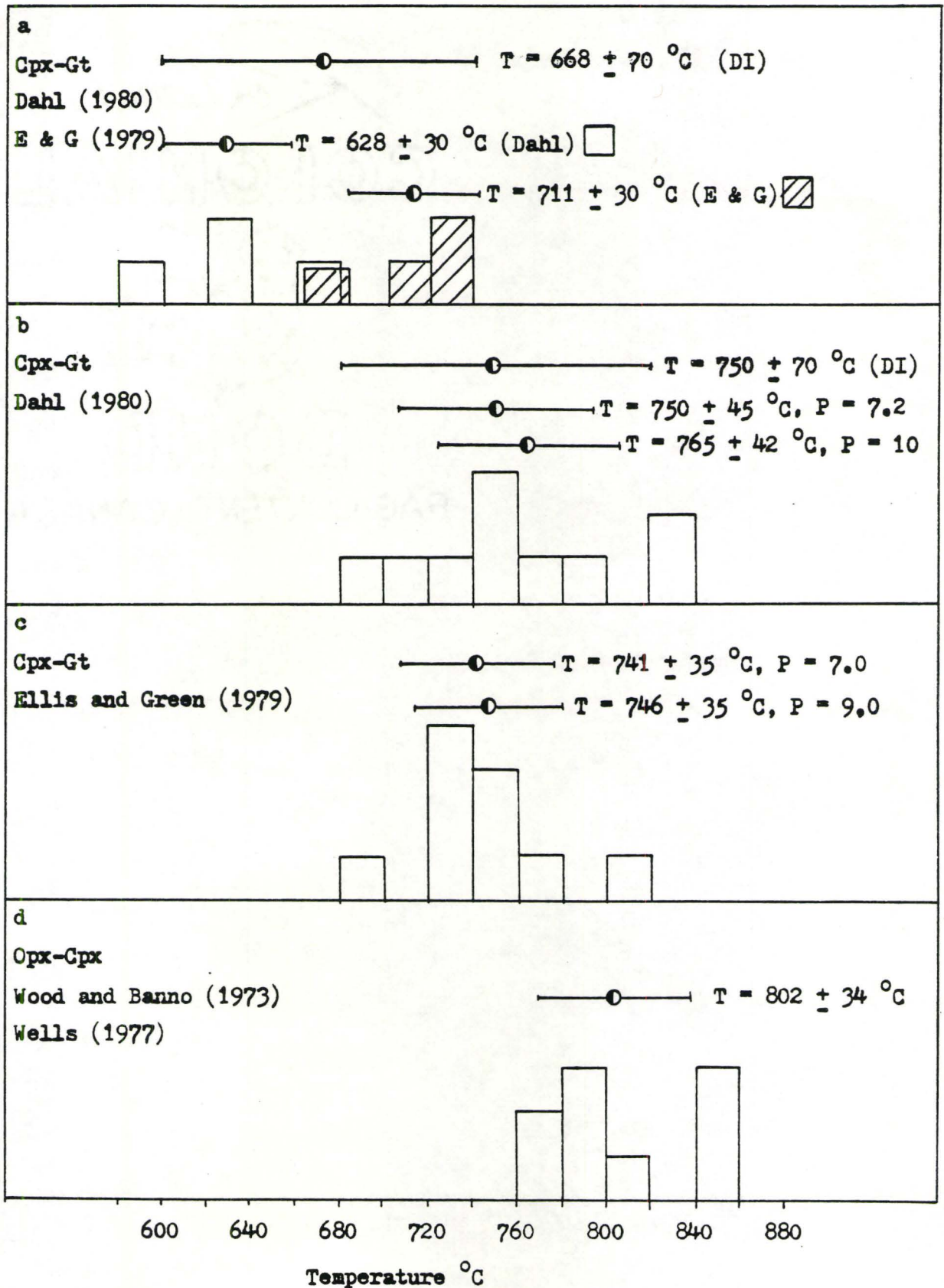


FIG 5-V Location of Samples Used in Temperature Determinations

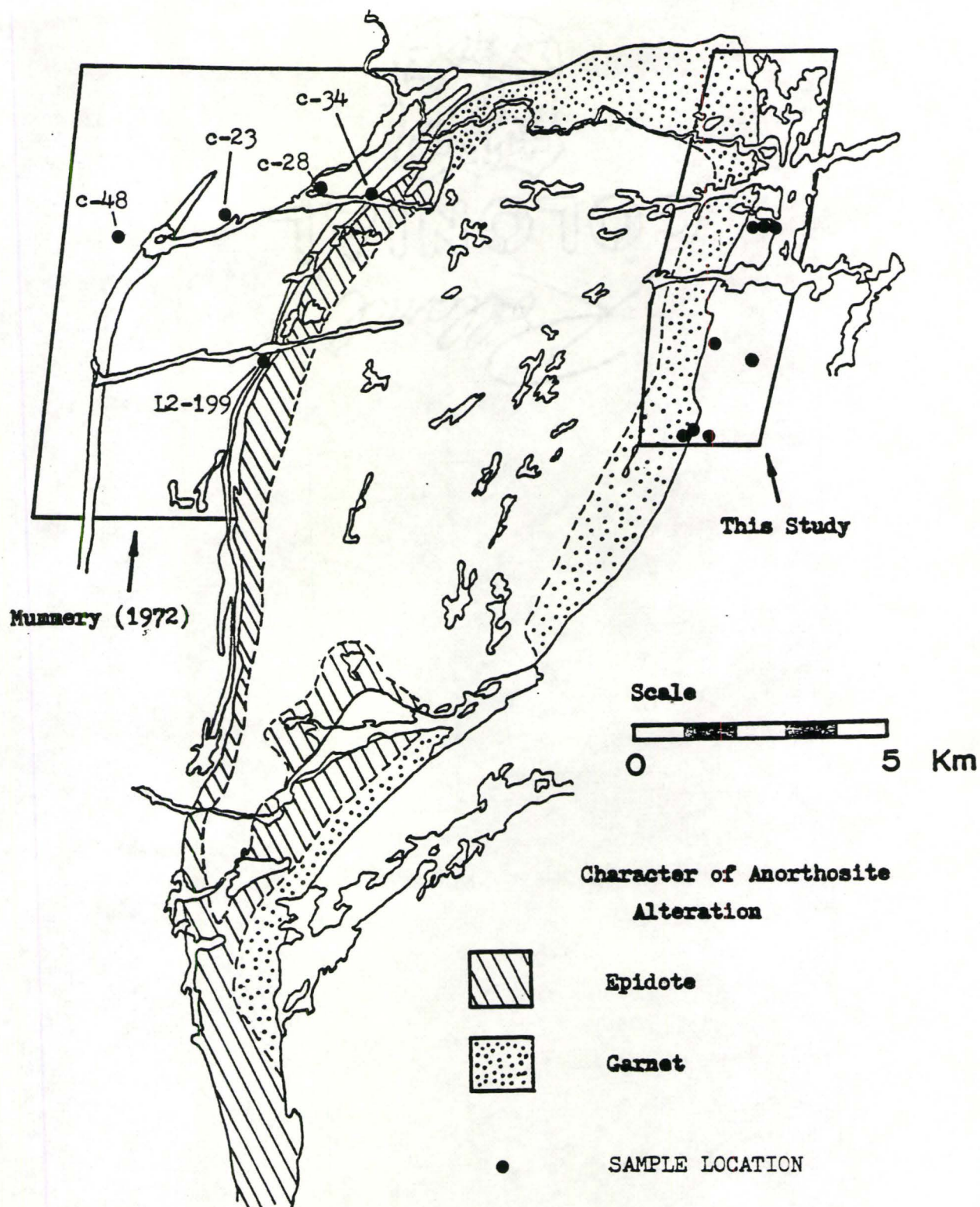
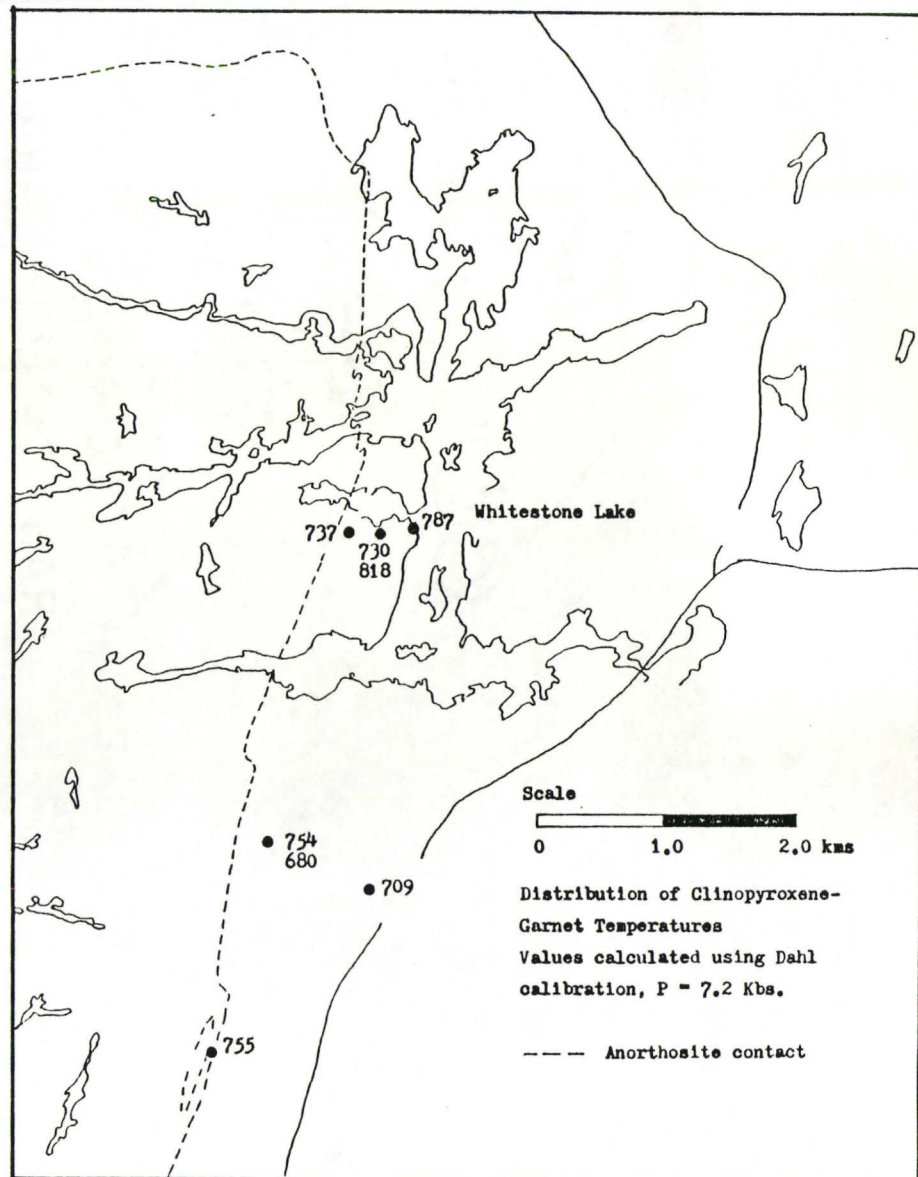
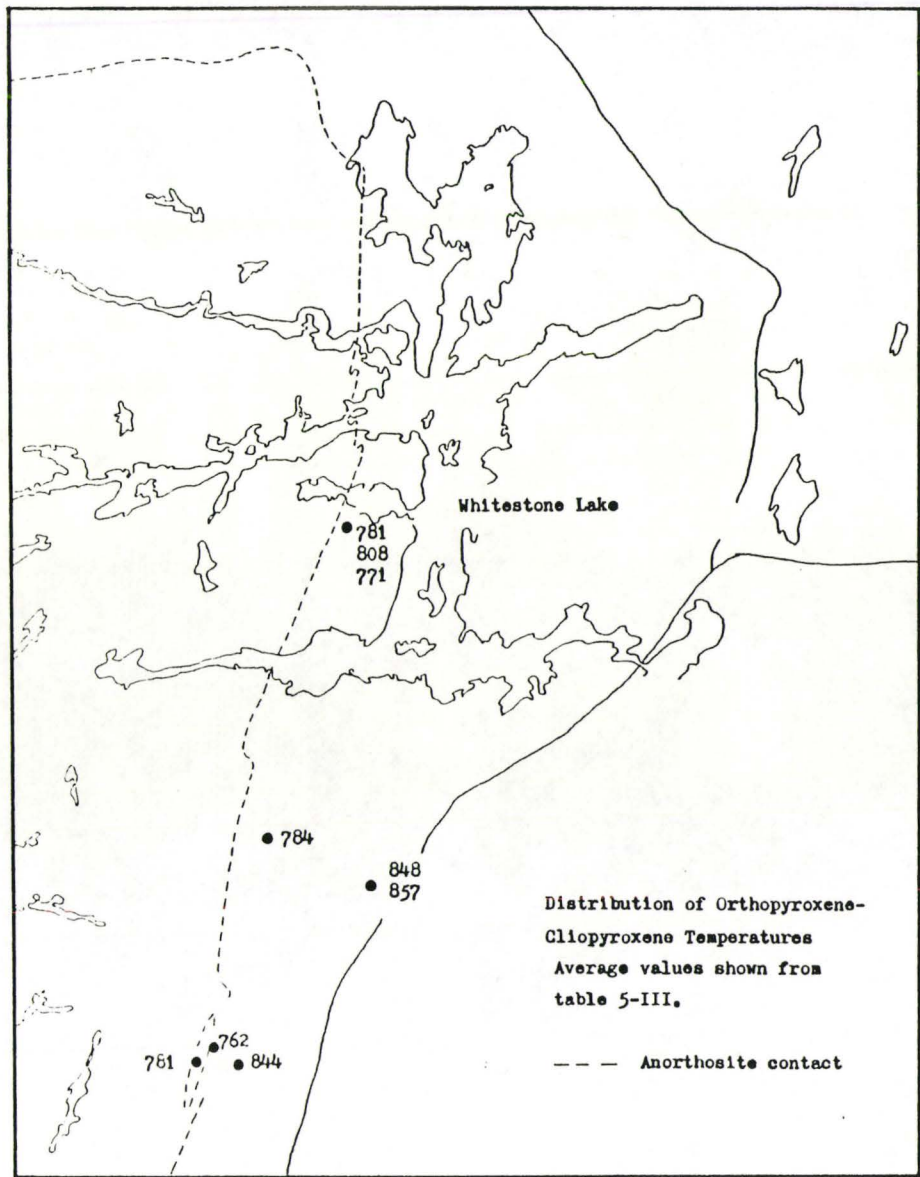


FIG 5-VI Distribution of Calculated Temperatures



east to west.

The average orthopyroxene-clinopyroxene temperature (obtained from an average of Wood and Banno 1973, and Wells 1977) is 802 °C (precision = ± 34 °C, accuracy = ± 70 °C). The lowest values are obtained from samples taken close to the anorthosite (see Figure 5-VI). It is possible that these assemblages originally formed at a temperature in excess of 850 °C, but have been partially to completely re-equilibrated to a lower temperature. They may also be non-equilibrium assemblages. Further discussion of the retrograde nature of these assemblages, as well as the significance of the apparent temperature gradient from east to west, will be deferred until several related observations have been presented.

At this point, it is appropriate to consider a more fundamental question: what do the measured temperatures actually represent?

There are three important points to be considered here:

1. What physio-chemical event(or solid state process) occurs at the time the temperature is locked in, i.e., what determines the blocking temperature?
2. Do calculated values represent peak metamorphic temperatures?
3. Is the blocking temperature fixed, i.e., is it independent of whole rock chemistry and kinetic history?

Up until recently, most workers assumed that the temperatures obtained using geothermometry represented (or closely approached) peak

metamorphic temperatures (Hewins 1975, Hensen 1977, Berg 1977, Bohlen and Essene 1977, 1979, Bohlen et al. 1980). The rather ill-defined basis for this belief is the common observation that many high grade assemblages, which exhibit only minor retrograde alteration, otherwise appear to be completely preserved. The normally accepted explanation for this phenomenon is that reverse reactions are kinetically unfavourable, therefore, upon relaxation of metamorphic conditions the highest grade assemblage is "frozen in". This metastable assemblage will persist indefinitely providing the system is not reactivated. While this concept is broadly true, recent workers (Stormer and Whitney 1977, O'Hara and Yarwood 1978, Dahl 1979, Stoddard 1980, Savage and Sills 1980) have demonstrated that many assemblages re-equilibrate to lower temperatures upon cooling. For slowly cooled, high grade terrains, the following general trend is apparent:

Highest T: comparison of the co-existing minerals with the existing petrogenetic grid.

Very high temperatures and pressures have been suggested, however, they are rarely supported by calculated values.

Intermediate
to high T: e.g., Gt-Cpx, Opx-Cpx, 700-900 °C, higher in some cases.

Intermediate
to low T: two-feldspar, two-oxide, 500-800 °C, variable but commonly lower than the above methods.

Lowest T: e.g., calcite-dolomite, quartz-magnetite
($0^{18}/0^{16}$), variable but commonly the lowest temperature of any method.

While there are exceptions to this general trend, it is apparent that the co-existing mineral pairs discussed above cannot necessarily be expected to record peak metamorphic temperatures, nor can they be expected to give coincident temperatures even under the same metamorphic conditions. The blocking temperature is generally thought to represent the threshold value, below which diffusion between co-existing minerals is not rapid enough to sustain equilibrium, however, it is very difficult to define this value. Below the peak metamorphic temperature (but above the so-called blocking temperature), diffusion will still occur, but it is debatable whether equilibrium is always achieved. In addition to temperature, the diffusion rate of any one particular ion is also dependent on the composition, orientation, and structural state of the mineral in which it is diffusing, as well as the density of dislocations and the presence of volatiles.¹ Minerals exhibiting complex chemical gradients have been reported by several workers (Hess 1971, Lonkers 1980), in which the variation shown by any one particular mineral is directly related to the surrounding minerals with which it is

1. For an introduction to recent developments in the kinetics of mineral reactions (particularly the structural and compositional dependency of diffusion mechanisms and rates), see: Loomis 1967, 1977, 1982, Brady 1975, Anderson and Buckley 1974, Nicolas and Poirier 1976, Putnis and McConnell 1980, Lasaga 1981, Onorato et al. 1981, Li 1981, Nolfi 1981, Freer 1981, Graham 1981, and Tracy and Dietsch 1982.

in contact. With respect to the entire system (active during prograde metamorphism), these localized ion exchange reactions are non-equilibrium.

It should be possible in theory, to calculate the volume over which equilibrium might be expected using existing silicate diffusion data. Since many of the processes of interest involve the simultaneous counter-movement of two or more related ions, the diffusion data should ideally be of the interdiffusion type. Unfortunately, there is little experimental data of this type available on major element diffusion in the silicates of interest in this study (garnet, hornblende and pyroxene). Recent work by Freer (1982), suggests that an average value for Ca, Mg, and Al diffusion rates in pyroxenes (under dry conditions) would be $D = 10^{-15} \text{ cm}^2 \text{ s}^{-1}$ at 1200 °C, at 800 °C, the value varies from $D = 10^{-17}$ to $10^{-22} \text{ cm}^2 \text{ s}^{-1}$. For these values of D , ions could be expected to diffuse only a distance of 0.56 to 0.0017 mm over a period of 10 Ma. Freer (1982) suggests that the pyroxenes should be amongst the slowest to reach equilibrium and therefore have the highest blocking temperatures.

A further problem, closely associated with the observations discussed above, is the recognition of equilibrium assemblages. It is commonly assumed that regular element distributions between co-existing minerals indicate a close approach to equilibrium (Kretz 1959, 1960, 1961, 1963, 1964, 1978, Muller and Saxena 1977, Lonkers 1980). The k_D for the Fe-Mg distribution between the co-existing minerals studied in this thesis is shown in Figure 5-VII (i) to (viii). For the distribution

of two components between two ideal solid solutions these curves obey the relation:¹

$$\frac{X_1 (1 - X_2)}{X_2 (1 - X_1)} = k_D = \text{a constant at fixed P and T}$$

where: X_1 = the mole fraction of component 1 in solid solution 1

X_2 = the mole fraction of component 1 in solid solution 2.

Unfortunately, few solid solutions of geological interest are ideal and there is the further problem of determining the best atomic ratio to represent mole fraction; consequently (as has been noted by Kretz 1977) these curves are largely empirical in nature.

Most of the curves in Figure 5-VII display systematic relationships, thus indicating equilibrium conditions. However, there are several problems with this interpretation. The biotite grains analyzed are very small (< .01 mm) retrograde blades and rosettes which are clearly not in equilibrium with the entire system. Garnet-orthopyroxene and garnet-clinopyroxene pairs, which also appear to be in equilibrium, give discordant temperatures, indicating that: either one of these mineral pairs is giving an erroneous apparent temperature (due to non-equilibrium), or that one or both of the geothermometers is incorrectly calibrated. A partial explanation for the orderly trends exhibited by

1. These diagrams are commonly called Roozenboom plots or distribution diagrams. For a full discussion of the assumptions involved in their development, see Kretz (1961).

FIGURE 5-VII

Mineral - Mineral Element Distributions

(i) Gt - Cpx

Sample	Fe/Mg Gt	Fe/Mg Cpx	k_D
28	.866	.468	7.35
25	.733	.292	6.66
30	.597	.209	5.61
32	.747	.330	5.60
34	.933	.631	8.14
35	.825	.441	5.98
36	.803	.394	6.27
98	.766	.339	6.38
176	.696	.268	6.25

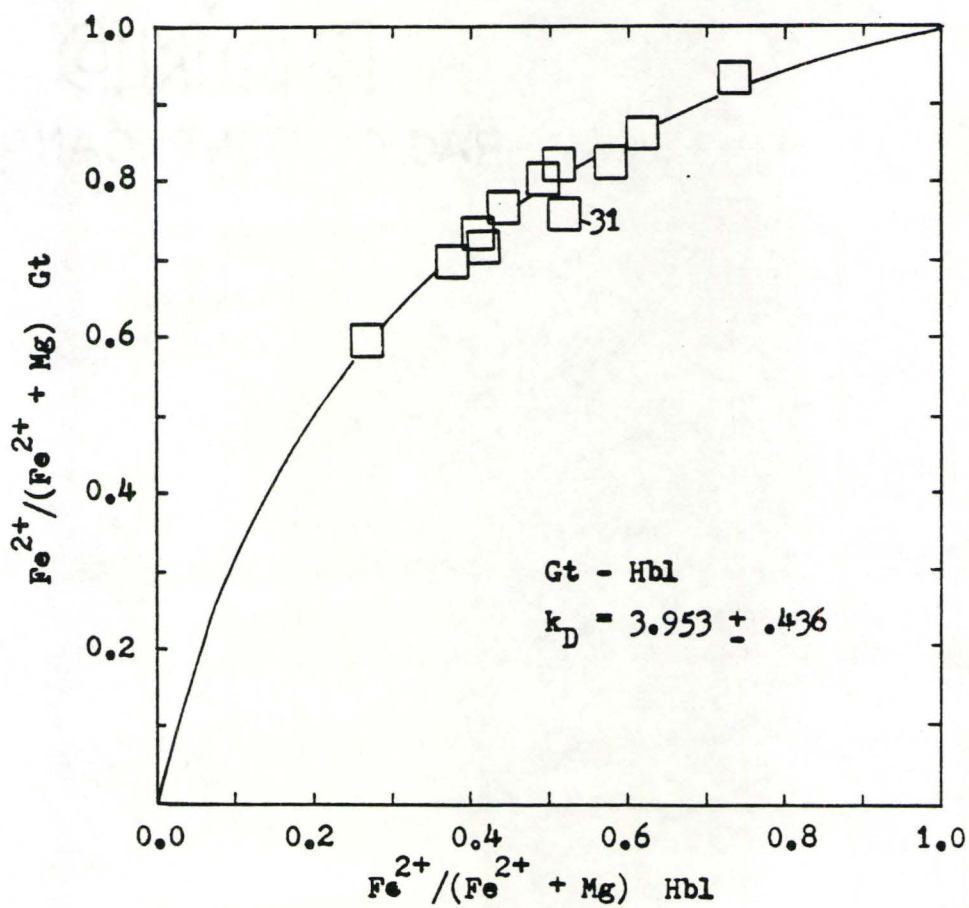
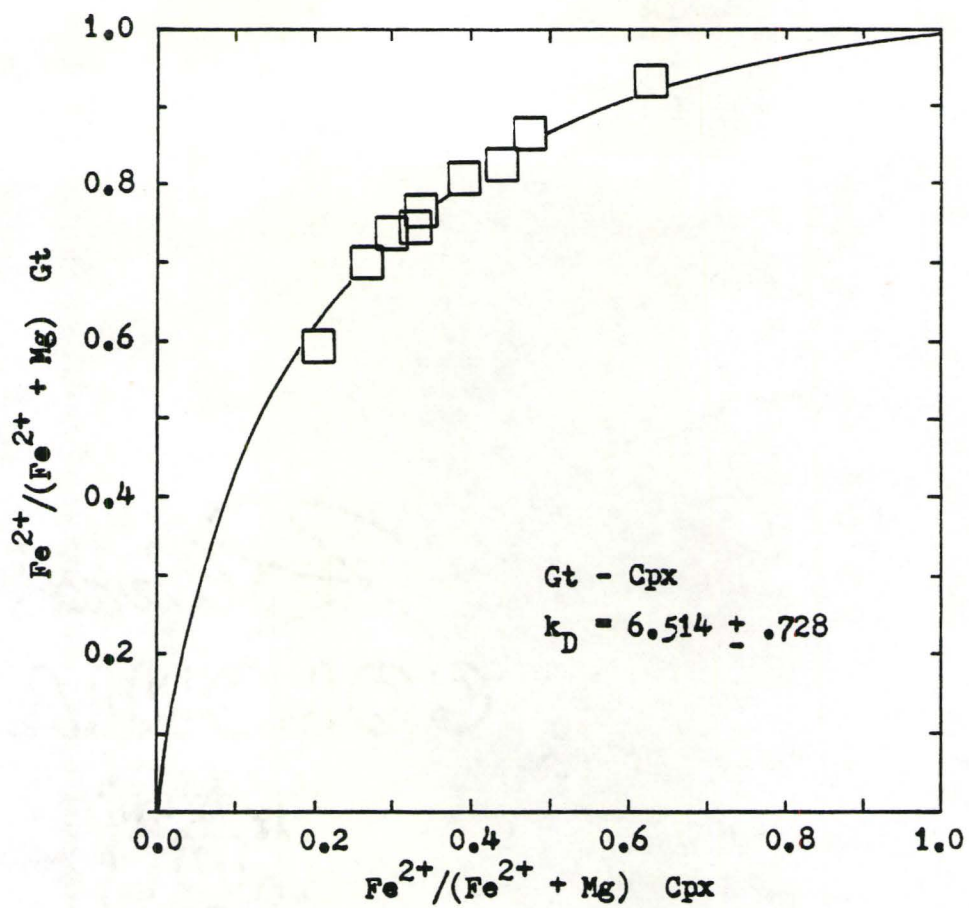
Ave. = $6.514 \pm .782$ (12.0%)

(ii) Gt - Hbl

Sample	Fe/Mg Gt	Fe/Mg Hbl	k_D
25	.733	.410	3.95
28	.866	.620	3.96
30	.597	.271	3.99
31*	.759	.521	3.44
34	.933	.741	4.87
35	.825	.583	3.37
36	.803	.495	4.16
37	.821	.511	4.39
98	.766	.446	4.07
176	.696	.378	3.77
178	.717	.418	3.53

Ave. = $3.953 \pm .436$ (11.0%)

*Sample DT-31 not included in calculation of Ave. k_D .



Mineral - Mineral Element Distributions

(iii) Gt - Bt

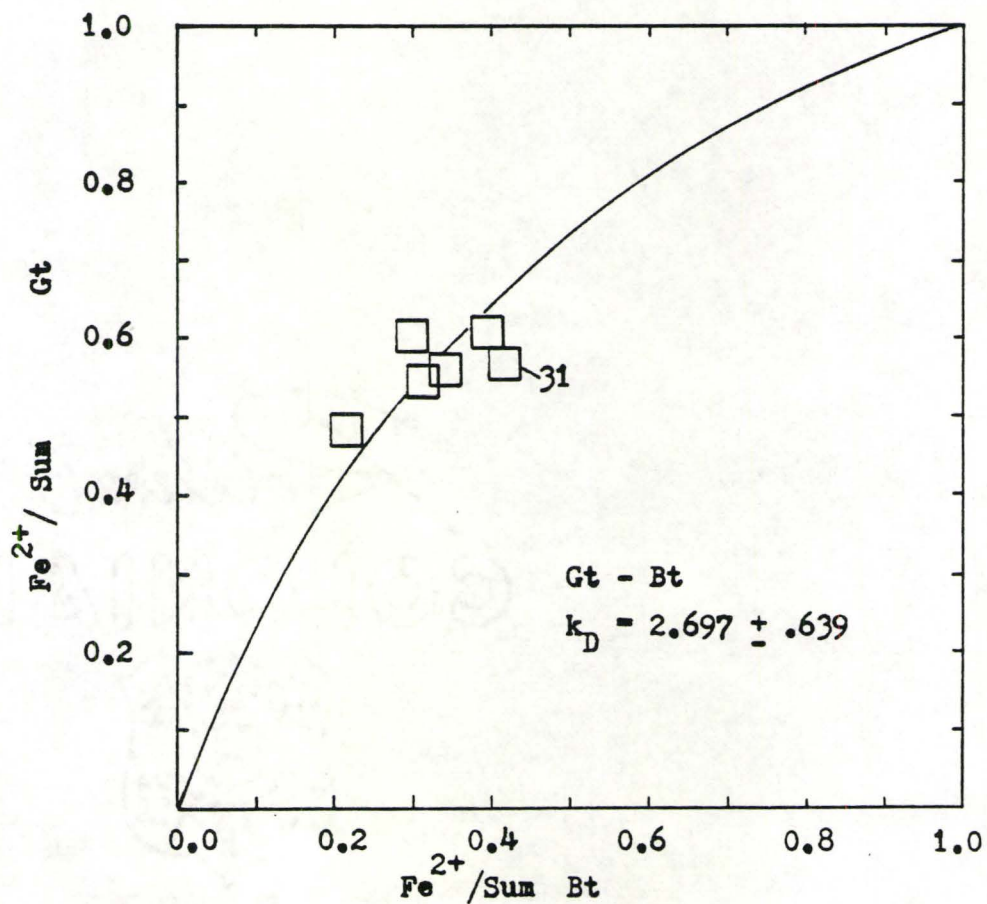
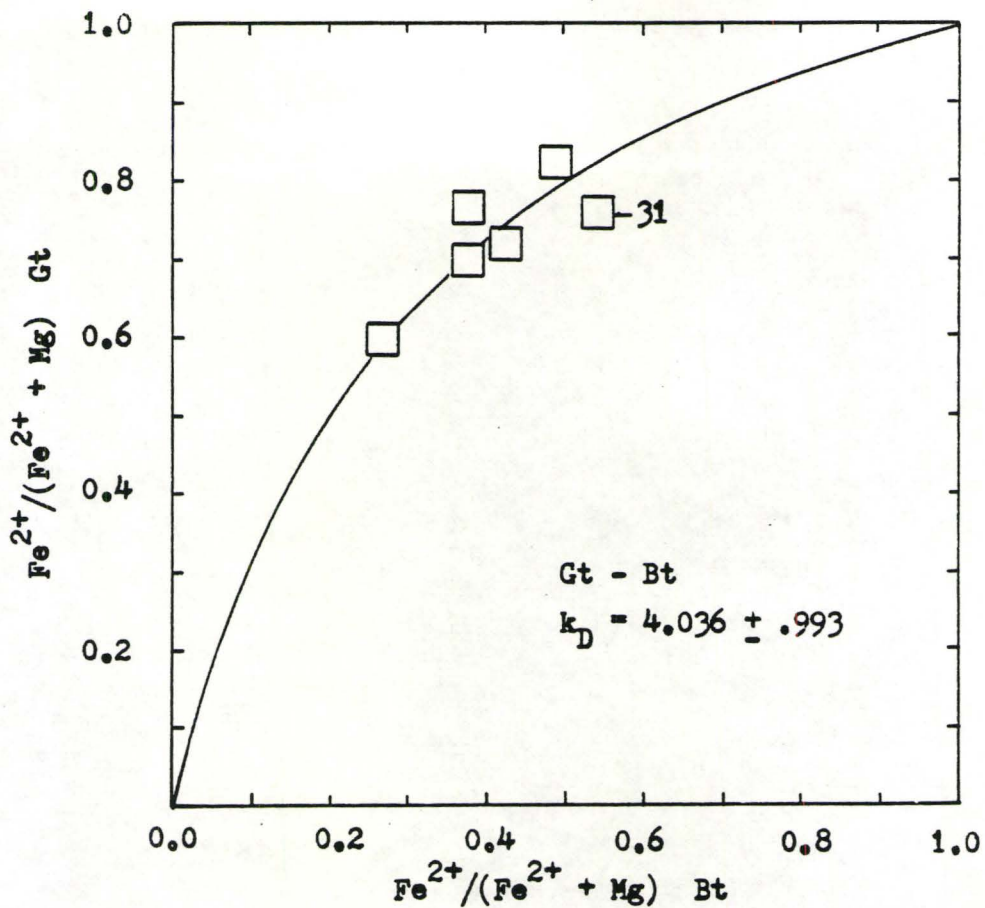
Sample	Fe/Mg Gt	Fe/Mg Bt	k_D
30	.597	.269	4.03
31	.759	.541	2.67
37	.821	.489	4.79
98	.766	.347	5.48
176	.696	.375	3.82
178	.717	.425	3.43

Ave. = $4.036 \pm .993$ (24.6%)

(iv) Gt - Bt

Sample	Fe/Sum Gt	Fe/Sum Bt	k_D
30	.482	.217	3.36
31	.570	.419	1.84
37	.608	.398	2.35
98	.602	.300	3.53
176	.545	.312	2.64
178	.560	.340	2.47

Ave. = $2.697 \pm .639$ (23.7%)



Mineral - Mineral Element Distributions

(iv) Opx - Hbl

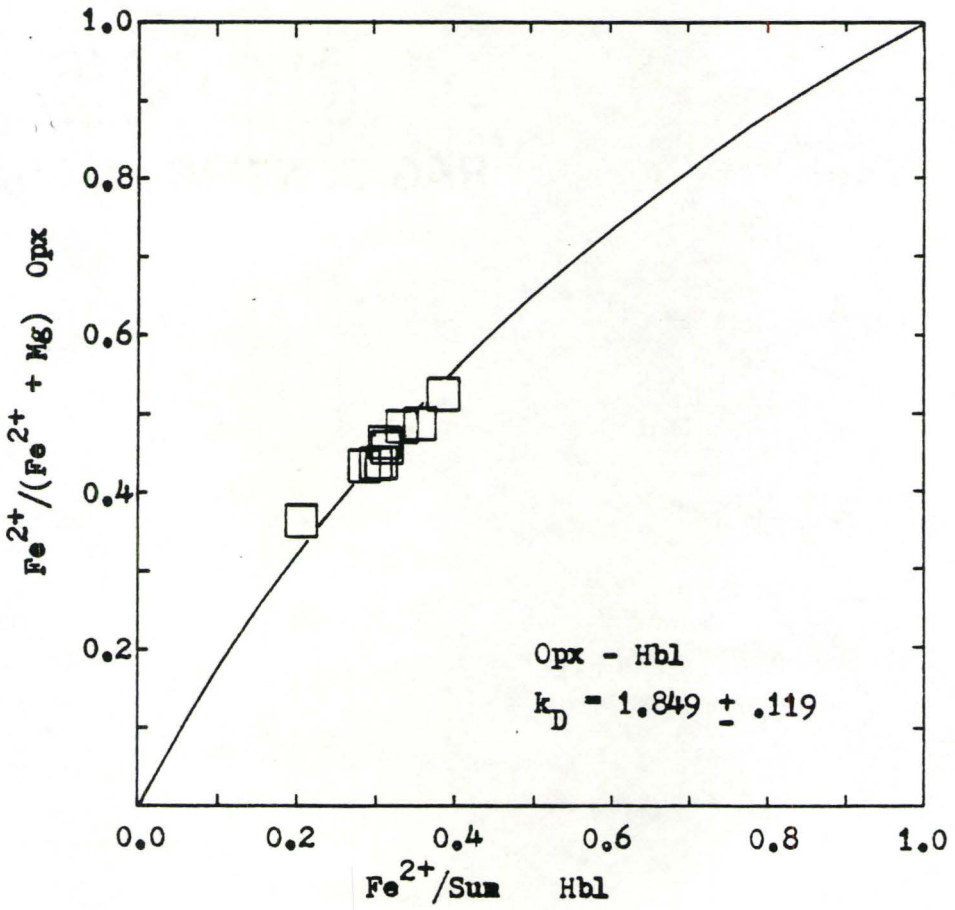
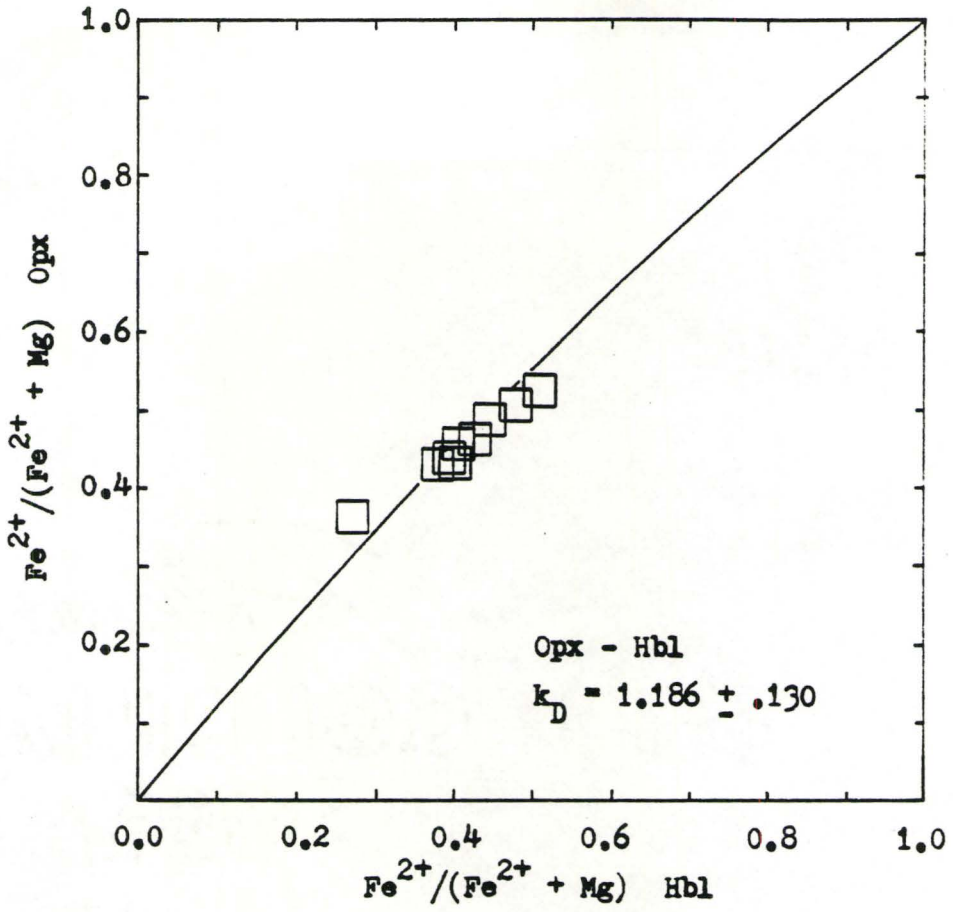
Sample	Fe/Mg Opx	Fe/Mg Hbl	k_D
24	.433	.398	1.16
25	.438	.410	1.12
30	.362	.271	1.53
32	.489	.467	1.09
33	.455	.410	1.20
37	.526	.511	1.06
98	.488	.446	1.18
174	.505	.474	1.13
176	.430	.378	1.24
177	.460	.426	1.15

Ave. = $1.186 \pm .130$ (11.0%)

(v) Opx - Hbl

Sample	Fe/Mg Opx	Fe/Sum Hbl	k_D
24	.433	.306	1.73
25	.438	.305	1.78
30	.362	.209	2.15
32	.489	.353	1.75
33	.455	.313	1.83
37	.526	.385	1.77
98	.488	.334	1.90
174	.505	.357	1.84
176	.430	.288	1.87
177	.460	.313	1.87

Ave. = $1.849 \pm .119$ (6.4%)



Mineral - Mineral Element Distributions

(vi) Opx - Cpx

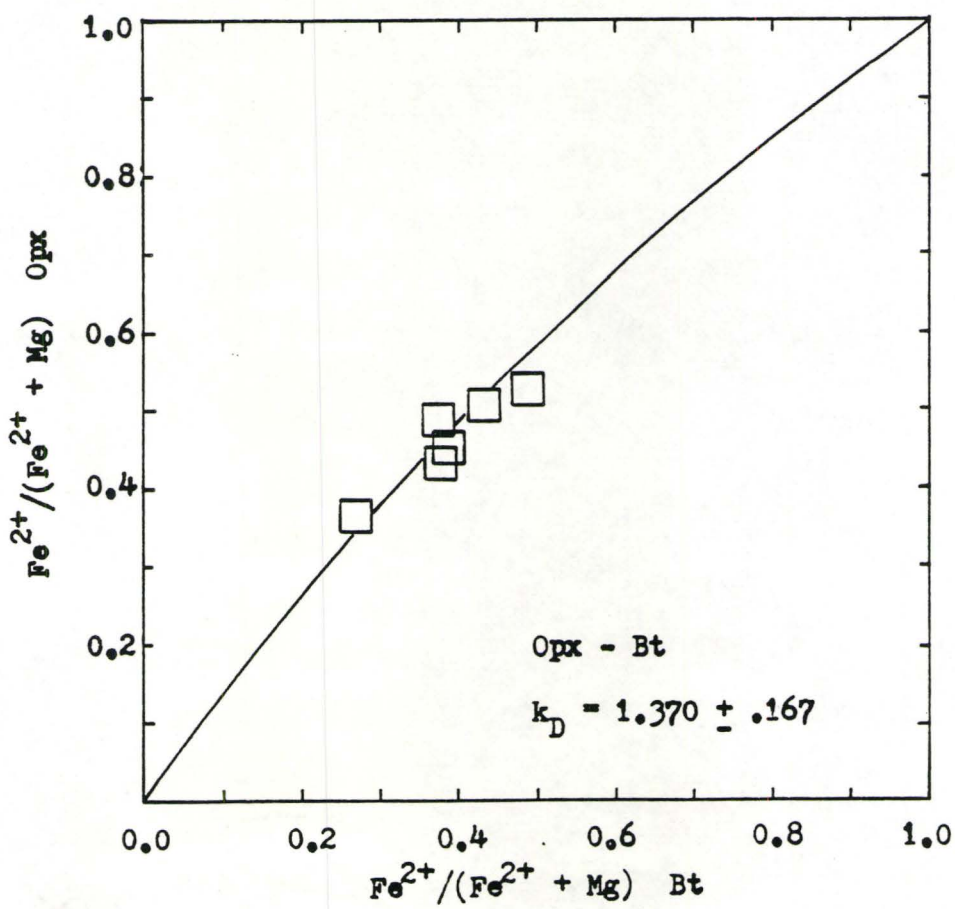
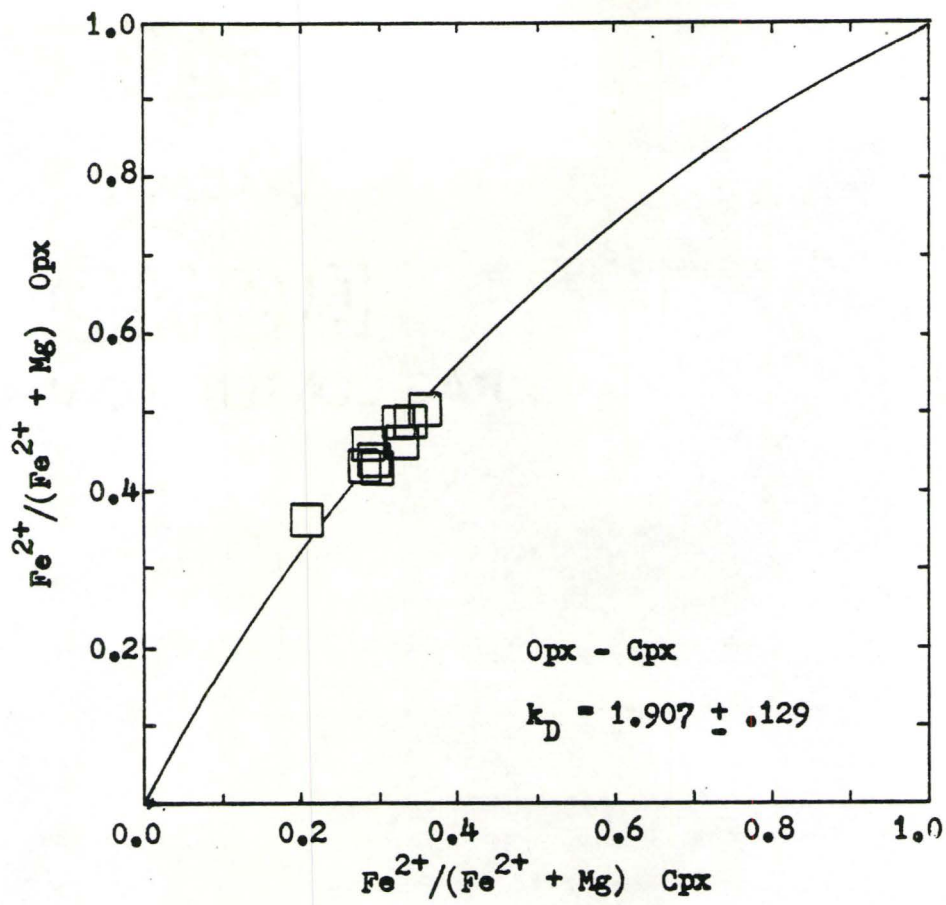
Sample	Fe/Mg Opx	Fe/Mg Cpx	k_D
24	.433	.294	1.83
25	.438	.292	1.89
30	.362	.209	2.15
32	.489	.330	1.94
33	.455	.288	2.06
98	.488	.339	1.86
174	.505	.360	1.81
176	.430	.286	1.88
177	.460	.330	1.73

Ave. = $1.907 \pm .129$ (6.7%)

(vii) Opx - Bt

Sample	Fe/Mg Opx	Fe/Mg Bt	k_D
30	.362	.269	1.54
33	.455	.387	1.32
37	.526	.489	1.16
98	.488	.374	1.60
174	.505	.432	1.34
176	.430	.375	1.26

Ave. = $1.370 \pm .167$ (12.2%)

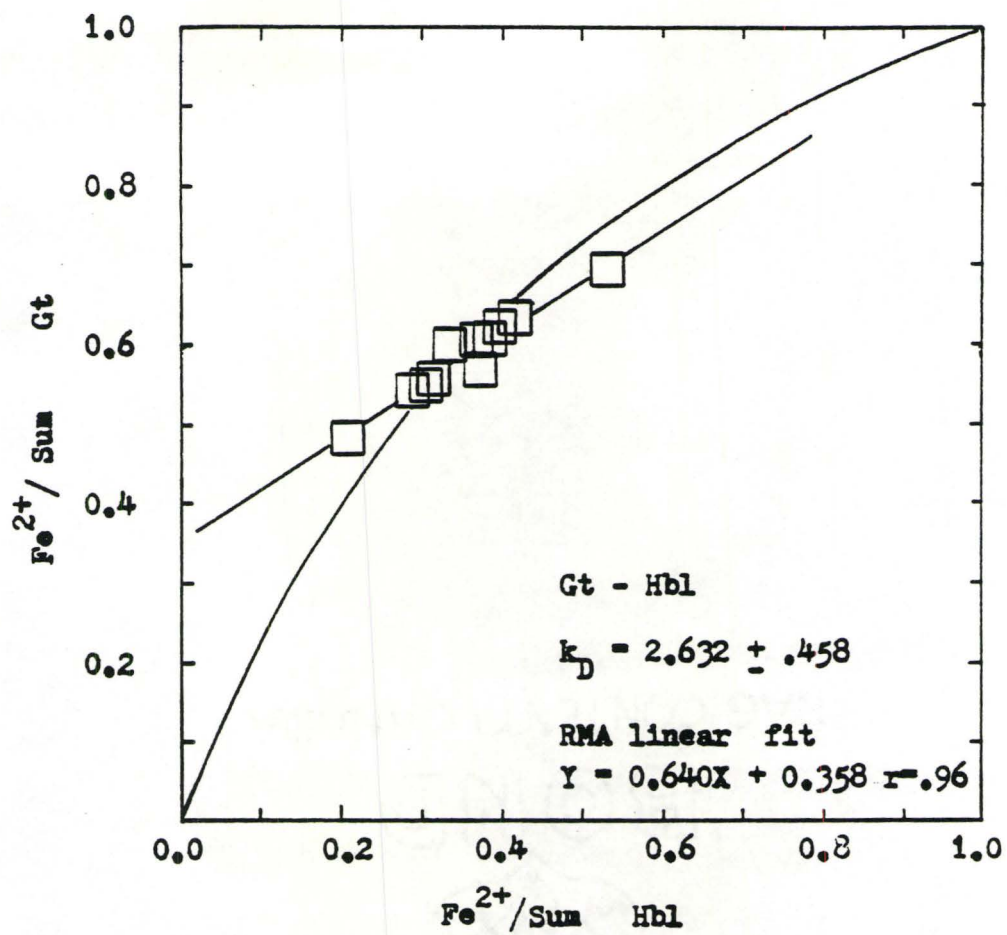


Mineral - Mineral Element Distributions

(viii) Gt - Hbl

Sample	Fe/Sum Gt	Fe/Sum Hbl	k_D
25	.555	.305	2.84
28	.623	.445	2.06
30	.482	.209	3.52
31	.570	.374	2.22
34	.693	.532	1.99
35	.632	.414	2.43
36	.605	.368	2.63
37	.608	.385	2.48
98	.602	.334	3.02
176	.545	.288	2.96
178	.560	.312	2.81

Ave. = $2.632 \pm .458$ (17.4%)



the distribution diagrams is shown in Figure 5-VIII. This plot demonstrates, as one might expect, that there is a strong correspondence between the whole rock and mineral Fe/Mg ratios, regardless of the state of equilibrium.

I conclude from these observations that retrograde (or partially re-equilibrated prograde) minerals can be expected to reflect the Fe/Mg ratio of the system in which they are reacting. Very well defined element distributions (such as the Gt-Cpx and Gt-Hbl curve, Figure 5-VII (i) and (ii)) may indicate equilibrium conditions. However, approximately linear (but scattered) distributions (Opx-Hbl and Opx-Bt, Figures 5-VII (iv) and (vii)) cannot be accepted as evidence of equilibrium. In fact, depending on the choice of atomic ratio chosen to represent the mole fraction of a component, many of these curves can be fit equally well to a linear relationship. This is shown clearly in Figure 5-VII (viii), where the atomic fraction of Fe in garnet is calculated as $X_{Fe}^{Gt} = Fe^{2+} / (Fe^{2+} + Mn + Mg + Ca)$, which gives a very different trend from Gt-Hbl distribution shown in Figure 5-VII (ii). This supports the hypothesis that we may be observing a crude relationship imposed by the whole rock chemistry of the system and not necessarily by an equilibrium assemblage.

The use of rim compositions has been recommended by some authors for the calculation of equilibrium temperatures, particularly in studies of retrograde metamorphism. While there are examples in the literature which appear to give good results (see for example, Russell 1981), all too often little effort is made to demonstrate equilibrium.

FIGURE 5-VIII

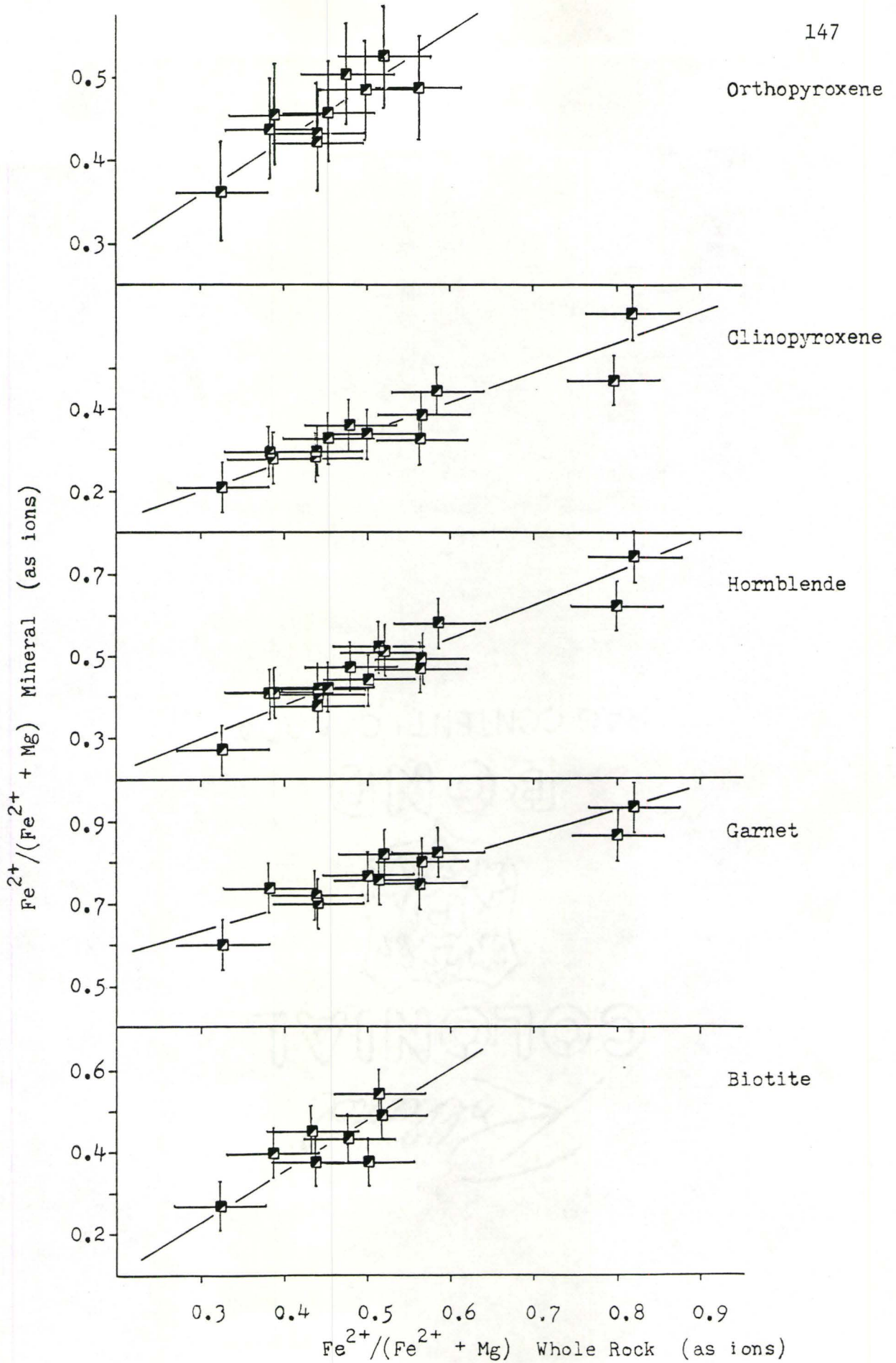
Whole Rock - Mineral Fe/Mg Distribution

Straight lines have been fit using the Reduced Major Axis Method.

Orthopyroxene	$Y = 0.662X + 0.162$	$r = .84$
Clinopyroxene	$Y = 0.713X - 0.011$	$r = .93$
Hornblende	$Y = 0.801X + 0.062$	$r = .93$
Garnet	$Y = 0.584X + 0.458$	$r = .91$
Biotite	$Y = 1.206X - 0.130$	$r = .80$

Mineral chemistry determined by microprobe, Fe^{2+}/Fe^{3+} by Mossbauer.

Whole Rock chemistry by XRF, Fe^{2+}/Fe^{3+} by titration. Error bars represent the precision (maximum expected error) in the determination of the Fe/Mg ratio. The accuracy of the whole rock compositions is decreased due to analyses of inhomogeneous samples. The magnitude of this error is generally unknown and is not considered in this plot.



To test the possibility of generating an erroneous result, Gt-Bt temperatures have been calculated using the mineral data from this thesis and the calibration of Ferry and Spear (1978). An average of five determinations (using garnet core compositions) gives a very reasonable, but completely fortuitous, temperature of $665\text{ }^{\circ}\text{C}$ (precision $\pm 60\text{ }^{\circ}\text{C}$).

5-V Summary

The average garnet-clinopyroxene value of $750 \pm 70\text{ }^{\circ}\text{C}$ is considered to represent the most accurate temperature determination. This is supported by the very regular Fe/Mg distribution shown in Figure 5-IV. Core compositions have been used in all calculations on the basis that they are the most representative of equilibrium conditions at the time of crystallization. The orthopyroxene-clinopyroxene temperatures may indicate partial re-equilibration of a pre-existing higher temperature assemblage.

The quoted inaccuracy in the geothermometer calibrations ($\pm 70\text{ }^{\circ}\text{C}$ for Gt-Cpx, Dahl 1980, and $\pm 70\text{ }^{\circ}\text{C}$ for Opx-Cpx, Wells 1977) is great enough to explain the observed disagreement, therefore, while it is suspected that a real temperature difference does exist, it is not possible to prove this supposition with the available data.

CHAPTER 6

REACTION RIM SLAB STUDY

6-I Introduction

As was noted in Chapter 2, the mineral assemblage garnet-clinopyroxene-opaques-plagioclase-apatite is of special significance, because its degree of development (particularly in mafic gneiss) appears to be directly related to the proximity of the anorthosite contact.

For example, outcrop 37 (sample DT-57)¹ shows a sharp increase in the development of this mineral assemblage over a distance of 10-20 meters as one approaches the contact. Right at the contact, the rock is a dark rusty red colour due to the increased concentration of garnet, clinopyroxene, and opaques, while hornblende is almost completely absent. Understanding the controls on the development of this assemblage is complicated by the fact that it occurs (locally) in a number of other locations throughout the study area (see Mineral Facies Map).

Approximately 300 meters from the anorthosite contact is an outcrop of mafic gneiss, exhibiting small leucocratic "pods" surrounded by a reaction rim rich in garnet and clinopyroxene. Because the mineralogy of these small-scale reaction rims is similar to the large-scale contact aureole, it was decided to examine them closer in hopes of

1. Other aspects of the mineralogy and chemistry of this sample have already been discussed, see plates 2-IV, 2-V, 2-VI, and 2-VII.

gaining some insight into the process responsible for the formation of the garnet-clinopyroxene assemblage. Details of this outcrop are shown in Plates 6-I, 6-II, and 6-III. The irregular-shaped pods are composed predominantly of plagioclase (oligoclase) and quartz. Concentrations of garnet, clinopyroxene and opaques occur as irregular clots "floating" in the melt, and as a rather poorly defined, discontinuous reaction rim surrounding the entire structure. Hornblende, which makes up a significant component of the surrounding mafic gneiss, is almost absent in the vicinity of the pods. Evidence that these patches represent incipient partial melting is:

1. their extremely irregular outline and gradational contact with the surrounding mafic gneiss;
2. most appear "rootless", that is, they do not appear to have any origin except in situ;
3. if one looks closely, it is possible to see fragments of gneiss which are in the process of entrainment. These fragments have irregular breaks which "match up" with similar irregular surfaces along the margin of the melt;
4. the presence of a mafic enriched reaction rim which is interpreted as a restite phase.

As it proved impossible to obtain a proper sample from this outcrop, samples were obtained from a similar outcrop approximately 100 meters away. The same style of reaction is present in this outcrop, however, the melt zones cannot be demonstrated to be formed in situ.



Plate 6-I

OTC-076

Mafic granulite exhibiting felsic segregations. Three hundred meters from the end of Farley's side road. Detail shown in opposite plates. Although it is not clear from the photo, the gneiss immediately surrounding the segregations is depleted in hornblende and enriched in garnet and clinopyroxene.



Plate 6-II



Plate 6-III

6-II Observations Made in Slab Study

Plates 6-IV, 6-V, 6-VI, and 6-VII show the location and general nature of the sample selected for detailed study of the garnet-clinopyroxene reaction rim. A large block was removed from the outcrop containing a mafic xenolith (of the local country rock) and sectioned perpendicular to the reaction rim. Smaller slabs were cut for thin sections and chemical analysis.¹ In thin section, one observes a systematic change in mineralogy across the melt/inclusion interface.

The mafic xenolith is composed of plagioclase (An_{12}), hornblende, clinopyroxene, garnet, opaques, and orthopyroxene, with minor apatite, carbonate, quartz, and secondary biotite. At the inner margin of the reaction rim, the modal concentration and crystal size of hornblende and most orthopyroxene decreases rapidly. Remaining, small orthopyroxene crystals are strongly altered to a very fine grained biotite mat,² which occurs along numerous cracks and cleavage planes giving the crystals a ragged appearance. The zone of the reaction rim, which is most obvious in thin section, is a thin lime-green band approximately 1 cm wide composed of plagioclase, garnet, and clinopyroxene, with lesser opaques, apatite, and quartz. Hornblende and orthopyroxene are completely absent. The high concentration of pink garnet and lime-

1. A special oversize thin section (5 x 11 cms) was used to study changes in mineralogy and texture across the reaction rim.

2. Other minerals may also be present, however the assemblage is too fine grained to properly identify all phases.

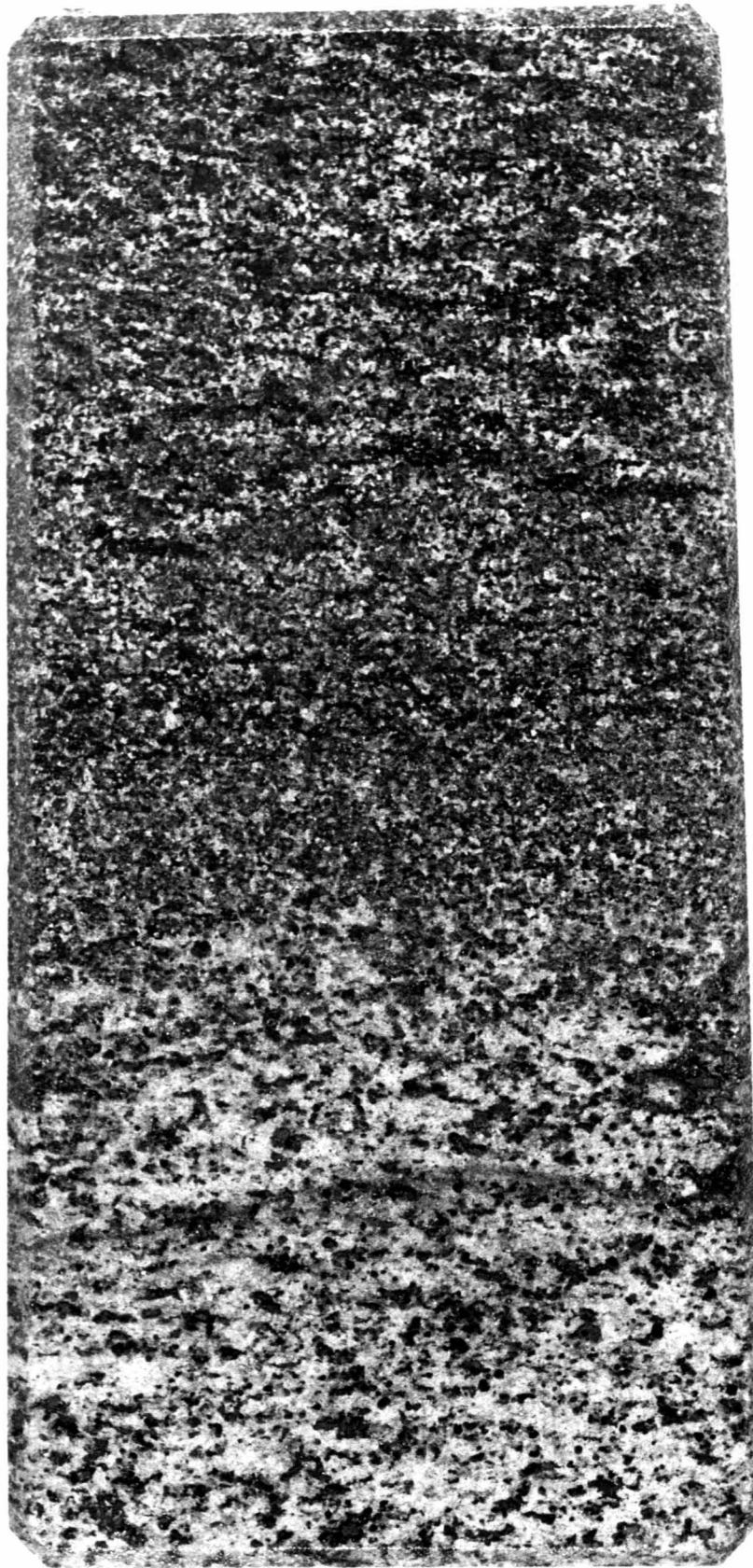
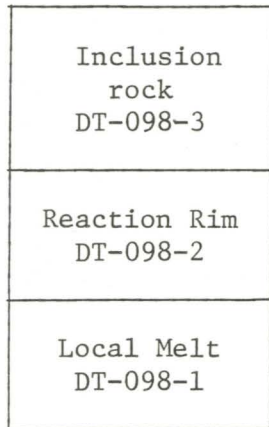




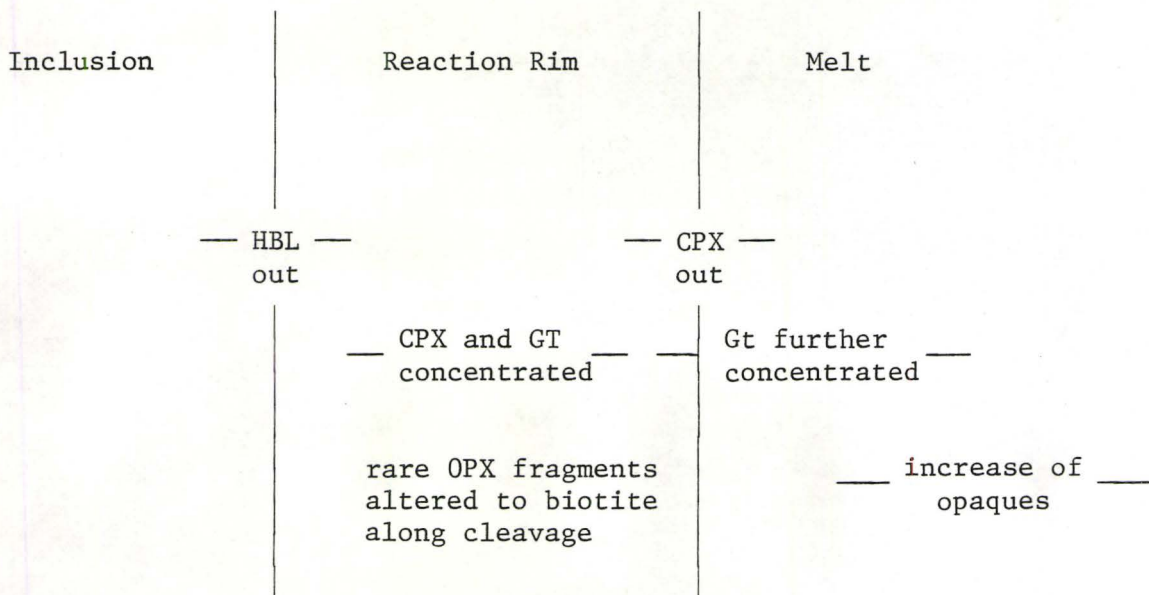
Plate 6-V
 OTC-021
 Sample DT-098

Field location of Slab section
 used in reaction rim study

← Detail of Slab shown opposite
 (Plate 6-IV)



Detail of Slab Section
(opposite Plates 6-VI, 6-VII)



Note: HBL - very dark grey

BT - dark grey (rare)

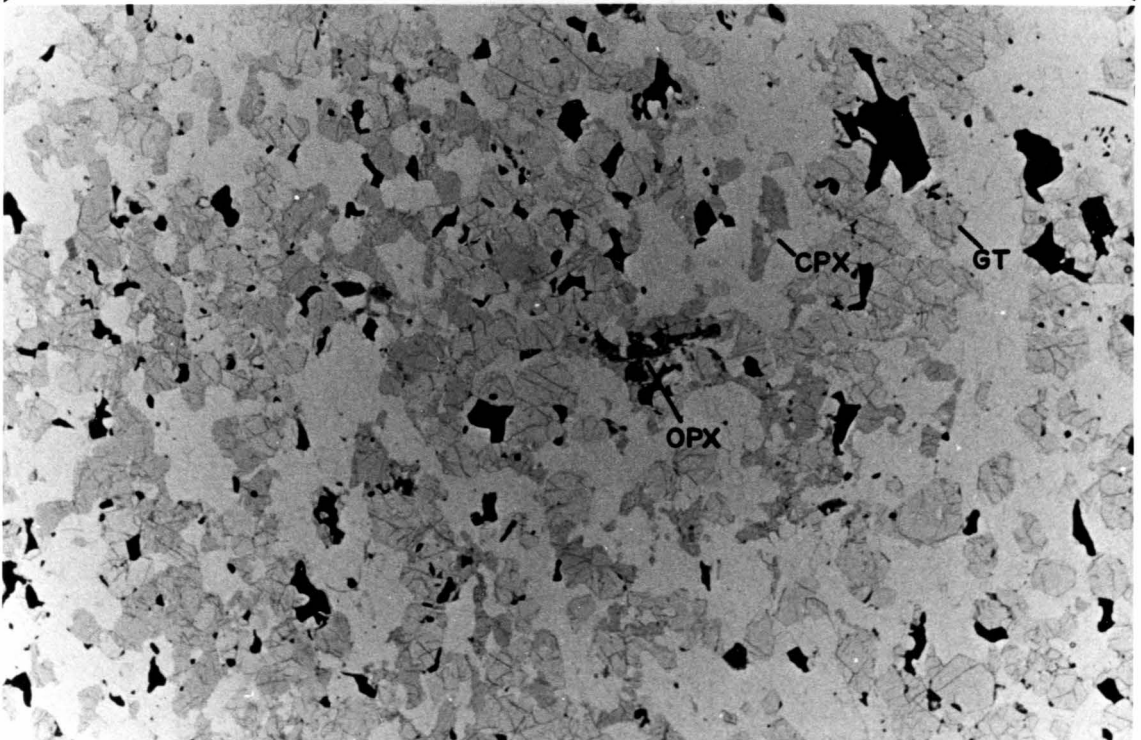
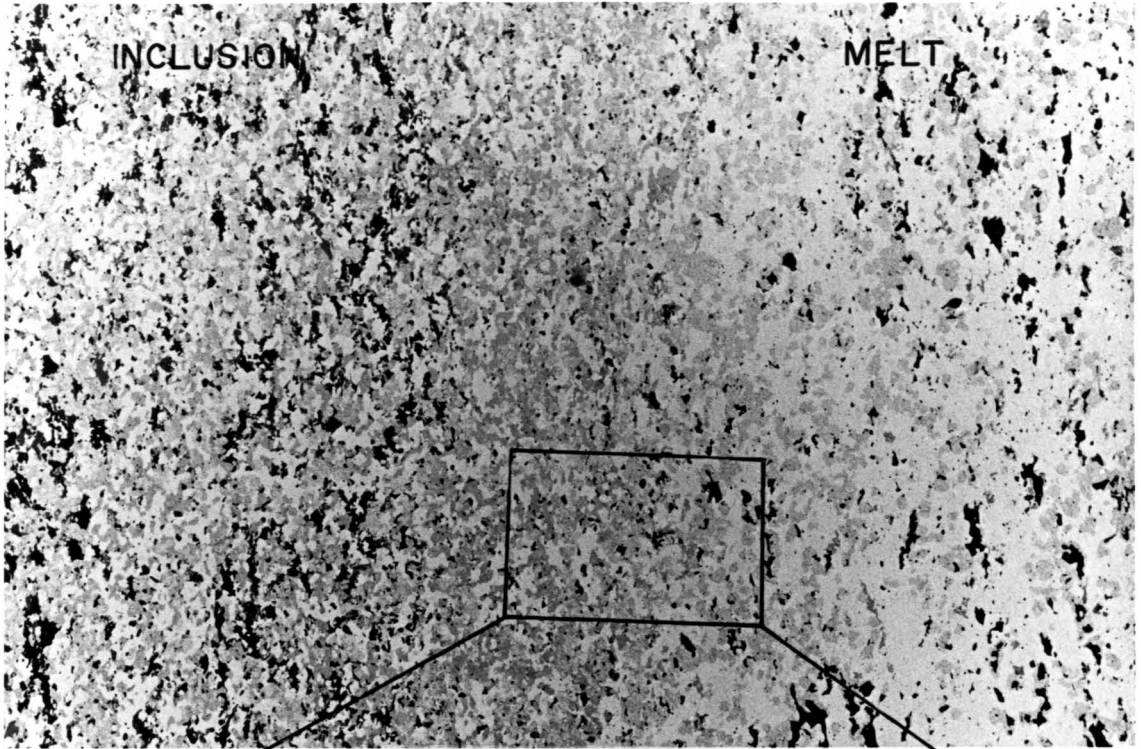
CPX - medium grey

OPX - medium grey (rare), altered to biotite

GT - light grey

OPAQ - black

Quartz, feldspar and apatite are also present and appear white.



1.0 mm

green clinopyroxene crystals gives this band a striking appearance in plane light, which is exactly similar to the garnet-clinopyroxene rich rocks already described from other localities. The outer edge of the reaction rim is defined by the breakdown of clinopyroxene in an analogous manner to that of hornblende; pyroxene crystals become smaller in size and less abundant over a very short distance. The only mafic minerals remaining in the melt are garnet and opaques (both ilmenite and magnetite are present). The systematic changes in modal mineralogy discussed above are shown in Figure 6-I. The reaction rim can be divided into two sections; an inner band containing an increased concentration of clinopyroxene (accounting for its lime-green colour), and an outer band containing mostly garnet, accounting for the pink "halo" which is visible along the melt/mafic gneiss interface in Plate 6-V. The garnet in the melt exhibits two distinctly different habits; approximately 80% or greater occurs as clean subhedral crystals, the remaining garnet occurs in a granular, symplectic corona (gt and qtz) surrounding some of the opaque grains. This texture is also present (but not as apparent) in the mafic inclusion, but is slightly different in morphology suggesting that the symplectic texture in the melt was not necessarily inherited from the "parent" gneiss.

Microprobe analyses of mafic minerals from the reaction zone are shown in Figure 6-II. These results indicate that there is little, if any, change in the composition of hornblende and clinopyroxene over most of the area investigated. Even the smallest hornblende and clinopyroxene fragments show no change in chemistry or systematic zoning,

FIGURE 6-I

Modal Mineralogy Across A Melt/Inclusion Reaction Rim

For each mineral, the raw point-counting data¹ is shown in the lower section by the small circles. The upper boxes show the same data after it has been filtered using a three point moving average (Davis 1970). The modal value of clinopyroxene has been determined by a second independent method² (shown by the larger overlapping circles) which is in excellent agreement with the point-counting data.

Independently determined modal mineralogy of each section (for all minerals) is given below.³

	DT-98-1 Melt	DT-98-2 Inner Rim	DT-98-3 Mafic Gneiss
Garnet	19.8	20.2	9.3
Clinopyroxene ₄	tr	30.4	21.1
Orthopyroxene	tr	tr	9.8
Hornblende	—	tr	20.9
Feldspar (plag)	60.1	39.7	34.1
Quartz	10.7	5.0	tr
Opaque ₅	8.1	3.1	2.2
Apatite ₆	1.2	1.5	0.5
Biotite	tr	tr	2.0
Carbonate	tr	tr	tr

1. Based on 8,000 counts in plane light: quartz, feldspar and apatite were grouped together.

2. Determination of % area using a planimeter.

3. Based on 1,200 counts each.

4. Commonly altered to biotite.

5. Estimated.

6. Retrograde.

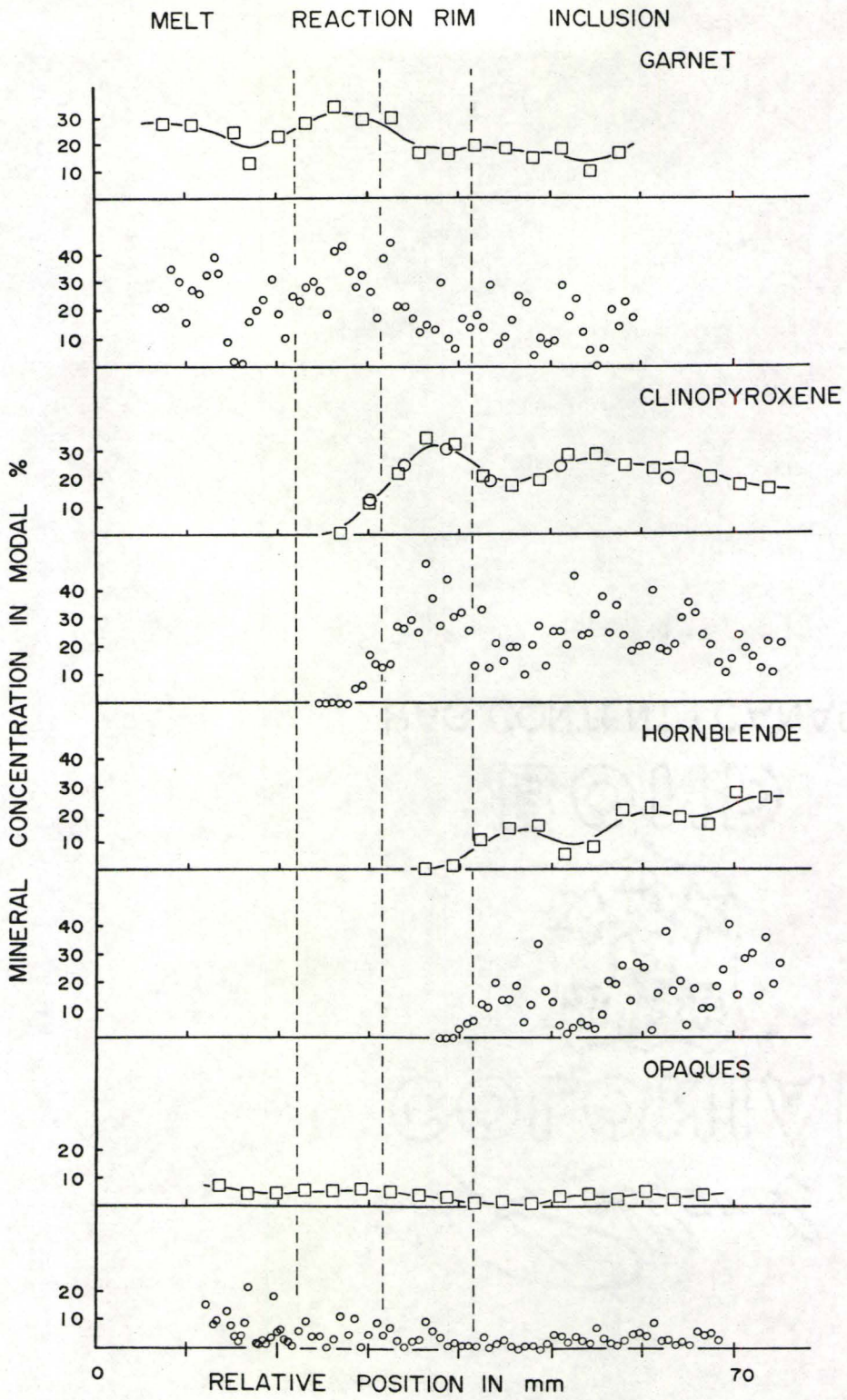
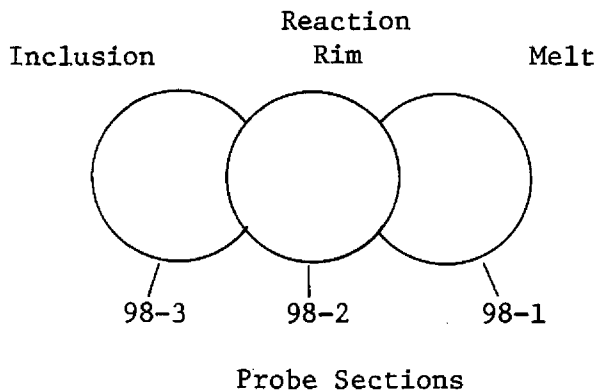


FIGURE 6-II

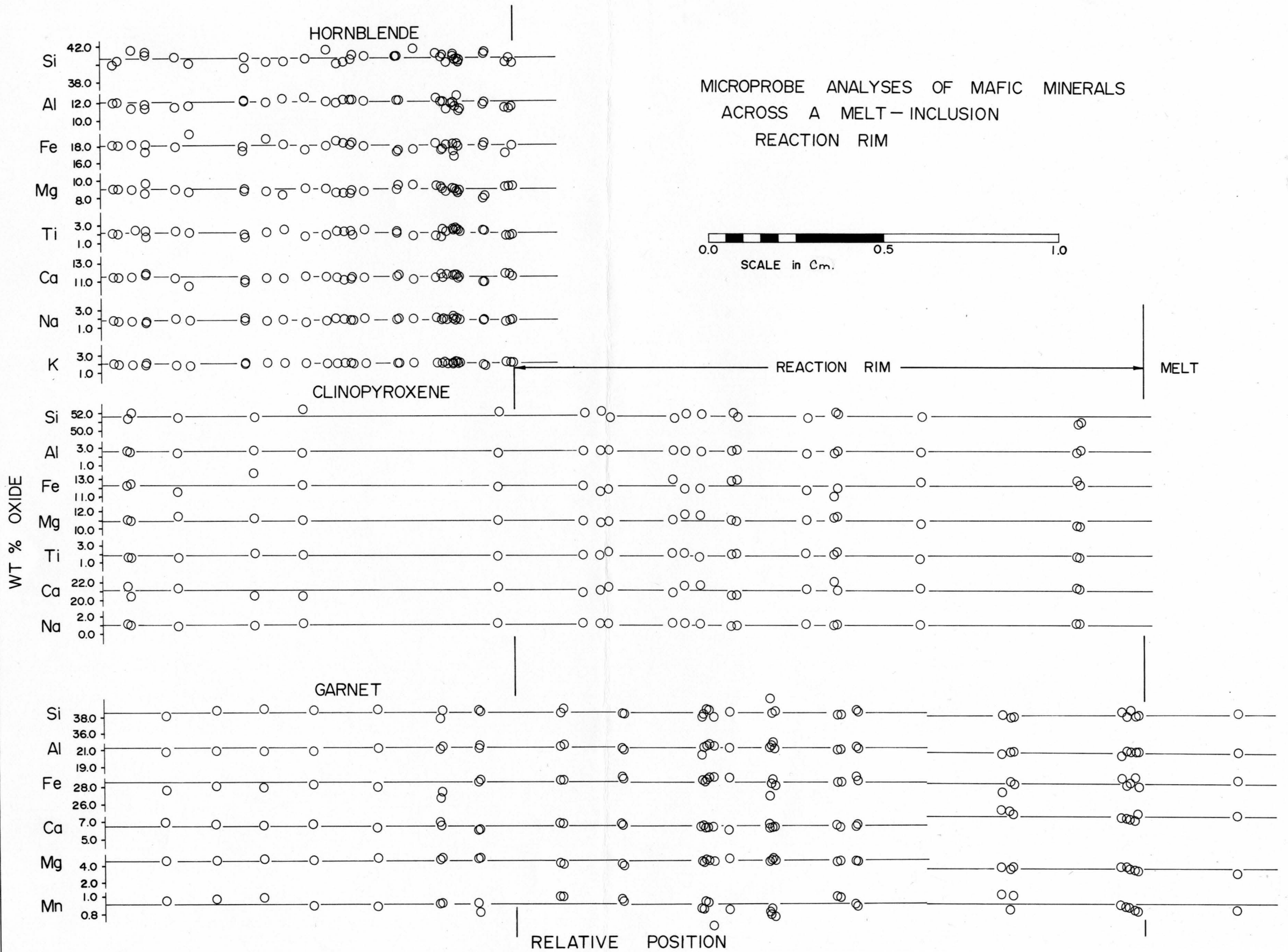
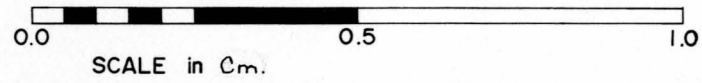
Microprobe Analyses Across A Melt/Inclusion Reaction Rim

This probe data has been compiled from three overlapping probe sections as shown:



The plot (right) shows the variation in chemistry (wt % oxide) of the three minerals hornblende, clinopyroxene, and garnet, across the reaction rim. The far right analyses of hornblende and clinopyroxene indicate the last occurrence of these minerals just before complete reaction. The central black line drawn through the data for each oxide is the average value for that oxide (based on all data shown). For garnet, two averages are shown: one for the country rock/reaction rim, and one for the melt (which appears slightly different).

MICROPROBE ANALYSES OF MAFIC MINERALS
ACROSS A MELT-INCLUSION
REACTION RIM



being exactly similar in chemistry to the equivalent larger crystals in the parent gneiss.¹ Garnets in the melt show a slight increase in Ca and a slight decrease in Mg with respect to garnets in the mafic parent. This trend is consistent with (but does not prove) the idea that, rather than melting, they are equilibrating with a lower temperature assemblage.

Based on the observations outlined above, one may make the following general conclusions concerning the formation of the reaction rim:

1. Hornblende breaks down first, either because it is the most unstable mineral or its rate of decomposition (reaction rate) is greater than the other minerals. The reason for this is almost certainly its hydrous nature.
2. The minerals are melting (under the specific conditions present in this example) by continuous, concentric decomposition. These reactions are non-equilibrium in nature, being controlled by the kinetics of the decomposition.
3. The uniformity in garnet and clinopyroxene compositions indicates that the increased modal values in the reaction rim result from mechanical concentration, due to the refractory nature of these minerals.

1. Several small hornblende crystals were investigated in detail to determine the exact nature of the breakdown reaction. It was found that there are subtle changes in chemistry throughout the crystal, however, they are only barely resolvable with the probe (approximately 2%-5% variation), and are extremely inconsistent, apparently being controlled by the proximity of surrounding crystals.

FIGURE 6-III (a)

Plot of Major Element Variation Across
Inclusion/Melt Reaction Rim

The horizontal bars on each data point indicate the size of the separate slab samples used in the analyses. The vertical error bars represent the estimated precision (2σ) in the XRF method. In most cases, the 2σ error bar is smaller than the size of the box and is therefore not visible.

The % variation represents the difference in chemistry between inclusion and the reaction rim/melt transition. The value of the oxide measured in the inclusion is taken as the 0 datum in each case.

Sample	Inclusion 98-3	Reaction Rim 98-2	Melt 98-1
SiO ₂	47.14	47.29	49.76
TiO ₂	1.87	3.34	3.24
Al ₂ O ₃	12.73	15.22	15.57
Fe ₂ O ₃	3.26	4.07	5.43
FeO	11.54	14.49	11.54
MnO	.27	.40	.27
MgO	6.42	2.34	.87
CaO	10.17	6.36	5.78
Na ₂ O	2.62	2.68	2.75
K ₂ O	.61	.49	.64
P ₂ O ₅	.13	.47	.41
CO ₂	.19	.16	.16
Total	96.95	97.31	96.42

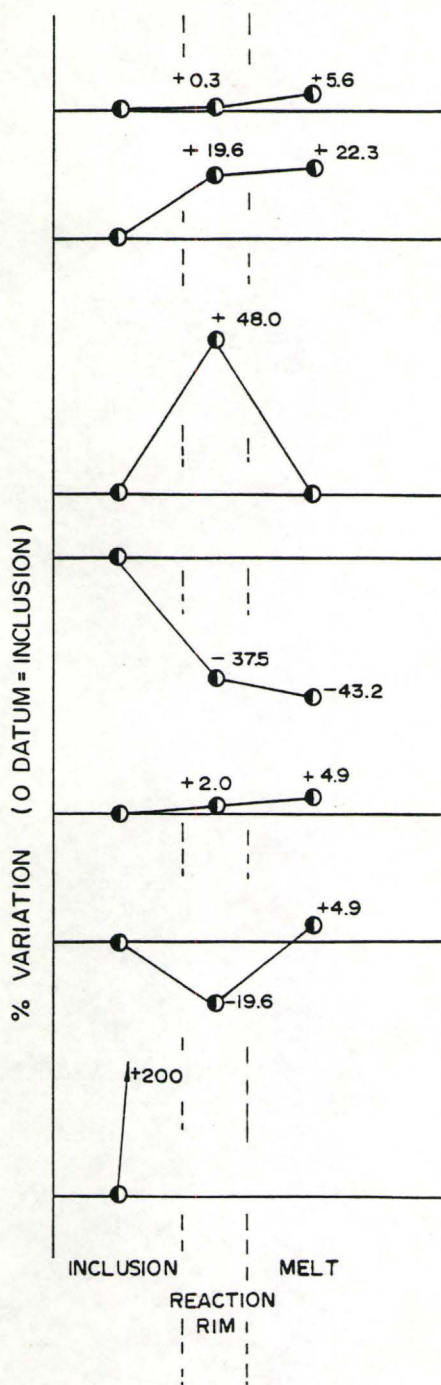
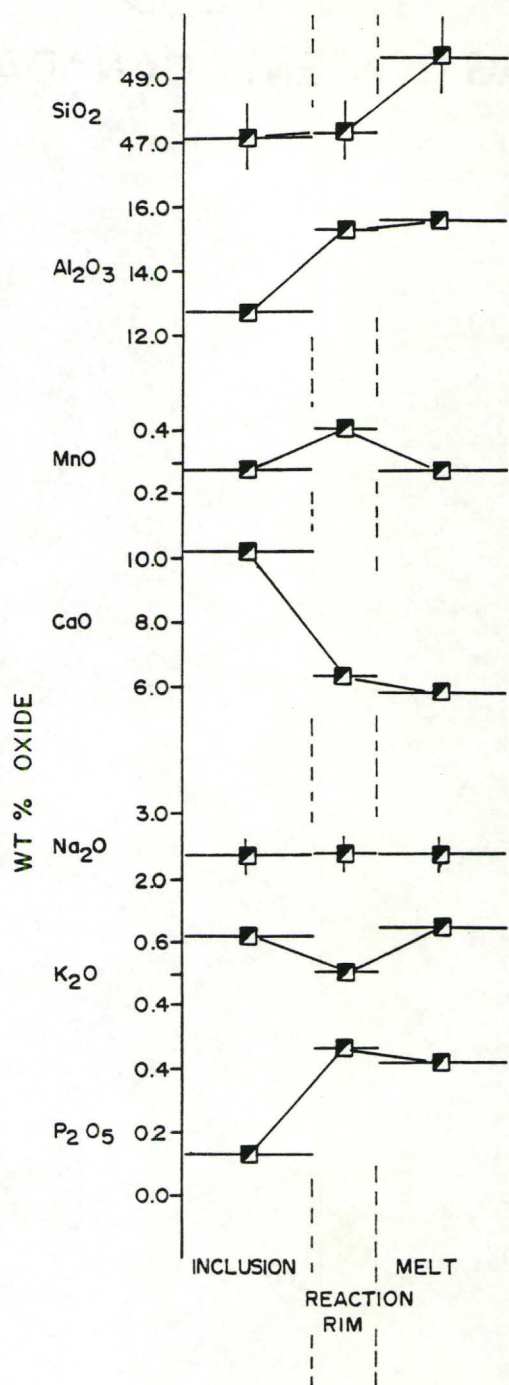


FIGURE 6-III(b)

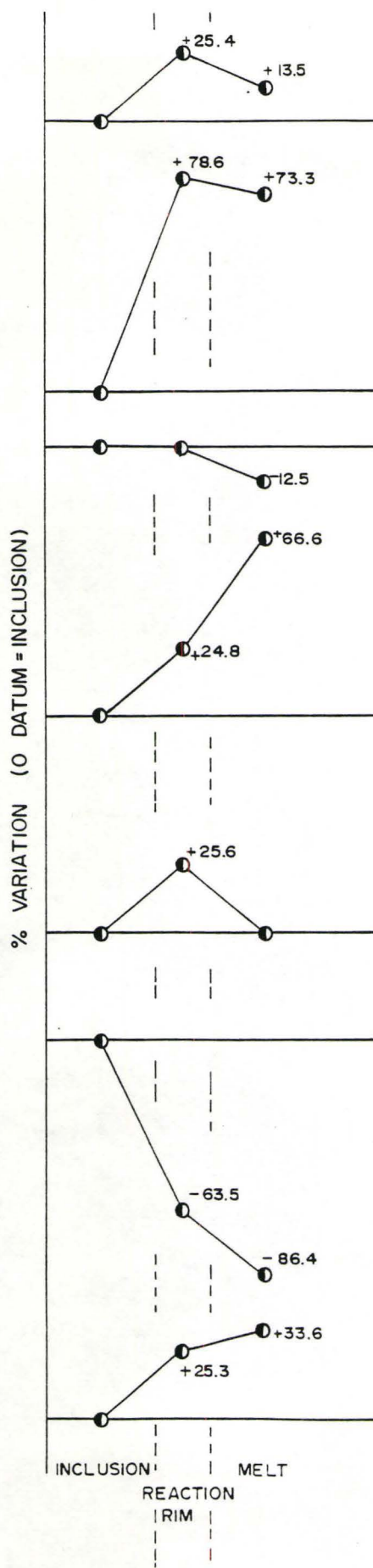
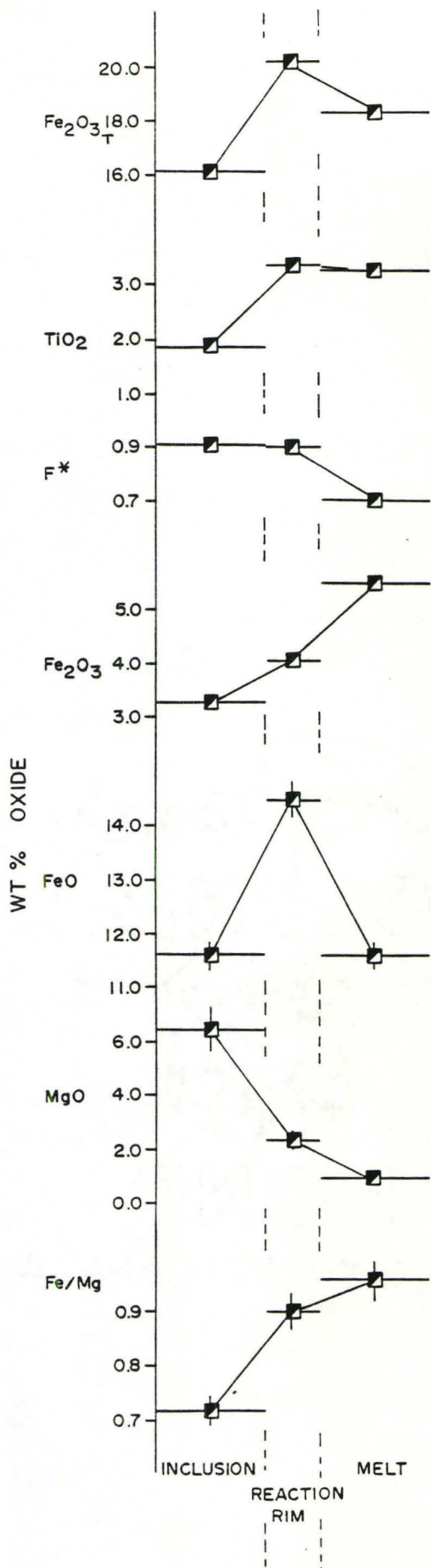
Plot of Major Element Variation Across An
Inclusion/Melt Reaction Rim

The details of the plot are the same as those defined in Figure 6-III(a).

$$F^* = \text{Fe}^{2+} / (\text{Fe}^{2+} + \text{Fe}^{3+}), \text{ as ions (wet chem method).}$$

$$\text{Fe/Mg} = \text{Fe}_T / (\text{Fe}_T + \text{Mg}), \text{ as ions.}$$

$$\text{Fe}_2\text{O}_{3_T} = \text{total Fe by XRF.}$$



Chemical analyses of slabs cut from the three zones are shown in Figures 6-III (a and b). The variation in the reaction rim relative to the parent gneiss is as follows:

25% increase in $\text{Fe}_2\text{O}_3(\text{tot})$	37% decrease in CaO
20% increase in Al_2O_3	19% decrease in K_2O
48% increase in MnO	63% decrease in MgO
78% increase in TiO_2	
200% increase in P_2O_5	

These changes are clearly related to the concentration of restite phases, namely, garnet, clinopyroxene, opaques, and apatite. The role of the latter two minerals is uncertain because, while it is fairly clear that garnet and clinopyroxene represent an unreacted mechanical concentrate; magnetite, ilmenite and apatite may have been recrystallized during the melting process, being concentrated in the reaction rim due to their incompatibility in the silicate melt structure (Hess 1977).

The analyses given as the "melt composition" is difficult to interpret, because the analyzed slab comes from the border zone of the melted area and consequently, contains a sizable proportion of restite minerals. Table 6-I outlines an attempt to calculate the approximate composition of the melt fraction by removal of garnet, ilmenite, magnetite and apatite in accordance with their modal concentration. Considering the rather crude assumptions involved in this calculation (for example, magnetite and ilmenite were visually estimated to be

TABLE 6-I

Calculation of Melt Composition by Removal of Restite Phase

Melt = Whole Rock composition - (20% garnet + 8% (Magnetite + Ilmenite) + Apatite)

$$C_i^{\text{Melt}} = C_i^{\text{WR}} - \sum (C_i^{\text{Restite}}), C_i = \text{the conc. of component } i$$

where: $C_i^{\text{Restite}} = \text{modal \%} \times \frac{\rho_{\text{Mineral}}}{\rho_{\text{Melt}}} \times C_i^{\text{Mineral}}$

	Melt	Restite			Melt-Restite
		Garnet	Ilmenite ²	Magnetite ³	
SiO ₂	51.61	38.08	0.42	0.40	69.63
TiO ₂	3.36	0.03	47.40	0.03	0.28
Al ₂ O ₃	16.15	20.69	0.16	0.43	17.99
Fe ₂ O ₃	5.63	2.20	7.34	67.71	-0.46
FeO	11.97	26.31	41.95	30.46	0.14
MnO	0.28	0.91	0.15	0.06	0.04
MgO	0.90	3.46	0.64	0.04	-0.03
CaO	5.99	7.74	0.01	0.02	5.72
Na ₂ O	2.85				4.76
K ₂ O	0.66				1.09
P ₂ O ₅	0.43				0.00 ⁴
CO ₂	0.17				0.28
Total	100 ¹	99.39	98.07	99.15	100 ¹

1. Total normalized to 100%.

2. FeO and Fe₂O₃ based on the recalculation procedure of Carmichael (1967).

3. FeO and Fe₂O₃ based on the theoretical composition of magnetite, in which F* = .333.

4. P₂O₅ and CaO removed in the ratio P₂O₅/CaO = .75, assumed to be in Apatite.

present in approximately equal amounts and representative mineral densities were taken from Deer et al. (1966)), it is rather surprising how close it comes to exact mass balance. The calculation is clearly not adequate because Fe and Mg have been reduced to zero, however, if small amounts of opaque minerals and symplectitic garnet (noted above) are added, the resultant melt composition is somewhat suggestive of a quartz diorite.

6-III Discussion

If the irregular-shaped felsic pods truly are partial melts, then they are of considerable interest for two reasons:

1. They represent an example of in situ partial melting of granulite facies gneisses under conditions of $P_{H_2O} < P_{Total}$.
2. They appear to be undeformed and therefore allow observation of the exact nature of the melting process.

The observations made in this chapter suggest that, once formed, the partial melt zones act as centers of dessication, extending into the surrounding rock by further decomposition of hydrous minerals. Refractory minerals such as garnet and clinopyroxene are mechanically concentrated as a restite phase. This behaviour contrasts sharply with the formation of upper amphibolite facies migmatites, in which hydrous minerals such as biotite typically form part of the restite phase (Dougan 1979, 1981).

Davidson (personal communication 1982) has noted similar irregular, "pod-shaped" structures at several locations within the Parry Sound block. He interprets them as "local sweats", that is, felsic concentrations formed by solid state migration and replacement. According to Wyllie (1977), partial melting of mafic rocks, undersaturated with respect to H_2O , to produce a melt having a tonalitic composition, only occurs at $T > 1000$ °C, and certainly not at the temperatures of 700-800 °C calculated for these rocks by geothermometry. Therefore, while the geometrical features exhibited by these zones seem to be compatible with a melting origin, the supposition does not appear to be supported by experimental evidence.

Of more importance to this thesis, are the observations made in the reaction rim slab study. Granulite facies mafic rocks displaying dark coloured reaction rims are quite common, for example, mafic xenoliths (in felsic melts) or thin mafic units in quartzofeldspathic gneisses (Ono 1977). In both cases, a complex mixing reaction has occurred at the interface between the two differing rock types. In general, the exact form of the exchange is difficult to predict because the availability and mobility of diffusing ions is directly related to the mineral reactions which are occurring. In the example under study, the breakdown of hornblende and orthopyroxene results in the loss of Ca, K, and Mg from the system and the concentration of Fe and Ti in the new phases, ilmenite and magnetite.

Mafic rocks are capable of stabilizing high modal concentrations of hydrous minerals, even under granulite conditions (see

Phillips 1980, and Phillips and Wall 1981), providing a local sink for H_2O is not available. When mafic rocks come in contact with a system having a reduced μH_2O , there is a net transport of H_2O out of the rock, resulting in the decomposition of hydrous minerals. The increased flux of volatile components through the rock accelerates reaction rates (diffusion and recrystallization). The mafic component can be expected to exhibit a recrystallized (restite-like) reaction rim; enriched in certain immobile elements (in this case Fe, Ti, P, and Al) and impoverished in the more mobile components, in particular volatiles. Most mafic/felsic interfaces metamorphosed under granulite conditions, can be expected to exhibit this behaviour.

CHAPTER 7

THE ASSOCIATION OF Gt-Cpx ASSEMBLAGES AND OXIDE-APATITE CONCENTRATIONS WITH ANORTHOSITE MASSIFS

7-I Review of Field Relations

(i) The Marcy Massif

The Adirondack region of Upper New York State is dominated by the Marcy Massif anorthosite complex. The Marcy Massif is one of the most studied anorthosite terrains in the world, however, its age, mode of emplacement and subsequent metamorphic history remain controversial. Early mapping distinguished two facies of anorthositic rocks (Buddington 1939):

1. The Marcy Anorthosite: characteristic of the core of the massif.
2. The Whiteface Facies: restricted to the borders of the massif or to bands closely involved with Grenville layers and inclusions.

The Marcy anorthosite is typically bluish-grey, coarse to very coarse grained anorthosite with less than 10% dark minerals. Much of it has an indistinct foliation or none at all. In contrast, the marginal Whiteface facies has a foliated, medium grained texture and is characterized by white feldspars, increased concentrations of pyroxene, garnet, hornblende, biotite, opaques, and apatite, and numerous, partially assimilated country rock fragments.

In Buddington's classic memoir on Adirondack geology, he aptly describes the complex and often enigmatic field relationships observed within the marginal facies of the Marcy massif. (The following quotations are from Buddington 1939, Adirondack igneous rocks and their metamorphism):

Hornblende is a common constituent of the anorthositic rocks, especially in the border facies, but it is questionable whether any of it is of primary origin, with the possible exception of some in the border facies where the latter has been modified in contact zones with Grenville. The hornblende may occur either as distinct grains or with corona relationship to the pyroxene. Biotite is also present locally in such contact zones. It may also appear locally as a late replacement of hypersthene and the plagioclase. It has rarely been observed with the relations of a primary magmatic mineral in the little metamorphosed core rocks.

There is a general tendency for an increase of apatite in the gabbroic anorthosite as compared with the true anorthosite. Some apatite as well as orthoclase appears to have been introduced into the border facies of the anorthosite where it adjoins the quartz syenitic and granite rocks, and there is in general an increase in apatite in the assimilation facies of the anorthositic rocks (p. 33).

These metamorphosed facies were in part subsequently broken up, included as layers or brecciated fragments, and locally injected, disintegrated, modified, or incorporated by the still mobile magma. At many localities, complete gradation can be traced between uniform layers of metamorphosed Grenville formation (pyroxene or garnet skarn), such layers with augen of andesine and injected anorthositic veinings, and diorite or gabbro representing anorthosite modified by incorporation of relics of such layers. (See Plate 1.) Such modified facies may be of coarser, finer, or similar grain; many have a more heterogeneous appearance and show an inherited ghost-like or nebulitic angular breccia or a shredded schlieren structure. Knots, shreds, and small lenses of

pyroxene granulite or of garnet-rich material are common. Anorthosite dikes have been noted across the modified Grenville. Every type of phenomenon found in contact zones between limestone and granite is duplicated in the contact zones between anorthosite and limestone, though the resulting products are different.

There are several types of variation and modification of the anorthositic rocks in the contact zones with Grenville which should be noted. The predominant variation is toward a more mafic character; another common development is the incoming of quartz; locally, sills of diorite in limestone have a coarse porphyritic fabric. This porphyritic development may also occur locally in the border facies involved with Grenville. The modified rocks may be exceptionally rich in garnet, exceptionally rich in pyroxene, or in both, depending on the character of the original skarn layer (p. 43).

These observations indicate a complex history of large-scale mixing (assimilation and metasomatism) at the anorthosite/country rock interface. Relic gneiss fragments, exhibiting all stages of assimilation, are commonly rich in garnet, clinopyroxene, and apatite. It is interesting to note that Buddington interprets many of Balk's so-called "gabbroic layers" as re-crystallized mafic xenoliths. Typical chemical analyses and modal mineralogy of the various Marcy massif facies are given in Table 7-I. Figure 7-I is a simplified geological map showing the distribution of the marginal Whiteface Facies.

Clearly, there is a gross similarity in the character of deformation, alteration, and general mineralogy between the Marcy massif and the Whitestone Anorthosite. Therefore it is possible, at least qualitatively, to model the "style" of interaction which takes place between anorthosite massifs and their contact rocks during granulite metamorphism.

TABLE 7-I

Average Chemical Analyses and Modal Mineralogy of Marcy and Whiteface Facies Anorthosite Rocks (Buddington 1939)

Chemical Analyses (Table 4)

- A- ave. of 4 unaltered anorthosite samples, Marcy facies.
- 16 ave. of 60 grab samples, Marcy facies.
- 17 ave. of 70 grab samples, Marcy facies.
- 18 ave. of 10 grab samples, Whiteface facies.
- 19 ave. of 72 grab samples, Whiteface facies.
- 20 ave. of 55 grab samples, Whiteface facies.
- B ave. of 7 analyses, Whiteface facies.

Modal Mineralogy (Table 5)

- 1. ave. of 20 unaltered anorthosite, Marcy facies.
- 2. ave. of 8 sections, Whiteface border facies.
- 3. ave. of 21 sections, Whiteface border facies.
- 4. ave. of 20 sections, Whiteface border facies, gabbroic anorthosite with numerous country rock inclusions.
- 5. ave. of 5 gabbroic facies, mafic character due to assimilation (Buddington 1939).
- 6. ave. of 5 noritic facies.

Table 4 from Buddington (1939, p. 30).

Table 5 from Buddington (1939, p. 32).

TABLE 4.—Average composition of Marcy and Whiteface facies of anorthositic rocks

	A	16	17	18	19	20	B
SiO ₂	54.54	55.03	53.21	54.55	53.40	55.10	53.34
Al ₂ O ₃	25.61	25.56	26.64	22.50	23.06	22.10	22.50
FerO ₂	1.00	.75	.35	1.31	.91	.66	1.26
FeO.....	1.26	1.59	1.24	3.89	3.02	4.17	4.14
MgO.....	1.03	1.02	1.16	1.01	1.88	1.67	2.21
CaO.....	9.92	9.56	11.48	7.81	9.85	8.69	10.12
Na ₂ O.....	4.58	4.67	4.75	4.61	4.17	4.06	3.79
K ₂ O.....	1.01	1.09	.69	1.93	.80	1.31	1.19
H ₂ O+.....	.55	.28	.33	.48	.62	.50
H ₂ O-.....		.03	.04	.08	.07	.04
TiO ₂67	.43	.24	1.12	.77	.92	.72
P ₂ O ₅09	.03	.35	.18	.27	.13
CO ₂1314	.42	.24	.41
S.....03
Cl.....0103	.01	.04
MnO.....0208	.07
Total.....	100.17	100.24	*100.20	99.81	100.06	*99.84	99.88

* Less .01 for O = Cl or S.

TABLE 5.—Average modes of some facies of anorthositic series

	1	2	3	4	5	6
Plagioclase.....	93.5	94	81.2	73	62.2	84.5
Potash feldspar.....	1.6	2	1.0	0.5
Hypersthene.....	2.6	0.3	4.4	11.3
Augite.....	2.8	2.6	0.8	7	16.5	1.9
Hornblende.....	0.2	1.7	0.5	4	0.9	0.6
Biotite.....	0.1	Tr.	1½	1.5	0.4
Magnetite and ilmenite.....	0.5	0.3	2.3	2	2.2	0.2
Apatite.....	0.2	Tr.	0.4	½	1.1	Tr.
Quartz.....	1.0	3	1.8	0.2
Garnet.....	0.2	0.2	2.7	7	6.6
Pyrite.....	Tr.	Tr.	Tr.	Tr.	Tr.	Tr.
Sphene.....	0.1	Tr.	Tr.	1.4
Chlorite, epidote, carbonate.....	1.0	3.1	0.4	0.3

FIGURE 7-1

Simplified Geology of the Marcy Massif



Anorthosite - Marcy facies.



Anorthosite gneiss - Whiteface facies (metasomatic overprint), includes numerous xenoliths.



Metasedimentary rocks - unsubdivided.



Calc - silicate gneiss and related rocks.



Pyroxene - hornblende - quartz syenitic gneiss, may contain interlayered amphibolite, paragneiss and migmitite.



Pyroxene granitic gneiss ± hornblende, leucocratic gneiss, locally with disseminated magnetite and magnetite ore bodies.

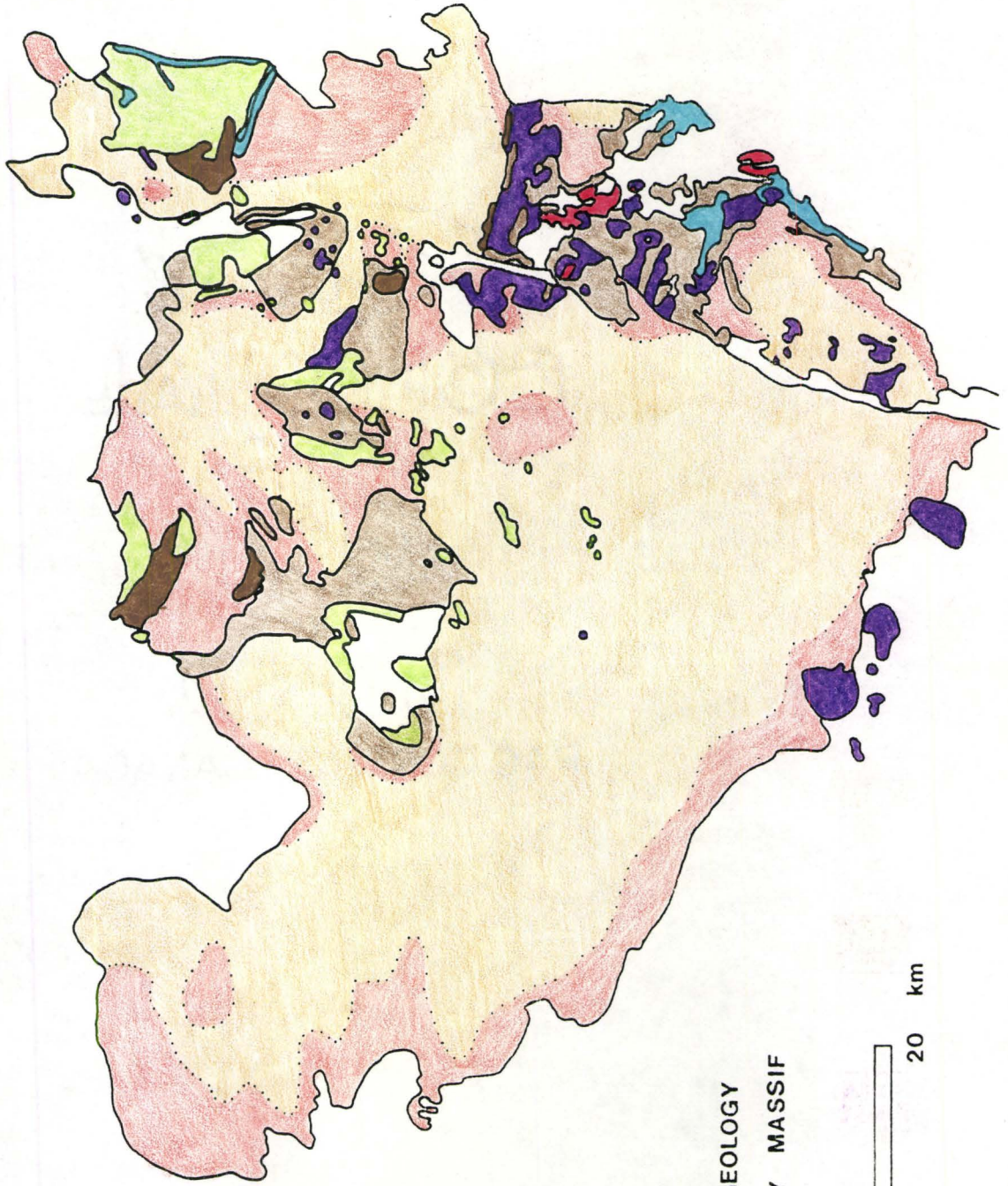


Metagabbro - includes some amphibolite of unknown origin.

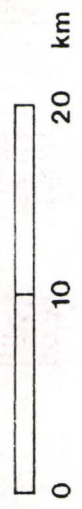


Leucogranitic gneiss - commonly contains metasedimentary layers, amphibolite, and magmitite; is a host to magnetite ore bodies.

Source: Simplified from the "Geological Map of New York State," Adirondack Sheet, Fisher W. D. et al. (1961).



SIMPLIFIED GEOLOGY
OF THE MARCY MASSIF



(ii) Allard Lake

In his study of the Allard Lake Anorthosite, Hargraves (1962) emphasized the occurrence of a gradational zone at the contact between the anorthosite and the local country rock (pyroxene syenite gneiss). The contact is characterized by a conformable gneissosity and enrichment in mafic minerals in both the anorthosite and the syenite. The syenite shows a progressive change in mineralogy away from the contact and eventually grades into a hornblende-biotite granite. There is a positive aeromagnetic anomaly associated with the anorthosite/syenite contact due to the local enrichment in magnetite. Within the anorthosite proper are several large units of "oxide rich norite", described by Hargraves as "somewhat irregular, elongated or curved sheets."¹ They are composed of plagioclase, pyroxene, apatite (8%-10%) and oxides, and are interpreted as injections of oxide rich norite into a crushed zone in the anorthosite. Based on the field descriptions and photographs of typical examples, I would submit that they are thoroughly re-crystallized mafic xenoliths.

(iii) The Morin Anorthosite

The complex structural history of the Morin anorthosite massif²

1. The Lac Tio ore body (massive ilmenite) occurs within one of these units. Allard Lake is situated approximately 15 miles inland from the St. Lawrence River and 400 miles east of Quebec City.

2. The Morin anorthosite massif underlies approximately 2500 km² and is situated 75 km north of Montreal.

has been described in detail by Martignole and Schrijver (1970a, 1970b). They believe that the large-scale dome and nappe structures resulted from the rise, and eventual lateral spreading of a buoyant anorthosite mass. The main body is partially surrounded by a thin jotunite rim, which appears to form the cover to the pluton.¹ The jotunite is described by Martignole and Schrijver (1970, p. 175) as follows:

. . . . A narrow jotunite zone is commonly present around the mass. The contact zone between anorthosite and jotunite is occupied by an oxide-clinopyroxene rich gabbroic layer a few meters thick. The gabbro encloses angular to subangular blocks of anorthosite and grades into jotunite with numerous small xenoliths of quartzite and calc-silicate rocks . . . both gabbro and jotunite contain garnet. . . . The jotunite is a dark, heavy rock rich in iron-titanium oxides and apatite. Where it is not too strongly deformed and gneissic, it has a palimpsest structure due to the growth of reaction rims of garnet, quartz and locally, clinopyroxene around plagioclase grains The contact between jotunite and mangerite cannot be shown to be a line, the change in mineralogy being completely gradational.

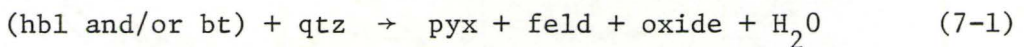
Of particular significance is their observation that in and around the anorthosite body, the granulite assemblage opx-plag is replaced by the equivalent, higher pressure assemblage gt-cpx-qtz-plag (less calcic). Garnet-quartz symplectics commonly surround ilmenite and orthopyroxene (originally in contact with plagioclase). Further study (Martignole and Schrijver 1971, 1973) has shown that within the gt-cpx "isograd", the development of garnet is directly proportional to

1. Due to the complexity of the field relations, the nature and significance of the contact is probably equivocal in many cases.

the bulk rock $\text{Fe}^{2+}/(\text{Fe}^{2+} + \text{Mg})$ and normative $\text{An}/(\text{An} + \text{Ab})$ ratios. They conclude that the presence of the anorthosite retarded regional cooling sufficiently to permit the garnet forming reaction to take place, therefore the gt-cpx assemblage is retrograde.¹

7-II Fe - Ti - P Concentrations and Their Relationship to Liquid Immiscibility

The relationship between granulite terrains and iron-titanium ores has been recognized for some time (Ramberg 1948, who sites Vogt, J. H. L. 1893). Based on his field work in West Greenland, Ramberg concludes that, "such a liberation of titanium and iron is actually connected with some of the most important mineral transformations which take place when certain rocks are exposed to the physical conditions of the granulite facies" (Ramberg 1948, p. 557). Ramberg envisioned the breakdown of Fe-Ti rich minerals to occur by the following type of reaction:



He supports this notion with the important observation that amphibolite inclusions in enderbitic gneiss are typically surrounded by a thin reaction rim enriched in opx and oxides, and that the concentration of oxide minerals in the reaction zone is considerably greater than that in either of the surrounding rocks.

1. The retrograde aspect of this assemblage is based primarily on textural evidence, e.g., undeformed corona structures.

Philpotts (1966, 1967) noted the close association between oxide rich rocks (in particular oxide-apatite rich ore bodies) and anorthosite massifs. The ore zones are commonly 2/3 oxide, 1/3 apatite (by volume), and have dikes rich in ferromagnesian minerals associated with them.¹ Exploratory experimental work (Philpotts 1967) in the system magnetite-fluorapatite indicated that a eutectic exists, having a composition of 2/3 magnetite and 1/3 apatite; and, further, that this oxide rich liquid is immiscible with a silicate melt.

More recent experimental work on liquid immiscibility has been undertaken by Freestone (1978), and Philpotts (1981). Freestone investigated the system fayalite-leucite-silica (analogous to alkali rich magmas), previously considered by Roedder (1951). He found that the addition of 1 mole % P_2O_5 and 3 mole % TiO_2 caused a marked expansion of the two liquid field towards the K rich compositions. Experimental observations having a more direct significance to the Anorthosite suite have been gathered by Philpotts, who prepared melts consisting of equal proportions (by wt) of jotunite and mangerite.² The melts were cooled very slowly (1/4 °C/hr) so that the development of the immiscible phase could be closely studied. At 1050 °C, plagioclase (An_{50}) begins to crystallize followed by augite at 1035 °C. At 1025 °C (after 5%

1. The dikes are described as being strongly altered, however, the details of the alteration are not given.

2. Based on the known chemistry and close spacial relation between these rocks in the field, he considers them to be good candidates for complimentary immiscible liquids.

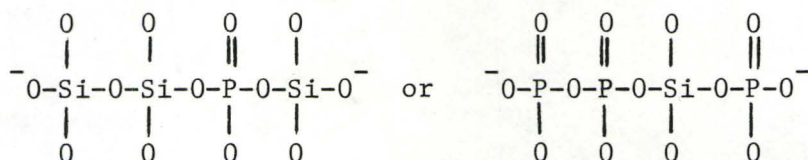
crystallization), magnetite is present, plus a second liquid forming small brown globules. At 995 °C, two liquids are still present in contact with all phases. The composition of glasses produced in the experiments show a consistent major element fractionation:

The Fe rich phase is enriched in: Fe, Ti, Mg, Mn, Ca, P, Zr.
The Si rich phase is enriched in: Si, Al, Na, K.

The phase separation is related to the compositional dependence of the melt structure. As the concentration of metal cations is increased, the melt begins to order by concentrating n.b.o.¹ around the metal cations (this local clustering reduces the free energy because the n.b.o. can more effectively screen the positively charged cations from one another). For melts containing highly charged metal cations, the screening problem becomes more critical. These melts are characterized by an inherently, higher degree of ordering than melts containing either monovalent or divalent cations. Hence, these melts contain few n.b.o.; they are solutions containing locally ordered regions of either free or bridging oxygen (Hess 1981). The positive free energy of mixing, associated with the interface between these localized, sub-microscopic regions of order, is minimized by collecting them into two distinct phases. The end result of this process is the formation of a pair of immiscible liquids (Hess 1977).

1. n.b.o. refers to non-bridging oxygen (see Hess 1981).

The role of Ti and P in silicate melts is of particular significance, because their presence expands the immiscibility field. At present, the exact reason for this is not clear. Freestone (1978) states that because Ti^{4+} and P^{5+} have high field strengths, they will not enter a tectosilicate network, thus their presence increases the oxygen screening problem--expanding the two liquid field. According to Hess (1981) the role of P is more complex. Experimental work on the system $P_2O_5-SiO_2$, indicates that in the range $N_{SiO_2} = 100-50$ mole % the two species may copolymerize with each other, thereby enhancing the stability of the melt. One possible explanation for this behaviour is the close similarity between the PO_4^{3-} and SiO_4^{4-} tetrahedra. Substitution of these structural units for one another may be viewed as follows:



The key difference between these two fundamental structural units is the double bond in the phosphate ion. This limits its cross-linking ability; therefore, unlike silica, PO_4^{3-} does not form extended polymerized networks, rather it is more likely to occur as a single molecule or in unbranched chains (Hess 1981). This may explain why P is strongly fractionated into the mafic fraction of the immiscible liquid pair. As the liquid orders into two separate structures, the PO_4^{3-} group is stabilized in the less polymerized, polyvalent, cation rich fraction where it can substitute for SiO_4^{4-} , whereas the bonding

requirements of PO_4^{3-} are incompatible with the strongly cross-linked nature of the highly polymerized silica rich fraction.

7-III Discussion

There are a number of ways to produce Fe, Ti, P enrichment in rocks associated with anorthosite complexes:

1. Magmatic Differentiation
2. Liquid Immiscibility
3. Metamorphic Differentiation

The ferrodiorites of the Harp Lake anorthosite complex are strongly fractionated and enriched in Fe, Ti, and P (Emslie 1980). They occur as small intrusions and dykes associated with contacts between adamellite and anorthosite. Magmas of this composition are characteristic of late-stage residual differentiates of tholeiitic magmas, for example, the Skaergaard intrusion (McBirney 1975). Although the ferrodiorites appear to be closely related to the basic rocks of the complex, their chemistry suggests that they are not residual liquids from the plagioclase rich rocks. Emslie (1980) suggests they may be differentiates of the primary magma, but in general their origin is not clear.

Philpotts (1981) has argued that the members of the anorthosite suite could be derived from a common parent magma by liquid immiscibility. Support of this concept is, in part, based on the field occurrence of Fe, Ti, P rich rocks which are gradational (?) into more typical

anorthositic rocks. However, in most cases, the rocks in question have been strongly deformed and metamorphosed, consequently the field relations are equivocal. Kolker (1982) has reviewed the occurrence and chemistry of nelsonite dykes and finds them consistent with the concept of an immiscible liquid, but while there is strong evidence in favour of the nelsonite dykes as immiscible liquids, the relationship of experimental immiscible granitic and ferrodiorite liquids to oxide-apatite liquids (if any) has not been determined. According to Morse (1982) and Emslie (personal communication 1982), the liquid immiscibility hypothesis is not a viable mechanism for the formation of the anorthosite suite.

Figure 7-II compares the Al_2O_3 concentration of known immiscible liquids with mafic granulites, jotunitites and ferrodiorites. Aluminum is known to be relatively immobile during metamorphism (Carmichael 1969), therefore one would expect to find it enriched in a restite phase. In contrast, during the formation of complimentary immiscible liquids, aluminum is fractionated into the Si rich phase. According to the criteria outlined above, very few of these rocks represent immiscible liquids.

Finally, it has been demonstrated in this thesis that under certain circumstances, mafic rocks may become enriched in Fe, Ti and P during high grade metamorphism (e.g., jotunite gneisses).

Ferrodiorites, nelsonite dykes and jotunite gneisses are all associated with anorthosite massifs. These rock types appear to be independent of one another, however, it is easy to see how considerable

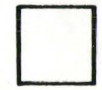
FIG 7-II

Comparison of Al_2O_3 Concentration in Known Immiscible Liquids

Mafic gneisses, Jotunites, and Ferrodiorites Associated with Anorthosite Massifs

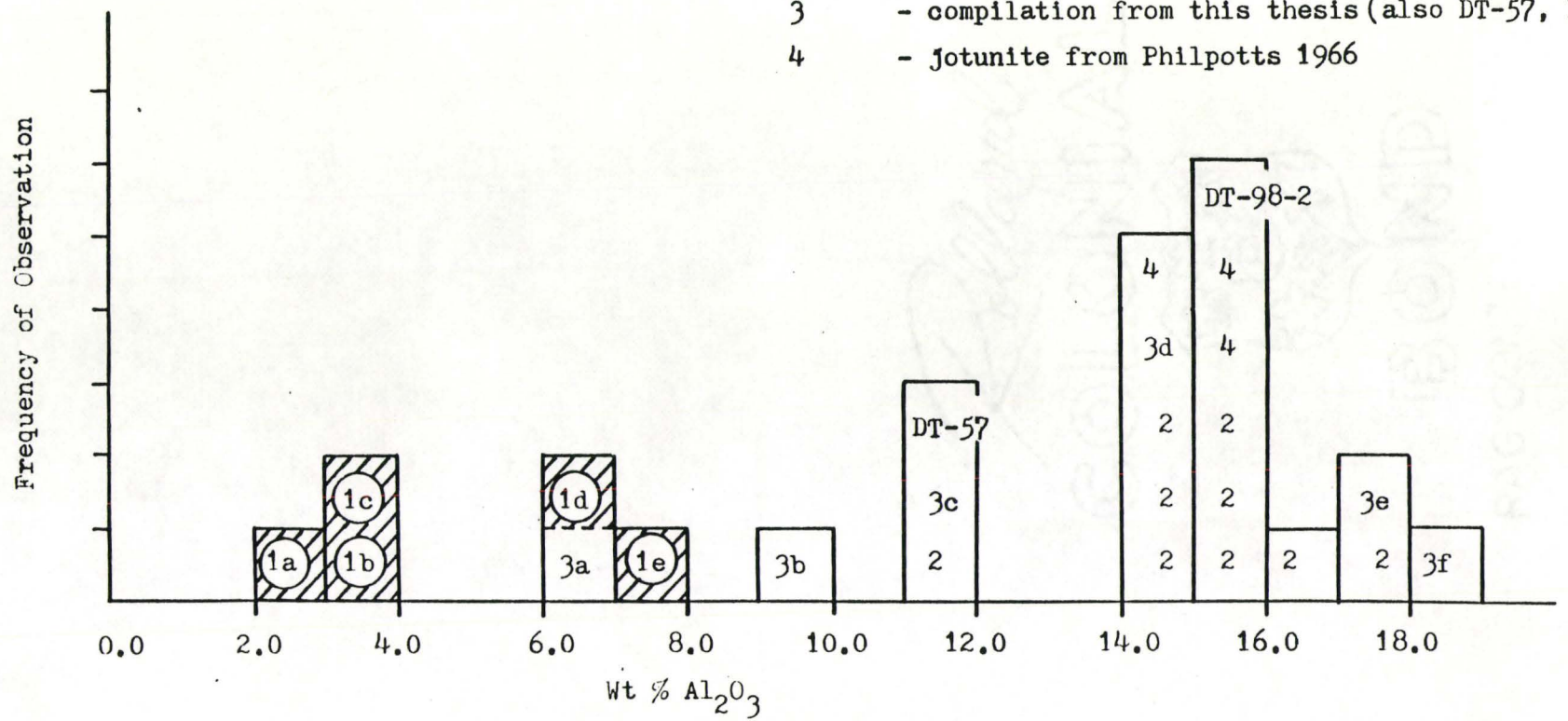


Known Immiscible Liquids ; 1a-1d - naturally occurring examples, Philpotts 1981 and Hess 1980.



1e - experimental composition, Philpotts 1981
 Gneisses, Jotunites and Ferrodiorites ;

- 2 - compilation from Emslie 1980
- 3 - compilation from this thesis (also DT-57, DT-98)
- 4 - jotunite from Philpotts 1966



confusion may arise when anorthosite massifs become strongly deformed and metamorphosed. Figure 7-III shows the distribution of TiO_2 and P_2O_5 measured in the granulite gneisses studied in this thesis. The calculated average values agree closely with those given by Emslie (1980) for average granulite terrains. A plot of TiO_2 vs. P_2O_5 (Figure 7-IV) gives a positive linear correlation. The anomalous samples (marked by their sample number) are the samples containing the garnet-clinopyroxene assemblage. Sample DT-57 (the mafic gneiss which was sampled close to the anorthosite contact) contains the best developed garnet-clinopyroxene assemblage (or the highest gt-cpx concentrations) of the rocks studied, and also, the greatest concentration of TiO_2 and P_2O_5 . Sample DT-98-2 is the mafic reaction rim discussed in the slab study. It is interesting to hypothesize that the linear relationship observed in this plot is due to a concentration process similar to that observed in the reaction rim study. Figure 7-V is a composite TiO_2 - P_2O_5 plot showing the field of samples from this thesis (Figure 7-IV), as well as jotunite gneisses and mafic intrusive rocks associated with anorthosite massifs. Also shown is the path of alteration for the Marcy Massif, the Whitestone Anorthosite, and the reaction rim study.

Observations made in the reaction rim study support the notion that the increased concentration of TiO_2 and P_2O_5 observed in the garnet-clinopyroxene assemblages (notably the mafic contact gneiss DT-57) is due to reactions taking place in the solid state. Two possible end-member processes may be envisioned:

FIG 7-III Distribution of TiO_2 and P_2O_5 in Granulite Facies Gneisses

Note: the shaded samples are considered to be anomalous and have not been included in the calculation of average values.

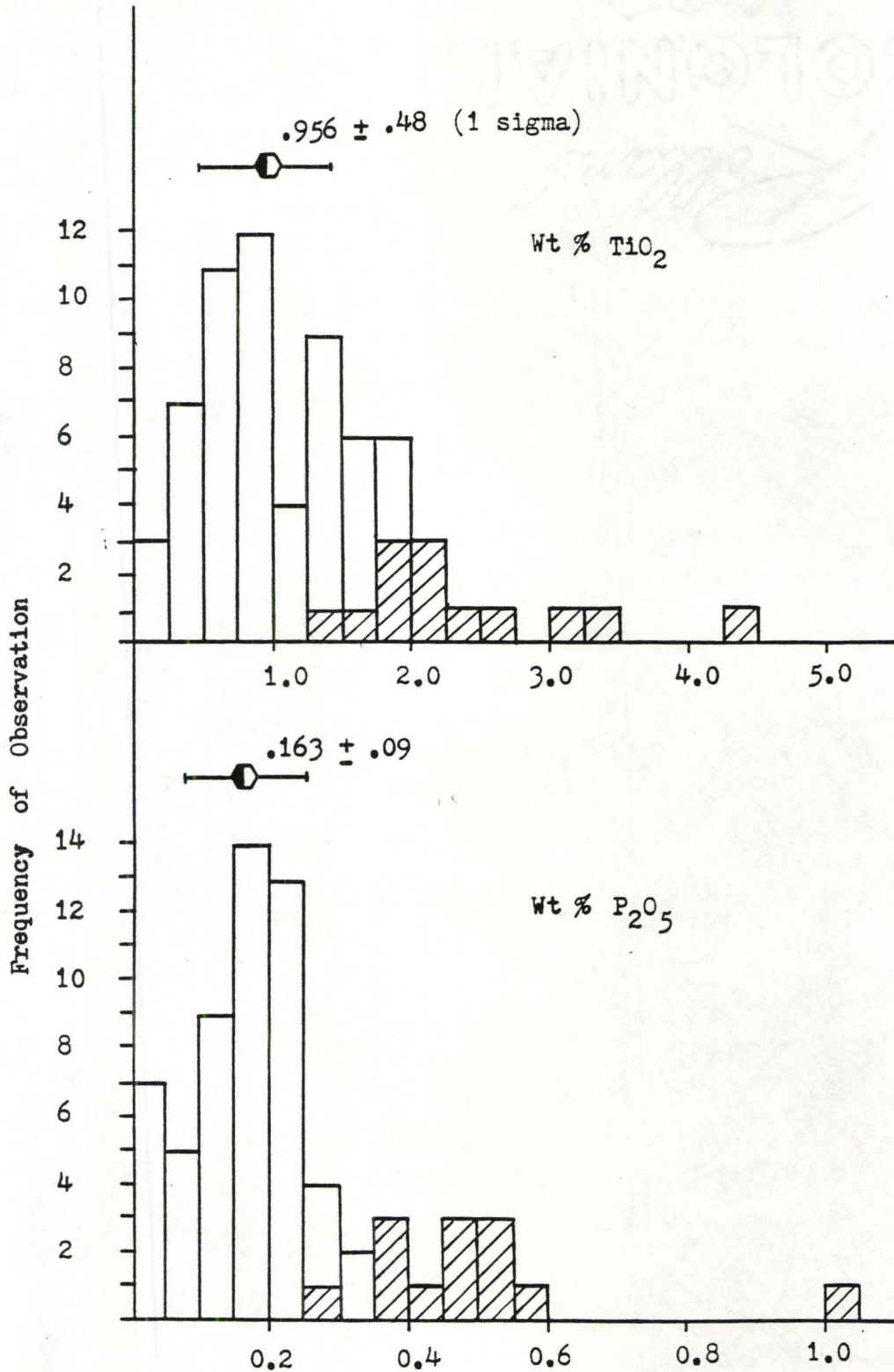


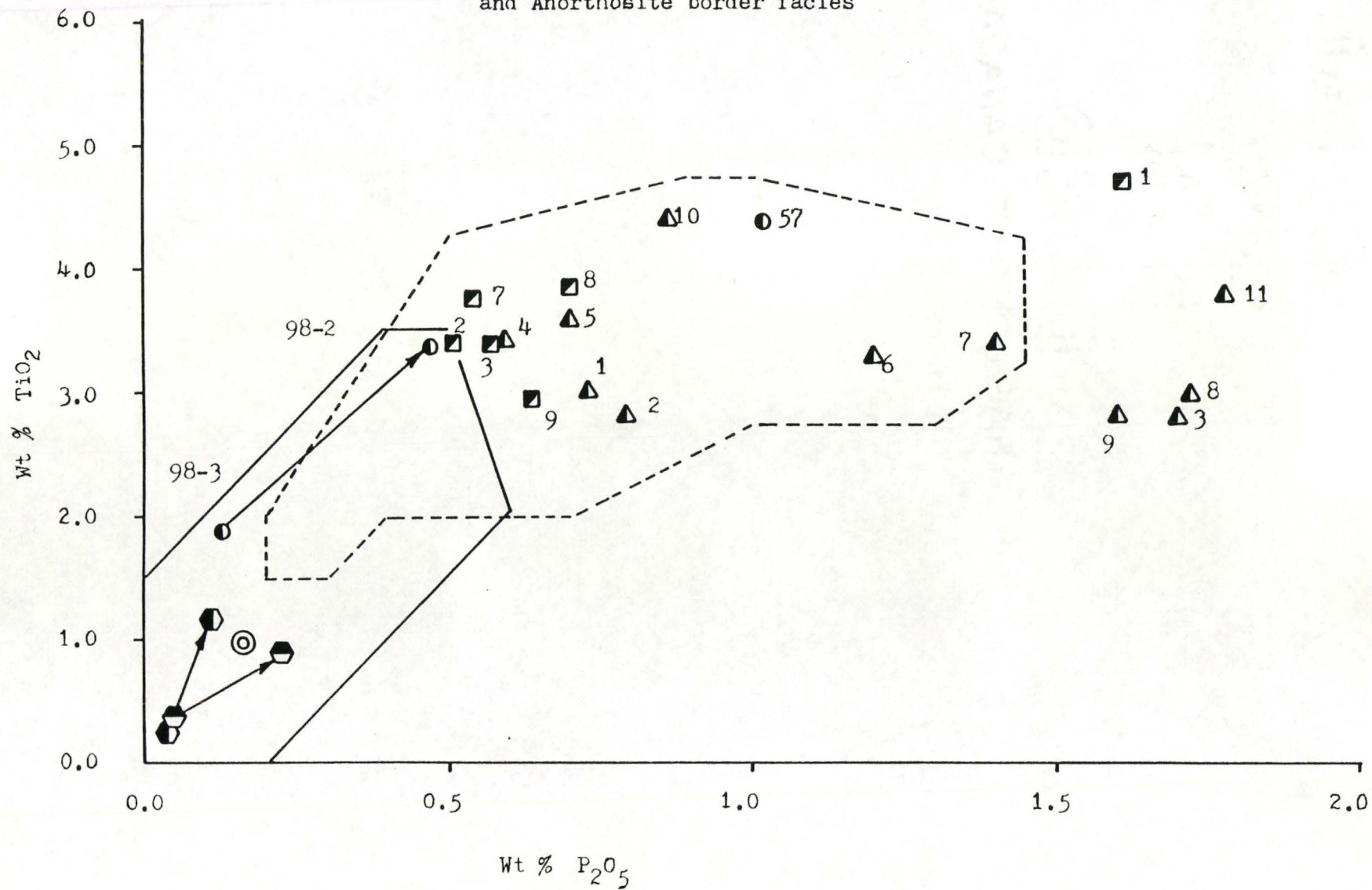
FIGURE 7-V

Variation of TiO_2 and P_2O_5 : Key to Figure

- 
 Compilation of Ferrodiorites from Emslie (1980, p. 133).
- 
 Ferrodiorites from other Anorthosite Massifs.¹
- 
 Path of concentration in reaction rim study:
 98-3 = mafic inclusion
 98-2 = reaction rim
- 
 Average value of TiO_2 and P_2O_5 in granulite facies gneisses, data from this study and Emslie (1980).
- 
 Path of alteration (core → foliated margin), White-stone Anorthosite, based on average analyses from Mason (1969), and this study.
- 
 Path of alteration (as above), Marcy Massif, analyses from Buddington (1939).
- 
 Field of ferrodiorites from the Harp Lake Anorthosite, Emslie (1980).
- 
 Field of all granulites and altered rocks, this study - taken from Figure 7-IV.

1. Analyses from: Buddington (1939), Philpotts (1966, 1967), and Mason (1969).

Variation of TiO_2 and P_2O_5 in Granulites, Ferrodiorites (Jotunite),
and Anorthosite border facies



1. In situ concentration of immobile elements as a restite phase, by partial leaching of inherently more mobile elements such as Si, K, Na, and volatiles.
2. A combination of infiltration and diffusion metasomatism in which a mobile fluid phase, enriched in the necessary mafic components, soaks into the rock thereby changing the relative concentration of all elements.
3. Some combination of the above two processes.

Infiltration metasomatism is favoured by Mason (1969) as an explanation for the garnet-clinopyroxene assemblages associated with the Whitestone Anorthosite contact. A number of objections may be raised to this conclusion. The contact gneisses in question have been re-crystallized to an approximately anhydrous, polygonal mosaic, at an estimated temperature of 750 °C and a pressure in excess of 7 kbs. If these rocks have been affected by a fluid phase, then it is unusual that there is no evidence of volatile alteration preserved in outcrop or in thin section. Solutions, having the necessary volatile concentrations required to complex and transport the metal ions supposedly added, are generally not considered to be present under these metamorphic conditions. Therefore, if metasomatism has played any part in the formation of these rocks, the addition must have occurred by solid state diffusion. The main objection to this conjecture is that the metal ions we are required to move are notorious for their immobility. In summary, it would appear that our present understanding of metamorphic transport processes negates the hypothesis of infiltration metasomatism, as a viable process

responsible for the unusual chemistry of these rocks.

7-IV Summary and Conclusions

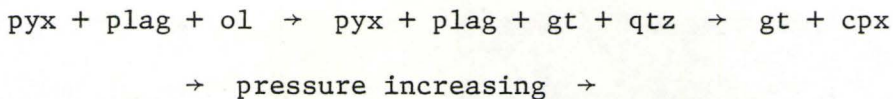
The Whitestone Anorthosite is, in many respects, characteristic of metamorphosed anorthosite bodies (see Review of Field Relations, 7-I). Therefore, one may conclude that tectonic mixing and metamorphic assimilation are important processes during granulite grade metamorphism of anorthosite massifs. Samples DT-098-2 (reaction rim study) and DT-057 (mafic contact gneiss) demonstrate that Fe, Ti, P enrichment in mafic gneisses can occur by solid state metamorphic processes. Figure 7-V indicates that there is a continuous variation in Ti and P between the mafic gneisses studied in this thesis and the jotunites and ferrodiorites reported in the literature. Therefore, it is critically important to determine in the field, the exact nature of each of these rock types, i.e., whether they were originally intrusive, and most importantly, to what degree they have been affected by metamorphism. The high concentration of Al_2O_3 in jotunites and ferrodiorites is not compatible with their formation by immiscible separation.

CHAPTER 8

CONTROLS ON THE DEVELOPMENT OF GARNET-CLINOPYROXENE ASSEMBLAGES

8-I Temperature Pressure Boundary Conditions of the Granulite Facies and the Significance of Garnet Granulites

In Figure 8-I, selected experimental data is used to bracket the location of the granulite facies in P, T space. The medium to high pressure granulite facies and the granulite-eclogite transition have been studied experimentally by Green and Lambert (1965), Green and Ringwood (1967, 1972), Ito and Kennedy (1971), and Kennedy and Ito (1972). These experiments established a general pattern of mineralogical variation with increasing pressure:



The width of the transition zone between these assemblages is strongly dependent on whole rock composition; the most significant parameters being:

- i) Degree of silica saturation.
- ii) Ab/An ratio of the plagioclase.
- iii) Fe/Mg ratio.

de Waard (1965) has subdivided the granulite facies into a number of subfacies on the basis of variations in P (total) and P (H₂O)

FIGURE 8-I

Pressure Temperature Boundary
Conditions of the Granulite Facies

1. Minimum melting of granite, excess H₂O (Wyllie 1977).
2. Granite liquidous, excess H₂O (Wyllie 1977).
3. $\text{Mu} + \text{Qtz} \rightarrow \text{Kspar} + \text{Al}_2\text{SiO}_5 + \text{H}_2\text{O}$ < 5.8 kbs.
 $\text{Mu} + \text{Qtz} \rightarrow \text{Kspar} + \text{sill} + \text{liq}$ > 5.8 kbs.
 (Muller and Saxena 1977)
4. First appearance of garnet in quartz tholeiites, Fe/Fe + Mg = 30-70 range. Curve represents an average of the P-T range (Green and Ringwood 1967).
5. Garnet in curve for average adamellite (Green and Lambert 1965).
6. Disappearance of plagioclase in quartz tholeiites: gabbro-eclogite transition. Curve represents an average of the P-T range (Green and Ringwood 1967).
7. Granite liquidous - dry (Wyllie 1977).
8. Tonalite liquidous - dry (Wyllie 1977).
9. $\text{An} + 2\text{En} \rightarrow \text{Pyrope} + \text{Diop} + \text{Qtz}$
 $\text{opx} \rightarrow \text{cpx} + \text{garnet}$ transition (Hansen 1981).
 Dotted line indicates displacement of curve with increasing Fe/Mg ratio (calculated by Hansen 1981).
10. Al₂SiO₅ triple point. Average from: Mueller and Saxena (1977), Holdaway (1971), and Richardson et al. (1969).
 Also indicated are the 20, 30, and 50 °C/km geotherms, and the critical point of H₂O (marked CP). Box indicates the best estimate of P-T conditions during final equilibration of garnet-clinopyroxene assemblage.

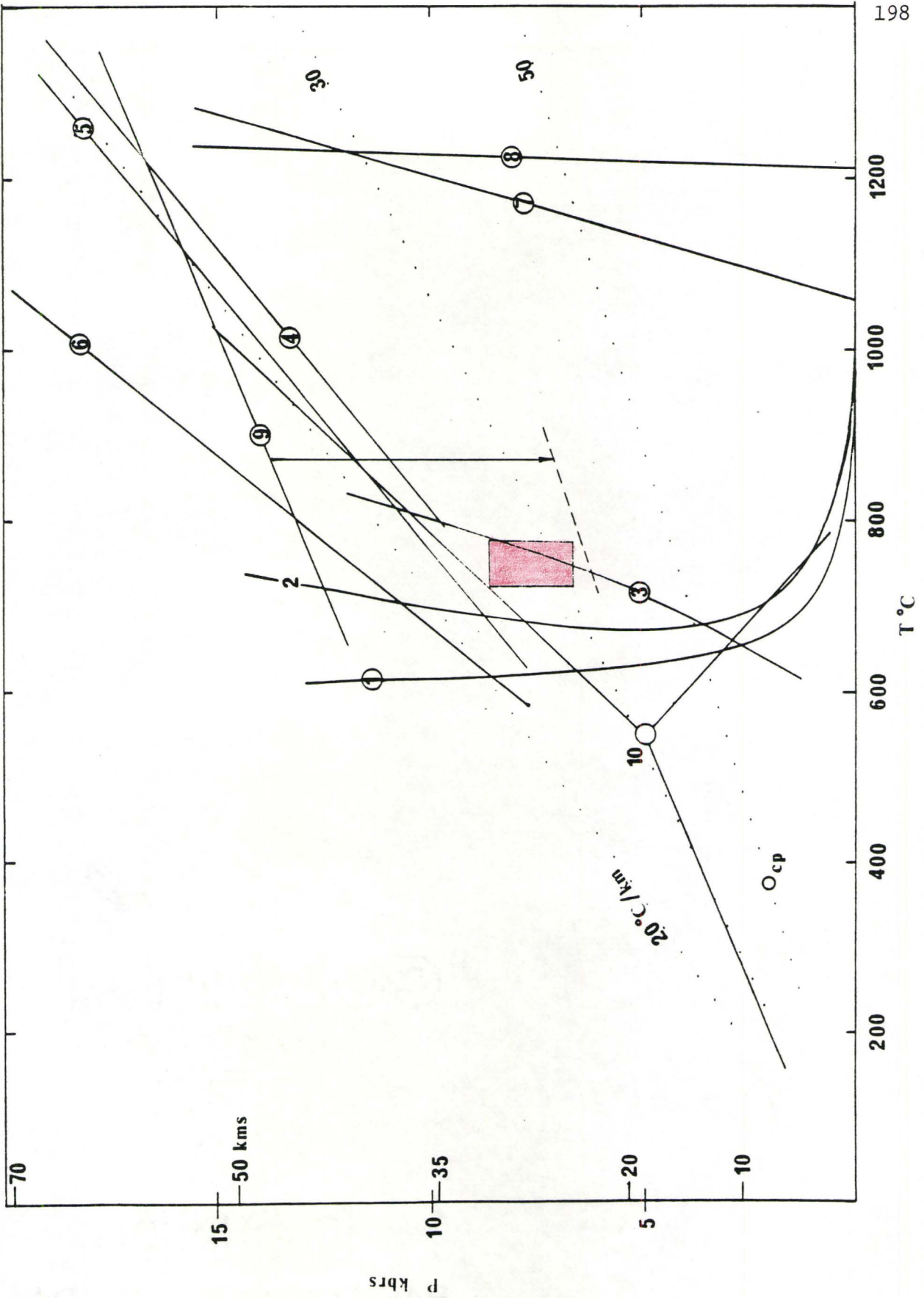


FIGURE 8-II

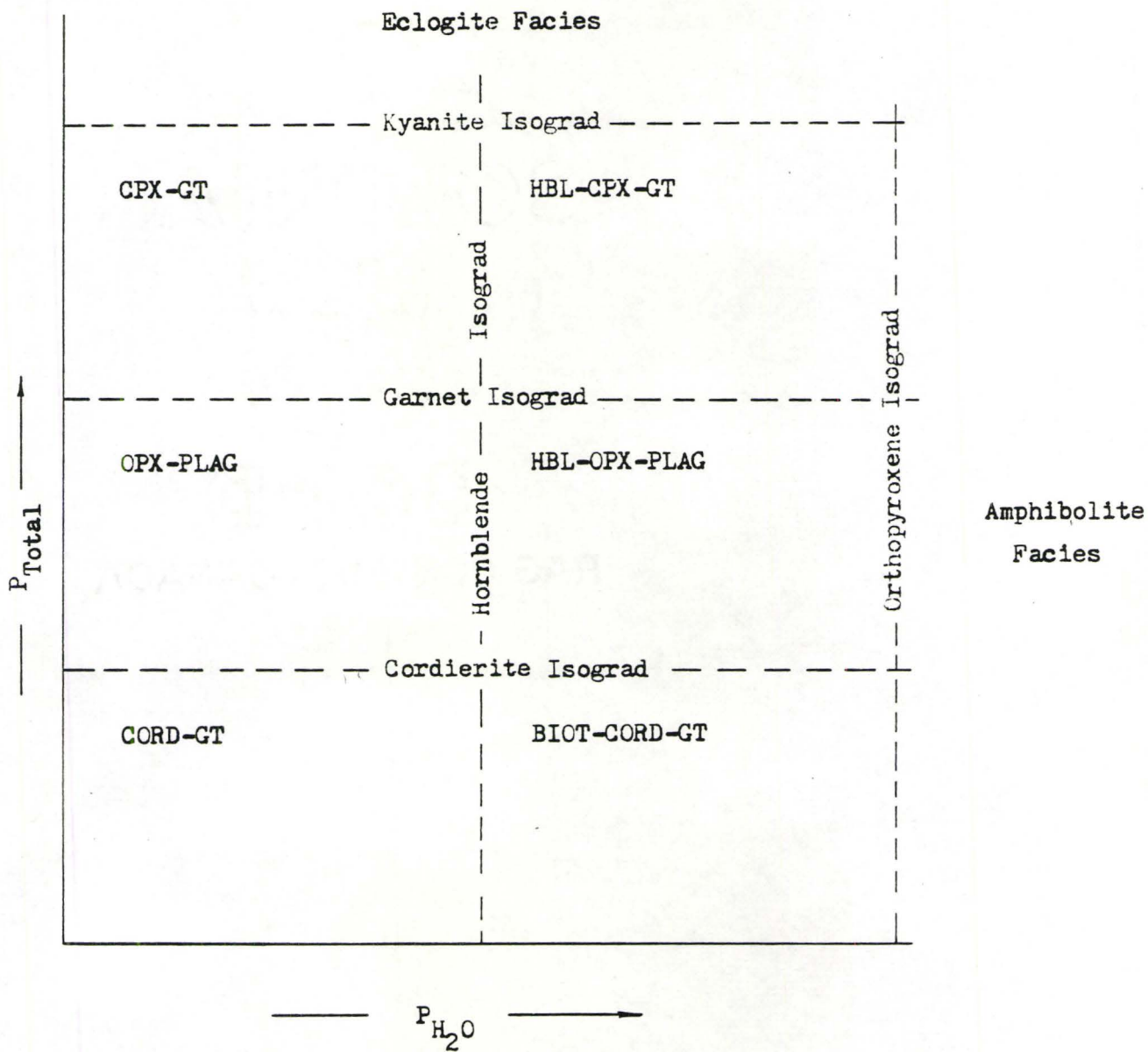
Subdivisions of the Granulite Facies

de Waard (1965) has subdivided the granulite facies into six subfacies, based on the intersection of two dehydration boundaries and two pressure dependent anhydrous reactions. The three subdivisions based on $P(\text{total})$, correspond to the high, medium, and low pressure subdivisions of the granulite facies suggested by Green and Ringwood (1967).

This approach is informative because it explains the considerable overlap which occurs in P-T space between the granulite facies and surrounding facies, however, the boundaries are somewhat subjective.

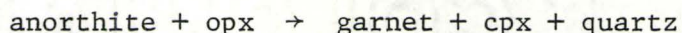
The boundary between the low P granulite facies and the pyroxene hornfels facies is difficult to define, because many of the representative mineral assemblages are the same for both facies. According to Turner (1981), quite often the distinction must be made on field criteria alone.

The high P granulite - eclogite transition is marked by the kyanite isograd. But if we accept the definition of "eclogite" as proposed by Green and Ringwood (1967), and Winkler (1979), then only kyanite bearing rocks of basaltic composition, and having a complete eclogite mineralogy, are truly within the granulite facies. Other rocks containing kyanite may or may not be within the eclogite facies, therefore, the kyanite isograd only indicates the "general region" in which the transition takes place.



(see Figure 8-II). The subdivisions are supported by experimental work, however, Green and Ringwood (1967) note that the presence of hydrous minerals will tend to suppress the formation of the experimental assemblages.

More recently, the transition from the pyroxene granulite facies to the garnet-clinopyroxene granulite facies has been studied by Hansen (1981) in the system CMAS. In this system, the reaction of interest becomes:



The right hand side of the reaction represents the higher pressure phase assemblage, and marks the beginning of "eclogite-like mineralogy". Two points are worthy of note; first, the garnet-clinopyroxene assemblage signifies high pressure only in SiO_2 saturated rocks. If quartz is not present, garnet + clinopyroxene may develop at lower pressure (and temperature), so the assemblage may appear before the orthopyroxene isograd is crossed in a prograde metamorphic sequence. And second, as is shown in Figure 8-II, the transition takes place at greatly reduced pressure for rocks having high Fe/Mg ratios (Hansen 1981).

8-II Composition Paragenesis Diagrams

AFM projections of the mineral assemblages studied in this thesis are shown in Figure 8-III (a, b, and c). The samples have been divided into three groups:

1. Figure 8-III(a): orthopyroxene, hornblende, clinopyroxene assemblages
2. Figure 8-III(b): garnet, orthopyroxene, hornblende, clinopyroxene assemblages.
3. Figure 8-III(c): garnet, hornblende, clinopyroxene assemblages.

Analyses were not available for orthopyroxene in sample DT-36 or clinopyroxene in sample DT-37 (Figure 8-III(b)), therefore, compositions consistent with the known tie lines have been assumed (these values are shown by filled circles).

Unfortunately, these plots are not rigorous composition paragenesis diagrams, because most of the samples do not meet the requirements of the projection, i.e., many do not contain K-spar and some do not contain quartz. With these reservations in mind, there are a number of empirical relationships evident which are worthy of consideration. The garnet rich gneisses fall on the extreme left of the field while the garnet absent felsic gneisses fall on the extreme right. Samples containing all four phases generally fall in the central region, overlapping both the garnet rich and garnet absent field. Whole rock values (shown in Figure 8-III(d)) fall into three separate fields which correspond to the three groups discussed above. These observations indicate that the whole rock Fe/Mg ratio is one of the most significant factors controlling the mafic mineral assemblages present in these rocks.

FIGURE 8-III

Composition Paragenesis Diagrams:
Diagrammatic Representation of the Relation Between Bulk
Chemistry and Mineral Composition

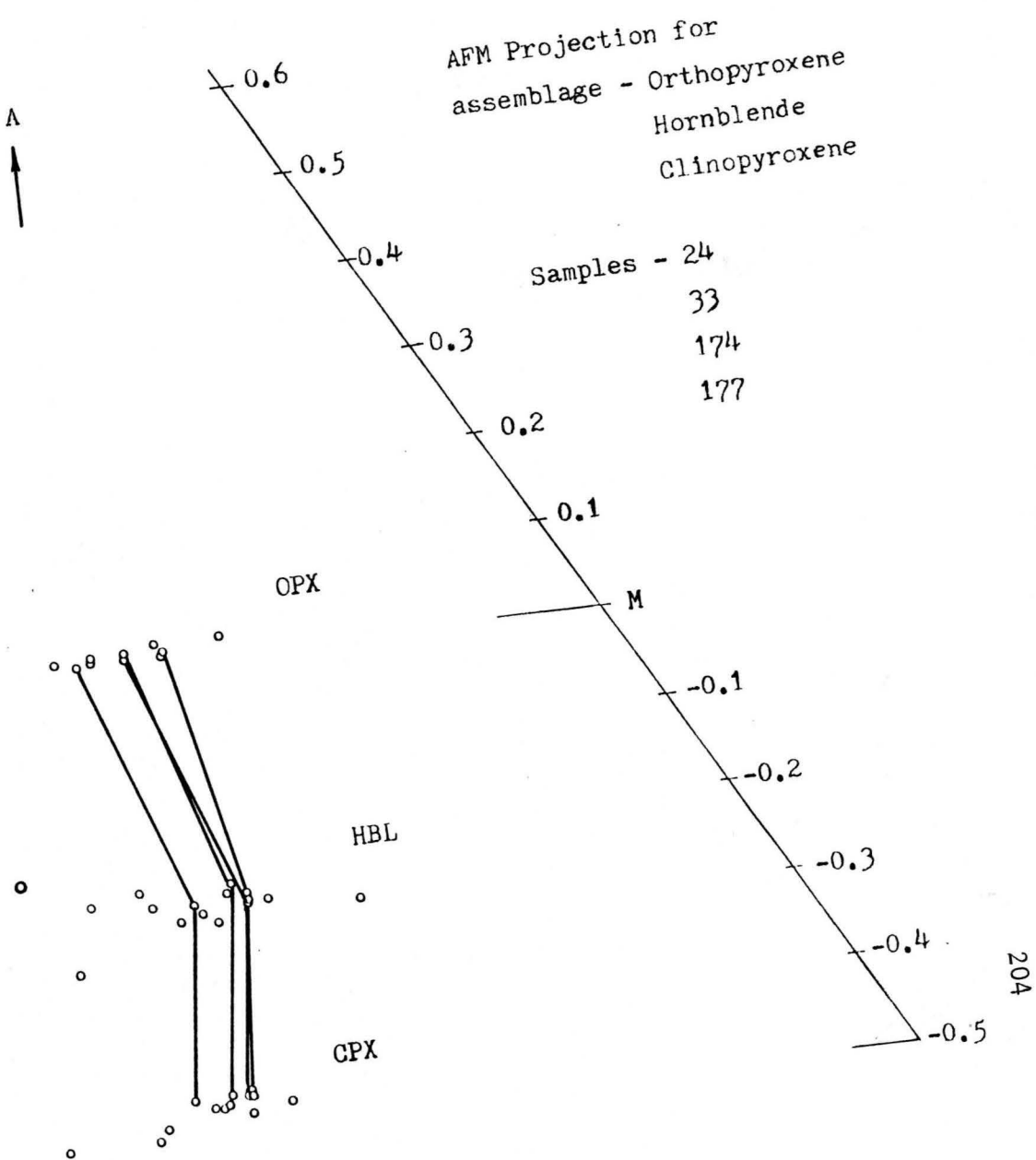
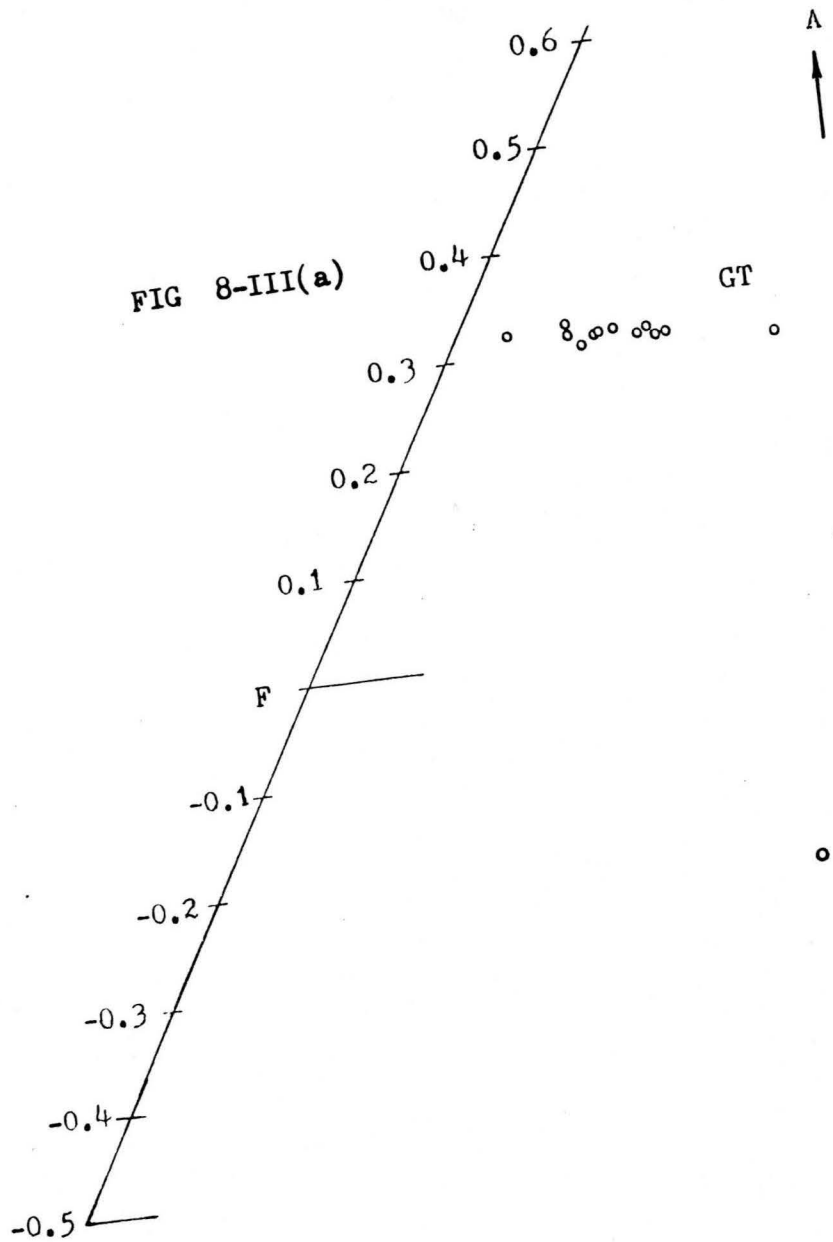
The AFM diagram is a graphical treatment developed by Thompson (1957) to represent mineral assemblages in muscovite bearing meta-pelites. Reinhardt (1968), and Reinhardt and Skippen (1970), devised an AFM projection applicable to high grade rocks having a wider range of composition than that of metapelites. The AFM compatibility triangle is derived by elimination of the common phases: K-spar, plagioclase, magnetite, and ilmenite (in addition to SiO_2 which is an excess component). H_2O is considered to be a perfectly mobile component whose chemical potential is fixed by an external system and, therefore, is not included in the projection (see below). A, F, and M, are calculated as follows:

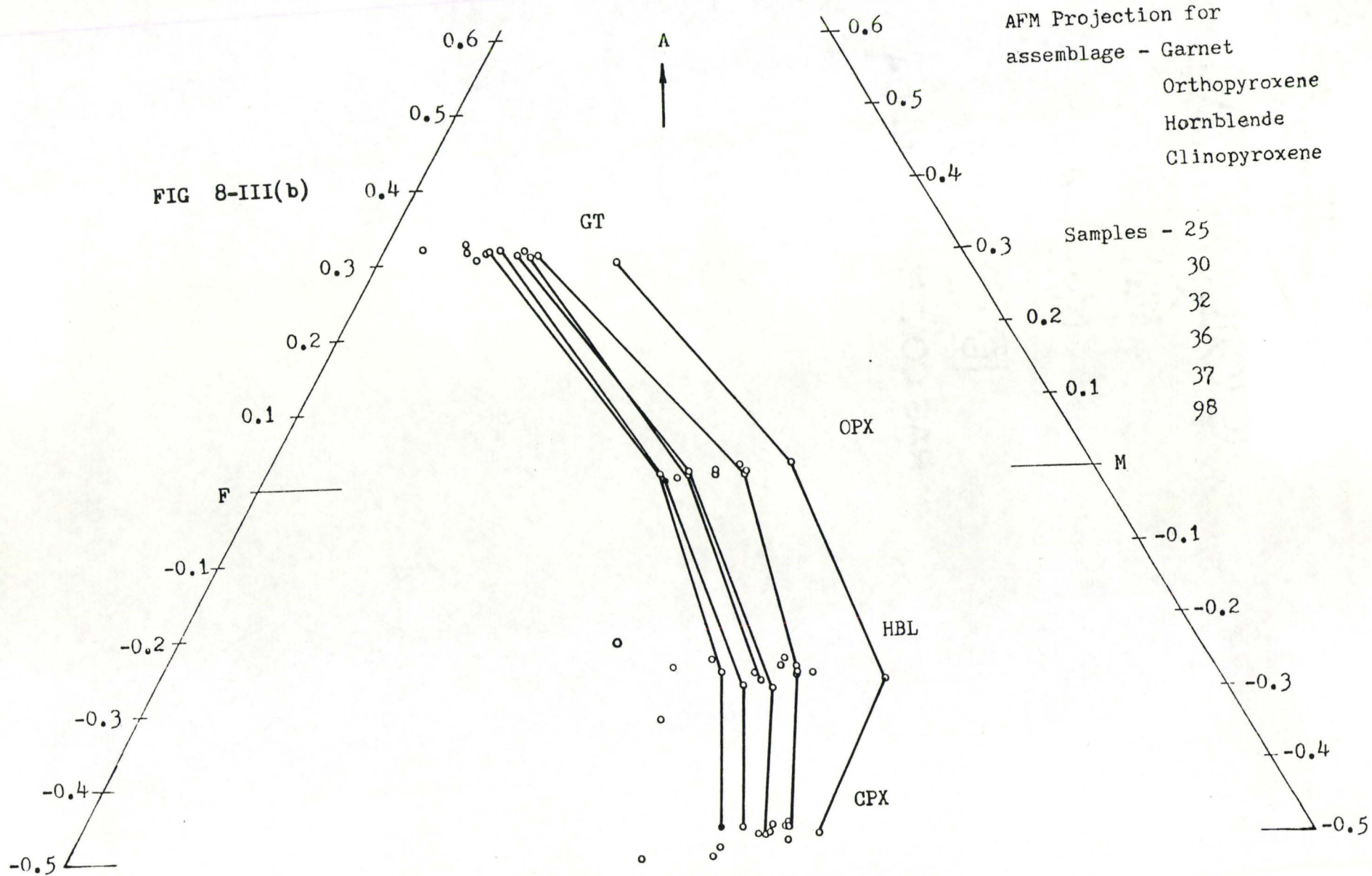
$$A = \text{Al}_2\text{O}_3 - (\text{K}_2\text{O} + \text{Na}_2\text{O} + \text{CaO})$$

$$F = \text{FeO} - (\text{Fe}_2\text{O}_3 + \text{TiO}_2)$$

$$M = \text{MgO}$$

1. For a discussion on the concept of perfectly mobile components and their relationship to the phase rule see: Thompson (1955, 1959, 1970), Korzhinskii (1959, 1966, 1967), and Weill and Fyfe (1964, 1967).





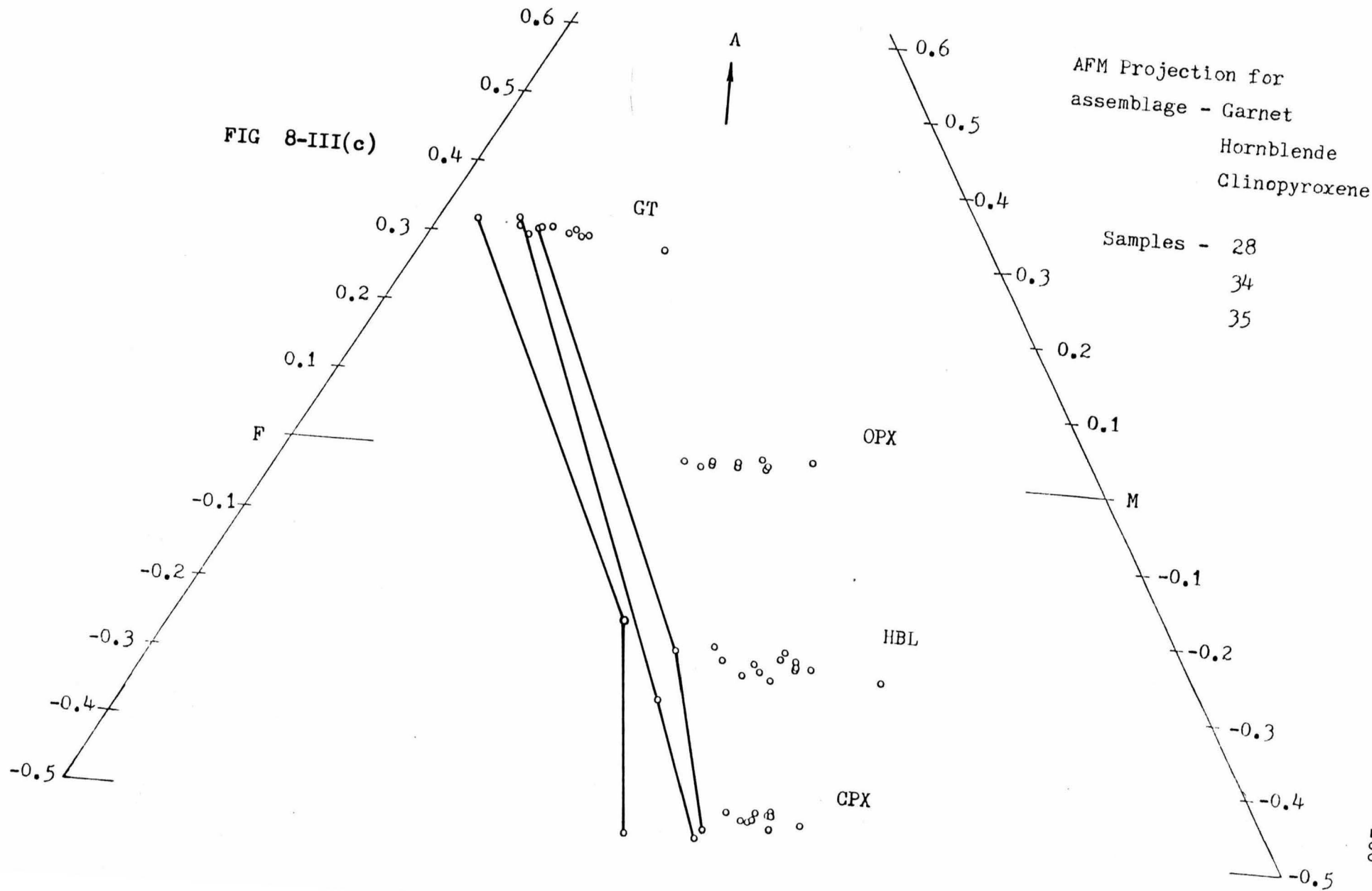
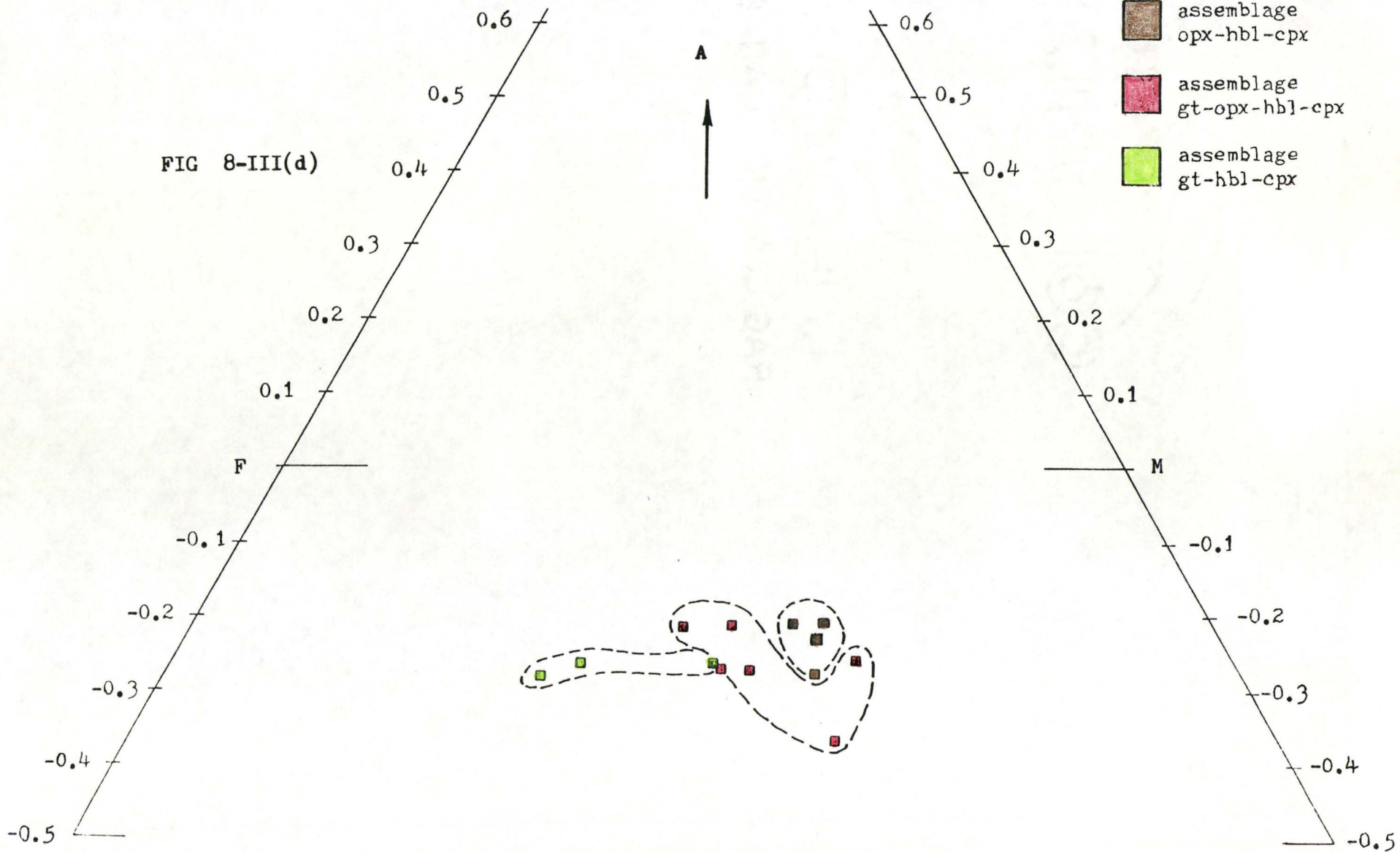


FIG 8-III(d)



8-III Significance of Hydrous Minerals

According to de Waard's (1965) classification scheme, the garnet rich gneisses fall in the high P(total), low P(H₂O) region of the granulite facies--the garnet-clinopyroxene subfacies. The AFM plot indicates that the garnet-clinopyroxene assemblage occurs in rocks having high Fe/Mg ratios, and as has been demonstrated by Hansen (1981), this will stabilize the assemblage at much lower pressures than might be expected.

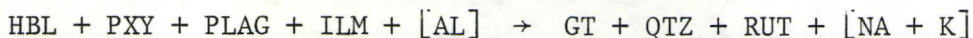
Although the mineral assemblages observed in this study are consistent with existing experimental studies, there is one important point which has not been addressed. This is the role of hornblende. Experimental studies dealing with granulite mineral assemblages and the granulite-eclogite transition have generally not included hydrous minerals, however, field studies indicate that these minerals are of significant importance. Blattner (1976) has documented the replacement of hornblende by garnet in granulite facies gneisses (metadiorite) from Milford Sound, New Zealand (see Figure 8-IV). The replacement takes place in narrow, bleached zones modelled after pre-existing subplanar fracture systems. Loss of H₂O from the rock is considered to be the primary cause of garnet formation.

Glassley et al. (1980) describe metamorphosed dolerite dykes from the Isortoq complex of central west Greenland which display an unusual zoning. The dyke margins exhibit amphibolite facies assemblages while the dyke cores are within the garnet granulite facies. Pyroxene granulite rocks intervene between the two. They conclude that the

FIGURE 8-IV

Replacement of Hornblende by Garnet
in Granulite Facies Assemblages

Detail of garnet replacement shown opposite (taken from Blattner 1976). The greenish-grey, medium grained hornblende metadiorite is transected by swarms of bleached "looking", subplanar zones approximately 5.0 cm wide, within which hornblende is replaced by garnet. Chemical analysis of the bleached zones shows loss of Na and K and an increase in Al, with respect to the unaltered rock. Blattner (1976) suggests the following generalized reaction:



Frequently (but not always), pegmatoid veins occupy the centre of the garnet zones, while others cross-cut at high angles. The veins consist almost entirely of plagioclase (oligoclase) and small amounts of scapolite.

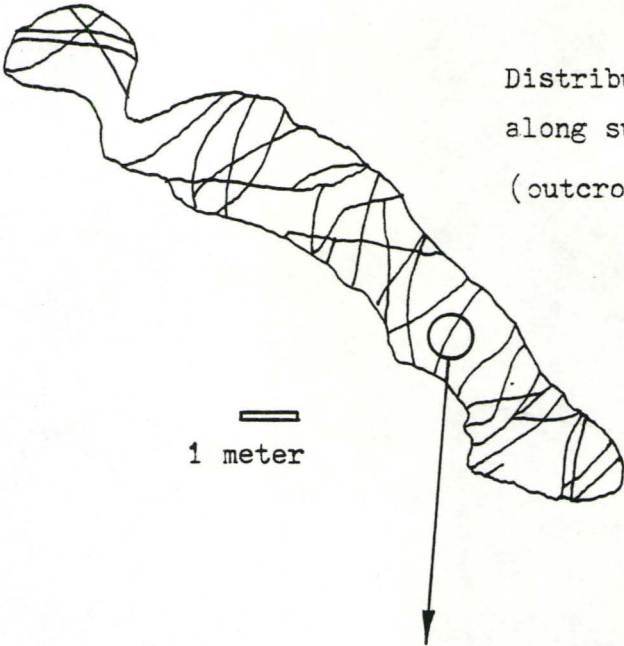
MODAL COMPOSITIONS

	Hornblende Granulite	Garnet-Pyroxene Granulite
Plag	56.0	49.0
CPX	12.0	9.0
OPX	11.0	7.0
HBL	13.0	—
GT	—	27.0
QTZ	2.0	4.0
ILM	2.0	—
RUT	—	tr
AP	tr	tr
S[HBL - EP]	3.0	2.0

Note: - = not detected

tr = trace amounts

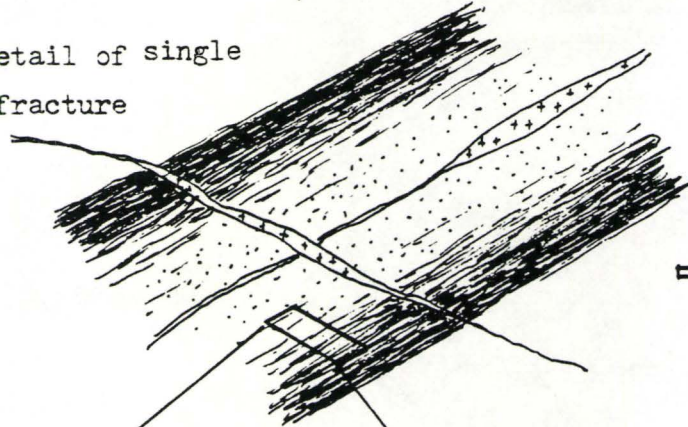
S[HBL - EP] = secondary hornblende and epidote.



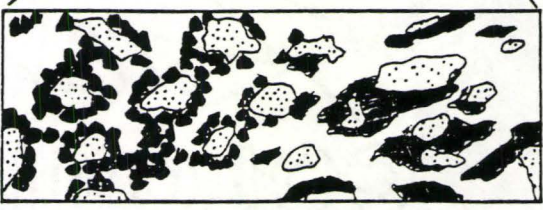
Distribution of garnet zones
along subplanar joint pattern
(outcrop sketch along creek)

1 meter

Detail of single
fracture



5 cms



- cpx and opx
- hbl
- gt

Detail in thin section

pattern resulted from reactions in compositionally zoned dykes, in which $a(\text{H}_2\text{O})$ was greatest near the margin and lowest in the core. This example demonstrates that amphibolite facies assemblages may develop contemporaneously with, and adjacent to, granulite facies assemblages during prograde metamorphism.

8-IV Conclusions

The majority of garnet rich gneisses studied in this thesis are within the clinopyroxene-garnet subfacies of the granulite facies. The characteristic assemblage is stabilized by a high Fe/Mg ratio, and the breakdown of hornblende as a result of dyhydration. The close correspondence of these two factors suggests that they may be related to the same physio-chemical event. Sample DT-030 (see Plate 2-VIII) has a very low Fe/Mg ratio but is garnet rich. This divergence from the normal trend is explained by its undersaturated nature.

CHAPTER 9
SUMMARY AND CONCLUSIONS

9-I General Statement

The following conclusions are supported by the observations reported in this thesis:

1. The metasomatic alteration exhibited by the Whitestone Anorthosite is thought to be due to a combination of two processes:
 - (i) Mechanical mixing at the anorthosite/country rock contact during intense deformation.
 - (ii) Widespread absorption of mobile components (predominantly volatiles) from both included material and the surrounding rocks.

2. The formation of the "contact aureole" (or reaction aureole) is a continuous solid state metamorphic process whereby mobile components are preferentially leached from the rock leaving a mafic restite. Pre-existing mafic rocks are affected to a much greater degree than felsic rocks as a consequence of the devolatilization process and resulting hornblende breakdown.

Post deformation cooling of the anorthosite combined with an increased volatile flux (which enhances reaction rates thereby facilitating re-crystallization) has imparted a polygonal mosaic texture to the contact gneisses suggestive of contact metamorphism.

3. The typical garnet-clinopyroxene-plagioclase-oxide-apatite \pm quartz assemblage exhibited by mafic gneisses within the reaction aureole, is a consequence of the increased Fe/Mg ratio which stabilizes this assemblage at lower P, T conditions. The temperature of final equilibration and re-crystallization of the contact rocks, estimated to be 750 ± 70 °C, is thought to represent a retrograde overprint on a pre-existing granulite assemblage. Garnet poor gneisses give an average temperature of 845 ± 70 °C. This may represent a minimum value for the earlier metamorphism, however, the exact significance of this temperature is not known and in general is not considered very reliable.
4. Garnet-clinopyroxene temperatures calculated using the data from Mummery (1972), give an average temperature of 670 ± 70 °C for the western margin of the Whitestone Anorthosite, while data from this thesis indicates an average temperature of 750 ± 70 °C for the eastern margin. Although there is little statistical difference between these temperatures, the K(D)'s are clearly different supporting the existence of a temperature difference. Davidson (personal communication) has noted that along the western margin of the Parry Sound block there has been almost complete retrogression to amphibolite assemblages, therefore the lower values may indicate the influence of increased $a(\text{H}_2\text{O})$ which would allow equilibration to a lower temperature. It is also possible that the assemblages (from Mummery) are non-equilibrium. In any case, because these temperatures are all interpreted as retrograde, a valid

difference between two regions is not necessarily indicative of a temperature gradient, rather it is more likely to represent differing kinetic control during retrogression.

5. The oxidation state of Fe in mafic minerals, measured by Mossbauer spectroscopy, is approximately constant throughout the study area and shows no significant correlation with mineral assemblage, whole rock chemistry or proximity to the anorthosite contact. The reason for this consistency has not been adequately explained. If these values are representative of granulite terrains in general, then they are quite useful for the correction of mineral analyses determined by microprobe.
6. The garnet rich mafic gneisses studied in this thesis do not fit the theoretical chemical partitioning (or separation) expected if liquid immiscibility were the predominant process responsible for their formation. Field relations also do not support this concept. I submit that a similar process to the one outlined in this thesis is to be expected at all anorthosite-country rock contacts which have been overprinted by granulite metamorphism.

9-II Final Word

The reaction aureole which partially surrounds the Whitestone Anorthosite is interpreted to be retrograde. This conclusion is based on:

1. The calculated lower temperature and/or pressure of the garnet-clinopyroxene assemblage.
2. The observation (in thin section) that the garnet-clinopyroxene assemblage appears to overprint an earlier orthopyroxene-clinopyroxene assemblage.
3. The undeformed nature of the re-crystallized contact rocks.

It was shown in Chapter 8 that the garnet-clinopyroxene assemblage is stabilized in rocks having a high Fe/Mg ratio, and this fact alone could explain the occurrence of this assemblage, i.e., during progressive metamorphism (and interaction with the anorthosite) the chemistry of these rocks changed slowly until they entered the stability field of the garnet-clinopyroxene assemblage. However, Buddington (1963) noted that garnet also tends to form in weakly sheared zones, in rocks otherwise poor in garnet. This observation suggests that there could be a kinetic control as well.

One important factor may be the unique thermal properties of anorthosite. Thermal diffusivity is defined as (Oxburgh, 1980):

$$K = \frac{k}{\rho C_p}$$

where: K = thermal diffusivity

k = thermal conductivity

ρ = density

C_p = heat capacity

The thermal conductivity (k) of anorthosite is approximately 25% lower than most other crustal rocks (Pollack and Roy 1968). In addition, the value of the thermal conductivity, measured normal to the foliation, may be reduced by more than a factor of two. For any thermal perturbation of the crust, a crude estimate of the time required for return to thermal equilibrium (by conduction alone) may be calculated from:

$$T = \frac{L}{K}$$

where: T = time

L = length

It is clear that as the thermal conductivity of a rock decreases, the time taken for thermal exchange increases. Therefore, a large body of anorthositic rock with a strongly foliated border, which has been heated to granulite temperatures, would cool very slowly and act as significant local heat source. This could explain the "contact aureole" effect, i.e., the growth of numerous, small, euhedral garnets and fairly complete polygonal re-crystallization in the vicinity of the anorthosite. At present this supposition remains highly speculative, because the tectonic (and thermal) history of the Parry Sound block is largely unknown.

REFERENCES

- Aldridge, L. P., Tse, J. S., and Bancroft, G. M. (1982). The identification of Fe^{2+} in the M4 site of calcic amphiboles: discussion. *Amer. Mineral.*, v. 67, pp. 335-339.
- Anderson, D. E., and Buckley, G. R. (1975). Modelling of diffusion controlled properties of silicates. In A. W. Hofmann (ed.), *Geochem. Transport and Kinetics*.
- Angeletos, S. (1975). Developments in oxidation of the (Mg, Fe) SiO_3 pyroxene series and use of thermogravimetry as a quantitative analytical method. *Chem. Geol.*, v. 15, pp. 145-153.
- Bancroft, G. M. (1967). Quantitative estimation of site populations in an amphibole by the Mossbauer effect. *Phys. Letters*, v. 26A, no. 1, pp. 17-18.
- Bancroft, G. M. (1970). Quantitative site population in silicate minerals by the Mossbauer effect. *Chem. Geol.*, v. 5, pp. 255-258.
- Bancroft, G. M. (1973). *Mossbauer Spectroscopy: An Introduction for Inorganic Chemists and Geochemists*. McGraw-Hill, U.K.
- Bancroft, G. M. (1979). Mossbauer spectroscopic studies of the chemical state of iron in silicate minerals. *Jour. de Physique. Colloque C2, Tome 40, C2-464*.
- Bancroft, G. M., and Brown, J. R. (1975). A Mossbauer study of co-existing hornblendes and biotites: quantitative $\text{Fe}^{3+}/\text{Fe}^{2+}$ ratios. *Amer. Mineral.*, v. 60, pp. 265-272.
- Bancroft, G. M., Burns, R. G., and Stone, A. J. (1967). Applications of the Mossbauer effect to silicate mineralogy - II. Iron silicates of unknown and complex crystal structures. *Geochim. Cosmochim. Acta*, v. 32, pp. 547-559.
- Bancroft, G. M., and Maddock, A. G. (1967). Applications of the Mossbauer effect to silicate mineralogy - I. Iron silicates of known crystal structure. *Geochim. Cosmochim. Acta*, v. 31, pp. 2219-2246.

- Barker, J. F. (1972). Rare earth elements in the Whitestone Anorthosite. Unpublished M.Sc. thesis, McMaster University, Hamilton, Ontario.
- Behr, H. J., den Tex, E., de Waard, D., Mehnert, K. R., Scharbert, H. G., St. Sobolev, V., Watznauer, A., Winkler, H. G. F., Wynne-Edwards, H. R., Zoubek, V., and Zwart, H. J. (1971). Granulites, Results of a discussion. *Neus Jahr. Mineralogie, Monatshefte*, v. 3, pp. 97-123.
- Bell, T. H., and Etheridge, M. A. (1973). Microstructure of mylonites and their descriptive terminology. *Lithos*, v. 6, pp. 337-348.
- Berg, J. H. (1977). Regional geothermometry in the contact aureoles of the anorthositic Nain Complex, Labrador. *Jour. Petrol.*, v. 18, pp. 399-430.
- Blattner P. (1976). Replacement of hornblende by garnet in granulite facies assemblages near Milford Sound, New Zealand. *Contrib. Min. Petrol.*, v. 55, pp. 181-190.
- Bohlen, S. R., and Essene, E. J. (1977). Feldspar and oxide thermometry of granulites in the Adirondack Highlands. *Contrib. Min. Petrol.*, v. 62, pp. 153-169.
- Bohlen, S. R., and Essene, E. J. (1979). A critical evaluation of two-pyroxene thermometry in Adirondack granulites. *Lithos*, v. 12, pp. 335-345.
- Bohlen, S. R., and Essene, E. J. (1980). Evaluation of coexisting garnet-biotite, garnet-clinopyroxene, and other Mg-Fe exchange thermometers in Adirondack granulites: Summary. *Geol. Soc. Amer. Bull.*, pt. 1, v. 91, pp. 107-109.
- Brady, J. B. (1975). Reference frames and diffusion coefficients. *Amer. Jour. Sci.*, v. 275, pp. 954-983.
- Brown, G. M. (1979). The problem of the diversity of igneous rocks. In H. S. Yoder (ed.), *The Evolution of Igneous Rocks, Fiftieth Anniversary Perspectives*, Princeton University Press, pp. 3-14.
- Buddington, A. F. (1939). Adirondack igneous rocks and their metamorphism. *Geol. Soc. Amer.*, Mem. 7, 354 p.

- Buddington, A. F. (1963). Isograds and the role of H₂O in metamorphic facies of orthogneisses of the Northwest Adirondack area, New York. *Geol. Soc. Amer. Bull.*, v. 74, pp. 1155-1182.
- Buddington, A. F., and Lindsley, D. H. (1964). Iron-titanium oxide minerals and synthetic equivalents. *Jour. Petrol.*, v. 5, pp. 310-357.
- Burns, R. G. (1972). Mixed valencies and site occupancies of iron in silicate minerals from Mossbauer spectroscopy. *Can. Jour. Spectros.*, v. 17, p. 17, no. 2, pp. 51-59.
- Burns, R. G., and Greaves, C. (1971). Correlations of infrared and Mossbauer site population measurements of actinolites. *Amer. Mineral.*, v. 56, pp. 2010-2033.
- Buseck, P. R., Nord, G. L., and Veblen, D. R. (1980). Subsolidus phenomena in pyroxenes. In C. T. Prewitt (ed.), *Pyroxenes. Mineral. Soc. Amer., Reviews in Mineralogy*, v. 7, pp. 117-204.
- Cameron, M., and Papike, J. J. (1980). Amphibole crystal chemistry: a review. *Fortschr. Mineral.*, v. 57, no. 1, pp. 28-67.
- Carmichael, D. M. (1969). On the mechanism of prograde metamorphic reactions in quartz-bearing pelitic rocks. *Contrib. Min. Petrol.*, v. 20, pp. 244-267.
- Carmichael, I. S. E. (1967). The iron-titanium oxides of salic volcanic rocks and their associated ferromagnesium silicates. *Contrib. Min. Petrol.*, v. 14, pp. 36-64.
- Cawthorn, R. G., and Collerson, K. D. (1974). The recalulation of pyroxene end-member parameters and the estimation of ferrous and ferric iron content from electron microprobe analyses. *Amer. Mineral.*, v. 59, pp. 1203-1208.
- Chinner, G. A. (1960). Pelitic gneisses with varying ferrous/ferric ratios from Glen Cova, Angus, Scotland. *Jour. Petrol.*, v. 1, pt. 2, pp. 178-217.
- Dahl, P. S. (1979). Comparative geothermometry based on major-element and oxygen isotope distributions in Precambrian metamorphic rocks from southwestern Montana. *Amer. Mineral.*, v. 64, pp. 1280-1293.

- Dahl, P. S. (1980). The thermal-compositional dependence of Fe^{2+} -Mg distributions between coexisting garnet and pyroxene: application to geothermometry. *Amer. Mineral.*, v. 65, pp. 854-866.
- Davidson, A., and Morgan, W. C. (1980). Preliminary notes on the geology east of Georgian Bay, Grenville Structural Province, Ontario. In *Current Research, Part A, Geol. Surv. Can.*, Paper 81-1A, pp. 291-298.
- Davidson, A., Culshaw, N. G., and Nadeau, L. (1982a). A tectono-metamorphic framework for part of the Grenville Province, Parry Sound region, Ontario. In *Current Research, Part A, Geol. Can. Surv.*, Paper 82-1A, pp. 175-190.
- Davidson, A., Culshaw, N. G., and Nadeau, L. (1982b). Tectonic features in the Central Gneiss Belt, Parry Sound region, Ontario. *Friends of the Grenville, Field Guide*.
- Davis, B. T., and Boyd, F. R. (1966). The join $\text{Mg}_2\text{Si}_2\text{O}_6 - \text{CaMgSi}_2\text{O}_6$ at 30 kilobars pressure and its application to pyroxenes from kimberlites. *Jour. Geophys. Res.*, v. 71, pp. 3567-3576.
- Davis, J. C. (1973). *Statistics and data analysis in geology*. John Wiley and Sons, Inc. 550 p.
- Deer, W. A., Howie, R. A., and Zussman, J. (1966). *An introduction to the rock forming minerals*. Longman Group, Great Britain, 528 pp.
- Deer, W. A., Howie, R. A., and Zussman, J. (1978). *Rock-forming minerals. Volume 2A: single-chain silicates (2nd ed.)*. Longman Group, Great Britain, 668 pp.
- de Waard, D. (1965). A proposed subdivision of the granulite facies. *Amer. Jour. Sci.*, v. 263, pp. 455-461.
- de Waard, D. (1971). Threefold division of the granulite facies in the Adirondack Mountains. *Krystalinkum*, v. 7, pp. 85-93.
- Dollase, W. A. (1975). Statistical limitations of Mossbauer spectral fitting. *Amer. Mineral.*, v. 60, pp. 257-264.

- Dougan, T. W. (1979). Compositional and modal relationships and melting relations in some migmatitic metapelites from New Hampshire and Maine. *Contrib. Min. Petrol.*, v. 279, pp. 897-935.
- Dougan, T. W. (1981). Melting reactions and trace element relationships in selected specimens of migmatitic pelites from New Hampshire and Maine. *Contrib. Min. Petrol.*, v. 78, pp. 337-344.
- Dowty, E., and Lindsley, D. H. (1973). Mossbauer spectra of synthetic hedenbergite-ferrosilite pyroxenes. *Amer. Mineral.*, v. 58, pp. 850-868.
- Ellis, J., and Green, D. H. (1979). An experimental study of the effect of Ca upon garnet-clinopyroxene Fe-Mg exchange equilibria. *Contrib. Min. Petrol.*, v. 71, pp. 13-22.
- Emslie, R. F. (1980). Geology and petrology of the Harp Lake Complex, central Labrador: an example of Elsonian magmatism. *Geol. Surv. Can. Bull.*, v. 293, 136 pp.
- Engel, A. E. J., and Engel, C. G. (1962). Progressive metamorphism of amphibolite, northwest Adirondack Mountains, New York. *Geol. Soc. Amer., Petrologic Studies, Buddington Volume*, pp. 37-82.
- Essene, E. J., and Fyfe, W. S. (1967). Omphacite in Californian metamorphic rocks. *Contrib. Min. Petrol.*, v. 15, pp. 1-23.
- Eugster, H. P. (1959). Reduction and oxidation in metamorphism. In P. H. Abelson (ed.), *Research in Geochemistry, Volume 1*, pp. 397-426.
- Ferry, J. M., and Spear, F. S. (1978). Experimental calibration of the partitioning of Fe and Mg between biotite and garnet. *Contrib. Min. Petrol.*, v. 76, pp. 113-117.
- Freer, R. (1981). Diffusion in silicate minerals and glasses: a data digest and guide to the literature. *Contrib. Min. Petrol.*, v. 76, pp. 440-454.
- Freer, R., Carpenter, M. A., Long, J. V. P., and Reed, S. J. B. (1982). "Null result" diffusion experiments with diopside: implications for pyroxene equilibria. *Earth Planetary Sci. Lett.*, v. 58, pp. 285-292.

- Freestone, J. C. (1978). Liquid immiscibility in alkali-rich magmas. *Chem. Geol.*, v. 23, pp. 115-123.
- Ganguly, J. (1979). Garnet and clinopyroxene solid solutions, and geothermometry based on Fe-Mg distribution coefficients. *Geochim. Cosmochim. Acta*, v. 43, pp. 1021-1029.
- Ganguly, J., and Kennedy, G. C. (1974). The energetics of natural garnet solid solution. I. Mixing of the aluminosilicate end-members. *Contrib. Min. Petrol.*, v. 48, pp. 137-148.
- Glassley, W. E., and Sorensen, K. (1980). Constant Ps-T amphibolite to granulite facies transition in Agto (West Greenland) meta-dolerites: implications and applications. *Jour. Petrol.*, v. 21, pp. 69-105.
- Goldman, D. S., and Rossman, G. R. (1977). The identification of Fe²⁺ in the M4 site of calcic amphiboles. *Amer. Mineral.*, v. 62, pp. 205-216.
- Goldman, D. S., and Rossman, G. R. (1982). The identification of Fe²⁺ in the M4 site of calcic amphiboles: reply. *Amer. Mineral.*, v. 67, pp. 340-342.
- Graham, C. M. (1981). Experimental hydrogen isotope studies. III. *Contrib. Min. Petrol.*, v. 76, pp. 216-228.
- Green, D. H., and Lambert, I. B. (1965). Experimental crystallization of anhydrous granite at high pressures and temperatures. *Jour. Geophys. Res.*, v. 70, pp. 5259-5268.
- Green, D. H., and Ringwood, A. E. (1967). An experimental investigation of the gabbro to eclogite transformation and its petrologic applications. *Geochim. Cosmochim. Acta*, v. 31, pp. 767-833.
- Green, D. H., and Ringwood, A. E. (1972). A comparison of recent experimental data on the gabbro-garnet granulite-eclogite transition. *Jour. Geol.*, v. 80, pp. 277-288.
- Grover, J. E. (1980). Thermodynamics of pyroxenes. In C. T. Prewitt (ed.), *Pyroxenes*. Mineral. Soc. Amer., *Reviews in Mineralogy*, pp. 341-414.

- Hamm, H. M., and Vieten, K. (1971). Zur berechnung der kristallchemischen formel und des Fe^{3+} -gehaltes von klinopyroxenen aus elektronenstrahl - mikroanalysen. *Neus Jahrb. fur Mineralogie, Monatsheft*, pp. 310-314.
- Hansen, B. (1981). The transition from pyroxene granulite facies to garnet-clinopyroxene granulite facies. Experiments in the system $\text{CaO-MgO-Al}_2\text{O}_3\text{-SiO}_2$. *Contrib. Min. Petrol.*, v. 76, pp. 234-242.
- Haggstrom, L., Wappling, R., and Annersten, H. (1969). Mossbauer study of oxidized iron silicate minerals. *Phys. Stat. Sol.*, v. 33, pp. 741-748.
- Hargraves, R. B. (1962). Petrology of the Allard Lake Anorthosite Suite, Quebec. *Geol. Soc. Amer., Petrologic Studies, Buddington Volume*, pp.
- Hawthorne, F. C. (1973). The crystal chemistry of the clino-amphiboles. Unpublished Ph.D. Thesis, McMaster University, Hamilton, Ontario.
- Hawthorne, F. C. (1981). Amphibole spectroscopy. In D. R. Veblen (ed.), *Amphiboles and Other Hydrous Pyriboles-Mineralogy*. *Mineral. Soc. Amer., Reviews in Mineralogy*, v. 9A, pp. 103-137.
- Heaman, L. M. (1982). The timing of igneous and metamorphic events in the Chandos Township Area, Grenville Province, Ontario. 1982 Grenville Workshop, (Program and Abstracts), Ottawa-Carleton Centre for Geoscience Studies.
- Hensen, B. J. (1977). Cordierite-garnet bearing assemblages as geothermometers and barometers in granulite facies terranes. In D. H. Green (ed.), *Experimental Petrology Related to Extreme Metamorphism, Tectonophysics*, v. 43, pp. 73-88.
- Holdaway, M. J. (1971). Stability of andalusite and the aluminum silicate phase diagram. *Amer. Jour. Sci.*, v. 271, pp. 97-131.
- Hess, P. C. (1971). Prograde and retrograde equilibria in garnet - cordierite gneisses in South-Central Massachusetts. *Contrib. Min. Petrol.*, v. 30, pp. 177-195.
- Hess, P. C. (1977). Structure of silicate melts. *Can. Mineral.*, v. 15, part 2, pp. 162-178.

- Hess, P. C. (1980). Polymerization model for silicate melts. In R. B. Hargraves (ed.), *Physics of Magmatic Processes*, Princeton University Press, pp. 3-44.
- Hewins, R. H. (1975). Pyroxene geothermometry of some granulite facies rocks. *Contrib. Min. Petrol.*, v. 50, pp. 205-209.
- Ito, K., and Kennedy, G. C. (1971). An experimental study of the basalt-garnet granulite - eclogite transition. In J. G. Hancock (ed.), *The Structure and Physical Properties of the Earth's Crust*, Amer. Geophys. Union, Geophys. Monogr., no. 14, pp. 303-314.
- Johnson, A. M., and Pollard, D. D. (1973). Mechanics of growth of some laccolithic intrusions in the Henry Mountains, Utah. I. Field observations, Gilberts model, physical properties and flow of the magma. *Tectonophysics*, v. 18, pp. 261-309.
- Kennedy, G. C., and Ito, K. (1972). Comments on: "A comparison of recent experimental data on the gabbro - garnet granulite - eclogite transition." *Jour. Geol.*, v. 80, pp. 289-292.
- Kolker, A. (1982). Mineralogy and geochemistry of Fe-Ti oxide and apatite (nelsonite) deposits and evaluation of the liquid immiscibility hypothesis. *Econ. Geol.*, v. 77, pp. 1146-1158.
- Korzhinskii, D. S. (1959). *Physiochemical basis of the analysis of the paragenesis of minerals*. Translated from Russian, Consultants Bureau Inc., New York, originally published in 1957.
- Korzhinskii, D. S. (1966). On thermodynamics of open systems and the phase rule (A reply to D. F. Weill and W. S. Fyfe.) *Geochim. Cosmochim. Acta*, v. 30, pp. 829-835.
- Korzhinskii, D. S. (1967). On thermodynamics of open systems and the phase rule (A reply to the second critical paper of D. F. Weill and W. S. Fyfe.) *Geochim. Cosmochim. Acta*, v. 31, pp. 1177-1180.
- Kretchmar, U. H. (1968). A study of the opaque minerals of the White-stone Anorthosite, Dunchurch, Ontario. Unpublished M.Sc. Thesis, McMaster University, Hamilton, Ontario.

- Kretz, R. (1959). Chemical study of garnet, biotite and hornblende from gneisses of Southwestern Quebec, with emphasis on distribution of elements in coexisting minerals. *Jour. Geol.*, v. 67, pp. 371-402.
- Kretz, R. (1960). The distribution of certain elements among coexisting calcic pyroxenes, calcic amphiboles and biotites in skarns. *Geochim. Cosmochim. Acta*, v. 20, pp. 161-191.
- Kretz, R. (1961). Some applications of thermodynamics to coexisting minerals of variable composition. Examples: orthopyroxene - clinopyroxene and orthopyroxene - garnet. *Jour. Geol.*, v. 69, no. 4, pp. 361-387.
- Kretz, R. (1963). Distribution of magnesium and iron between orthopyroxene and calcic pyroxene in natural mineral assemblages. *Jour. Geol.*, v. 71, pp. 773-785.
- Kretz, R. (1964). Analysis of equilibrium in garnet - biotite - sillimanite gneisses from Quebec. *Jour. Petrol.*, v. 5, part 1, pp. 1-20.
- Kretz, R. (1978). Distribution of Mg, Fe²⁺, and Mn in some calcic pyroxene - hornblende - biotite - garnet gneisses and amphibolites from the Grenville Province. *Jour. Geol.*, v. 86, pp. 599-619.
- Kretz, R. (1981). Site - occupancy interpretation of the distribution of Mg and Fe between orthopyroxene and clinopyroxene in metamorphic rocks. *Can. Mineral.*, v. 19, pp. 493-500.
- Lacy, W. C. (1960). Geology of the Dunchurch Area, Ontario, Canada: *Geol. Soc. Amer. Bull.*, v. 71, pp. 1713-1718.
- Lasaga, A. C. (1981). Rate laws of chemical reactions. In A. C. Lasaga and R. J. Kirkpatrick (eds.), *Kinetics of Geochemical Processes*. *Mineral. Soc. Amer., Reviews in Mineralogy*, v. 8, pp. 1-67.
- Law, A. D. (1973). Critical evaluation of "statistical best fits" to Mossbauer Spectra. *Amer. Mineral.*, v. 58, pp. 128-131.

- Leake, B. E. (1978). Nomenclature of amphiboles. *Amer. Mineral.*, v. 63, pp. 1023-1052.
- Li, J. C. M. (1981). Chemical potential for diffusion in a stresses solid. *Scripta Metallurgia*, v. 15, pp. 21-28.
- Lonkers, S. (1980). Conditions of metamorphism in high-grade pelitic gneisses from the Frontenac axis, Ontario, Canada. *Can. Jour. Earth Sci.*, v. 17, no. 12, pp. 1666-1684.
- Loomis, T. P. (1967). A natural example of metastable reactions involving garnet and sillimanite. *Jour. Petrol.*, v. 20, part 2, pp. 271-292.
- Loomis, T. P. (1977). Kinetics of a garnet granulite reaction. *Contrib. Min. Petrol.*, v. 62, pp. 1-22.
- Loomis, T. P. (1982). Numerical simulation of the disequilibrium growth of garnet in chlorite-bearing aluminous pelitic rocks. *Can. Mineral.*, v. 20, part 3, pp. 411-423.
- Martignole, J., and Schrijver, K. (1970a). Tectonic setting and evolution of the Morin Anorthosite, Grenville Province, Quebec. *Geol. Soc. Finland Bull.*, v. 42, pp. 165-209.
- Martignole, J., and Schrijver, K. (1970b). The level of anorthosite and its tectonic pattern. *Tectonophysics*, v. 10, pp. 403-409.
- Martignole, J., and Schrijver, K. (1971). Association of (hornblende) garnet - clinopyroxene "subfacies" of metamorphism and anorthosite masses. *Can. Jour. Earth Sci.*, v. 8, pp. 698-704.
- Martignole, J., and Schrijver, K. (1973). Effect of rock composition on appearance of garnet in anorthosite - charnokite suites. *Can. Jour. Earth Sci.*, v. 10, pp. 1132-1139.
- Mason, I. M. (1969). Petrology of the Whitestone Anorthosite. Unpublished Ph.D. Thesis, McMaster University, Hamilton, Ontario.
- May, L. (1971). An introduction of Mossbauer spectroscopy. Plenum Press, New York.

- McBirney, A. R. (1975). Differentiation of the Skaergaard intrusion. *Nature*, v. 253, pp. 691-694.
- Meagher, E. P. (1980). Silicate garnets. In P. H. Ribbe (ed.), *Ortho-silicates*. Mineral. Soc. Amer., *Reviews in Mineralogy*, v. 5, pp. 25-58.
- Middleton, G. V. (1963). Statistical inference in geochemistry. In D. M. Shaw (ed.), *Studies in Analytical Geochemistry*, The Royal Soc. Can., Special Pub., no. 6.
- Miyashiro, A. (1973). *Metamorphism and metamorphic belts*. George Allen and Unwin, London, 492 pp.
- Morse, S. A. (1982). A partisan review of Proterozoic anorthosites. *Amer. Mineral.*, v. 67, pp. 1087-1100.
- Mueller, R. F., and Saxena, S. K. (1977). *Chemical Petrology*. Springer-Verlag, New York, 394 pp.
- Mummery, B. C. (1972). Coronite amphibolites from the Whitestone area, Parry Sound, Ontario. Unpublished Ph.D. Thesis, McMaster University, Hamilton, Ontario.
- Neumann, E. R. (1976). Two refinements for the calculation of structural formula for pyroxenes and amphiboles. *Norsk Geologisk Tidsskrift*, v. 56, pp. 1-6.
- Nicolas, A., and Poirier, J. P. (1976). *Crystalline plasticity and solid state flow in metamorphic rocks*. John Wiley and Sons, London, 444 pp.
- Nolfi, F. V. Jr. (1981). Driving forces for mass transport in solids. *Scripta Metallurgica*, v. 15, pp. 7-13.
- O'Hara, M. J., and Yarwood, G. (1978). High pressure - temperature point on an archaean geotherm, implied magma genesis by crustal anatexis and consequences for garnet - pyroxene thermometry and barometry. *Phil. Trans. R. Soc. Lond., A*, no. 288, pp. 411-456.
- Ono, A. (1977). Chemical reactions at the boundary between gneiss and amphibolite in the Ryoke metamorphic terrain at Takato, Japan. *Jour. Geol. Soc. Japan*, v. 83, no. 1, pp. 33-40.

- Onorato, P. I. K., Hopper, R. W., Yinnon, H., Uhlmann, D. R., Taylor, L. A., Garrison, J. R., and Hunter, R. (1981). Solute partitioning under continuous cooling conditions as a cooling rate indicator. *Jour. Geophys. Res.*, v. 86, pp. 9511-9518.
- Oxburgh, E. R. (1980). Heat flow and magma genesis. In R. B. Hargraves (ed.), *Physics of Magmatic Processes*, Princeton University Press, pp. 161-194.
- Phillips, G. N. (1980). Water activity changes across an amphibolite - granulite facies transition, Broken Hill, Australia. *Contrib. Min. Petrol.*, v. 75, pp. 377-386.
- Phillips, G. N., and Wall, V. J. (1981). Evaluation of prograde regional metamorphic conditions: their implications for the heat source and water activity during metamorphism in the Willyama Complex, Broken Hill, Australia. *Bull. Mineral.*, v. 104, pp. 801-810.
- Philpotts, A. R. (1966). Origin of anorthosite - mangerite rocks in Southern Quebec. *Jour. Petrol.*, v. 7, part 1, pp. 1-64.
- Philpotts, A. R. (1967). Origin of certain iron - titanium oxide apatite rocks. *Econ. Geol.*, v. 62, no. 3, pp. 303-315.
- Philpotts, A. R. (1981). A model for the generation of massif-type anorthosites. *Can. Mineral.*, v. 19, pp. 233-253.
- Putnis, A., and McConnell, J. D. C. (1980). Principles of mineral behaviour. *Geosci. Texts*, v. 1, Elsevier, New York, 255 pp.
- Pollard, D. D. (1973). Derivation and evaluation of a mechanical model for sheet intrusions. *Tectonophysics*, v. 19, pp. 233-269.
- Raheim, A., and Green, D. H. (1974). Experimental determination of the temperature and pressure dependence of the Fe-Mg partition coefficient for coexisting garnet and clinopyroxene. *Contrib. Min. Petrol.*, v. 48, pp. 179-203.
- Ramberg, H. (1948). Titanic iron ore formed by dissociation of silicates in the granulite facies. *Econ. Geol.*, v. 43, pp. 553-570.

- Reinhardt, E. W. (1968). Phase relations in cordierite-bearing gneisses from the Gananoque Area, Ontario. *Can. Jour. Earth Sci.*, v. 5, p. 455.
- Reinhardt, E. W., and Skippen, G. B. (1970). Petrochemical study of Grenville granulites. In Report of Activities, part B. *Geol. Surv. Can.*, paper 70-1, pp. 48-54.
- Richardson, S. W., Gilbert, M. C., and Bell, P. M. (1969). Experimental determination of kyanite-andalusite and andalusite-sillimanite equilibria: the aluminum silicate triple point. *Amer. Jour. Sci.*, v. 267, pp. 259-272.
- Roedder, E. (1951). Low temperature liquid immiscibility in the system $K_2O-FeO-Al_2O_3-SiO_2$. *Amer. Mineral.*, v. 36, pp. 282-286.
- Rossman, G. R. (1980). Pyroxene spectroscopy. In C. T. Prewitt (ed.), *Pyroxenes*. Mineral. Soc. Amer., *Reviews in Mineralogy*, v. 7, pp. 93-113.
- Ross, M., and Huebner, J. S. (1975). A pyroxene geothermometer based on composition-temperature relationships of naturally occurring orthopyroxene, pigeonite, and augite (abstr.). *Int. Conf. Geothermometry and Geobarometry*, The Pennsylvania State University, University Park, Pennsylvania.
- Russell, J. K. (1981). Metamorphism of the Thompson Nickel Belt gneisses: Paint Lake, Manitoba. *Can. Jour. Earth Sci.*, v. 18, pp. 191-209.
- Savage, D., and Sills, J. D. (1980). High pressure metamorphism in the Scourian of N. W. Scotland: evidence from garnet granulites. *Contrib. Min. Petrol.*, v. 74, pp. 155-163.
- Sawatzky, G. A., Vander Woude, F., and Morrish, A. H. (1969). Recoilless - fraction ratios for Fe^{57} in octahedral and tetrahedral sites of a spinel and a garnet. *Physical Review*, v. 183, no. 2, pp. 383-
- Saxena, S. K. (1968). Distribution of iron and magnesium between co-existing garnet and clinopyroxene in rocks of varying metamorphic grade. *Amer. Mineral.*, v. 53, pp. 2018-2024.

- Schwarcz, H. P. (1966). Chemical and mineralogic variations in an arkosic quartzite during progressive metamorphism. *Geol. Soc. Amer. Bull.*, v. 77, pp. 509-532.
- Stoddard, E. F. (1980). Metamorphic conditions at the northern end of the northwest Adirondack Lowlands: summary. *Geol. Soc. Amer. Bull.*, v. 91, part 1, pp. 100-102.
- Stone, A. J. (1969). General constrained non-linear regression for Mossbauer spectra (modifications for the CDC-6400 and additional programming by H. D. Grundy). Obtained from A. J. Stone, University Chemical Laboratory, Lensfield Road, Cambridge, England.
- Stormer, J. C. Jr., and Whitney, J. A. (1977). Two-feldspar geothermometry in granulite facies metamorphic rocks. *Contrib. Min. Petrol.*, v. 65, pp. 123-133.
- Thom, R. (1975). *Structural Stability and Morphogenesis. An Outline of a General Theory of Models.* Reading: Benjamin.
- Thompson, J. B. (1955). The thermodynamic basis for the mineral facies concept. *Amer. Jour. Sci.*, v. 253, pp. 65-103.
- Thompson, J. B. (1957). The graphical analysis of mineral assemblages in pelitic schists. *Amer. Mineral.*, v. 42, pp. 842-858.
- Thompson, J. B. (1959). Local equilibrium in metasomatic processes. In P. H. Abelson (ed.), *Res. in Geochemistry*, v. 1, pp. 427-457.
- Thompson, J. B. (1970). Geochemical reaction and open systems. *Geochim. Cosmochim. Acta*, v. 34, pp. 529-551.
- Tracy, R. J., and Dietsch, C. W. (1982). High-temperature retrograde reactions in pelitic gneiss, central Massachusetts. *Can. Mineral.*, v. 20, part 3, pp. 425-437.
- Turner, F. J. (1981). *Metamorphic petrology.* Second edition, McGraw-Hill, New York, 524 pp.
- Turner, F. J. (1968). *Metamorphic petrology.* First edition, McGraw-Hill.

- Turnock, A. C., and Lindsley, D. H. (1981). Experimental determination of pyroxene solvi for ≤ 1 kbar at 900 and 1000 °C. *Can. Mineral.*, v. 19, pp. 255-267.
- Violet, C. E., and Pipkorn, D. N. (1971). Mossbauer line positions and hyperfine interactions in α iron. *Jour. Applied Phys.*, v. 42, no. 11, pp.
- Virgo, D., and Hafner, S. S. (1968). Re-evaluation of the cation distribution in orthopyroxenes by the Mossbauer effect. *Earth Planetary Sci. Let.*, v. 4, pp. 265-269.
- Virgo, D., and Hafner, S. S. (1969). Fe^{2+} , Mg order-disorder in heated orthopyroxenes. *Mineral. Soc. Amer. Spec. Pap.* 2, pp. 67-81.
- Virgo, D., and Hafner, S. S. (1970). Fe^{2+} , Mg order-disorder in natural orthopyroxenes. *Amer. Mineral.*, v. 55, pp. 201-223.
- Vogt, J. H. L. (1983). Bildung von erzlagerstätten durch differentiationsprozesse in basische eruptivmagma. *Zeitschr. prakt. Geologie*, v. 1, pp. 4-11 (not seen, referenced by Ramberg 1948).
- Weill, D. F., and Fyfe, W. S. (1964). A discussion of the Korzhinskii and Thompson treatment of thermodynamic equilibrium in open systems. *Geochim. Cosmochim. Acta*, v. 28, pp. 565-576.
- Weill, D. F., and Fyfe, W. S. (1967). On equilibrium thermodynamics of open systems and the phase rule (a reply to D. S. Korzhinskii). *Geochim. Cosmochim. Acta*, v. 31, pp. 1167-1176.
- Wells, P. R. A. (1977). Pyroxene thermometry in simple and complex systems. *Contrib. Min. Petrol.*, v. 62, pp. 129-139.
- White, S. (1977). Geological significance of recovery and recrystallization processes in quartz. *Tectonophysics*, v. 39, pp. 143-170.
- Winkler, H. G. F. (1979). Petrogenesis of metamorphic rocks. Fifth edition, Springer-Verlag, New York, 348 pp.
- Wood, B. J., and Banno, S. (1973). Garnet - orthopyroxene and orthopyroxene - clinopyroxene relationships in simple and complex systems. *Contrib. Min. Petrol.*, v. 42, pp. 109-124.

- Wyllie, P. J. (1977). Crustal anatexis: an experimental review. In D. H. Green (ed.), *Experimental Petrology Related to Extreme Metamorphism, Tectonophysics*, v. 43, pp. 41-71.
- Wynne-Edwards, H. R. (1972). The Grenville Province. In R. A. Price and R. J. W. Douglas (eds.), *Variations in Tectonic Styles in Canada*, Geol. Assoc. of Can., Spec. Pap. 11, pp. 263-334.

APPENDIX A

A-I General Theory of Mossbauer Spectroscopy (Recoil Free Nuclear Gamma Resonance)

(i) Introduction

For certain atomic species the probability exists that during the emission or absorption of a gamma ray, no energy will be transferred to the crystal lattice due to the quantized nature of the lattice energy levels, hence no energy is lost due to recoil. Such atoms are said to exhibit the Mossbauer effect (May 1971). In general, atoms may be excited resonantly if the radiation has an energy exactly equal to the energy levels within the sample. For resonance to be observable, the source line width must be smaller than the energy range (or scan) over which resonance is being studied. In Mossbauer spectroscopy, the effective line width is the natural line width of the gamma ray energy distribution. This narrow energy range is extremely small in comparison with the energies of interaction between the nucleus and its surrounding environment, therefore, it is possible to resolve small differences in the energy required to raise a particular nucleus to an excited state (Bancroft 1973).

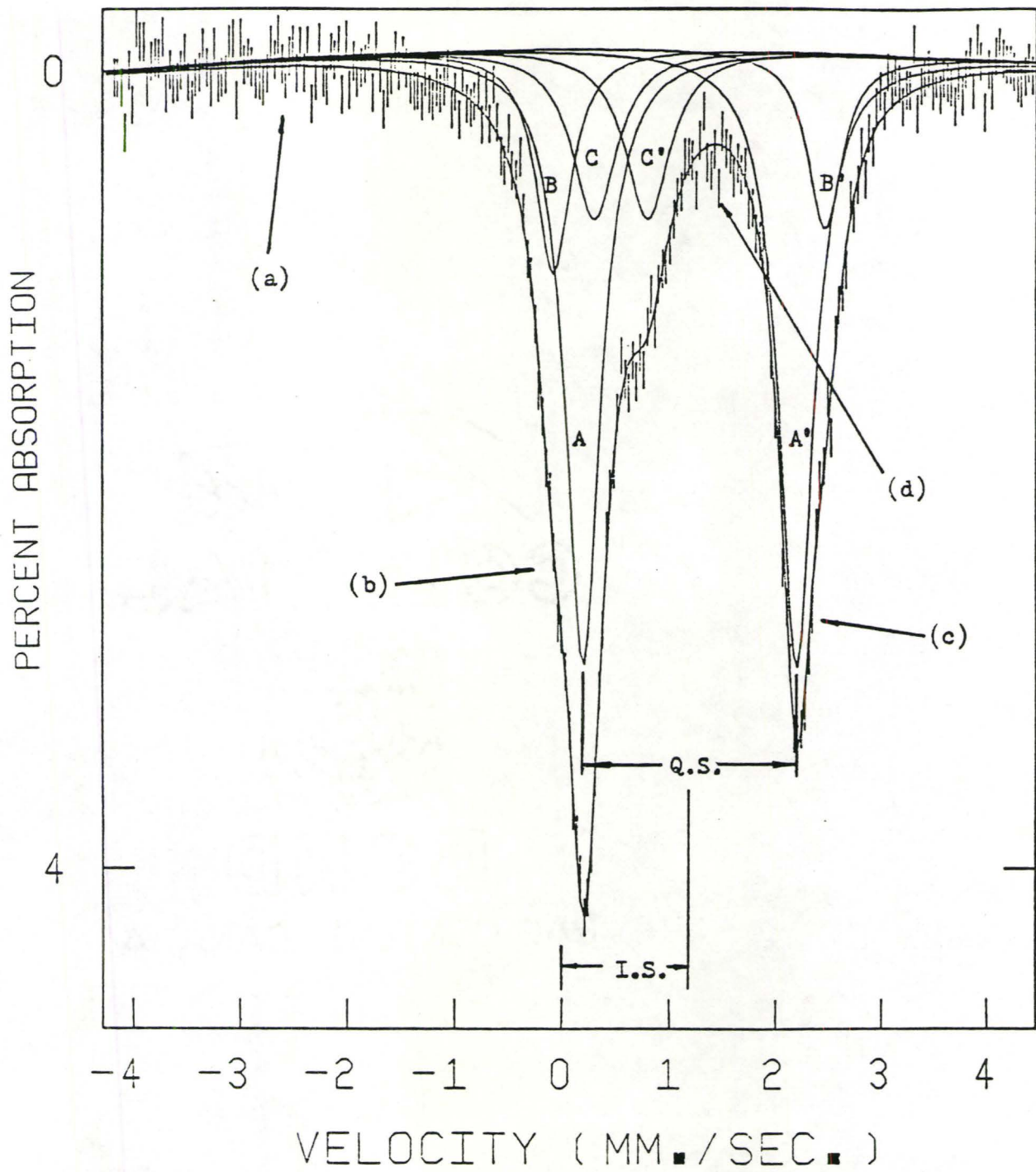
In a typical Mossbauer experiment, the gamma ray energy from a radioactive source is modulated, so as to repeatedly scan a certain energy range.¹ The photon beam is passed through a randomly oriented,

Figure A-I

General Characteristics of a Typical
Mossbauer Spectra

- (a) Baseline or background count, also referred to as the off resonance count. Due to the nature of the source drive, there is a slight sinusoidal component to the baseline which is evident in this example. Each vertically ruled line represents the counts accumulated in one channel, the length of the line is one sigma.
- (b) Low velocity envelope.
- (c) High velocity envelope.
- (d) Indicates either a minor impurity which has not been taken into consideration in the filtering, or channels which have "dropped out" during the counting process. Dropped channels which deviate considerably from the envelope are removed before fitting.

This example clinopyroxene spectra has been fit to 3 sets of peaks marked A-A', B-B', and C-C'. Each set of peaks is referred to as a quadrupole doublet and represents absorption of gamma rays by one particular nuclear species. The two Mossbauer parameters (or hyperfine parameters) normally measured are the quadrupole splitting (Q.S.), which is the distance between the component peaks of the doublet, and the isomer shift (I.S.), which is the deviation of the centroid of the quadrupole doublet from zero velocity. For the doublet A-A', the A peak is referred to as the low velocity peak and the A' as the high velocity peak.



powdered absorber (the mineral sample) and for certain gamma ray energies the system is brought into resonance and absorption occurs. The resultant absorption spectra is recorded by a multichannel analyzer, each channel corresponding to a particular narrow velocity or energy range.

An example of a typical Mossbauer spectra is shown in Figure A-I. Each set of peaks corresponds to the energy required for excitation of a specific nuclear species. This transition energy is dependent on the electronic configuration surrounding the nucleus, therefore it is impossible to measure and compare the nuclear transition energies of nuclei in various crystallographic environments.

Of the various isotopes which are sensitive to the Mossbauer effect, ^{57}Fe is the only one which is of practical use in mineralogical studies. ^{57}Fe has a natural abundance of 2.19% (of natural Fe) and is assumed to be representative of all Fe in the phase being studied (Bancroft 1973).

(ii) Hyperfine Parameters

The two Mossbauer parameters (or hyperfine parameters) normally measured from Mossbauer spectra are the quadrupole splitting (Q.S.) and the chemical shift (C.S.). The chemical shift (or centre shift)

1. The photon beam is modulated by imparting a Doppler velocity to it using a electromechanical vibrator. Velocity is monitored by a laser path difference technique, or with an Fe foil (standard) calibration spectrum.

observed in Mossbauer experiments is composed of two components: the isomer shift (I.S.) and the second order doppler shift (S.O.D.). The S.O.D. shift arises from the thermal motion of the Mossbauer atoms and because it is much smaller than the I.S., is normally neglected.¹

The I.S. results from the electrostatic interaction between the charge distribution of the nucleus and those electrons which have a finite probability of overlapping, and thus interacting with the nuclear charge density (Bancroft 1973). Because the s electron density at the nucleus is sensitive to both the p and d electron density, the isomer shift is a measure of the overall electronic environment of the Mossbauer nucleus and may be used to characterize both valence state and coordination number (Hawthorne 1981). In iron compounds, the I.S. has a negative dependence on the s electron density, therefore one would expect that the Fe^{2+} (electron configuration $3d^6$) would have an appreciably larger I.S. than Fe^{3+} (electron configuration $3d^5$). This is because increasing the population of 3d orbitals will shield the nucleus more effectively from the s electrons, causing the s radial functions to expand, thus reducing the s electron density at the nucleus and increasing the I.S. (Bancroft 1973).

The Q.S. arises from the interaction of a non-cubic extranuclear electric field with a non-spherical nuclear charge density. Some

1. The discussion of Mossbauer hyperfine parameters given here is necessarily brief and covers only the major points of importance to this study. A more thorough discussion may be found in Bancroft 1973, May 1971.

nuclei possess angular momenta, a property usually expressed by the spin I . For a nucleus with spin I , the allowable nuclear spins are quantized and have component levels $m_I = I, I - 1, \dots -I$. For ^{57}Fe , $I_e = 3/2$ and $I_g = 1/2$; the $I = 3/2$ level splits into two components ($\pm 3/2, \pm 1/2$), while the $I = 1/2$ levels remain degenerate. The perturbation of those nuclear energy levels with spin $I > 1/2$ by a non-spherical electric field results in a two line spectrum. For a given nucleus, the Q.S. is proportional to the Z component of the EFG (electric field gradient).¹ The EFG is the gradient of the electric field at the Mossbauer nucleus and can be thought of as a strongly geometry dependent sum of the contributions from the surrounding charges. There are two major contributions to the quadrupole splitting; first, the EFG due to the electron environment--the valence term, and second, the EFG originating from surrounding charged entities--the lattice term. This may be expressed as:

$$q = f(q_{\text{val}}) + f(q_{\text{lat}})$$

It is commonly observed, experimentally, that divalent iron has a much larger Q.S. than trivalent iron. This is because in a weak crystal field where Hund's rule is obeyed, divalent iron has one d electron outside a half-filled shell with spherical symmetry. The field gradient arises predominantly from this 6th electron (i.e., q_{val}

1. The Z-EFG axis often coincides with the highest symmetry axis of the molecule or crystal (Bancroft 1973).

$\gg q_{\text{lat}}$). Trivalent iron has the electron configuration $3d^5$. In a weak crystal field, the five 3d electrons are in a half-filled shell with spherical symmetry which does not contribute to the field gradient. The observed Q.S. must arise from the field gradient due to the other ions in the crystal (i.e., $(q_{\text{val}} \ll q_{\text{lat}})$). Alternatively, the variation in Q.S. may be related to the following three factors:

1. The distortion of the oxygen coordination polyhedra from cubic symmetry.
2. The field gradient due to the neighbouring metallic cations.
3. The variation in effective charge on the coordinating oxygens or OH groups.

A-II Precision of Mossbauer Parameters: calculated using the Method of Dollase (1975)

How well defined spectral parameters are, depends on the peak to background ratio of the specific peak in question. The peak depth (the difference between the number of counts observed at the peak and the off resonance count) may be defined as:

$$R = (N_{\infty} - N_0) / \sqrt{N_{\infty}} \quad (1)$$

where: R = the peak depth in units of counting standard deviation

N_0 = the count at the peak

N_{∞} = the off resonance count

For spectra measured under constant experimental conditions, R is in fact, proportional to the statistical quality of a given peak. To compare various spectra, it is necessary to take into account the peak width (Γ) and the MCA velocity increment/channel. Equation (1) now becomes:

$$E = (N_{\infty} - N_0) \sqrt{G/N_{\infty}} \quad (2)$$

where: E : is defined as the statistical quality of the peak

$G = \Gamma$, the full width at half maximum in channel numbers

= Γ'/v where Γ' = the peak width in mm sec^{-1}

v = the velocity increment/channel

We now introduce the fractional dip $p = (N_{\infty} - N_0)/N_{\infty}$, and note that for Lorentzian peaks, the area under the peak is related to the dip and

width parameters by:

$$A = \pi G(N_{\infty} - N_0)/2 \quad (3)$$

- substituting (3) into (2), we have:

$$\Xi = 2A/(\pi\sqrt{N_{\infty}G})$$

For isolated peaks, the statistical uncertainty with which each peak parameter may be determined is an inverse function of the peak Ξ value, however, for spectra with partially overlapping peaks, parameter uncertainty further depends on component peak separation. To investigate the effect of Δ (the relative peak separation) on ϵ_i (the standard error of parameter i). Dollase fit synthetic spectra (computer generated) using standard techniques, and compared the resultant parameters with the known parameters used to generate the synthetic spectra. His results indicate that for peak separation below 0.6Γ (where the eye no longer discerns a separate maxima), there is a rapid decrease in the precision with which all peak parameters can be determined. Dollase provides plots of $(\Xi\epsilon)$ vs. Δ (for area, width, and position) which allow estimation of ϵ , when Ξ and Δ are known.

Standard errors calculated for the spectra collected in this thesis are shown in Table A-I. Unfortunately, these values are approximations only because Dollase employed computer generated synthetic spectra in his analysis, consisting of only two partially overlapping peaks of equal intensity. In natural spectra, partially overlapping peaks are often of considerably different intensity, consequently the results in Table A-I must be considered minimum errors, especially for the smaller ferrous peaks.

TABLE A-I

Precision of Mossbauer Parameters

Key to Tables

- (i) $\epsilon_1\%$ = the standard error from least squares fitting program.
- (ii) $\Xi (Xi)$: this parameter is a statistical measure of the quality of a peak. Values of typical spectra should fall in the 100-200 range. Peaks with higher values are exceptionally well determined, whereas peaks with Ξ values significantly less than 100 are only indistinctly resolved in a given spectra.
- (iii) Δ = relative peak separation

$$= \frac{\text{position of peak 1} - \text{position of peak 2}}{\text{peak width}}$$
- (iv) $\epsilon_2\%$ = standard error for a single isolated peak

$$= K_i / \Xi$$

 where: K_i is a constant for each parameter
- (v) $\epsilon_3\%$ = the approximate standard error for overlapped peaks

$$\epsilon_3 = f(\Xi \epsilon_2 \Delta) \text{ (non-linear function)}$$

Precision of Mossbauer Parameters for Orthopyroxene

Peak	Parameter	$\epsilon_1\%$	Ξ	Δ	$\epsilon_2\%$	$\epsilon_3\%$
A	Width	0.85			3.41	6.86
	Area	2.70	66	1.02	2.49	7.25
	Pos	0.16			1.24	1.60
A'	W	0.85			3.41	6.03
	A	2.37	66	1.17	2.49	6.06
	P	0.08			1.24	1.55
B	W	0.85			0.71	1.46
	A	0.92	327	1.02	0.52	1.49
	P	0.04			0.26	0.33
B'	W	0.85			0.70	1.26
	A	0.81	332	1.17	0.51	1.26
	P	0.02			0.25	.032
C	W	8.06			9.47	50.52
	A	7.59	25	0.29	6.92	500
	P	0.35			3.44	26.68
C'	W	8.06			9.47	14.05
	A	7.59	25	1.53	6.92	12.74
	P	0.20			3.44	4.12

Precision of Mossbauer Parameters for Clinopyroxene

Peak	Parameter	$\epsilon_1\%$	Ξ	Δ	$\epsilon_2\%$	$\epsilon_3\%$
A	Width	1.19			2.46	5.50
	Area	2.94	92	.67	1.80	13.55
	Pos	0.13			0.89	2.10
A'	W	1.19			3.07	6.88
	A	4.04	76	.66	2.25	17.39
	P	0.07			1.12	2.57
B	W	1.19			0.80	1.78
	A	1.48	303	.67	0.58	4.58
	P	0.14			0.29	0.69
B'	W	1.19			0.80	1.78
	A	1.48	303	.66	0.58	4.58
	P	0.08			0.29	0.69
C	W	2.99			2.62	11.74
	A	2.35	91	.32	1.92	200
	P	0.08			0.95	6.14
C'	W	2.99			2.62	4.33
	A	2.35	91	1.13	1.92	4.48
	P	0.10			0.95	1.18

Precision of Mossbauer Parameters for Hornblende

Peak	Parameter	$\epsilon_1\%$	Ξ	Δ	$\epsilon_2\%$	$\epsilon_3\%$
A	Width	1.37			1.09	3.73
	Area	2.02	219	.43	0.80	15.63
	Pos	0.08			0.40	1.95
A'	W	1.37			1.09	2.38
	A	2.45	219	.70	0.80	4.68
	P	0.05			0.40	0.82
B	W	1.37			1.50	5.21
	A	2.45	157	.35	1.10	37.42
	P	0.11			0.54	3.35
B'	W	1.37			1.50	4.58
	A	2.45	157	.69	1.10	5.11
	P	0.08			0.54	1.26
C	W	1.37			4.38	24.02
	A	4.58	59	.27	3.20	200
	P	0.37			1.59	15.56
C'	W	1.37			4.38	9.68
	A	4.58	59	.74	3.20	15.38
	P	0.14			1.59	3.35
D	W	1.86			1.45	3.36
	A	1.31	170	.41	1.06	15.70
	P	0.12			0.53	1.79
D'	W	1.86			1.45	2.27
	A	1.31	170	1.40	1.06	1.95
	P	0.06			0.53	0.65

Precision of Mossbauer Parameters for Garnet

Peak	Parameter	$\epsilon_1\%$	E	Δ	$\epsilon_2\%$	$\epsilon_3\%$
A	Width	0.46			0.39	0.50
	Area	0.38	583	1.88	0.28	0.41
	Pos	0.01			0.14	0.16
A'	W	0.48			0.40	
	A	0.42	564	2.0	0.29	
	P	0.01			0.15	
B	W	4.64			5.14	6.67
	A	4.24	43	1.88	3.75	5.56
	P	0.18			1.87	2.11
B'	W	4.68			5.20	8.44
	A	4.19	43	1.09	3.80	8.89
	P	0.16			1.89	2.22

A-III Mossbauer Sample Preparation

1. Hand specimen size samples were crushed in a jaw crusher to chips approximately 1.0 cm in size, and then further reduced in a bico grinder with a maximum disk separation of approximately 1.5 mm.
2. This material was then washed in acetone and sieved into four fractions:

> 50	mesh
50-100	mesh
100-150	mesh
< 150	mesh

In most cases, the 50-100 size fraction was used for further separation because the 100-150 size fraction proved too difficult to hand pick.

3. Separation of mafic minerals (hornblende, pyroxene, etc.) from the lighter minerals was achieved using the Carpo magnetic separator and a density stratification water column. Further separation of mafic minerals was made with a hand magnet and the Franze isodynamic magnetic separator.
4. Final separation was made by hand picking under a binocular microscope using a glass fibre. This method effectively achieves complete separation, however, purity is reduced in many cases due to small inclusions of other minerals within the separated grains. The worst offender is hornblende because of its very dark brown, almost opaque nature.

5. The mineral separate is ground by hand, under acetone, to a fine flour, then mixed with approximately 1/3 sucrose (by volume) and re-ground to reduce any asymmetry effects in the spectrum due to sample orientation. This mixture is pressed into the central cavity (1.0 mm by 15 mm dia.) of a copper disk and held in place with scotch tape. For low temperature spectra (78 °K), the tape is reinforced with two cardboard disks which are perforated to avoid explosion upon exposure to vacuum.

A-IV Key to Constraints Used in Fitting

1. Doublet H.W.'s constrained to be equal.
2. H.W.'s of all ferrous peaks constrained to be equal.
3. Doublet areas constrained to be equal.
4. Centre Shift (C.S.) constrained.
5. Quadrupole splitting (Q.S.) constrained.
6. Peak position constrained.
7. Peak H.W. constrained.

Note: (i) Constraints 1, 2, and 3, do not constrain the parameters to have a specific value, rather they constrain the two component peaks of the doublet to have the same value.

(ii) Constraints 4, 5, 6, and 7, constrain the parameters to have a specific value.

Example: 1, 2, 3(C), 6(C) = (i) H.W.'s are constrained to be the same for all ferrous peaks.

(ii) Areas of doublet peaks CC' are constrained to be equal.

(iii) The peaks positions of doublet CC' are constrained to a specific value.

A-V Mossbauer Calibration Values

File Name	Geometry	Zero velocity channel position	Vel. Increment/channel in mm sec ⁻¹
MSFOR	H	124.7523	.0345
MSFIV	H	124.7238	.0347
MSSIX	H	124.7578	.0347
MSSEV	V (300 °K)	124.6658	.0351
	H (78 °K)	124.7508	.0353
MSEGT	V	124.6334	.0330
	H	123.4343	.0330
MSNIN	H	124.0857	.0329

A-VI Listing of Mossbauer Parameters

C.S.: Centre Shift (quoted relative to Fe⁰ metal)

Q.S.: Quadrupole Splitting

H.W.: Width of Peak at Half Height

TABLE A-II MOSSBAUER PARAMETERS FOR CLINOPYROXENES (mm sec⁻¹)

SAMPLE	CODE	χ^2	Fe ²⁺						Fe ³⁺			Constraints used in fitting
			PEAKS AA ^a (M1)			PEAKS BB ^a (M2)			PEAKS CC ^a (M1,M2)			
			C.S.	Q.S.	H.W.	C.S.	Q.S.	H.W.	C.S.	Q.S.	H.W.	
DT-24	BOH	563	1.13	2.55	.39	1.13	2.01	.39	.52	.53	.43	1,2,3(B,C)
DT-24	EOV	574	1.13	2.54	.39	1.13	2.00	.39	.51	.54	.45	1,2,3(A,C)
DT-24	DUD	490	1.16	2.55	.39	1.14	2.00	.39	.50	.55	.46	1,2,3(C)
DT-25	BFB	251	1.14	2.54	.39	1.14	2.00	.39	.50	.50	.50	1,2,3(B,C)
DT-28	ANI	607	1.16	2.56	.42	1.17	2.03	.42	.55	.54	.39	1,2,3(B,C)
DT-30	CUG	243	1.14	2.57	.42	1.13	2.02	.42	.54	.48	.41	1,2,3(B,C)
DT-33	BIG	110	1.15	2.57	.37	1.13	2.00	.37	.51	.49	.45	1,2,3(B,C)
DT-35	CDA	1010	1.12	2.57	.40	1.13	2.02	.40	.51	.52	.42	1,2,3(B,C)
DT-36	BOF	361	1.14	2.54	.40	1.14	2.01	.40	.51	.49	.43	1,2,3(B,C)
DT-174	CUN	355	1.14	2.58	.40	1.13	2.02	.40	.52	.50	.44	1,2,3(B,C)
DT-174	BHQ	365	1.14	2.58	.41	1.13	2.03	.41	.52	.50	.41	1,2,3(B,C)
DT-176	CFC	263	1.14	2.55	.44	1.14	2.03	.44	.54	.51	.48	1,2,3(B,C)
DT-177	BFG	272	1.15	2.57	.42	1.14	2.03	.42	.55	.52	.43	1,2,3(B,C)
DT-003	BPB	340	1.15	2.55	.43	1.15	2.01	.43	.53	.49	.47	1,2,3(B,C)
		\bar{x}	1.14	2.56	.41	1.14	2.02	.41	.52	.51	.44	
		S	.01	.01	.02	.01	.01	.02	.02	.02	.03	

TABLE A-III MOSSBAUER PARAMETERS FOR ORTHOPYROXENES (mm sec⁻¹)

SAMPLE	CODE	χ^2	Fe ²⁺						Fe ³⁺		
			PEAKS AA ^a (M1)			PEAKS BB ^a (M2)			PEAKS CC ^a (M1, M2)		
			C.S.	Q.S.	H.W.	C.S.	Q.S.	H.W.	C.S.	Q.S.	H.W.
DT-24	CBG	708	1.13	2.38	.33	1.13	2.05	.33	.51	.66	.23
DT-25	DWO	341	1.55	3.39	.43	1.27	2.15	.33	.58	.71	.37
DT-30	BVF	239	1.25	2.93	.38	1.26	2.15	.38	.61	.62	.17
DT-32	DIK	251	1.13	2.38	.32	1.16	2.06	.32	.51	.66	.12
DT-32	BCH	319		N/F		1.16	2.10	.35	.51	.71	.35
DT-33	BBT	385	1.12	2.93	.39	1.26	2.10	.33	.59	.72	.30
DT-37	AXF	247	1.29	2.95	.34	1.26	2.11	.34	.58	.71	.24
DT-37	BAZ	250	1.29	2.95	.34	1.26	2.11	.34	.57	.72	.26
DT-174	DER	125	1.28	2.99	.39	1.25	2.14	.39	.61	.61	.31
DT-176	BZP	96	1.28	2.89	.41	1.26	2.15	.41	.62	.58	.23
DT-177	BGZ	358	1.28	2.93	.36	1.26	2.15	.39	.60	.65	.25
DT-177	BGW	362	1.28	2.92	.39	1.26	2.15	.39	.60	.65	.26
DT-177	DZW	602	1.10	2.40	.34	1.13	2.06	.34	.51	.66	.28
DT-177	ECT	781	1.14	2.40	.34	1.14	2.07	.34	.51	.66	.26
		\bar{x}	1.28	2.93	.38	1.25	2.13	.36	.59	.66	.25
		S	.12	.24	.03	.03	.03	.03	.03	.05	.07

TABLE A-IV Mossbauer Parameters for Amphiboles (mm sec^{-1})

SAMPLE	CODE	χ^2	Fe^{2+}									Fe^{3+}		
			PEAKS AA' (M1)			PEAKS BB' (M3)			PEAKS CC' (M2)			PEAKS DD' (M1, M2, M3)		
			C.S.	Q.S.	H.W.	C.S.	Q.S.	H.W.	C.S.	Q.S.	H.W.	C.S.	Q.S.	H.W.
DT-12	DWG	576	1.12	2.72	.34	1.10	2.37	.34	1.01	2.03	.34	.45	.62	.43
DT-25	DVD	557	1.12	2.67	.34	1.10	2.31	.34	1.02	1.96	.34	.46	.61	.43
DT-30	DRT	337	1.13	2.66	.38	1.09	2.28	.38	1.02	1.93	.38	.46	.63	.48
DT-31	DDH	693	1.13	2.75	.32	1.10	2.39	.32	1.03	1.95	.32	.45	.61	.50
DT-32	BHI	264	1.12	2.62	.36	1.08	2.27	.36	1.03	1.96	.36	.44	.63	.43
DT-33	BHF	254	1.13	2.66	.33	1.10	2.31	.33	1.03	1.99	.33	.45	.62	.43
DT-36	BVX	387	1.13	2.63	.35	1.10	2.29	.35	1.03	1.93	.35	.44	.57	.46
DT-36	BGM	450	1.13	2.71	.30	1.11	2.39	.37	1.03	2.01	.38	.45	.55	.43
DT-37	BRL	313	1.13	2.64	.35	1.10	2.27	.35	1.02	1.90	.35	.45	.58	.49
DT-176	DXL	273	1.12	2.65	.37	1.08	2.28	.37	.99	1.86	.37	.45	.63	.46
DT-004	DQT	433	1.12	2.69	.35	1.10	2.33	.35	1.03	2.00	.35	.47	.60	.44
		\bar{X}	1.13	2.67	.35	1.10	2.31	.35	1.02	1.95	.35	.45	.61	.46
		S	.01	.04	.02	.01	.04	.02	.01	.05	.02	.01	.02	.03

Plots show 3 peak (low velocity component of AA' and BB' doublet superimposed)
and 4 peak (2 doublet) computer fit.

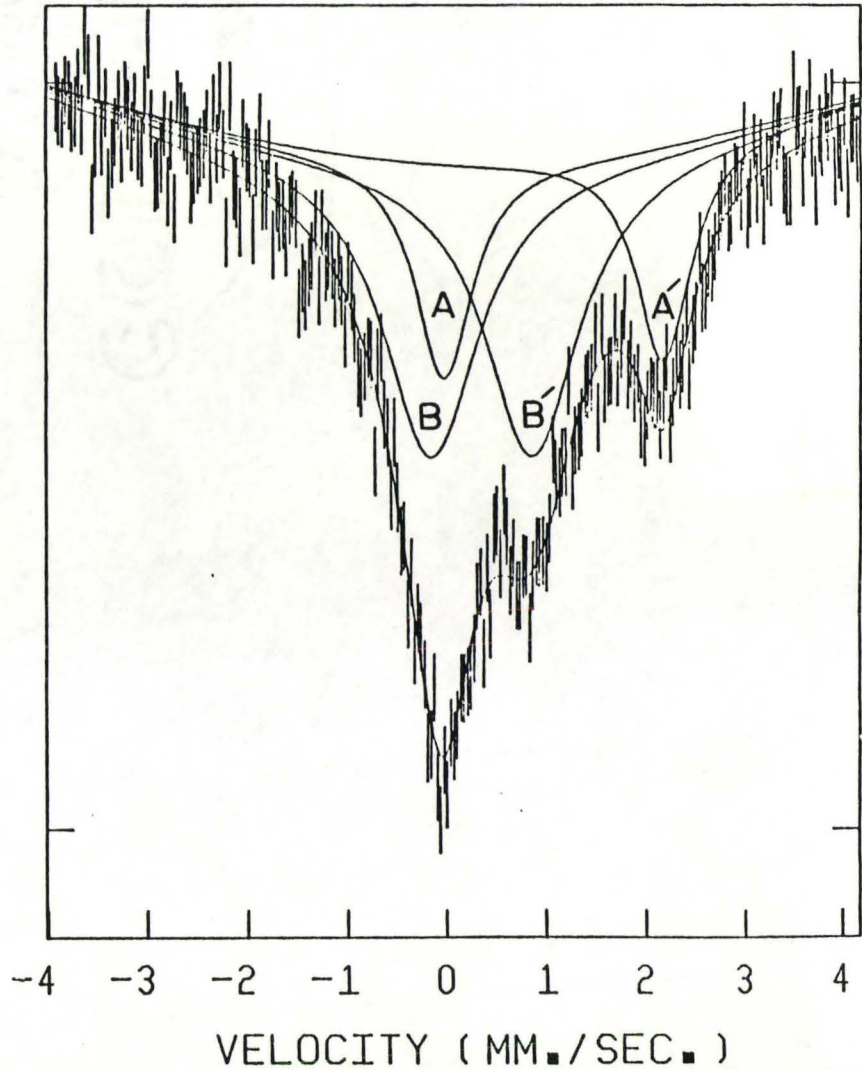
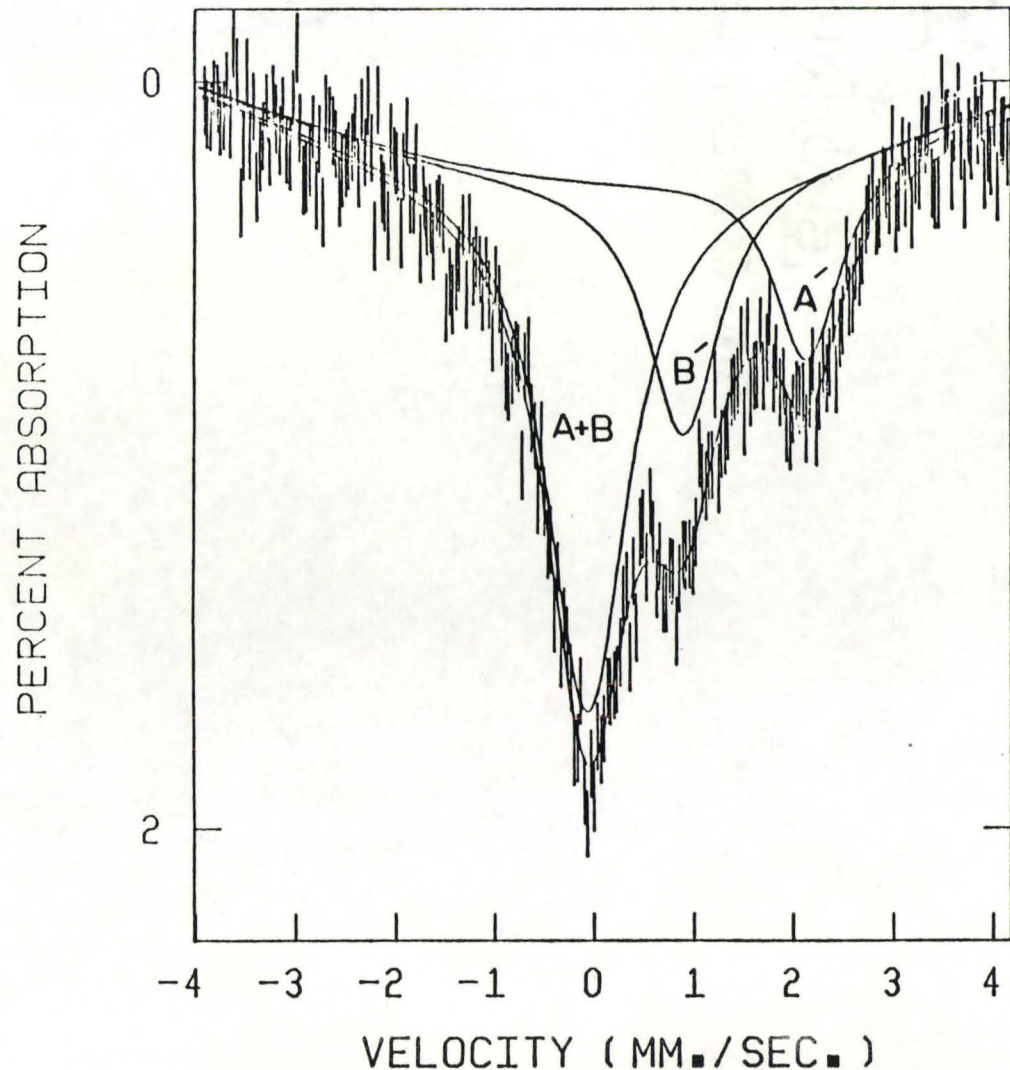
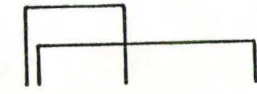
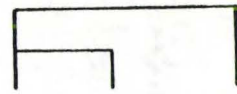


TABLE A-V

MCSSBAUER PARAMETERS (mm sec⁻¹) and RELATIVE PEAK AREAS FOR GLASSES

SAMPLE	CODE	χ^2	Fe ²⁺			Fe ³⁺			Number of Peaks Fit	Fe ²⁺	Fe ³⁺	Constraints in fitting
			PEAKS AA'			PEAKS BB'				%AREA AA'	%AREA BB'	
			C.S.	Q.S.	H.W.	C.S.	Q.S.	H.W.				
DT-28	EGH	255	.99	2.32	.84	.34	1.02	.80	3	.331	.669	0
DT-28	CGS	252	.91	2.46	.84	.38	.92	.80	4	.367	.633	1
DT-28	DLL	270	.96	2.42	.85	.34	.98	.86	4	.316	.684	1,3
DT-30	GGL	227	.99	2.27	.80	.36	1.01	.84	3	.354	.646	0
DT-32	CGP	65	1.00	2.29	.81	.35	.99	.83	3	.367	.633	0
DT-33	DXD	215	1.00	2.21	.81	.38	.96	.90	3	.415	.586	0
DT-33	AIA	220	1.03	2.20	.67	.31	1.01	1.14	4	.303	.697	1,3
DT-36	AIC	226	1.04	2.27	.81	.38	.95	.85	3	.522	.478	0
DT-57	DTV	244	.87	2.54	.92	.35	.97	.82	4	.734	.266	1,3
DT-57	AIB	231	.86	2.54	.86	.37	.95	.80	4	.732	.268	1
DT-98-1	BIC	217	.90	2.67	.75	.32	1.04	.84	4	.883	.117	1,3
DT-98-2	BSV	283	1.05	2.22	.85	.40	.93	.72	3	.716	.284	0
DT-98-3	BTK	267	1.05	2.25	.83	.39	.92	.70	3	.714	.286	0
3 Peak Fit		$\bar{\chi}$	1.02	2.26	.82	.37	.97	.81				
		S	.03	.04	.02	.02	.04	.07				
4 Peak Fit		$\bar{\chi}$.92	2.47	.82	.35	.98	.88				
		S	.06	.16	.09	.03	.04	.13				

A-VII Listings of Individual Spectra

Example: OPX DT-37 T(78) AXF

OPX: mineral type

OPX = orthopyroxene

CPX = clinopyroxene

GT = garnet

HBL = hornblende

OPAQ = opaque mineral separate

GLASS = glass (XRF fusion pellet)

GRUN = grunerite

ACTN = actinolite

SAPPH = sapphirine

DT-37: sample number

T(78): temperature

T(78) = liquid nitrogen

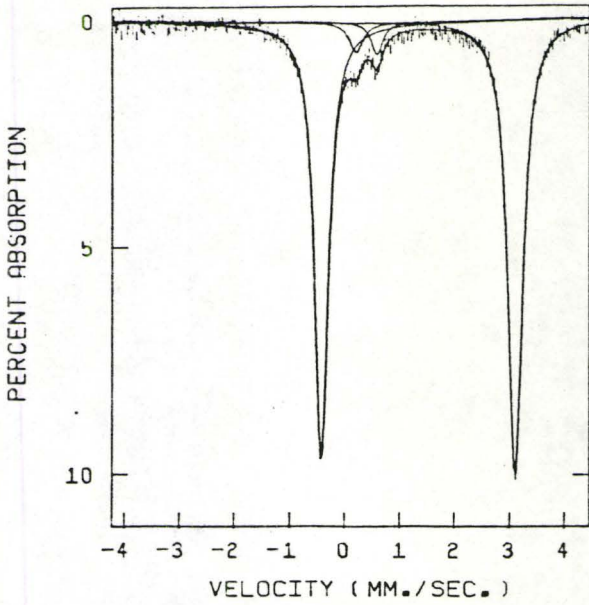
T(RT) = room temperature

Where not given room temperature is assumed.

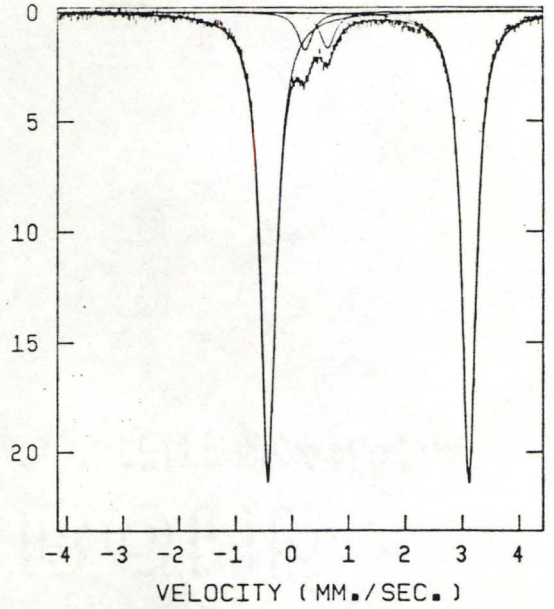
AXF: computer hash code

This code can be used to find the corresponding Mossbauer parameters in Tables 3-II to 3-VIII.

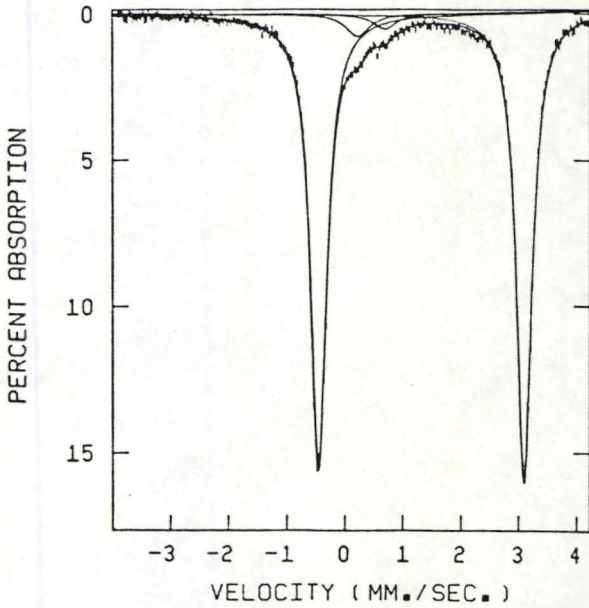
GT DT-25 CJF



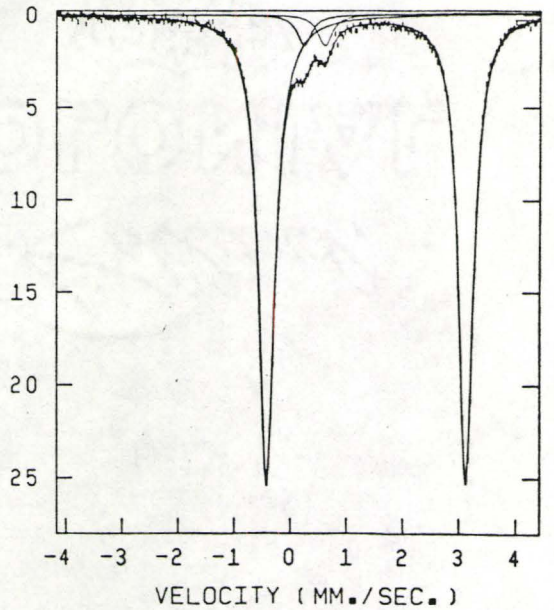
GT DT-28 BAH



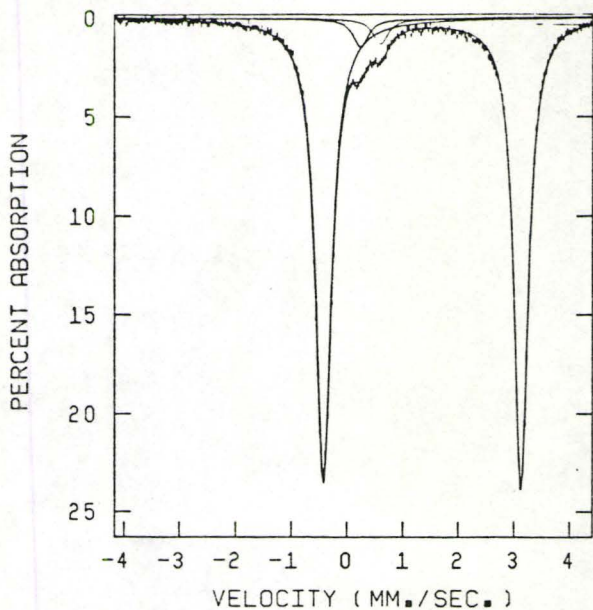
GT DT-30 AGV



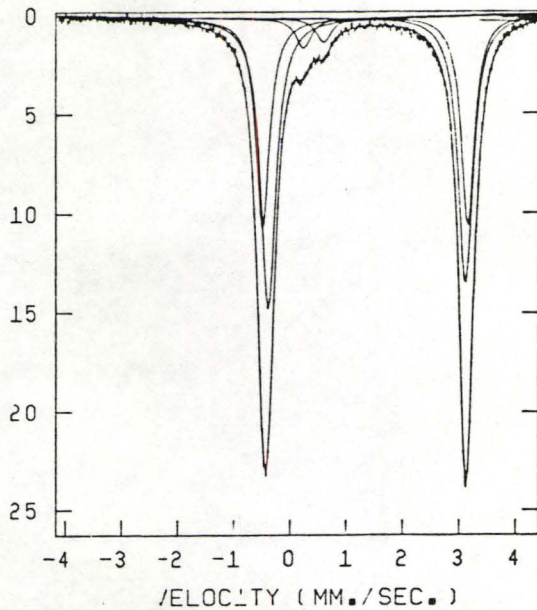
GT DT-31 BAK



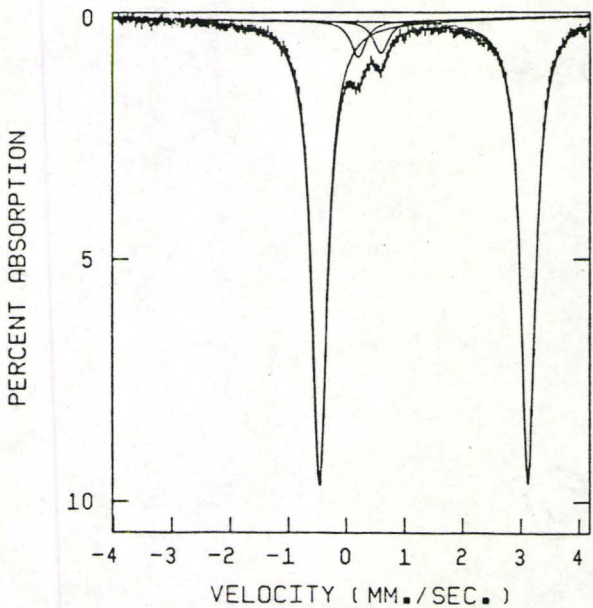
GT DT-32 BJH



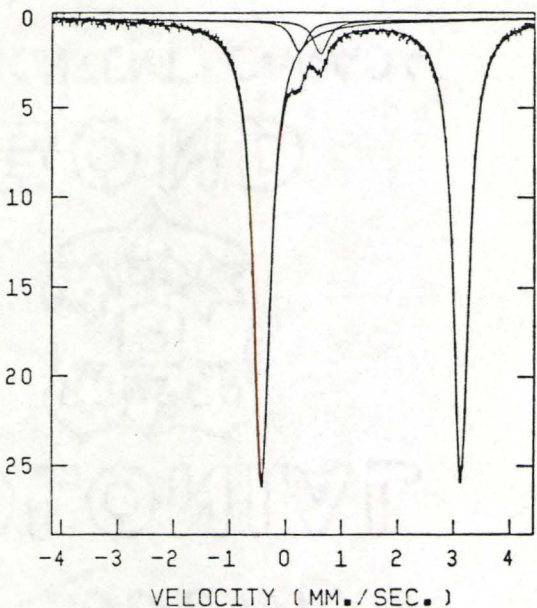
GT DT-32 BEM

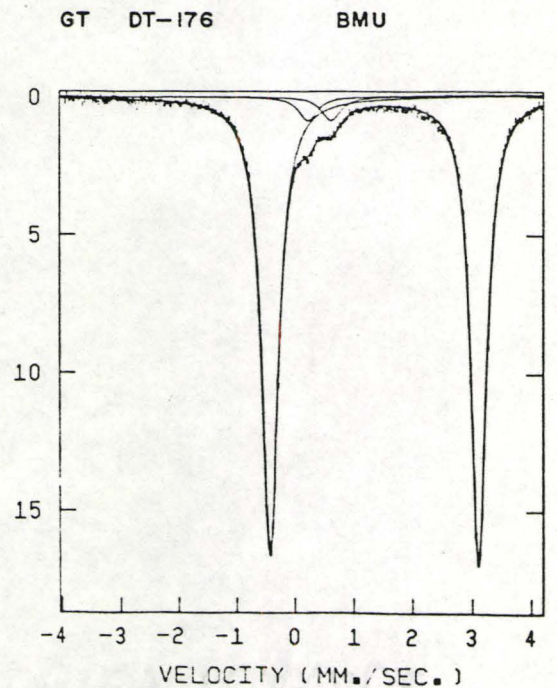
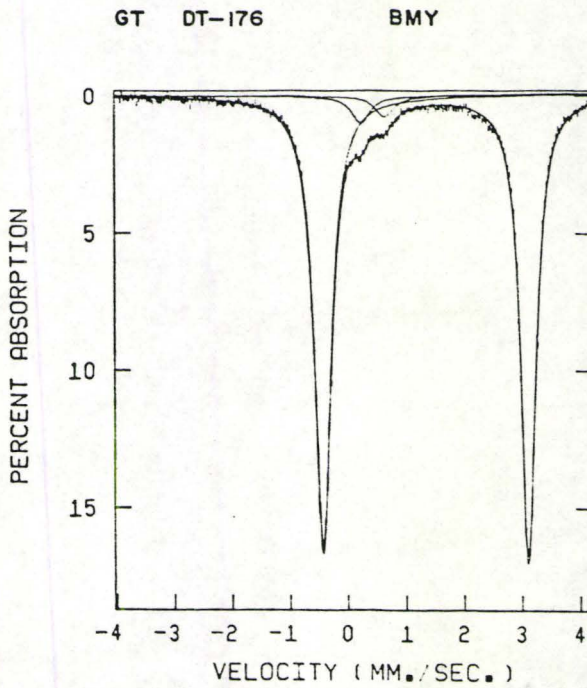
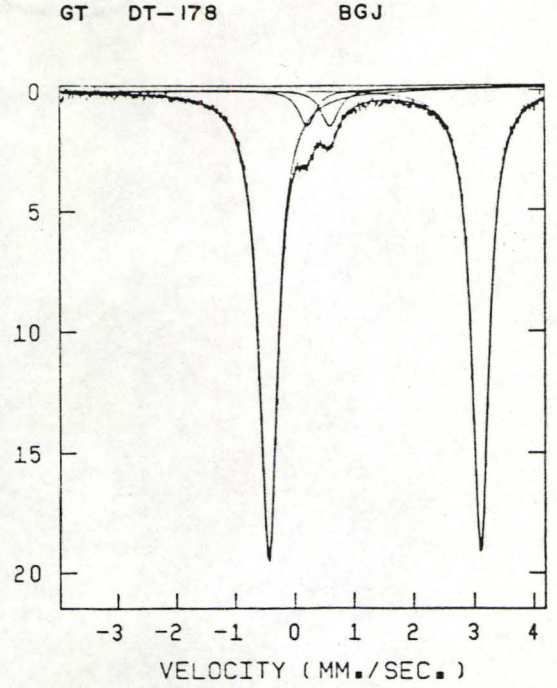
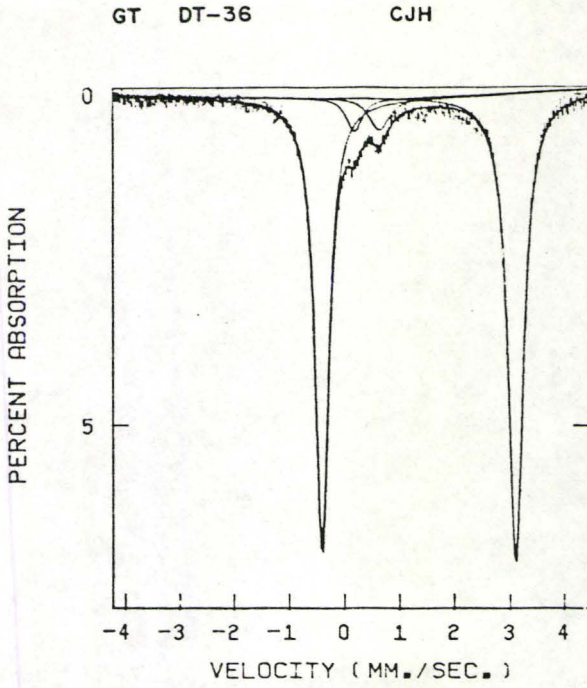


GT DT-34 CZH

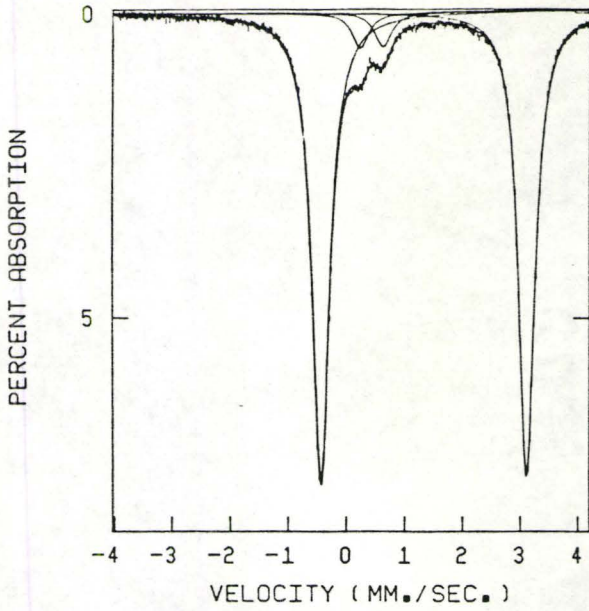


GT DT-35 BEN

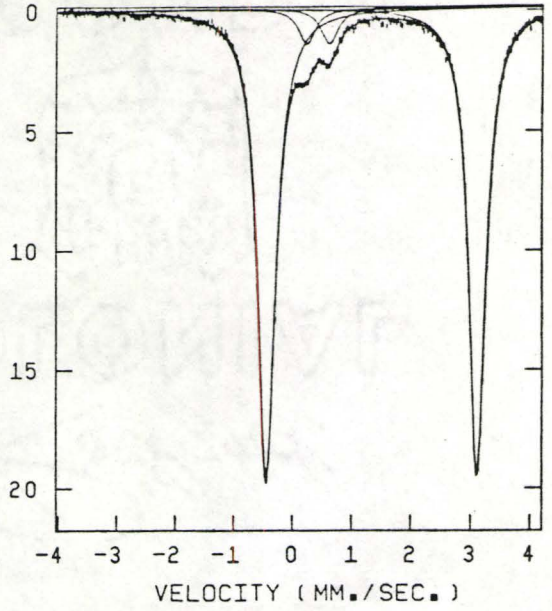




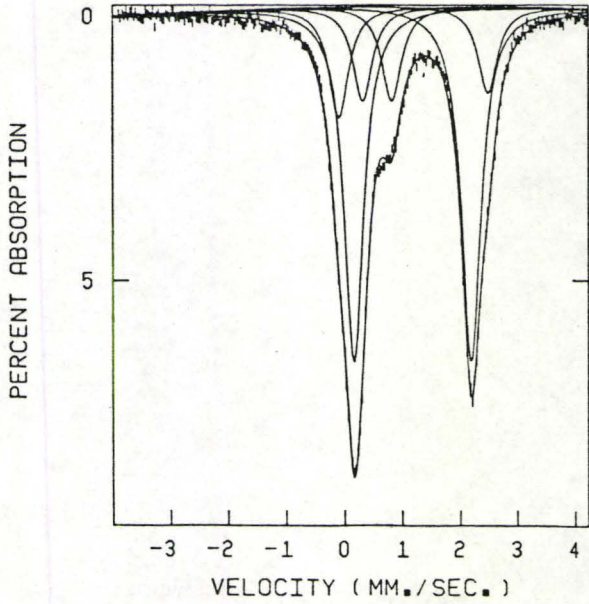
GT DT-002 BFK



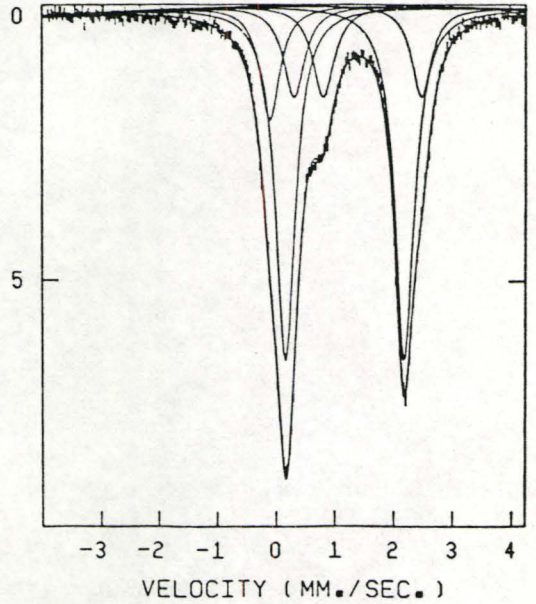
GT DT-002 BGL



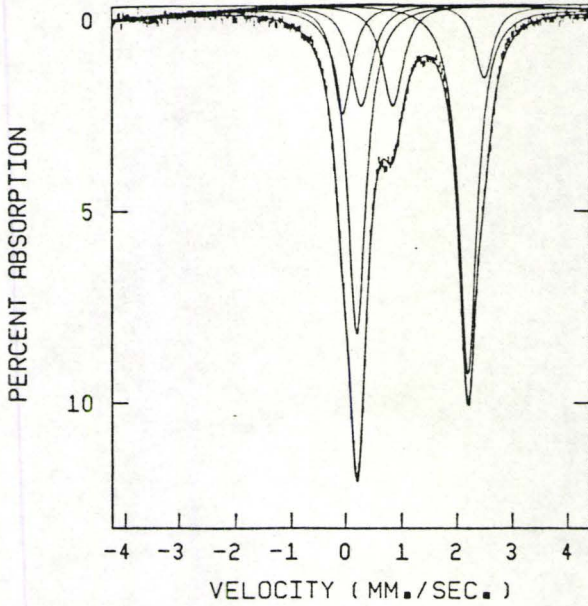
CPX DT-174 BHQ



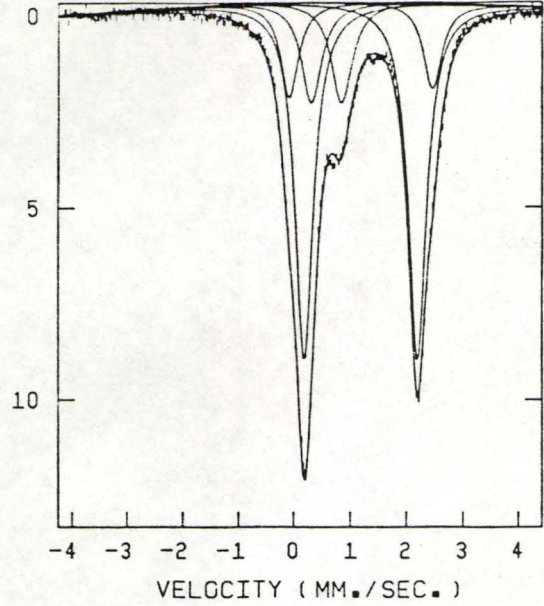
CPX DT-174 CUN



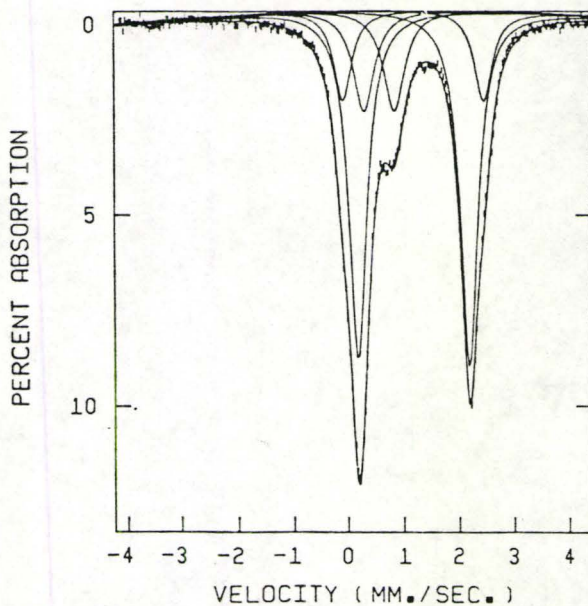
CPX DT-24 DUD



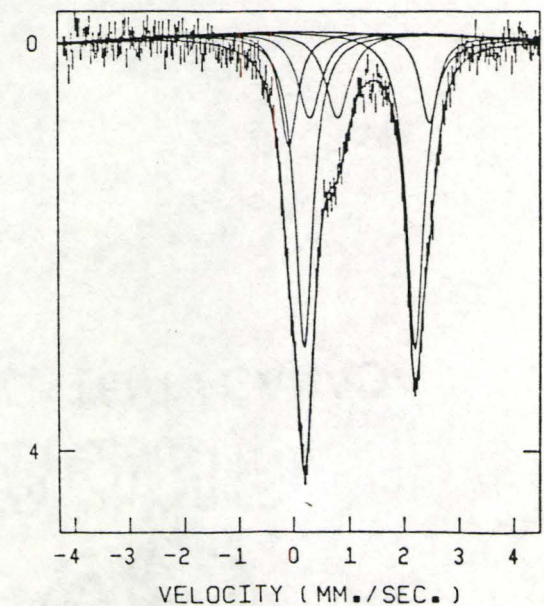
CPX DT-24 BOH



CPX DT-24 ECQ



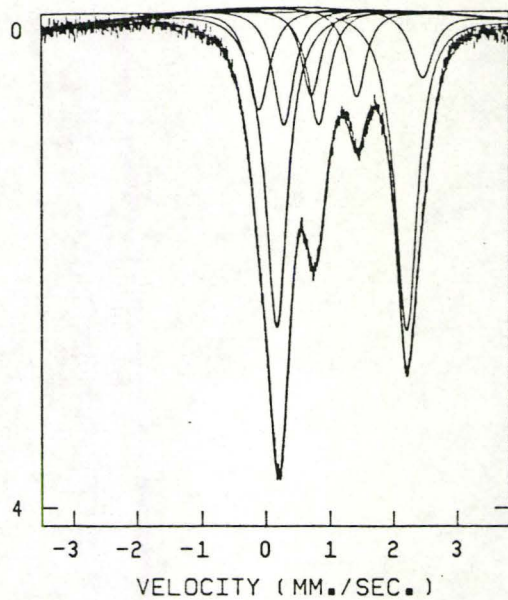
CPX DT-25 BPZ



CPX DT-28

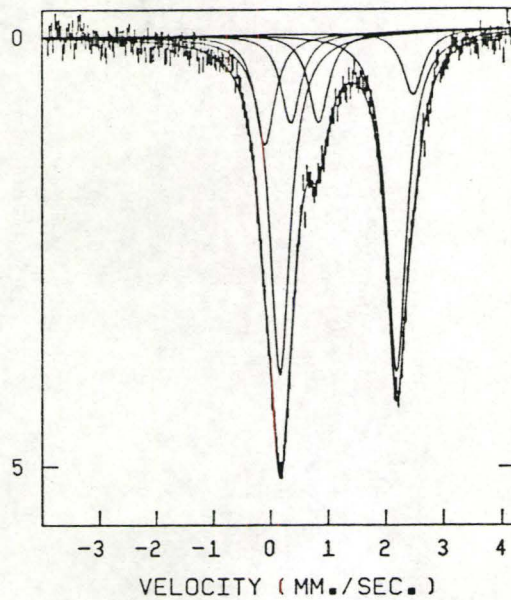
ANI

PERCENT ABSORPTION



CPX DT-30

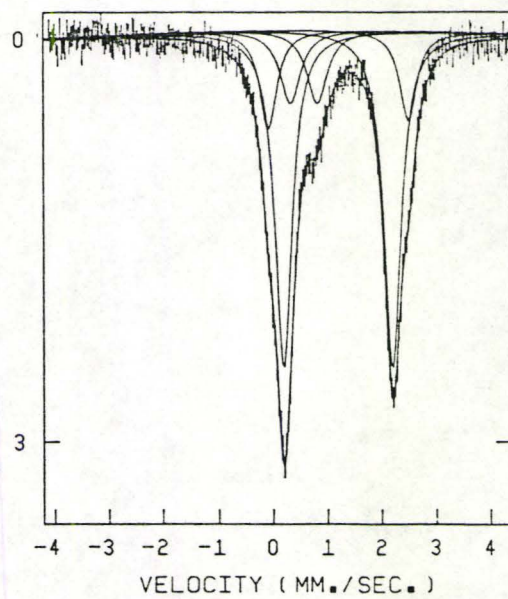
CUG



CPX DT-33

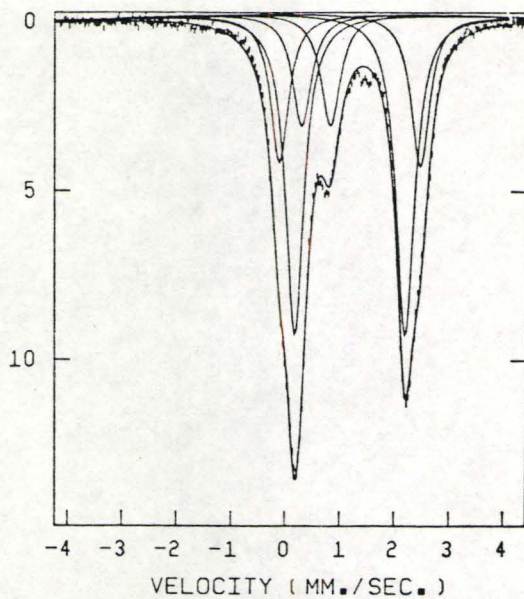
BQO

PERCENT ABSORPTION



CPX DT-35

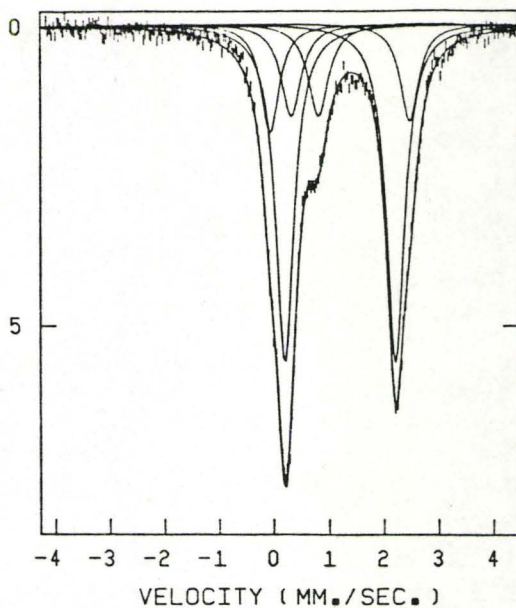
CDA



CPX DT-36

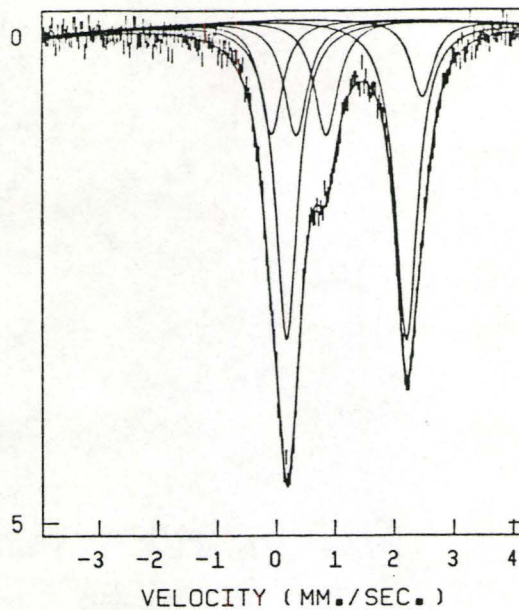
BQF

PERCENT ABSORPTION



CPX DT-176

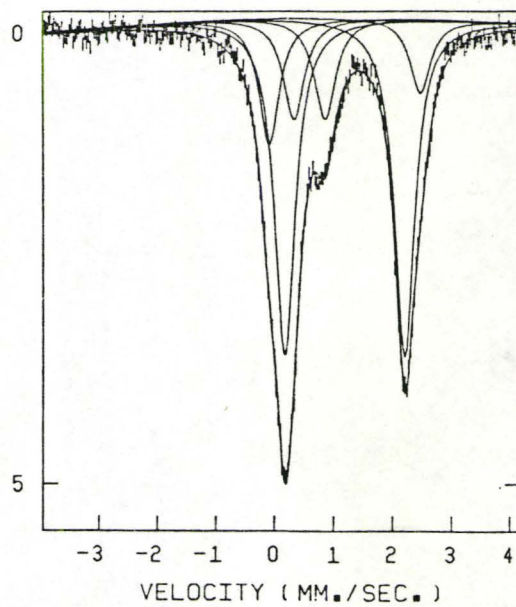
CFC



CPX DT-177

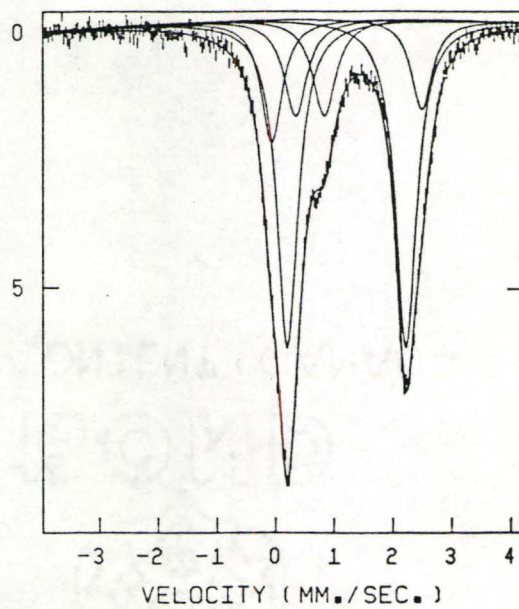
BPG

PERCENT ABSORPTION

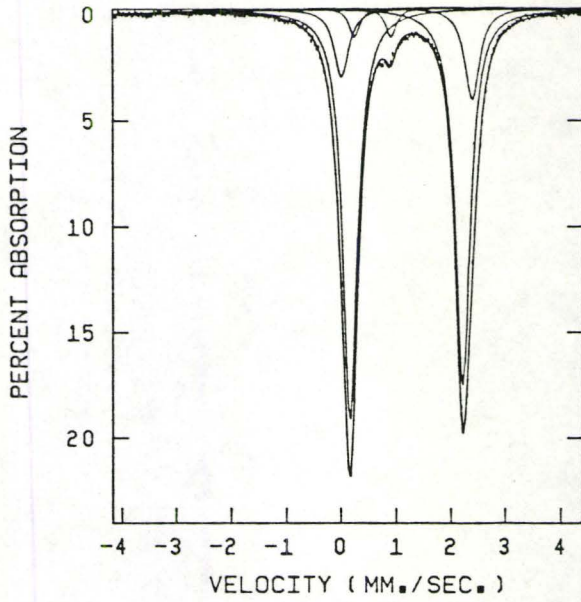


CPX DT-003

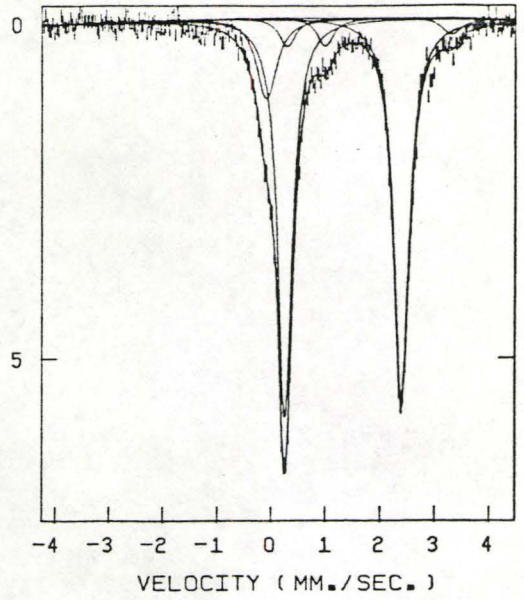
BPB



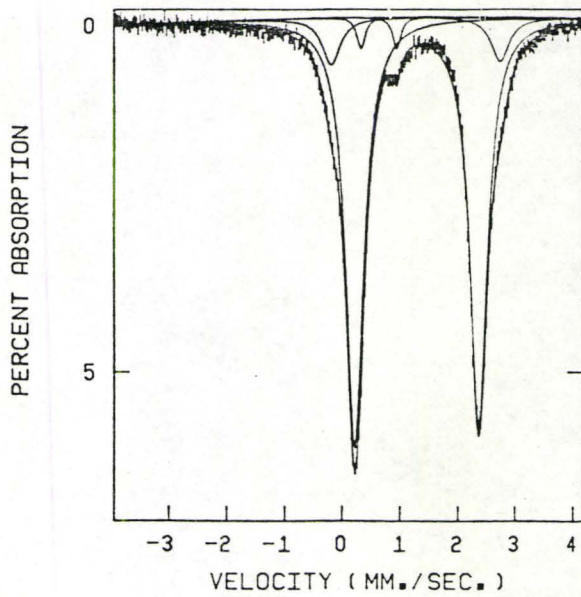
OPX DT-24 T(RT) CBG



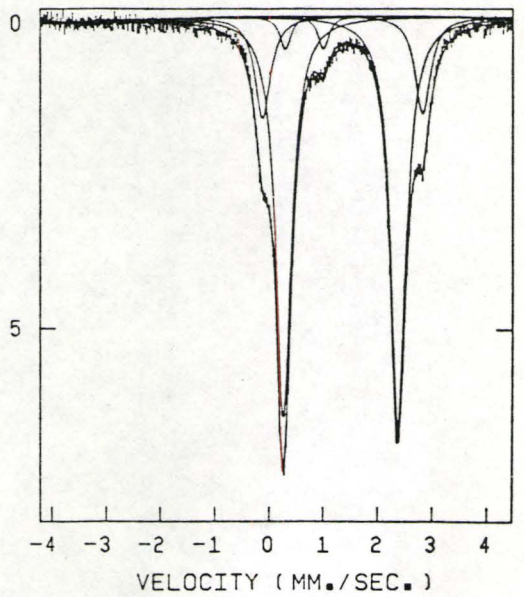
OPX DT-25 T(78) DWO



OPX DT-30 T(78) BPF

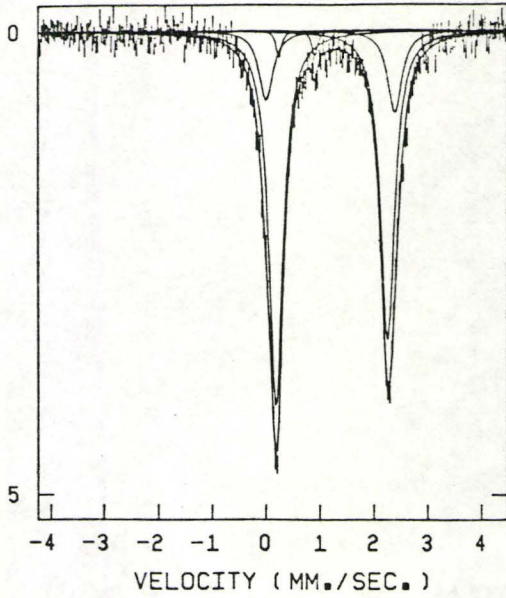


OPX DT-37 T(78) AXF

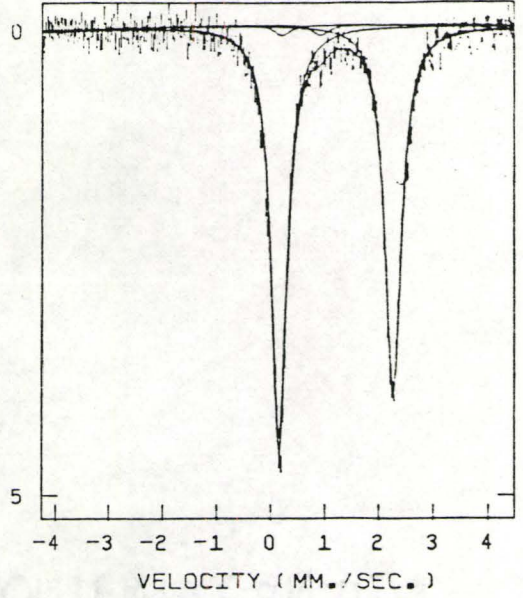


OPX DT-32 T(78) DIK

PERCENT ABSORPTION

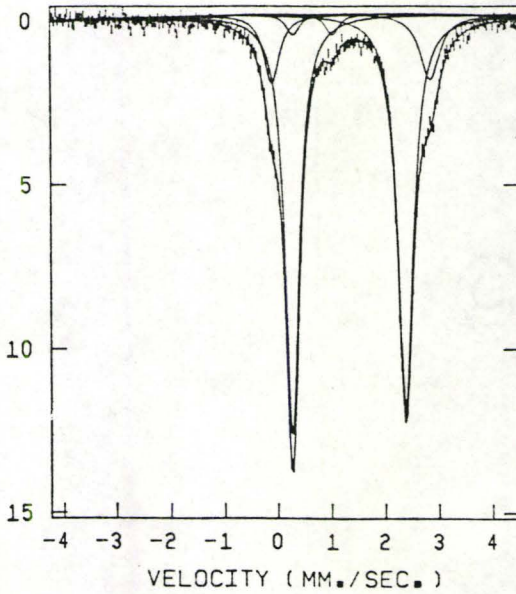


OPX DT-32 T(78) BOH

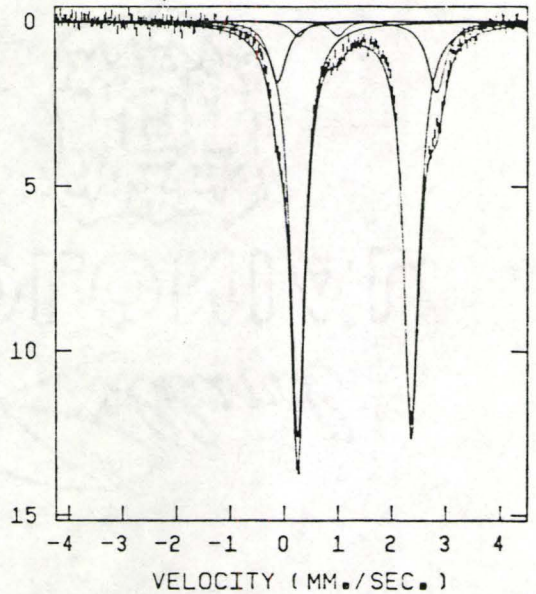


OPX DT-33 T(78) BBT

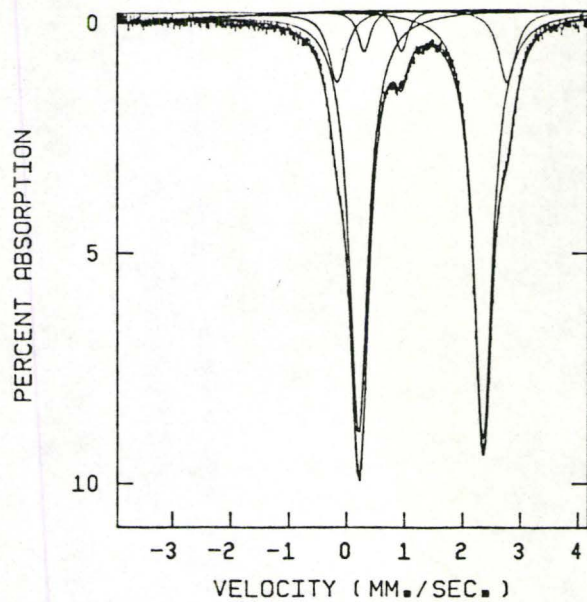
PERCENT ABSORPTION



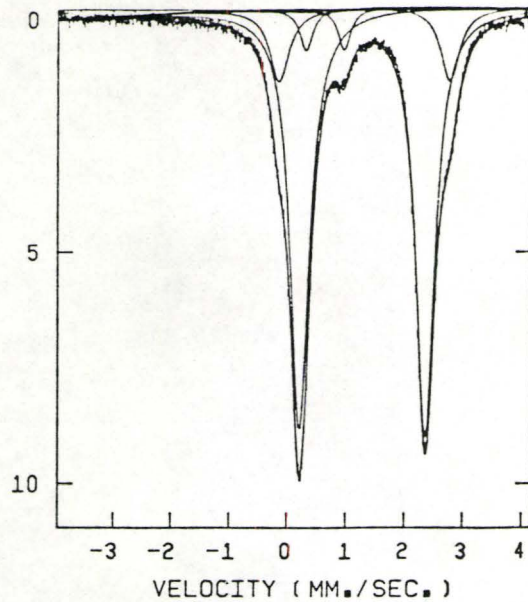
OPX DT-33 T(78) BLV



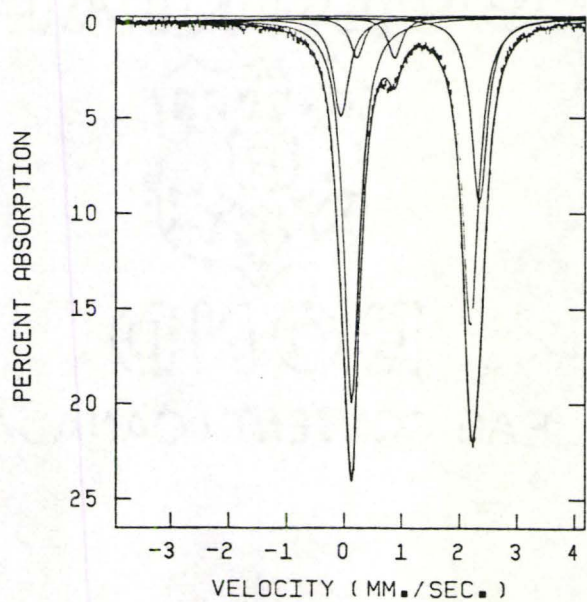
OPX DT-177 T(78) BGZ



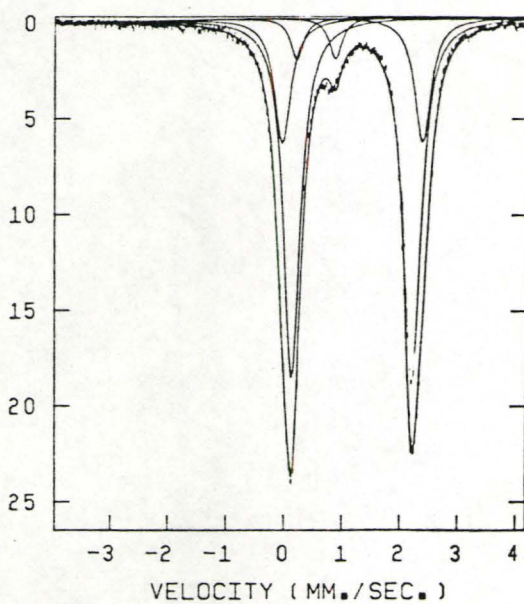
OPX DT-177 T(78) BGW



OPX DT-177 T(RT) DZW

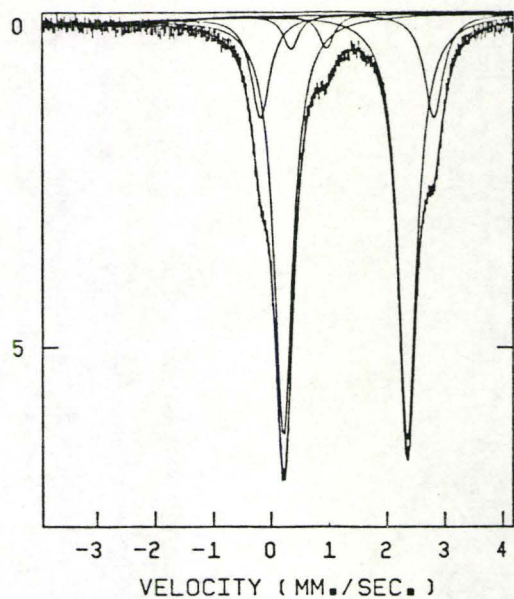


OPX DT-177 T(RT) ECT

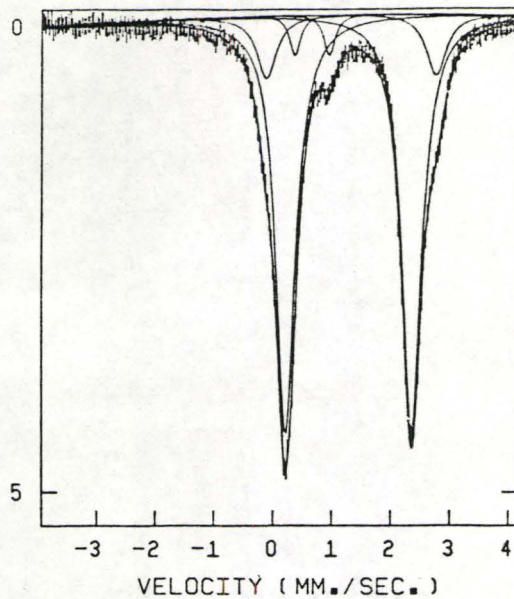


OPX DT-174 T(78) DZR

PERCENT ABSORPTION

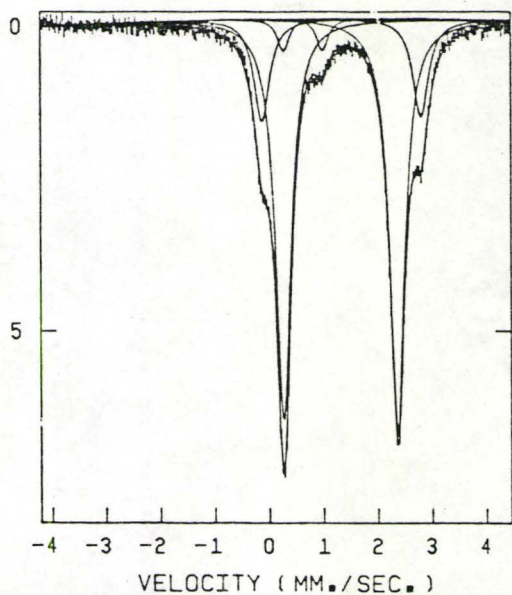


OPX DT-176 T(78) BZP

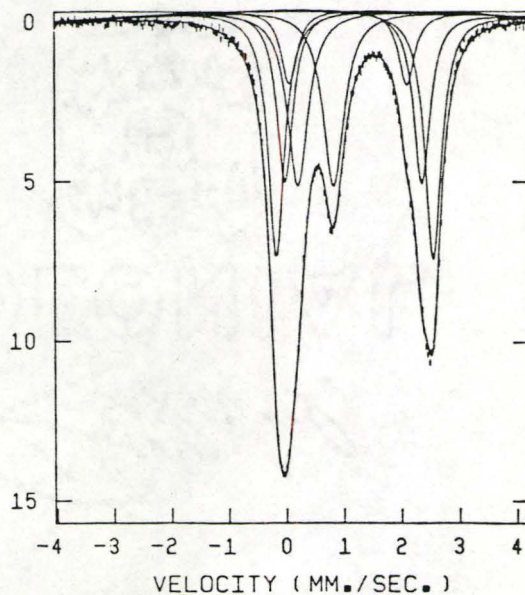


OPX DT 37 T(78) BAZ

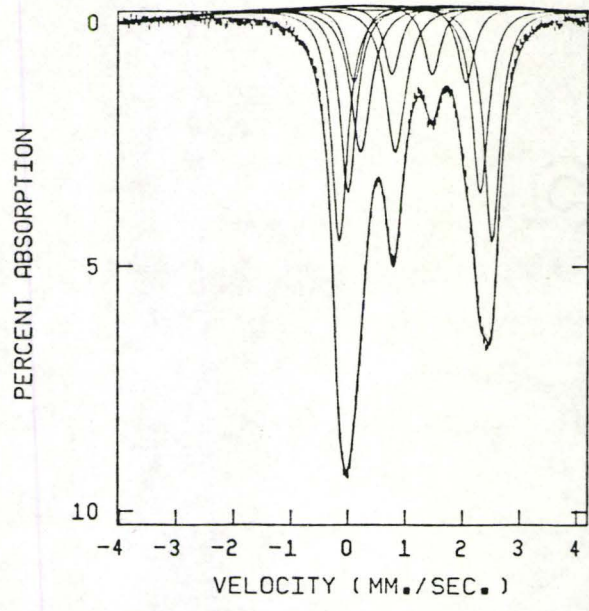
PERCENT ABSORPTION



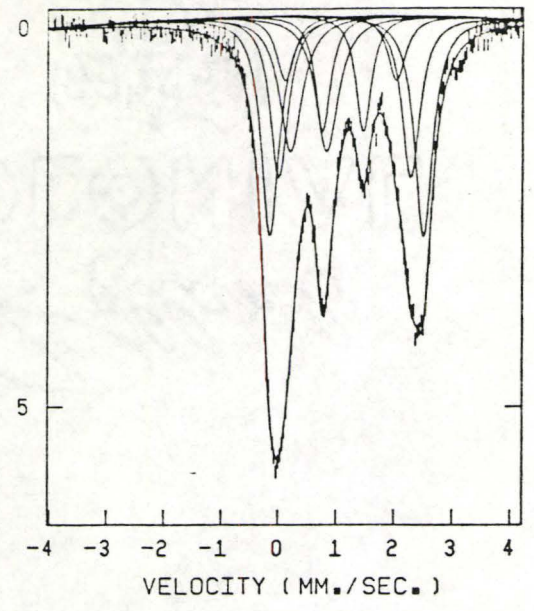
HBL DT-12 DWG



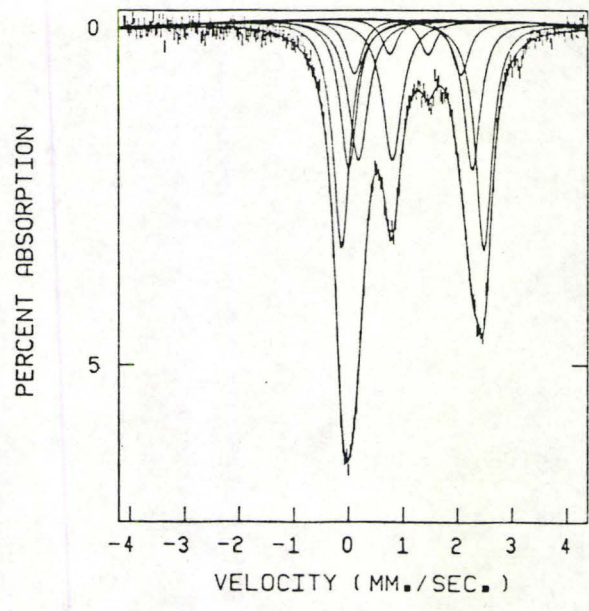
HBL DT-25 DVD



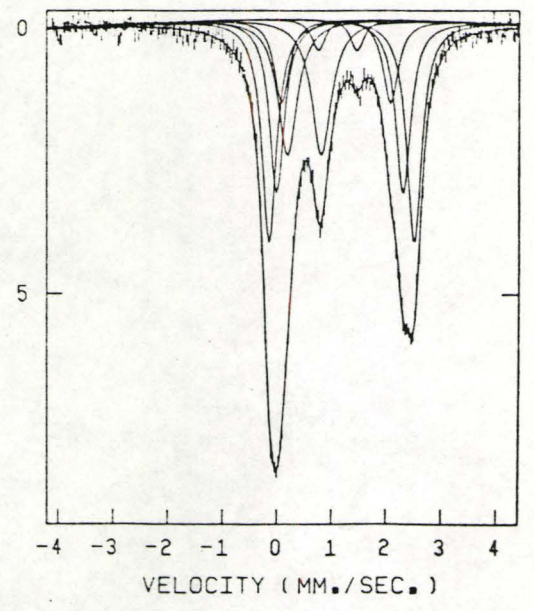
HBL DT-30 DRT



HBL DT-32 BHI

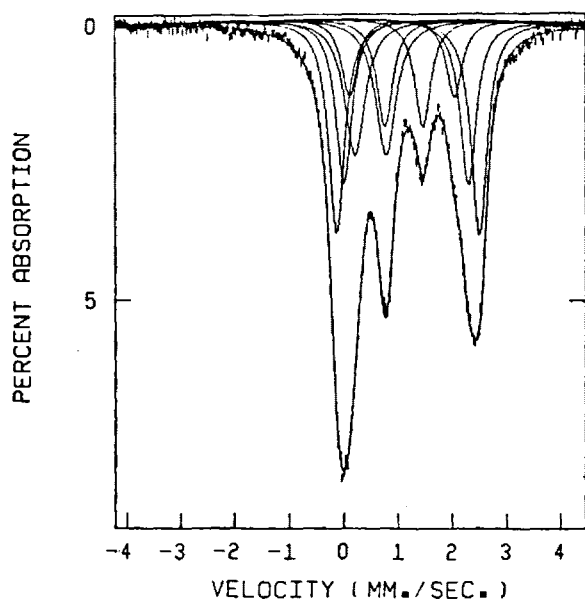


HBL DT-33 BHF



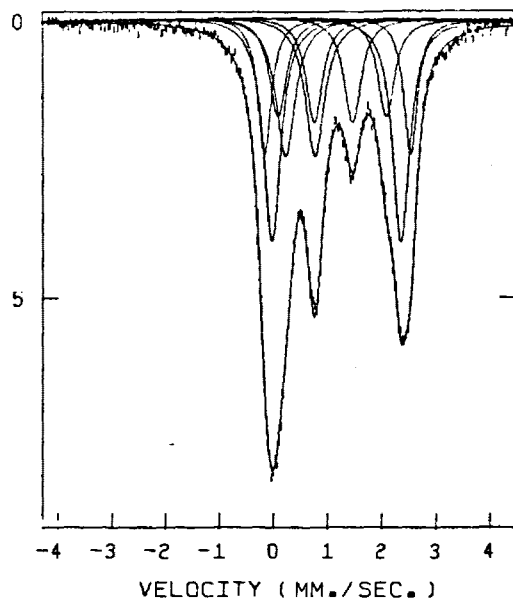
HBL DT-36

BVX



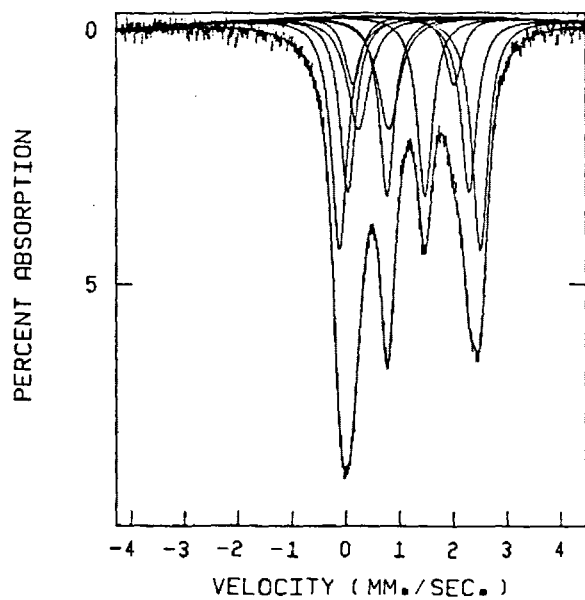
HBL DT-36

BGM



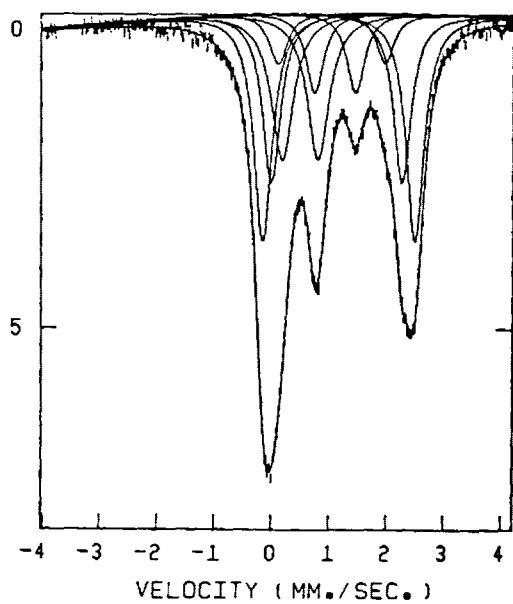
HBL DT-37

BRL



HBL DT-176

DXL



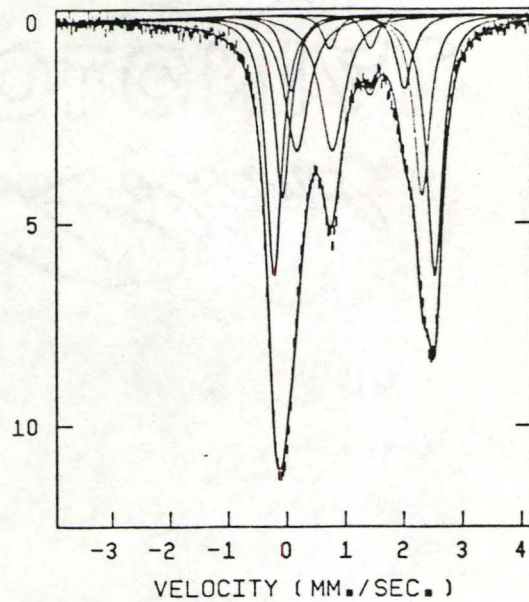
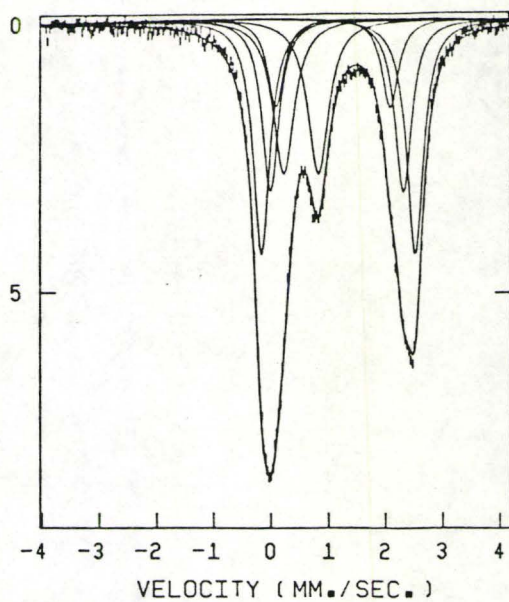
HBL DT-004

DQT

HBL DT 31

DDH

PERCENT ABSORPTION



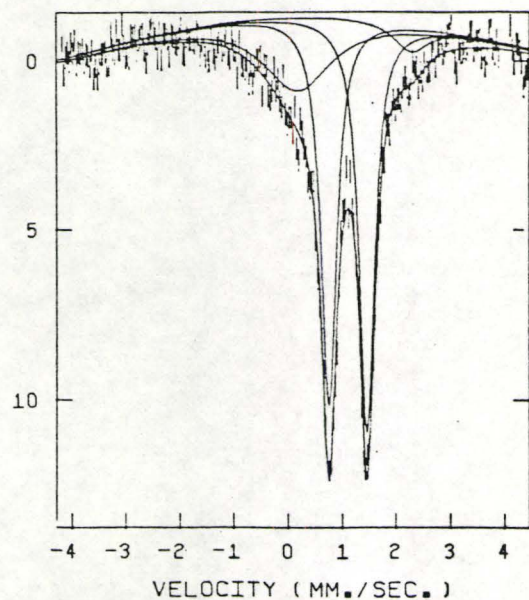
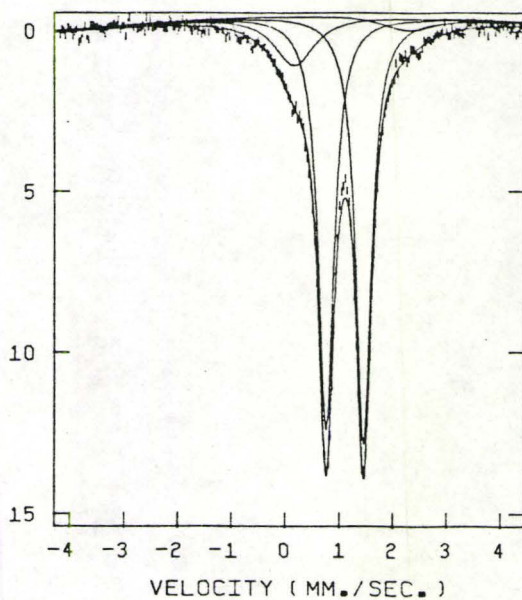
OPAQ

DT-35 BBZ

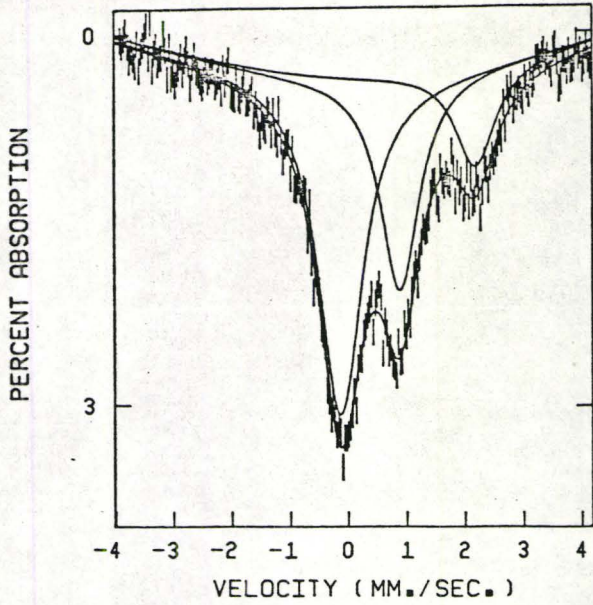
OPAQ

DT-37 BCA

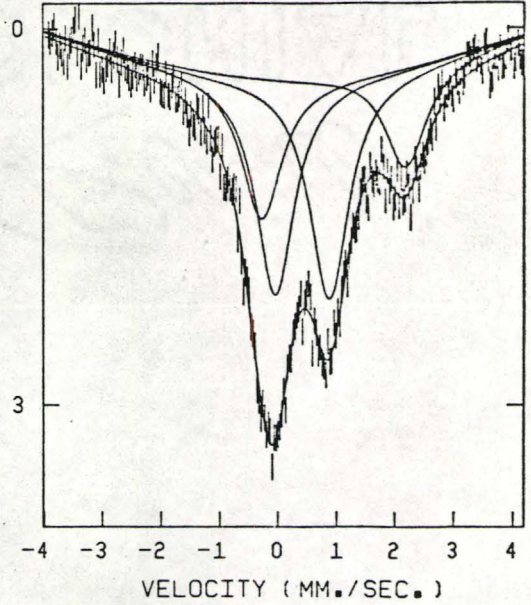
PERCENT ABSORPTION



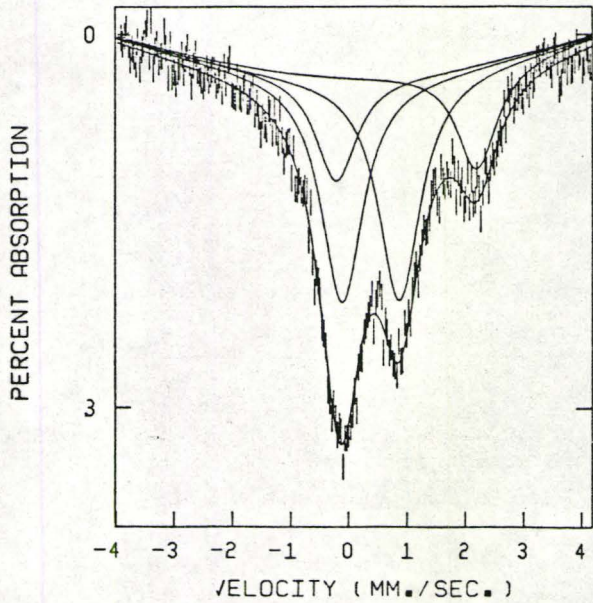
GLASS DT-28 EGH



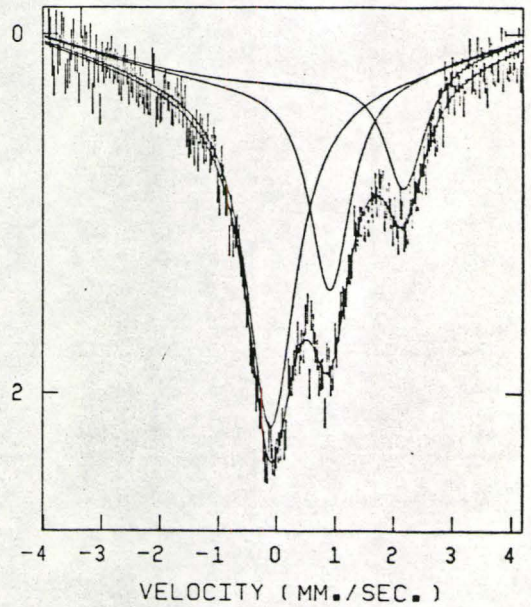
GLASS DT-28 CGS



GLASS DT-28 DLL

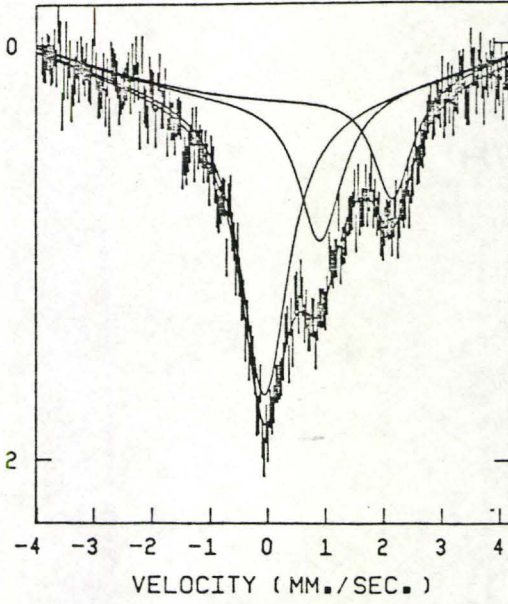


GLASS DT-30 CGL

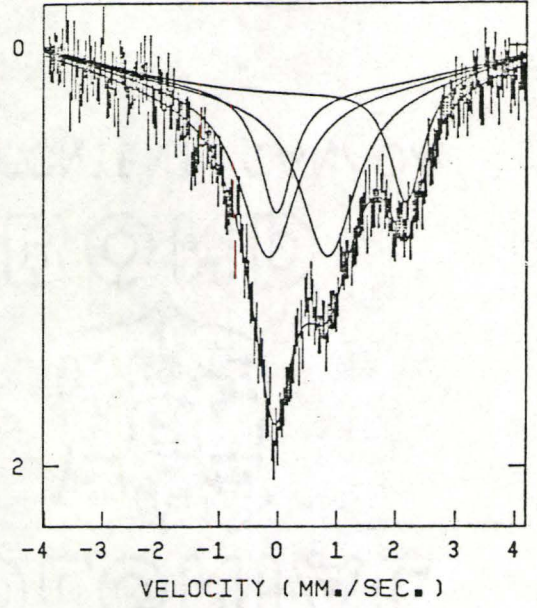


GLASS DT-33 DXD

PERCENT ABSORPTION

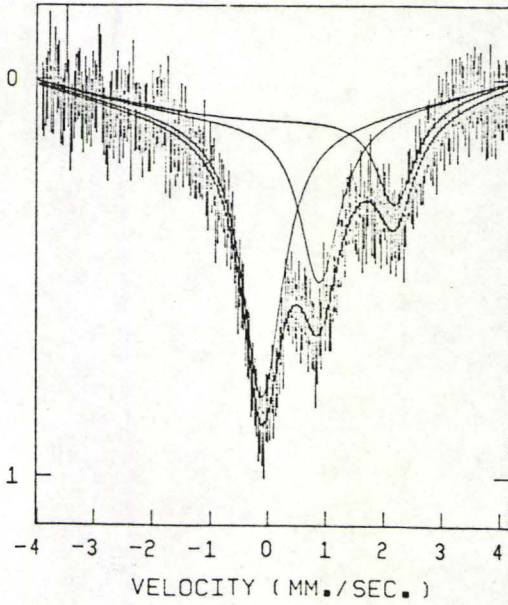


GLASS DT-33 AIA

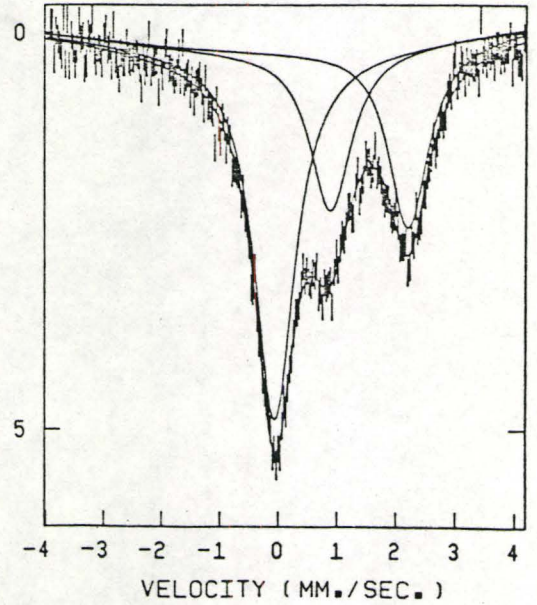


GLASS DT-32 CGP

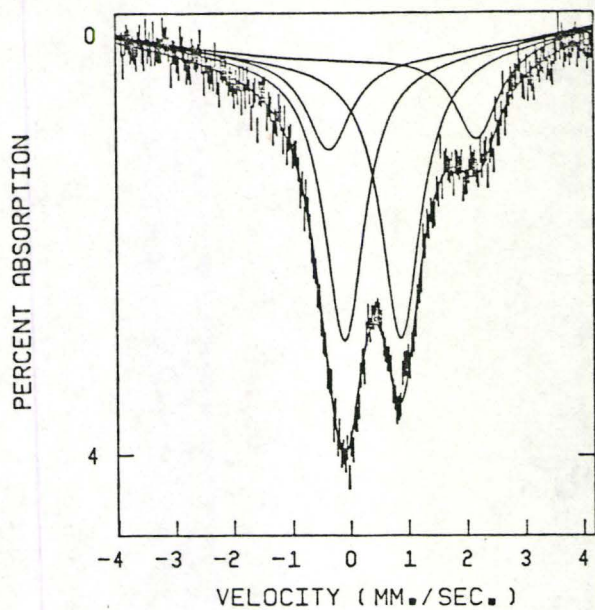
PERCENT ABSORPTION



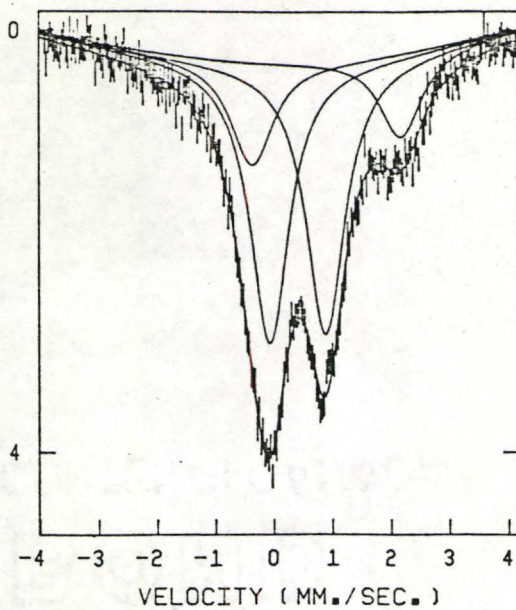
GLASS DT-36 AIC



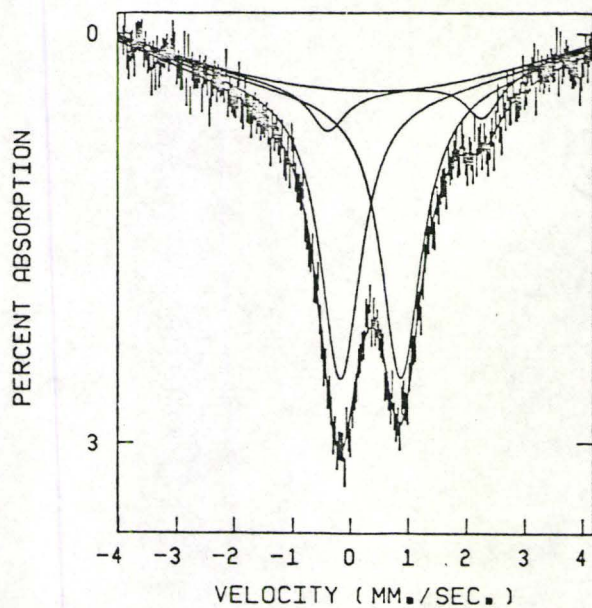
GLASS DT-57 DTV



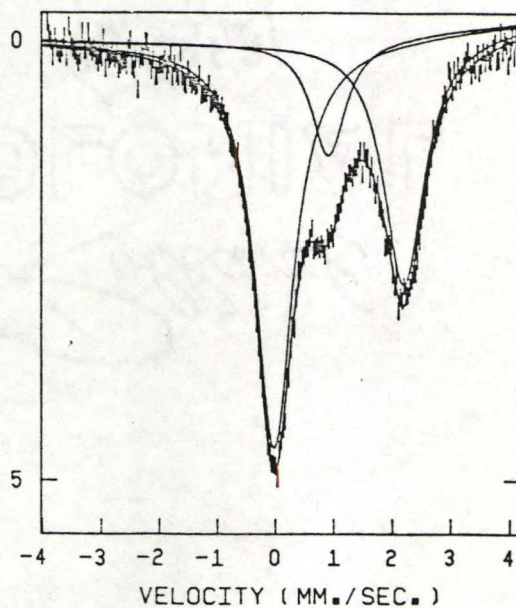
GLASS DT-57 AIB



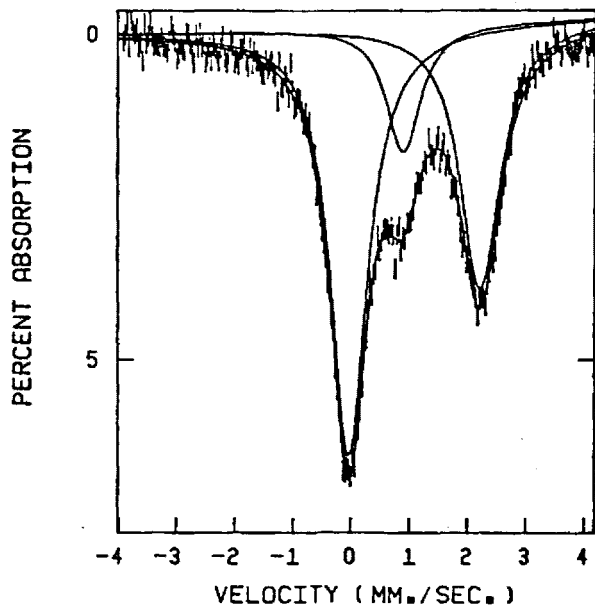
GLASS DT-98-1 BJC



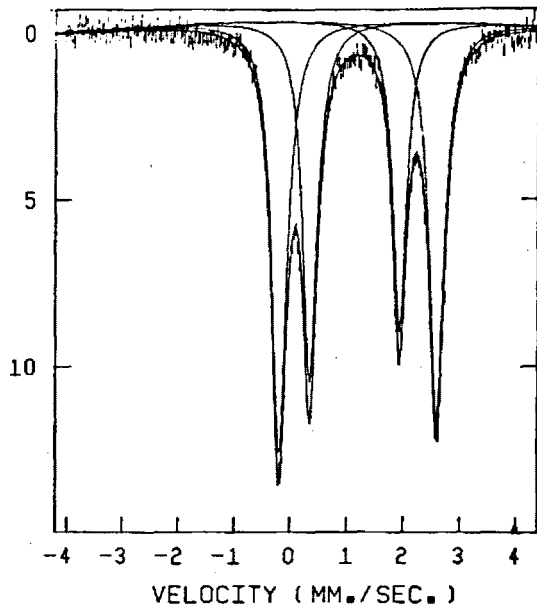
GLASS DT-98-2 BSV



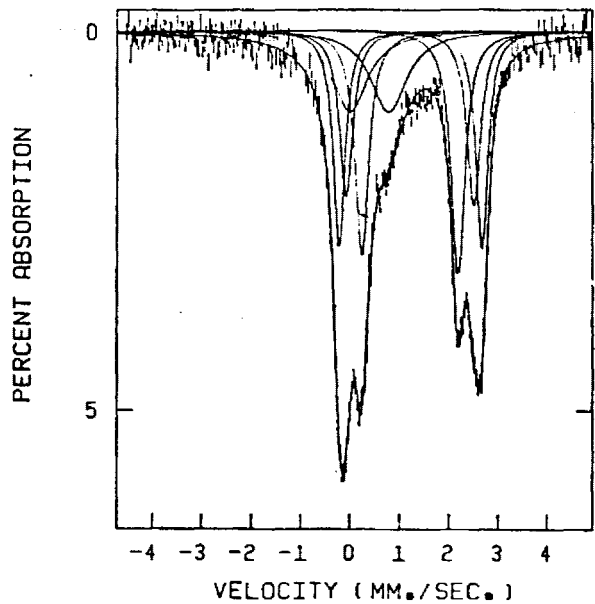
GLASS DT-98-3 BTK



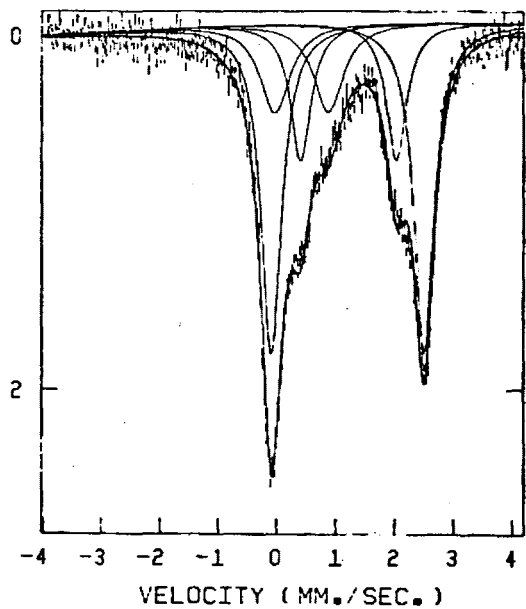
GRUN ADX



ACTN ADY



SAPPH ATF



APPENDIX B

B-I Accuracy and Precision of Chemical Analyses

(i) XRF

Whole rock samples were analysed by X-Ray Fluorescence analysis, using U.S.G.S. standards, GSP-1, AGV-1, JB-1, W-1, B-3, and SY-2, to establish a working curve. Samples were prepared by the fusion method (O. Mudroch, personal communication). The final values (including determination of FeO and CO₂) are given in Table B-I.

Precision of XRF analyses have been determined by multiple analysis of samples, DT-034, DT-160, and DT-165. These samples were chosen to cover a wide range of composition. The average one sigma error for each element is given in Table B-II. Accuracy has been determined by comparison of standards, BM, TB, GS-N, and DRN (analysed as unknowns) with published values. In each case, this error (or bias) has been found to be approximately the same or less than the measured precision.

The oxidation state of Fe in whole rock samples has been determined using the following method (O. Mudroch, personal communication 1982):

1. Place the powdered sample (0.4000 g) in a 90 ml platinum crucible with 10 ml of H₂SO₄ (1:3) and 5 ml of HF.

Table B-I

	DT-012	DT-023	DT-024	DT-025	DT-026	DT-027	DT-028	DT-029	DT-030	DT-31
SiO ₂	43.22	54.33	58.21	49.03	61.80	56.58	56.04	45.36	49.22	52.77
TiO ₂	1.35	.77	.66	1.69	.71	.79	2.13	.38	1.38	1.34
Al ₂ O ₃	14.88	17.87	16.23	12.02	16.02	18.74	11.58	18.44	13.61	20.50
Fe ₂ O ₃	4.33	9.08	2.88	5.17	2.14	2.43	5.86	8.51	2.79	2.80
FeO	10.02		4.86	8.35	4.15	5.65	10.99		8.32	5.17
MnO	.24	.13	.15	.23	.11	.13	.36	.09	.17	.11
MgO	6.86	4.26	3.46	7.55	2.72	3.49	1.56	10.93	9.69	2.73
CaO	9.66	7.55	6.36	11.80	5.13	7.45	6.75	11.24	11.99	10.47
Na ₂ O	3.11	3.98	3.88	2.72	3.77	3.93	1.89	2.04	1.77	3.46
K ₂ O	1.05	1.05	1.63	1.07	2.39	.65	.81	.83	.40	.70
P ₂ O ₅	.27	.20	.18	.18	.15	.18	.50	.04	.04	.28
CO ₂									.06	.93
Total	94.99	99.21	98.50	99.86	99.09	100.02	98.47	97.86	99.44	101.26

Table B-I con't

	DT-032	DT-033	DT-034	DT-035	DT-036	DT-037	DT-045	DT-046	DT-047	DT-048
SiO ₂	54.33	57.58	55.02	57.91	47.95	63.95	52.59	57.13	47.52	56.85
TiO ₂	.59	.92	1.81	.99	2.53	.46	2.18	1.58	1.48	1.97
Al ₂ O ₃	12.20	13.01	12.07	19.13	11.91	15.51	10.18	13.96	12.29	13.23
Fe ₂ O ₃	2.31	2.31	3.08	1.56	3.49	.86	18.79	11.22	10.55	16.52
FeO	12.24	6.94	11.90	4.81	12.55	3.52				
MnO	.45	.19	.32	.10	.28	.06	.33	.18	.15	.34
MgO	5.30	6.18	1.47	1.91	5.40	1.82	2.35	1.05	7.06	2.30
CaO	9.03	8.49	6.98	7.45	9.26	4.18	11.41	8.38	18.49	6.14
Na ₂ O	1.69	3.22	2.92	4.82	2.36	4.69	1.17	4.13	1.69	2.62
K ₂ O	.81	1.06	.86	.96	.90	2.29	.38	2.53	.25	1.19
P ₂ O ₅	.17	.22	.45	.23	.26	.08	.54	.21	.16	.52
CO ₂	.46	.25			.15					
Total	99.58	100.37	96.88	99.87	97.04	97.42	99.92	100.37	99.64	101.67

Table B-I con't

	DT-049	DT-051	DT-052	DT-054	DT-055	DT-056	DT-057	DT-069	DT-070	DT-071
SiO ₂	66.22	50.99	50.09	50.00	53.85	50.95	45.83	67.34	55.21	61.47
TiO ₂	1.16	.82	.36	.65	.20	1.04	4.39	.40	2.25	1.41
Al ₂ O ₃	13.16	22.03	24.36	21.08	27.86	23.11	11.80	13.17	13.45	12.44
Fe ₂ O ₃	8.36	4.41	3.91	6.46	1.31	5.91	4.66	1.14	3.53	11.93
FeO							13.00	3.62	9.62	
MnO	.16	.07	.03	.07	.00	.07	.23	.13	.30	.25
MgO	1.16	1.96	1.54	5.12	.19	1.62	2.93	2.27	1.89	1.19
CaO	3.72	14.58	12.63	12.31	10.78	10.73	11.96	6.88	7.43	5.08
Na ₂ O	2.41	2.50	4.35	3.18	5.07	4.58	2.23	4.38	2.94	3.04
K ₂ O	2.99	1.28	.74	.36	.68	.80	.61	1.05	1.59	1.87
P ₂ O ₅	.22	.20	.01	.02	.05	.12	1.02	.10	.56	.39
CO ₂							.08			
Total	99.56	98.58	98.02	99.24	99.99	98.92	98.74	100.48	98.77	99.07

Table B-I con't

	DT-072	DT-073	DT-074	DT-075	DT-077	DT-078	DT-079	DT-080	DT-081	DT-082
SiO ₂	61.33	54.65	48.33	12.17	55.76	58.91	47.62	46.07	56.80	57.19
TiO ₂	1.51	.65	1.55	.13	.72	.68	1.69	.98	.72	1.63
Al ₂ O ₃	12.92	19.92	13.39	1.17	18.22	17.70	12.96	26.24	17.38	16.22
Fe ₂ O ₃	11.42	8.02	12.91	1.29	7.76	6.57	14.41	12.35	9.16	8.15
FeO										
MnO	.25	.15	1.55	.00	.11	.11	.20	.17	.18	.13
MgO	1.03	4.29	7.09	5.35	3.28	2.36	6.55	4.45	1.37	2.07
CaO	5.37	8.15	12.66	48.80	6.49	5.33	10.81	4.85	5.52	6.55
Na ₂ O	3.16	5.10	3.11	.65	5.19	5.46	2.83	3.71	4.57	4.73
K ₂ O	1.45	.71	.58	.29	1.19	1.40	.45	1.06	2.92	2.96
P ₂ O ₅	.39	.22	.13	.07	.18	.16	.11	.00	.33	.32
CO ₂										
Total	98.83	101.85	99.94	69.93	98.90	98.68	97.63	99.89	98.95	99.95

Table B-I con't

	DT-083	DT-085	DT-086	DT-088	DT-89	DT-90	DT-091	DT-093	DT-098-1	DT-098-2
SiO ₂	46.90	56.34	55.42	57.86	58.11	49.93	60.69	48.17	49.76	47.29
TiO ₂	1.88	.45	.55	1.87	1.02	2.22	1.31	1.83	3.24	3.34
Al ₂ O ₃	13.58	22.92	18.31	12.47	18.72	13.94	17.94	12.38	15.57	15.22
Fe ₂ O ₃	13.58	22.92	18.31	12.47	18.72	13.94	17.94	12.38	5.43	4.07
FeO						10.19			11.54	14.49
MnO	.21	.07	.14	.36	.14	.26	.10	.26	.27	.40
MgO	6.45	1.71	3.16	1.67	1.94	5.94	1.13	6.49	.87	2.34
CaO	11.08	8.85	6.83	6.77	7.31	9.03	3.57	10.85	5.78	6.36
Na ₂ O	2.55	33.57	4.94	2.91	4.72	2.48	4.67	2.67	2.75	2.68
K ₂ O	.56	1.39	.78	.89	.92	.68	3.14	.51	.64	.49
P ₂ O ₅	.21	.11	.19	.46	.21	.37	.18	.16	.41	.47
CO ₂									.16	.16
Total	97.98	99.35	98.80	99.95	99.96	99.03	100.41	98.27	96.42	97.31

Table B-I con't

	DT-098-3	DT-160	DT-161	DT-162	DT-164	DT-165	DT-166	DT-167	DT-172	DT-173
SiO ₂	47.14	53.35	51.51	52.21	48.64	73.75	51.05	56.90	52.28	50.66
TiO ₂	1.87	.89	.67	1.31	1.37	.19	.80	.93	.62	.33
Al ₂ O ₃	12.73	17.52	23.09	18.52	15.59	13.05	18.53	17.01	24.35	25.98
Fe ₂ O ₃	3.26	10.47	5.24	9.77	11.52	1.70	9.46	7.87	5.13	4.50
FeO	11.54									
MnO	.27	.19	.04	.11	.15	.01	.15	.13	.04	.06
MgO	6.42	4.74	1.27	2.82	8.46	.53	4.64	3.14	1.23	1.72
CaO	10.17	7.77	9.92	9.13	10.94	1.29	7.42	6.98	10.90	9.67
Na ₂ O	2.62	4.25	4.62	3.73	2.14	2.96	4.46	5.22	4.04	4.24
K ₂ O	.61	.55	.82	.81	.37	4.34	1.34	.77	.35	1.01
P ₂ O ₅	.13	.23	.13	.14	.16	.01	.19	.20	.09	.05
CO ₂	.19									
Total	96.95	99.92	97.32	98.55	99.32	97.83	98.04	99.15	99.02	98.21

Table B-I con't

	DT-174	DT-175	DT-176	DT-177	DT-178	DT-179
SiO ₂	51.19	52.78	50.02	58.45	54.32	64.33
TiO ₂	1.31	.89	1.41	.68	.75	.47
Al ₂ O ₃	14.89	23.69	17.70	17.46	18.21	15.98
Fe ₂ O ₃	4.59	1.21	3.40	2.41	4.15	1.61
FeO	8.79	3.87	7.13	4.13	5.12	3.15
MnO	.21	.06	.15	.10	.19	.10
MgO	5.38	1.20	5.09	2.80	3.74	2.52
CaO	6.60	10.19	8.83	6.49	7.35	3.51
Na ₂ O	4.83	4.55	4.05	4.87	4.55	4.70
K ₂ O	.72	.73	.50	.78	.82	2.54
P ₂ O ₅	.26	.17	.20	.17	.23	.08
CO ₂			.14		.79	
Total	98.77	99.34	98.35	98.34	100.22	98.99

TABLE B-II

Precision of XRF Whole Rock Analyses

	DT-34	DT-160	DT-165	Ave. 1 sigma (%)
SiO ₂	2.32	0.30	0.74*	1.12
Al ₂ O ₃	1.14	1.46	0.91	1.17
Fe ₂ O ₃	1.36	0.76	1.22	1.11
MgO	4.76	7.05	9.56	7.12
CaO	0.74	0.86	1.19	0.93
Na ₂ O	7.64	4.41	6.56	6.20
K ₂ O	1.78	1.82	0.13	1.24
TiO ₂	0.84	0.65	0.00	0.50
MnO	0.00	2.99	43.30**	1.50
P ₂ O ₅	3.42	4.35	0.00	2.59

* - 1 sigma error (% relative error) based on three analyses.

** - excluded from calculation due to the very low concentration of MnO in sample DT-165.

2. Boil the mixture "gently" for exactly 10 minutes.
3. Remove the crucible from the heat and submerge in a beaker containing 50 ml of boric acid, 15 ml of H_2SO_4 (1:3) and O_2 free H_2O to the 380 ml mark.
4. Titrate using pre-mixed potassium dichromate solution. %Fe in sample = ml of $K_2Cr_2O_7$ * calibration factor.

The analysis is repeated for each sample until 3 equivalent results were obtained. This procedure was found to give very good results. The values of FeO, Fe_2O_3 , and F* (the oxidation ratio) are given in Table B-III.

TABLE B-III

Whole Rock Iron Oxidation State

1. $\text{Fe}_2\text{O}_3(\text{T})$ = total Fe as Fe_2O_3 , determined by XRF.
2. FeO determined by titration, Fe_2O_3 by difference.
3. $F^* = \text{Fe}^{2+} / (\text{Fe}^{2+} + \text{Fe}^{3+})$ atomic fraction.
4. Sample DT-012 is a hornblendite (hornblende-plagioclase gneiss) from outside the study area. It is not included in the calculation of average values and is not plotted in Figure 4-IV.

Whole Rock Oxidation State

Sample Number	Fe ₂ O ₃ (T)	FeO	Fe ₂ O ₃	F*
DT-12	15.47	10.02	4.33	0.72
DT-24	8.28	4.86	2.88	0.65
DT-25	14.45	8.35	5.17	0.64
DT-26	6.75	4.15	2.14	0.68
DT-27	8.71	5.65	2.43	0.72
DT-28	18.07	10.99	5.86	0.68
DT-30	12.04	8.32	2.79	0.77
DT-31	8.55	5.17	2.80	0.67
DT-32	15.91	12.24	2.31	0.85
DT-33	10.02	6.94	2.31	0.77
DT-34	16.30	11.90	3.08	0.81
DT-35	6.91	4.81	1.56	0.77
DT-36	17.44	12.55	3.49	0.80
DT-37	4.77	3.52	0.86	0.82
DT-57	19.11	13.00	4.66	0.76
DT-69	5.16	3.62	1.14	0.78
DT-70	14.22	9.62	3.53	0.75
DT-90	15.31	10.19	3.99	0.74
DT-98-1	18.25	11.54	5.43	0.70
DT-98-2	20.17	14.49	4.07	0.80
DT-98-3	16.08	11.54	3.26	0.80
DT-174	14.36	8.79	4.59	0.68
DT-175	5.51	3.87	1.21	0.78
DT-176	11.32	7.13	3.40	0.70
DT-177	7.00	4.13	2.41	0.66
DT-178	9.84	5.12	4.15	0.58
DT-179	5.11	3.15	1.61	0.69

(ii) Microprobe

Mineral analyses were obtained using a Material Analyses Co. (MAC) microprobe, and a Krisel control probe system V4C-M6SP1, with MAGIC corrections. An operating voltage of 15 kv, reference current of 250 or 500 ma, and a preset time and count of 30 seconds or 20,000 counts, were used for all samples. Natural minerals were used as standards. Samples were prepared by cutting 1.0 inch dia. disks from commercially prepared polished thin sections.

Precision has been determined by multiple analyses. The general procedure is to perform a number of analyses on the same crystal, moving the beam only slightly each time. The movement ensures a fresh surface for each analyses, but presumably is not great enough to move the beam to an area of differing composition. For most probe sections a large number of analyses were performed on each mineral, which were then averaged (following the removal of clearly spurious data). The mineral compositions determined in this way are given in Tables B-IV (Clinopyroxene), B-V (Orthopyroxene), B-VI (Amphibole), B-VII (Garnet), and B-VIII (Biotite). Most represent the average of between 5 and 15 individual analyses. The 1 sigma error (% relative error or dispersion) of the averaged values is approximately the same as the precision determined on a single crystal, even though there is likely to be greater chemical variability between a number of separate crystals. Several examples are given in Table B-IX. Accuracy has been determined by comparison of standards (analysed as unknowns) with published values. In each case, this error is approximately the same or less than the

calculated precision.

One further point is worthy of mention. During the storage of intensity data (measured on standards), it is necessary to make a value judgement on the quality of the data. Following the storage of intensity data for each element, a number of unknowns are analysed. If they are approximately correct, you may decide to accept the set of standard data you have collected, and proceed with the analyses of your samples. This leads to a fundamental problem: the standard intensity data varies with each use of the machine. This results in a systematic error, which is particularly noticeable for minerals in which the oxides total to less than 100. For these minerals it is often not possible to adequately judge the quality of the data due to the natural variability of the mineral. For example, a hornblende total which falls between 97.8 and 98.8 must be accepted as correct, if no other information is available. Analyses of the same probe section on different occasions, indicates the error due to differing standardization is probably less than the calculated precision.

TABLE B-IV Mean Composition and Structural Formula of Clinopyroxenes
(calculated on the basis of 6 oxygen)

Sample	DT-24	DT-25	DT-28	DT-30	DT-32	DT-33	DT-34	DT-35	DT-36	DT-174	DT-176	DT-177	DT-98
SiO ₂	51.667	51.022	50.860	51.835	51.800	51.587	49.687	49.278	51.766	51.783	51.597	51.352	51.527
TiO ₂	0.180	0.238	0.242	0.555	0.187	0.169	0.180	0.191	0.173	0.218	0.238	0.222	0.181
Al ₂ O ₃	2.230	2.660	2.864	4.275	2.413	2.294	1.820	2.937	2.501	2.285	3.215	3.055	2.578
Cr ₂ O ₃	0.060	0.04	0.016	0.048	0.104	0.091	0.010	0.04	0.001	0.010	0.003	0.017	0.093
Fe ₂ O ₃	2.622	2.785	3.906	1.372	2.760	2.005	4.641	3.470	3.020	2.569	2.898	2.752	2.745
FeO	9.148	8.884	12.460	6.028	9.934	8.810	16.704	12.489	11.584	10.531	8.256	9.905	9.871
MnO	0.397	0.375	0.148	0.080	0.092	0.296	0.257	1.443	0.311	0.455	0.230	0.367	0.164
MgO	12.320	12.080	7.956	12.793	11.332	12.239	5.485	8.867	9.984	10.518	11.548	11.285	10.785
CaO	21.073	21.083	20.978	22.165	21.321	21.551	20.292	21.563	19.937	20.768	21.938	20.392	21.197
Na ₂ O	0.863	0.967	1.358	0.878	1.151	0.890	1.160	0.971	1.117	0.993	0.908	0.917	0.984
K ₂ O	0.003	0.008	0.016	0.0	0.0	0.025	0.012	0.0	0.010	0.013	0.012	0.0	0.007
Total	100.563	100.142	100.803	100.028	101.095	99.957	100.247	101.250	100.405	100.140	100.844	100.263	100.128
Si	1.933	1.918	1.934	1.915	1.935	1.938	1.944	1.884	1.954	1.955	1.920	1.929	1.942
Al	0.067	0.082	0.066	0.085	0.065	0.062	0.056	0.116	0.046	0.045	0.080	0.071	0.058
Tot	2.0	2.0	2.0	2.0	2.0	2.0	2.0	2.0	2.0	2.0	2.0	2.0	2.0
Al	0.032	0.036	0.062	0.101	0.041	0.040	0.028	0.017	0.066	0.057	0.061	0.064	0.056
Ti	0.005	0.007	0.007	0.015	0.005	0.005	0.005	0.006	0.005	0.006	0.006	0.006	0.005
Cr	0.002	0.001	0.001	0.001	0.003	0.003	0.0	0.001	0.0	0.0	0.0	0.001	0.003
Fe ³⁺	0.074	0.079	0.112	0.038	0.078	0.057	0.137	0.100	0.086	0.073	0.081	0.078	0.078
Fe ²⁺	0.286	0.279	0.396	0.186	0.310	0.277	0.547	0.399	0.366	0.333	0.257	0.311	0.311
Mn	0.013	0.012	0.005	0.003	0.003	0.009	0.009	0.047	0.010	0.014	0.007	0.012	0.065
Mg	0.687	0.677	0.451	0.704	0.631	0.685	0.320	0.505	0.562	0.592	0.641	0.632	0.606
Ca	0.845	0.849	0.855	0.877	0.853	0.868	0.851	0.883	0.807	0.840	0.875	0.821	0.856
Na	0.063	0.071	0.100	0.063	0.083	0.065	0.088	0.072	0.082	0.073	0.066	0.067	0.072
K	0.0	0.0	0.001	0.0	0.0	0.001	0.001	0.0	0.001	0.001	0.001	0.0	0.0
Tot	2.007	2.011	1.990	1.988	2.007	2.010	1.986	2.030	1.985	1.989	1.995	1.992	2.052

TABLE B-V Mean Composition and Structural Formula of Orthopyroxenes
(calculated on the basis of 6 oxygen)

Sample	DT-24	DT-25	DT-30	DT-32	DT-33	DT-37	DT-174	DT-176	DT-177	DT-98(3)
SiO ₂	50.811	51.843	51.714	50.717	49.990	50.242	50.572	50.394	50.839	49.850
TiO ₂	0.059	0.107	0.048	0.030	0.060	0.070	0.067	0.058	0.060	0.035
Al ₂ O ₃	1.534	1.620	2.554	1.167	1.334	1.192	1.073	2.110	1.896	1.435
Cr ₂ O ₃	0.019	0.017	0.118	0.040	0.022	0.030	0.065	0.004	0.026	0.065
Fe ₂ O ₃	1.267	1.887	0.739	0.663	0.183	1.618	1.689	1.346	1.638	0.664
FeO	25.877	25.345	22.269	29.243	27.759	30.262	29.013	25.939	26.870	29.258
MnO	0.929	1.045	0.280	0.418	0.872	0.872	0.983	0.690	0.781	0.375
MgO	18.999	18.280	21.990	17.142	18.676	15.310	15.938	19.290	17.674	17.230
CaO	0.593	0.675	0.452	0.448	0.526	0.526	0.582	0.472	0.596	0.475
Na ₂ O	0.013	0.082	0.102	0.045	0.044	0.002	0.037	0.00	0.020	0.010
K ₂ O	0.029	0.003	0.014	0.00	0.044	0.004	0.012	0.012	0.00	0.00
Total	100.129	100.904	100.280	99.913	99.510	100.128	100.030	100.314	100.400	99.397
Si	1.938	1.957	1.925	1.960	1.934	1.958	1.962	1.918	1.941	1.941
Al	0.062	0.044	0.075	0.040	0.061	0.042	0.038	0.082	0.059	0.059
Tot	2.0	2.0	2.0	2.0	1.995	2.0	2.0	2.0	2.0	2.0
Al	0.007	0.009	0.037	0.014	0.0	0.012	0.011	0.012	0.027	0.007
Ti	0.002	0.003	0.001	0.001	0.002	0.002	0.002	0.002	0.002	0.001
Cr	0.001	0.001	0.004	0.001	0.001	0.001	0.002	0.0	0.001	0.002
Fe ³⁺	0.036	0.054	0.021	0.019	0.005	0.047	0.047	0.039	0.047	0.019
Fe ²⁺	0.826	0.800	0.693	0.945	0.898	0.986	0.941	0.825	0.858	0.953
Mn	0.030	0.033	0.009	0.014	0.029	0.029	0.032	0.022	0.025	0.012
Mg	1.080	1.028	1.220	0.986	1.077	0.889	0.922	1.094	1.006	1.000
Ca	0.024	0.027	0.018	0.0	0.022	0.022	0.024	0.019	0.024	0.020
Na	0.001	0.006	0.007	0.003	0.003	0.0	0.003	0.0	0.002	0.001
K	0.001	0.0	0.001	0.0	0.002	0.0	0.001	0.001	0.0	0.0
Tot	2.008	1.981	2.011	1.983	2.039	1.988	1.985	2.014	1.992	2.015

TABLE B-VI Mean Composition and Structural Formula of Amphiboles
(calculated on the basis of 23 oxygen)

Sample No.	DT-24	DT-25	DT-28	DT-30	DT-31	DT-32	DT-33	DT-34	DT-35	DT-36	DT-37	DT-174	DT-176	DT-177	DT-178	DT-98	DT-12
SiO ₂	40.081	41.925	38.610	41.913	40.294	40.254	40.614	38.783	40.852	40.548	40.347	40.575	40.728	40.694	40.956	40.574	40.530
TiO ₂	1.606	2.238	1.910	2.607	.869	2.129	2.272	1.703	1.013	2.452	1.853	1.983	1.811	1.724	1.001	2.158	1.437
Al ₂ O ₃	12.936	12.481	12.283	12.737	13.755	11.989	12.157	11.082	13.083	11.972	12.245	12.012	13.220	13.510	12.880	12.107	12.373
Cr ₂ O ₃	.064	.079	.073	.170	.140	.127	.148	.025	.037	.010	.023	.057	.007	.035	.010	.085	.008
Fe ₂ O ₃	5.040	5.073	6.966	3.514	6.529	5.835	5.047	8.461	6.967	6.131	5.482	6.018	5.182	5.334	5.889	5.641	6.477
FeO	12.094	12.174	16.199	8.204	14.383	13.684	12.278	19.675	16.201	14.293	14.990	13.993	11.399	12.402	12.365	12.847	12.733
MnO	.160	.204	.040	.010	.275	.063	.158	.103	.123	.097	.165	.202	.082	.170	.252	.082	.311
MgO	10.278	9.846	5.560	12.364	7.432	8.747	9.917	3.852	6.505	8.168	8.045	8.702	10.519	9.368	9.677	8.944	9.041
CaO	11.628	11.136	11.883	12.291	11.517	11.246	11.354	10.892	11.313	11.022	10.927	11.230	12.179	11.275	11.918	11.442	11.897
Na ₂ O	1.511	1.695	1.437	1.800	1.225	1.667	1.637	1.828	1.263	1.857	1.735	1.662	1.515	1.398	1.637	1.806	1.891
K ₂ O	2.076	1.884	2.427	1.661	1.690	2.033	1.958	1.837	2.038	1.993	2.013	1.790	2.024	2.119	1.169	1.982	1.469
Total	97.473	98.733	97.398	97.272	98.108	97.775	97.539	98.241	99.396	98.543	97.826	98.223	98.666	98.027	97.754	97.668	98.169
T																	
Si	6.064	6.225	6.028	6.191	6.109	6.109	6.138	6.101	6.171	6.137	6.158	6.145	6.063	6.110	6.160	6.152	6.120
Al ^{IV}	1.936	1.775	1.972	1.809	1.809	1.875	1.862	1.899	1.829	1.866	1.842	1.855	1.937	1.891	1.841	1.841	1.880
Tot	8.0	8.0	8.0	8.0	8.0	8.0	8.0	8.0	8.0	8.0	8.0	8.0	8.0	8.0	8.0	8.0	8.0
C																	
Al ^{VI}	.371	.410	.289	.409	.568	.276	.304	.157	.501	.273	.362	.290	.383	.501	.443	.316	.322
Cr	.008	.009	.009	.020	.017	.016	.017	.003	.004	.001	.003	.007	.001	.004	.001	.010	.001
Ti	.183	.250	.224	.290	.099	.244	.258	.202	.115	.279	.213	.226	.203	.195	.113	.246	.163
Fe ³⁺	1.135	.567	.819	.391	.745	.668	.574	1.002	.792	.698	.630	.686	.581	.603	.667	.644	.736
Mg	2.317	2.19	1.294	2.722	1.679	1.984	2.233	.903	1.464	1.842	1.830	1.964	2.334	2.096	2.169	2.021	2.035
Fe ²⁺	1.530	1.512	2.115	1.013	1.871	1.742	1.552	2.589	2.047	1.809	1.914	1.773	1.419	1.557	1.555	1.629	1.608
Mn	.018	.026	.005	.001	.021	.008	.020	.014	.016	.012	.021	.026	.010	.022	.032	.011	.040
Tot	5.0	4.951	4.755	4.846	5.0	4.937	4.958	4.868	4.946	4.915	4.972	4.971	4.930	4.977	4.981	4.877	4.905
B																	
Pn	.003				.014												
Ca	1.885	1.772	1.988	1.945	1.871	1.834	1.839	1.836	1.831	1.787	1.787	1.822	1.943	1.814	1.92	1.859	1.925
Na	.112	.229	.012	.055	.115	.166	.162	.164	.169	.213	.213	.178	.057	.186	.080	.141	.075
Tot	2.0	2.0	2.0	2.0	2.0	2.0	2.0	2.0	2.0	2.0	2.0	2.0	2.0	2.0	2.0	2.0	2.0
A																	
Na	.331	.259	.423	.461	.246	.326	.318	.394	.201	.332	.301	.310	.380	.221	.398	.390	.479
K	.401	.357	.485	.313	.327	.395	.378	.369	.169	.385	.392	.346	.384	.406	.224	.383	.283
Tot	.732	.616	.908	.774	.572	.720	.696	.762	.593	.717	.693	.656	.764	.626	.622	.773	.761

TABLE B-VII Mean Composition and Structural Formula of Garnets
(calculated on the basis of 24 oxygen)

Sample	DT-25	DT-28	DT-30	DT-31	DT-32	DT-34	DT-35(C)	DT-35(R)	DT-36	DT-37	DT-176	DT-178(C)	DT-178(R)	DT-98(1)	DT-98(2 and 3)
SiO ₂	38.431	37.853	39.906	38.059	37.970	37.173	37.996	38.043	38.016	37.773	38.443	38.583	38.078	38.049	38.433
TiO ₂	0.0	0.041	0.016	0.059	0.0	0.026	0.064	0.043	0.033	0.190	0.084	0.090	0.085	0.032	0.023
Al ₂ O ₃	20.959	20.544	21.526	21.297	21.237	20.701	20.840	20.940	20.943	20.385	21.331	21.180	21.058	20.694	21.244
Cr ₂ O ₃										0.050					
Fe ₂ O ₃	1.759	2.491	1.486	1.805	1.705	2.506	1.995	1.847	2.619	2.617	1.731	2.120	2.163	2.201	2.212
FeO	25.236	27.290	22.247	25.769	26.356	30.146	27.727	25.684	26.773	27.083	24.838	24.436	24.934	26.312	26.447
MnO	0.976	1.546	0.616	0.885	1.093	1.301	1.086	0.880	1.558	1.128	1.033	0.657	2.600	0.908	0.917
MgO	5.146	2.379	8.431	4.582	5.013	1.219	3.296	2.847	3.683	3.305	6.090	5.403	3.998	3.461	4.536
CaO	7.874	8.366	6.474	8.115	6.801	7.684	7.144	9.497	7.285	8.125	6.923	8.013	7.705	7.738	6.630
Na ₂ O										0.0					
K ₂ O										0.013					
Total	100.204	100.510	100.702	100.571	100.173	100.757	100.148	99.781	100.908	100.667	100.474	100.482	100.619	99.395	100.441
Si	5.991	5.994	6.054	5.942	5.950	5.940	6.005	6.010	5.960	5.959	5.959	5.983	5.964	6.030	6.000
Al	0.009	0.006		0.058	0.050	0.060			0.040	0.041	0.041	0.017	0.036		
Tot	6.0	6.0	6.054	6.0	6.0	6.0	6.005	6.010	6.0	6.0	6.0	6.0	6.0	6.030	6.000
Al	3.844	3.830	3.850	3.862	3.874	3.841	3.883	3.900	3.832	3.750	3.857	3.855	3.852	3.866	3.910
Cr										0.006					
Fe ³⁺	0.206	0.297	0.170	0.212	0.201	0.301	0.237	0.220	0.309	0.311	0.202	0.247	0.255	0.263	0.260
Ti		0.005	0.002	0.007		0.003	0.008	0.005	0.004	0.023	0.010	0.011	0.010	0.004	0.003
Tot	4.050	4.132	4.022	4.081	4.075	4.145	4.128	4.125	4.145	4.090	4.069	4.113	4.117	4.133	4.173
Fe ²⁺	3.290	3.614	2.823	3.365	3.454	4.029	3.665	3.394	3.511	3.573	3.220	3.169	3.266	3.487	3.453
Mn	0.129	0.207	0.079	0.117	0.145	0.176	0.145	0.118	0.207	0.151	0.136	0.086	0.345	0.122	0.121
Mg	1.196	0.561	1.906	1.066	1.171	0.290	0.776	0.570	0.861	0.777	1.407	1.249	0.933	0.817	1.056
Ca	1.315	1.420	1.052	1.358	1.142	1.316	1.210	1.608	1.224	1.373	1.150	1.331	1.293	1.314	1.109
Na										0.0					
K										0.003					
Tot	5.930	5.802	5.860	5.906	5.912	5.811	5.796	5.790	5.803	5.877	5.913	5.835	5.837	5.740	5.739

TABLE B-VIII

Mean Composition and Structural Formula of Biotites
(calculated on the basis of 23 oxygen)

Sample	DT-30	DT-31	DT-33	DT-37	DT-98	DT-174	DT-176	DT-178
SiO ₂	36.893	35.11	35.670	35.94	37.020	38.570	37.390	35.585
TiO ₂	5.537	4.07	4.483	4.64	4.425	4.395	4.000	3.400
Al ₂ O ₃	13.900	15.21	13.483	13.05	14.040	13.720	14.01	15.125
Cr ₂ O ₃	0.153	0.14	0.073	0.02	0.100	0.	0.00	0.00
FeO	11.457	21.67	16.03	20.51	15.935	18.390	16.99	17.940
Fe ₂ O ₃								
MnO	0.300	0.14	0.017	0.02	0.010	0.145	0.00	0.135
MgO	15.690	9.27	13.673	10.36	13.490	12.235	14.32	12.270
CaO	0.050	0.04	0.00	0.05	0.00	0.110	0.07	0.070
Na ₂ O	0.04	0.05	0.093	0.00	0.00	0.00	0.00	0.00
K ₂ O	9.747	9.73	9.937	9.747	9.280	7.900	10.60	9.950
Total	93.467	95.43	93.460	95.02	94.300	95.480	97.38	94.415
Si	5.806	5.696	5.768	5.933	5.872	6.038	5.812	5.733
Al	2.194	2.304	2.232	2.167	2.128	1.962	2.188	2.267
Al	0.385	0.606	0.338	0.330	0.498	0.570	0.380	0.606
Ti	0.655	0.497	0.545	0.566	0.528	0.517	0.468	0.405
Cr	0.019	0.018	0.009	0.003	0.013	0.002	0.00	0.00
Fe ³⁺	0.151	0.294	0.217	0.280	0.211	0.241	0.221	0.242
Fe ²⁺	1.357	2.646	1.951	2.518	1.903	2.167	1.987	2.175
Mn	0.00	0.019	0.002	0.003	0.001	0.019	0.000	0.018
Mg	3.680	2.242	3.295	2.627	3.189	2.854	3.318	2.946
Tct	6.247	6.322	6.357	6.327	6.343	6.370	6.374	6.392
Ca	0.008	0.007	0.00	0.009	0.00	0.019	0.012	0.011
K	1.957	2.014	2.050	2.035	1.878	1.578	2.102	2.045
Na	0.012	0.016	0.029	0.00	0.00	0.00	0.00	0.00
Tot	1.977	2.037	2.079	2.044	1.878	1.597	2.114	2.056

TABLE B-IX

Listing of Individual Microprobe Analyses,
Calculated Average and Precision (1σ)

DT-24 ORTHOPYROXENE

	1.	2.	3.	4.	5.	6.	7.	\bar{x}	S	%
SiO ₂	51.09	52.16	49.10	49.00	51.08	51.21	52.04	50.8114	1.28	2.52
TiO ₂	.04	.09	.09	.06	.04	.06	.03	.0586	.024	41.13
Al ₂ O ₃	1.65	1.47	1.26	1.73	1.66	1.44	1.53	1.5343	.161	10.50
Cr ₂ O ₃	.10	.00	.03	.00	.00	.00	.00	.0186	.038	202.15
FeO	26.38	27.00	28.42	27.44	26.98	26.73	26.17	27.0171	.748	2.77
MnO	.89	.96	.85	.84	.96	1.02	.98	.9286	.069	7.42
MgO	19.27	18.82	18.90	19.22	19.62	18.55	18.61	18.9986	.388	2.04
CaO	.67	1.18	.38	.53	.41	.45	.53	.5929	.276	46.58
Na ₂ O	.00	.00	.00	.09	.00	.00	.00	.0129	.034	263.57
K ₂ O	.05	.03	.03	.03	.00	.02	.04	.0286	.016	54.90
Total	100.15	101.71	99.05	98.93	100.77	99.48	99.92	100.002		

DT-25 Orthopyroxene

	1.	2.	3.	4.	5.	6.	\bar{x}	S	%
SiO ₂	50.93	52.14	51.00	52.07	52.66	52.26	51.8433	.771	1.49
TiO ₂	.09	.08	.16	.09	.09	.13	.1067	.031	29.05
Al ₂ O ₃	1.48	1.89	1.56	1.72	1.46	1.61	1.620	.162	10.00
Cr ₂ O ₃	.05	.02	.01	.00	.00	.02	.0167	.019	113.77
FeO	27.29	27.09	28.13	26.70	26.51	26.54	27.0433	.616	2.28
MnO	1.12	.91	1.08	1.05	1.04	1.07	1.0450	.072	6.89
MgO	17.88	18.91	17.90	18.05	18.55	18.39	18.280	.410	2.24
CaO	.60	.54	.95	.84	.63	.49	.6750	.181	26.81
Na ₂ O	.09	.03	.05	.21	.11	.00	.0817	.074	90.58
K ₂ O	.00	.00	.01	.00	.01	.00	.0033	.005	151.52
Total	99.52	101.61	100.85	100.73	101.06	100.50	100.715		

DT-30 Orthopyroxene

	1.	2.	3.	4.	5.	\bar{x}	S	%
SiO ₂	51.80	51.14	52.48	51.52	51.63	51.7140	.492	.951
TiO ₂	.08	.02	.05	.02	.07	.0480	.028	57.8
Al ₂ O ₃	2.72	2.64	2.70	2.12	2.59	2.5540	.248	9.70
Cr ₂ O ₃	.08	.21	.11	.10	.09	.1180	.053	44.6
FeO	23.16	23.33	22.60	22.65	22.93	22.9340	.316	1.38
MnO	.25	.35	.25	.22	.33	.2800	.057	20.2
MgO	21.94	22.14	21.80	22.18	21.89	21.9900	.164	.745
CaO	.49	.54	.43	.39	.41	.4520	.062	13.7
Na ₂ O	.08	.34	.00	.04	.05	.1020	.136	133
K ₂ O	.01	.03	.01	.00	.02	.0140	.011	81.4
Total	100.61	100.75	100.42	99.25	100.01	100.206		

DT-32 Orthopyroxene

	1.	2.	3.	4.	5.	6.	\bar{x}	S	%
SiO ₂	50.91	50.60	50.96	50.06	50.23	51.54	50.7167	.540	1.06
TiO ₂	.03	.05	.03	.05	.02	.00	.0300	.019	63.3
Al ₂ O ₃	1.21	1.30	1.22	1.09	1.16	1.02	1.1667	.100	8.57
Cr ₂ O ₃	.04	.04	.07	.03	.03	.03	.0400	.016	38.7
FeO	30.01	29.59	30.48	30.54	29.44	28.98	29.8400	.615	2.06
MnO	.48	.44	.45	.43	.37	.34	.4183	.053	12.6
MgO	16.80	16.98	17.14	16.71	17.82	17.40	17.1417	.414	2.41
CaO	.34	.44	.55	.55	.41	.40	.4483	.085	19.0
Na ₂ O	.15	.00	.02	.00	.09	.01	.0450	.062	137
K ₂ O	.00	.00	.00	.00	.00	.00	.0000	.000	.000
Total	99.98	99.43	100.91	99.46	99.56	99.72	99.8467		

DT-33 ORTHOPYROXENE

297

	1.	2.	3.	4.	5.	\bar{X}	S	%
SiO ₂	49.85	48.57	48.64	51.55	51.34	49.9900	1.424	2.85
TiO ₂	.03	.07	.06	.07	.07	.0600	.017	28.83
Al ₂ O ₃	1.35	1.39	1.38	1.31	1.24	1.3340	.361	4.58
Cr ₂ O ₃	.00	.01	.09	.01	.00	.0220	.038	174.09
FeO	28.71	28.55	28.53	26.94	26.89	27.9240	.924	3.31
MnO	.87	.82	.86	.90	.91	.8720	.036	4.08
MgO	18.98	18.84	19.03	18.34	18.19	18.6760	.385	2.06
CaO	.46	.58	.54	.53	.52	.5260	.043	8.25
Na ₂ O	.18	.00	.04	.00	.00	.0440	.078	177.27
K ₂ O	.04	.04	.06	.04	.04	.0440	.009	20.23
Total	100.47	98.88	99.23	99.69	99.20	99.492		

DT-37 Orthopyroxene

	1.	2.	3.	4.	5.	\bar{X}	S	%
SiO ₂	49.80	49.88	51.01	50.04	50.48	50.2420	.503	1.00
TiO ₂	.08	.07	.04	.07	.09	.07	.019	26.7
Al ₂ O ₃	1.36	1.32	.94	1.11	1.23	1.1920	.171	14.3
Cr ₂ O ₃	.03	.07	.03	.02	.00	.0300	.025	84.9
FeO	31.55	31.32	31.75	31.98	31.99	31.7180	.287	.906
MnO	.88	.86	.91	.82	.89	.8720	.034	3.92
MgO	15.30	15.21	15.43	15.39	15.22	15.3100	.099	.645
CaO	.63	.58	.37	.41	.64	.5260	.127	24.1
Na ₂ O	.00	.00	.01	.00	.00	.0020	.004	232
K ₂ O	.00	.00	.01	.00	.01	.0040	.010	136
Total	99.63	99.31	100.50	99.83	100.55	99.966		

DT-174 Orthopyroxene

	1.	2.	3.	4.	5.	6.	\bar{X}	S	%
SiO ₂	50.59	50.43	50.71	50.79	50.71	50.20	50.5717	.221	.437
TiO ₂	.07	.06	.08	.07	.04	.08	.0667	.015	22.6
Al ₂ O ₃	1.00	1.12	1.09	1.06	1.16	1.01	1.0733	.063	5.82
Cr ₂ O ₃	.09	.05	.07	.05	.08	.05	.0650	.018	27.1
FeO	30.57	30.22	30.17	30.02	31.04	31.18	30.533	.484	1.58
MnO	.95	1.05	1.00	1.04	.95	.91	.9833	.056	5.67
MgO	15.97	16.27	16.22	16.01	15.90	15.26	15.9383	.363	2.28
CaO	.64	.70	.46	.60	.54	.55	.5817	.084	14.4
Na ₂ O	.09	.09	.00	.04	.00	.00	.0367	.044	120
K ₂ O	.00	.01	.00	.01	.04	.01	.0117	.015	126
Total	99.96	99.98	99.82	99.70	100.46	99.26	99.8617		

DT-176 Orthopyroxene

	1.	2.	3.	4.	5.	\bar{X}	S	%
SiO ₂	49.77	50.34	51.00	50.82	50.04	50.3940	.516	1.02
TiO ₂	.04	.07	.04	.10	.04	.0580	.027	46.3
Al ₂ O ₃	2.14	2.21	1.95	2.25	2.00	2.1100	.131	6.19
Cr ₂ O ₃	.00	.02	.00	.00	.00	.0040	.009	224
FeO	27.15	27.66	27.24	26.50	27.20	27.1500	.416	1.53
MnO	.61	.76	.78	.62	.68	.6900	.078	11.3
MgO	19.06	19.05	19.27	19.64	19.43	19.2900	.252	1.30
CaO	.53	.50	.43	.52	.38	.4720	.065	13.7
Na ₂ O	.00	.00	.00	.00	.00			
K ₂ O	.02	.00	.04	.00	.00	.0120	.018	149
Total	99.32	100.61	100.74	100.46	99.77	100.1680		

DT-177 Orthopyroxene

	1.	2.	3.	4.	5.	6.	7.	\bar{x}	S	%
SiO ₂	51.46	51.18	51.27	50.13	50.61	50.46	50.76	50.8386	.482	.948
TiO ₂	.13	.03	.04	.08	.05	.04	.05	.06000	.446	57.7
Al ₂ O ₃	1.81	1.93	1.77	1.18	2.14	2.25	2.19	1.8957	.367	19.4
Cr ₂ O ₃	.02	.04	.00	.03	.00	.07	.02	.0257	.024	94.9
FeO	28.57	28.66	28.45	28.08	28.31	28.35	27.99	28.3443	.244	.862
MnO	.82	.70	.81	.73	.69	.80	.82	.7814	.081	10.4
MgO	17.61	17.01	17.18	18.39	17.51	18.04	17.98	17.6743	.493	2.79
CaO	.47	.52	.52	.47	.29	.98	.92	.5957	.255	42.8
Na ₂ O	.06	.00	.00	.00	.00	.05	.03	.0200	.027	132
K ₂ O	.00	.00	.00	.00	.00	.00	.00	.0000		
Total	100.94	100.07	100.04	100.14	99.61	101.06	100.76	100.2357		

298

DT-98-3 Orthopyroxene

	1.	2.	\bar{x}	S	%
SiO ₂	50.50	49.20	49.8500	.919	1.84
TiO ₂	.05	.02	.0350	.021	60.6
Al ₂ O ₃	1.46	1.41	1.4350	.035	2.46
Cr ₂ O ₃	.03	.10	.0650	.049	76.2
FeO	29.43	30.28	29.8550	.601	2.01
MnO	.37	.38	.3750	.007	1.88
MgO	17.64	16.82	17.2300	.5798	3.36
CaO	.50	.45	.4750	.035	7.44
Na ₂ O	.00	.02	.0100	.014	141
K ₂ O	.00	.00	.00	.00	.00
Total	99.98	98.69	99.330		

DT-24 Clinopyroxene

	1.	2.	3.	\bar{x}	S	%
SiO ₂	51.36	51.67	51.97	51.6667	.305	.59
TiO ₂	.16	.25	.13	.1800	.062	34.69
Al ₂ O ₃	2.38	2.13	2.18	2.2300	.132	5.93
Cr ₂ O ₃	.11	.05	.02	.0600	.046	76.38
FeO	10.46	12.08	11.98	11.5057	.908	7.89
MnO	.38	.38	.43	.3967	.029	7.28
MgO	12.20	12.50	12.26	12.3200	.159	1.29
CaO	21.99	20.71	20.52	21.0733	.799	3.79
Na ₂ O	.90	.80	.89	.8633	.055	6.38
K ₂ O	.01	.00	.00	.0033	.006	173.21
Total	99.94	100.59	100.38	100.300		

DT-25 Clinopyroxene

	1.	2.	3.	4.	5.	6.	\bar{x}	S	%
SiO ₂	51.47	51.17	51.49	51.15	50.81	50.04	51.0217	.542	1.06
TiO ₂	.24	.20	.24	.30	.27	.18	.2383	.044	18.46
Al ₂ O ₃	2.59	2.46	2.71	2.86	2.83	2.51	2.6600	.167	6.26
Cr ₂ O ₃									
FeO	10.93	11.59	11.11	11.70	11.06	11.95	11.3900	.412	3.62
MnO	.27	.39	.43	.46	.25	.45	.3750	.092	24.67
MgO	12.19	12.20	12.06	11.91	11.76	12.36	12.0800	.217	1.80
CaO	20.97	20.76	21.50	21.23	21.25	20.79	21.0833	.292	1.38
Na ₂ O	.96	1.01	.95	.90	1.05	.93	.9667	.055	5.66
K ₂ O	.00	.00	.03	.02	.00	.00	.0083	.013	160.24
Total	99.62	99.79	100.53	100.52	99.28	99.21	99.823		

DT-28 Clinopyroxene

	1.	2.	3.	4.	5.	\bar{X}	S	%
SiO ₂	50.64	50.68	50.71	51.46	50.81	50.8600	.341	.671
TiO ₂	.18	.26	.28	.21	.28	.2420	.045	18.6
Al ₂ O ₃	3.05	2.88	2.82	2.88	2.69	2.8640	.130	4.53
Cr ₂ O ₃	.00	.02	.00	.05	.01	.0160	.021	130
FeO	15.37	15.43	16.17	16.15	16.75	15.9740	.577	3.61
MnO	.14	.13	.16	.12	.19	.1480	.028	18.7
MgO	8.29	7.98	7.67	7.90	7.94	7.9560	.222	2.79
CaO	21.12	20.80	20.97	20.92	21.08	20.9780	.128	.611
Na ₂ O	1.29	1.41	1.28	1.38	1.43	1.3580	.069	5.09
K ₂ O	.01	.02	.02	.02	.01	.0160	.006	34.2
Total	100.09	99.63	100.09	101.08	101.18	100.4120		

299

DT-30 Clinopyroxene

	1.	2.	3.	4.	\bar{X}	S	%
SiO ₂	51.93	52.02	51.73	51.66	51.8350	.169	.325
TiO ₂	.61	.54	.60	.47	.5550	.065	11.6
Al ₂ O ₃	4.26	4.24	4.22	4.38	4.2750	.072	1.68
Cr ₂ O ₃	.07	.05	.02	.05	.0475	.021	43.4
FeO	7.34	7.15	7.35	7.21	7.2625	.098	1.36
MnO	.11	.04	.10	.07	.0800	.032	39.5
MgO	13.18	12.53	12.81	12.65	12.7925	.283	2.21
CaO	22.42	22.08	22.05	22.11	22.1650	.172	.775
Na ₂ O	.91	.85	.81	.94	.8775	.059	6.67
K ₂ O	.00	.00	.00	.00	.00		
Total	100.82	99.49	99.70	99.55	99.8900		

DT-32 Clinopyroxene

	1.	2.	3.	4.	5.	6.	7.	8.	9.	10.	\bar{X}	S	%
SiO ₂	51.66	52.04	51.70	51.93	50.97	51.87	51.98	52.10	52.15	51.60	51.8000	.347	.67
TiO ₂	.23	.21	.13	.15	.19	.20	.18	.13	.19	.26	.1870	.042	22.41
Al ₂ O ₃	2.40	2.36	2.48	2.55	2.70	2.63	2.27	2.30	2.23	2.21	2.4130	.171	7.09
Cr ₂ O ₃	.16	.07	.09	.06	.29	.12	.09	.01	.07	.08	.1040	.076	73.12
FeO	13.26	12.55	10.90	13.03	12.65	13.23	11.39	12.57	12.32	12.28	12.4180	.762	6.14
MnO	.13	.04	.05	.11	.14	.11	.07	.19	.07	.11	.0920	.047	51.44
MgO	11.18	11.11	11.85	10.89	10.80	10.93	11.88	11.70	11.89	11.09	11.3320	.445	3.93
CaO	21.02	21.23	22.15	21.11	21.27	20.80	21.75	21.25	20.98	21.65	21.3210	.411	1.93
Na ₂ O	1.14	1.15	1.11	1.18	1.36	1.21	1.07	1.09	.98	1.22	1.1510	.102	8.88
K ₂ O	.00	.00	.00	.00	.00	.00	.00	.00	.00	.00	.00		
Total	101.19	100.75	100.45	101.02	100.27	101.10	100.68	101.35	100.89	100.50	100.818		

DT-33 Clinopyroxene

	1.	2.	3.	4.	5.	6.	7.	8.	9.	10.	\bar{X}	S	%
SiO ₂	51.71	52.14	51.79	51.77	50.75	51.73	50.95	51.80	52.23	51.00	51.5870	.508	.99
TiO ₂	.11	.20	.21	.10	.09	.19	.21	.23	.15	.20	.1690	.052	30.74
Al ₂ O ₃	2.34	2.31	2.19	2.21	2.16	2.32	2.27	2.54	2.30	2.30	2.2940	.105	4.60
Cr ₂ O ₃	.02	.12	.04	.10	.05	.09	.25	.09	.04	.11	.0910	.065	71.86
FeO	11.14	10.90	11.59	9.88	9.48	10.46	10.14	10.09	11.64	10.82	10.6140	.727	6.85
MnO	.37	.23	.29	.20	.25	.28	.27	.35	.41	.31	.2960	.065	22.02
MgO	12.27	12.15	12.33	12.59	12.43	12.23	11.98	12.11	12.17	12.13	12.2390	.175	1.43
CaO	21.55	21.78	21.54	22.42	22.18	21.35	21.39	22.01	20.65	20.64	21.5510	.589	2.73
Na ₂ O	.77	.88	.83	.88	1.00	.83	.87	1.01	.90	.93	.8900	.075	8.41
K ₂ O	.00	.00	.00	.00	.23	.00	.00	.00	.02	.00	.0250	.072	289.21
Total	100.35	100.69	100.81	100.18	98.61	99.47	98.32	100.23	100.52	98.44	99.756		

	1.	2.	3.	4.	5.	6.	\bar{x}	S	%
SiO ₂	49.56	50.12	49.11	48.54	50.51	50.28	49.6867	.760	1.53
TiO ₂	.18	.21	.14	.16	.18	.21	.1800	.028	15.3
Al ₂ O ₃	1.87	1.80	1.81	1.76	1.87	1.81	1.8200	.043	2.36
Cr ₂ O ₃	.03	.00	.01	.00	.00	.02	.0100	.013	126.5
FeO	20.79	20.37	20.78	21.01	21.19	21.14	20.8800	.303	1.45
MnO	.24	.27	.24	.31	.25	.23	.2567	.029	11.5
MgO	5.63	5.56	5.51	5.38	5.48	5.35	5.4850	.106	1.94
CaO	20.39	20.46	20.52	20.42	19.91	20.05	20.2917	.249	1.23
Na ₂ O	.98	1.25	1.01	.98	1.37	1.37	1.1600	.192	16.5
K ₂ O	.02	.01	.01	.01	.01	.01	.0117	.004	34.9
Total	99.68	100.05	99.14	98.57	100.77	100.46	99.7818		

DT-35 Clinopyroxene

	1.	2.	3.	4.	5.	6.	7.	\bar{x}	S	%
SiO ₂	49.78	49.41	49.11	49.25	49.17	49.43	48.80	49.2780	.306	.621
TiO ₂	.14	.14	.13	.21	.28	.23	.21	.1914	.056	29.47
Al ₂ O ₃	3.22	3.04	2.72	2.90	2.90	2.85	2.93	2.9371	.157	5.35
Cr ₂ O ₃										
FeO	14.59	15.23	16.14	15.61	16.02	15.60	16.09	15.6114	.557	3.57
MnO	.20	.15	.19	.09	.17	.11	.10	1.443	.045	30.98
MgO	9.34	8.78	8.78	8.64	8.80	9.00	8.73	8.8671	.235	2.65
CaO	21.78	21.62	21.16	21.67	21.68	21.78	21.25	21.5629	.253	1.1715
Na ₂ O	.92	.77	1.05	1.00	1.00	1.01	1.05	.9714	.099	10.18
K ₂ O	.00	.00	.00	.00	.00	.00	.00	.00		
Total	99.96	99.13	99.28	99.36	100.02	100.02	99.17	99.564		

DT-36 Clinopyroxene

	1.	2.	3.	4.	5.	6.	7.	\bar{x}	S	%
SiO ₂	52.58	51.78	51.48	52.05	51.41	51.66	51.40	51.7657	.428	.826
TiO ₂	.16	.18	.21	.23	.11	.14	.18	.1729	.041	23.5
Al ₂ O ₃	2.46	2.49	2.49	2.54	2.39	2.55	2.59	2.5014	.066	2.64
Cr ₂ O ₃	.01	.00	.00	.00	.00	.00	.00	.0014	.004	264
FeO	14.67	14.23	14.87	14.45	14.57	13.82	13.50	14.3014	.489	3.42
MnO	.33	.25	.36	.33	.32	.31	.28	.3114	.036	11.6
MgO	9.99	10.02	9.86	10.02	9.87	10.01	10.12	9.9843	.091	.916
CaO	19.57	20.66	20.11	19.56	19.45	19.83	20.38	19.9371	.461	2.31
Na ₂ O	1.18	1.06	1.14	1.05	1.13	1.09	1.17	1.1171	.052	4.61
K ₂ O	.00	.00	.00	.02	.02	.02	.01	.0100	.010	100
Total	100.96	100.69	100.54	100.24	99.34	99.44	99.63	100.1020		

DT-174 Clinopyroxene

	1.	2.	3.	4.	\bar{x}	S	%
SiO ₂	51.89	51.84	51.61	51.79	51.7825	.122	.236
TiO ₂	.24	.23	.21	.19	.2175	.022	10.2
Al ₂ O ₃	2.07	2.39	2.20	2.48	2.2850	.185	8.09
Cr ₂ O ₃	.00	.04	.00	.00	.0100	.020	200
FeO	13.21	12.70	12.80	12.66	12.8425	.252	1.96
MnO	.41	.43	.50	.48	.4550	.042	9.24
MgO	10.55	10.67	10.49	10.36	10.5175	.129	1.23
CaO	20.87	20.87	20.87	20.46	20.7675	.205	.988
Na ₂ O	.97	1.06	.99	.95	.9925	.048	4.83
K ₂ O	.01	.00	.03	.01	.0125	.013	101
Total	100.21	100.23	99.70	99.37	99.8825		

DT-12 Hornblende

	1.	2.	3.	4.	5.	6.	7.	8.	9.	10.	11.	12.	13.	14.	15.
SiO ₂	40.39	40.54	40.09	41.14	40.74	40.47	41.06	40.85	40.60	40.66	39.60	40.82	40.29	40.10	40.60
TiO ₂	1.47	1.43	1.48	1.44	1.78	1.58	1.66	1.44	1.50	1.34	1.49	1.29	1.38	1.11	1.17
Al ₂ O ₃	12.61	12.68	12.43	12.88	12.29	12.52	12.57	11.69	11.64	11.78	12.49	12.28	12.55	12.65	12.54
Cr ₂ O ₃	.00	.00	.02	.00	.00	.01	.00	.01	.00	.08	.00	.00	.00	.00	.00
FeO	18.70	18.60	18.52	18.87	17.81	17.98	18.44	18.00	18.66	18.57	19.14	18.65	18.48	18.91	19.09
MnO	.29	.40	.34	.30	.21	.34	.34	.35	.31	.30	.26	.34	.32	.30	.27
MgO	8.93	9.00	9.04	8.89	8.97	9.30	8.98	9.32	9.08	9.43	8.88	9.22	8.68	8.76	9.14
CaO	11.76	11.74	12.00	11.96	11.86	11.82	11.79	12.21	11.96	11.91	11.73	12.02	11.79	11.93	11.98
Na ₂ O	1.93	1.97	1.90	1.90	1.68	1.96	2.13	1.97	1.89	1.74	1.82	1.91	1.96	1.55	2.06
K ₂ O	1.49	1.54	1.54	1.45	1.44	1.42	1.49	1.38	1.37	1.46	1.55	1.43	1.57	1.38	1.52
Total	97.57	97.89	97.36	98.83	96.79	97.41	98.46	97.23	97.02	97.28	96.96	97.97	97.02	96.69	98.36

	\bar{x}	s	%
SiO ₂	40.5300	.400	.986
TiO ₂	1.4373	.171	11.9
Al ₂ O ₃	12.3733	.377	3.05
Cr ₂ O ₃	.0080	.021	260
FeO	18.5613	.388	2.09
MnO	.3113	.045	14.4
MgO	9.0413	.211	2.33
CaO	11.8973	.131	1.10
Na ₂ O	1.8913	.146	7.72
K ₂ O	1.4687	.066	4.50
Total	97.5198		

DT-24 Hornblende

	1.	2.	3.	4.	5.	6.	7.	8.	9.	\bar{x}	s	%
SiO ₂	40.10	39.44	39.86	39.54	40.53	39.65	40.05	40.75	40.81	40.0811	.515	1.28
TiO ₂	1.45	2.04	2.15	1.95	1.34	.76	1.04	1.87	1.85	1.6056	.483	30.06
Al ₂ O ₃	12.67	13.14	13.09	13.14	12.86	13.43	12.93	12.22	12.94	12.9356	.343	2.65
Cr ₂ O ₃	.04	.00	.00	.16	.15	.08	.10	.00	.05	.0644	.062	97.05
FeO	16.73	16.92	17.10	17.05	15.72	16.70	16.29	16.25	16.90	16.6289	.455	2.74
MnO	.11	.19	.11	.21	.20	.14	.11	.19	.18	.1600	.042	26.31
MgO	10.13	9.70	10.09	9.62	11.44	10.49	10.54	10.42	10.07	10.2778	.542	5.28
CaO	11.63	11.44	11.78	11.21	11.66	11.83	11.68	11.59	11.83	11.6278	.200	1.72
Na ₂ O	1.39	1.50	1.56	1.65	1.47	1.46	1.60	1.45	1.52	1.5111	.081	5.36
K ₂ O	2.04	2.18	2.07	2.18	1.95	2.07	2.04	2.03	2.12	2.076	.074	3.58
Total	96.30	96.55	97.81	96.70	97.32	96.60	96.37	96.77	98.27	96.9679		

DT-25 Hornblende

	1.	2.	3.	4.	5.	6.	7.	8.	9.	10.	11.	\bar{x}	s	%
SiO ₂	42.42	41.32	41.07	41.41	42.10	41.22	41.36	42.68	42.43	42.99	42.17	41.9245	.669	1.60
TiO ₂	2.34	2.33	2.16	2.22	2.11	2.20	2.14	2.34	2.16	2.29	2.33	2.2382	.090	4.00
Al ₂ O ₃	11.79	12.40	11.52	12.55	12.48	13.07	13.13	12.74	12.51	12.62	12.48	12.4809	.476	.72
Cr ₂ O ₃	.11	.05	.05	.11	.05	.23	.02	.10	.05	.10	.00	.0791	.062	78.63
FeO	17.10	17.35	16.63	16.77	17.06	16.90	16.74	16.80	16.47	15.54	16.77	16.7391	.465	2.78
MnO	.33	.24	.24	.22	.19	.23	.24	.12	.19	.11	.13	.2036	.065	32.02
MgO	10.16	10.13	10.01	9.97	10.08	9.35	9.47	9.84	9.75	10.07	9.47	9.8455	.294	2.99
CaO	11.13	11.30	11.02	11.10	10.91	11.23	11.10	11.12	11.03	11.30	11.25	11.1355	.124	1.12
Na ₂ O	1.87	1.58	1.75	1.55	1.78	1.42	1.57	1.88	1.75	1.84	1.65	1.6945	.151	8.89
K ₂ O	1.74	1.85	1.83	1.93	1.93	2.03	1.95	1.83	1.83	1.92	1.88	1.8836	.079	4.17
Total	98.99	98.53	96.29	97.82	98.69	97.93	97.71	99.46	98.17	98.77	98.14	98.224		

DT-28 Hornblende

	1.	2.	3.	\bar{x}	S	%
SiO ₂	38.44	38.70	38.69	38.6100	.147	.382
TiO ₂	1.81	1.98	1.94	1.9100	.089	4.65
Al ₂ O ₃	12.39	12.05	12.41	12.2833	.202	1.65
Cr ₂ O ₃	.05	.08	.09	.0733	.021	28.4
FeO	22.06	22.89	22.45	22.4667	.415	1.85
MnO	.05	.03	.04	.0400	.010	25.0
MgO	5.75	5.59	5.34	5.5600	.207	3.72
CaO	11.92	11.97	11.76	11.8833	.110	.923
Na ₂ O	1.36	1.50	1.45	1.4367	.071	4.94
K ₂ O	2.47	2.45	2.39	2.4367	.042	1.71
Total	96.29	97.22	96.55	96.7000		

302

DT-30 Hornblende

	1.	2.	3.	4.	5.	6.	7.	\bar{x}	S	%
SiO ₂	40.57	41.66	41.43	43.06	42.97	41.63	42.07	41.9129	.879	2.10
TiO ₂	2.59	2.64	2.25	2.65	2.60	2.72	2.80	2.6071	.174	6.66
Al ₂ O ₃	13.22	13.01	12.86	12.20	11.80	13.05	13.02	12.7371	.527	4.14
Cr ₂ O ₃	.21	.17	.20	.17	.13	.11	.20	.1700	.038	22.3
FeO	11.68	11.80	11.20	10.93	10.64	11.67	11.64	11.3657	.447	3.93
MnO	.02	.05	.00	.00	.00	.00	.00	.0100	.019	191
MgO	11.93	12.14	12.50	12.78	12.68	12.20	12.32	12.3643	.305	2.47
CaO	12.21	12.17	12.46	12.58	12.25	12.21	12.16	12.2914	.163	1.32
Na ₂ O	1.86	1.87	1.59	1.85	1.62	1.89	1.92	1.8000	.135	7.52
K ₂ O	1.76	1.69	1.60	1.55	1.60	1.60	1.83	1.6614	.102	6.15
Total	96.03	97.17	96.09	97.75	96.36	97.09	97.97	96.9199		

DT-31 Hornblende

	1.	2.	3.	4.	5.	6.	7.	8.	9.	10.	\bar{x}	S	%
SiO ₂	39.12	40.13	40.86	39.79	39.50	41.71	40.70	40.56	39.96	40.61	40.2940	.750	1.66
TiO ₂	1.62	.88	.91	1.04	1.23	.56	.48	.71	.67	.59	.8696	.352	40.51
Al ₂ O ₃	14.20	13.72	14.26	13.83	14.50	13.42	12.86	13.44	13.47	13.85	13.7550	.485	3.53
Cr ₂ O ₃	.11	.25	.29	.05	.08	.06	.12	.08	.25	.11	.1400	.089	63.29
FeO	21.39	20.23	21.07	20.81	20.14	20.07	19.71	19.98	19.46	19.71	20.2570	.633	3.13
MnO	.28	.28	.47	.28	.20	.21	.26	.21	.36	.20	.2750	.085	30.95
MgO	6.66	7.13	7.36	7.11	6.99	7.89	8.00	7.49	7.62	8.07	7.4320	.468	6.29
CaO	11.28	11.52	11.51	11.55	11.36	11.63	11.56	11.47	11.63	11.66	11.5170	.121	1.05
Na ₂ O	1.12	1.55	1.26	1.32	1.25	1.20	1.15	1.13	1.31	.96	1.2250	.156	12.77
K ₂ O	2.26	1.84	1.74	1.75	1.70	1.55	1.48	1.53	1.55	1.50	1.6900	.235	13.93
Total	98.03	97.54	99.72	97.52	96.94	98.31	96.31	96.61	96.29	97.25	97.4540		

DT-32 Hornblende

	1.	2.	3.	4.	5.	6.	7.	\bar{x}	S	%
SiO ₂	40.06	40.06	40.00	40.73	40.66	40.25	40.02	40.2543	.312	.78
TiO ₂	2.58	2.25	2.34	1.70	1.57	2.39	2.05	2.1286	.368	17.28
Al ₂ O ₃	11.85	11.97	12.20	12.06	12.02	11.86	11.96	11.9886	.121	1.01
Cr ₂ O ₃	.10	.20	.11	.06	.15	.14	.14	.1286	.044	34.29
FeO	19.26	19.36	19.67	18.14	18.53	18.65	18.83	18.9343	.523	2.76
MnO	.16	.02	.06	.00	.11	.02	.07	.0629	.057	90.30
MgO	8.25	8.15	8.20	9.00	9.66	8.95	9.02	8.7471	.565	6.46
CaO	11.21	11.12	10.99	11.34	11.35	11.50	11.21	11.2457	.167	1.49
Na ₂ O	1.65	1.46	1.77	1.55	1.77	1.65	1.82	1.6671	.130	7.81
K ₂ O	2.05	2.10	2.07	1.84	1.97	2.11	2.09	2.0329	.097	4.78
Total	97.20	96.69	97.40	96.43	97.89	97.52	97.21	97.1901		

	1.	2.	3.	4.	5.	6.	7.	8.	9.	\bar{x}	s	%
SiO ₂	40.53	41.10	40.33	41.13	40.36	40.08	40.40	40.78	40.82	40.6144	.363	.89
TiO ₂	2.34	2.27	2.24	2.28	2.26	2.51	2.12	2.16	2.27	2.2722	.111	4.87
Al ₂ O ₃	12.08	12.28	12.13	12.00	12.04	12.76	12.51	11.82	11.79	12.1567	.316	2.60
Cr ₂ O ₃	.12	.18	.09	.13	.14	.20	.09	.18	.20	.1478	.044	29.63
FeO	16.85	16.48	16.71	16.45	16.99	16.92	16.98	16.86	17.13	16.8189	.023	.14
MnO	.11	.19	.14	.09	.21	.20	.07	.20	.21	.1578	.056	35.42
MgO	9.77	10.14	9.88	9.86	10.10	9.71	9.75	9.93	10.11	9.9167	.165	1.66
CaO	11.32	11.30	11.10	11.29	11.14	11.57	11.72	11.30	11.45	11.3544	.197	1.74
Na ₂ O	1.75	1.63	1.56	1.67	1.82	1.52	1.58	1.63	1.57	1.6367	.097	5.91
K ₂ O	1.89	1.82	2.00	1.97	1.89	2.10	2.00	1.93	2.02	1.9578	.084	4.30
Total	96.76	97.38	96.17	96.87	96.95	97.57	97.23	96.77	97.57	97.0357		

DT-34 Hornblende

	1.	2.	3.	4.	5.	6.	\bar{x}	s	%
SiO ₂	38.76	39.54	38.76	39.06	38.67	37.91	38.7833	.534	1.38
TiO ₂	1.68	1.61	1.66	1.80	1.80	1.67	1.7033	.079	4.62
Al ₂ O ₃	11.35	11.24	11.43	10.74	10.86	10.87	11.0817	.293	2.64
Cr ₂ O ₃	.05	.00	.04	.06	.00	.00	.0250	.028	112.4
FeO	27.68	26.85	27.01	27.61	27.27	27.31	27.2883	.325	1.19
MnO	.07	.10	.09	.13	.11	.12	.1033	.022	20.9
MgO	3.70	4.07	3.99	3.72	3.80	3.83	3.8517	.146	3.86
CaO	11.07	11.04	11.05	10.80	10.68	10.71	10.8917	.182	1.67
Na ₂ O	1.89	1.77	1.61	1.97	1.82	1.91	1.8283	.128	6.99
K ₂ O	1.39	1.97	1.87	1.88	1.89	2.02	1.8367	.227	12.34
Total	98.18	98.19	97.50	97.78	96.90	96.35	97.3933		

DT-35 Hornblende

	1.	2.	3.	4.	5.	6.	\bar{x}	s	%
SiO ₂	39.46	39.81	40.15	40.41	42.79	42.49	40.8517	1.425	3.49
TiO ₂	1.48	1.71	1.70	.55	.36	.28	1.0133	.686	67.71
Al ₂ O ₃	13.65	13.42	13.00	12.68	12.64	13.11	13.0833	.400	3.06
Cr ₂ O ₃	.00	.16	.04	.01	.00	.01	.0367	.062	169.48
FeO	23.59	23.58	22.59	23.12	20.65	21.29	22.4700	1.235	5.50
MnO	.14	.16	.17	.11	.09	.07	1.233	.040	32.28
MgO	5.46	5.52	5.60	6.32	8.16	7.97	6.505	1.25	19.20
CaO	11.15	11.21	11.32	11.26	11.41	11.53	11.3133	.139	1.23
Na ₂ O	1.14	1.23	1.36	1.13	1.37	1.35	1.2633	.112	8.84
K ₂ O	2.29	2.27	2.39	1.90	1.66	1.72	2.0383	.318	15.58
Total	98.38	99.07	98.32	97.48	99.12	99.81	98.698		

DT-36 Hornblende

	1.	2.	3.	4.	5.	6.	\bar{x}	s	%
SiO ₂	40.32	39.99	40.63	41.37	40.24	40.74	40.5483	.485	1.19
TiO ₂	2.28	2.21	2.67	2.70	2.39	2.46	2.4517	.201	8.18
Al ₂ O ₃	12.48	12.25	11.57	11.50	11.99	12.04	11.9717	.381	3.18
Cr ₂ O ₃	.05	.00	.01	.00	.00	.00	.0100	.020	200
FeO	20.41	19.98	18.86	19.08	20.26	20.27	19.810	.670	3.38
MnO	.14	.12	.07	.07	.11	.07	.0967	.031	31.8
MgO	8.01	7.80	8.48	8.67	7.96	8.09	8.1683	.334	4.09
CaO	11.01	11.05	11.00	10.96	11.06	11.05	11.0217	.039	.351
Na ₂ O	1.89	1.69	2.05	1.79	1.80	1.92	1.8567	.0125	6.72
K ₂ O	2.00	2.05	1.94	1.94	1.98	2.05	1.9933	.050	2.49
Total	98.59	97.15	97.28	98.07	97.79	98.70	97.9284		

DT-37 HORNBLENDE

	1.	2.	3.	4.	5.	6.	\bar{x}	S	%
SiO ₂	40.61	40.55	40.61	40.14	39.98	40.19	40.3467	.276	.685
TiO ₂	1.93	2.00	1.68	1.75	1.91	1.85	1.8533	.119	6.44
Al ₂ O ₃	12.01	12.09	11.87	12.17	12.70	12.63	12.2450	.341	2.78
Cr ₂ O ₃	.03	.00	.02	.01	.04	.04	.0233	.016	69.98
FeO	19.28	19.65	19.88	20.17	20.35	20.21	19.9233	.484	2.03
MnO	.11	.14	.16	.14	.23	.21	.1650	.046	27.8
MgO	8.33	8.09	8.18	8.13	7.76	7.78	8.0450	.228	2.84
CaO	10.97	10.93	11.02	10.89	10.92	10.83	10.9267	.065	.598
Na ₂ O	1.70	1.79	1.80	1.80	1.71	1.61	1.7350	.076	4.39
K ₂ O	2.01	2.00	1.86	2.00	2.14	2.07	2.0133	.093	4.61
Total	97.07	97.23	97.09	97.20	97.75	97.42	97.2766		

DT-174 Hornblende

	1.	2.	3.	4.	5.	6.	\bar{x}	S	%
SiO ₂	39.98	40.73	40.16	40.73	40.59	41.26	40.5750	.457	1.13
TiO ₂	1.95	1.98	1.92	2.14	2.11	1.80	1.9833	.126	6.35
Al ₂ O ₃	11.70	11.90	12.39	11.97	12.11	12.00	12.0117	.230	1.91
Cr ₂ O ₃	.05	.05	.09	.03	.08	.04	.0567	.023	41.3
FeO	20.79	19.94	19.77	18.86	18.29	18.80	19.4083	.921	4.75
MnO	.23	.25	.32	.13	.18	.10	.2017	.081	40.3
MgO	8.97	8.58	8.60	8.67	8.59	8.80	8.7017	.155	1.78
CaO	10.43	10.66	10.85	11.87	11.89	11.68	11.2300	.657	5.85
Na ₂ O	1.58	1.51	1.72	1.85	1.64	1.67	1.6617	.118	7.07
K ₂ O	1.61	1.63	1.86	1.89	1.85	1.90	1.7900	.133	7.44
Total	97.29	97.23	97.68	98.13	97.34	98.04	97.4386		

DT-176 Hornblende

	1.	2.	3.	4.	5.	6.	7.	8.	9.	10.	11.	12.	13.	14.
SiO ₂	40.63	40.83	40.60	40.76	40.96	40.95	40.13	40.31	40.29	41.18	41.05	40.60	40.63	41.27
TiO ₂	1.75	1.75	1.80	1.61	1.63	1.88	1.81	1.93	1.91	1.89	1.44	2.07	1.93	1.95
Al ₂ O ₃	13.30	13.06	13.43	13.08	13.03	13.05	13.56	13.57	13.74	13.02	13.48	12.93	12.97	12.86
Cr ₂ O ₃	.08	.00	.02	.00	.00	.00	.00	.00	.00	.00	.00	.00	.00	.00
FeO	15.74	15.72	14.72	15.59	16.07	16.17	16.79	15.64	15.90	16.38	16.61	16.46	16.71	16.37
MnO	.16	.02	.05	.06	.11	.13	.11	.04	.21	.04	.12	.04	.01	.05
MgO	10.86	10.70	10.69	10.86	10.80	10.30	10.17	10.29	10.46	10.35	10.65	10.17	10.52	10.45
CaO	12.19	12.34	12.22	12.21	12.29	12.14	12.25	11.85	12.07	12.32	12.14	12.16	11.92	12.40
Na ₂ O	1.64	1.73	1.34	1.46	1.44	1.48	1.44	1.49	1.67	1.44	1.44	1.62	1.59	1.43
K ₂ O	2.04	2.03	2.10	2.07	1.95	2.03	2.04	1.99	2.09	2.04	1.84	2.00	2.10	2.02
Total	98.39	98.17	96.96	97.48	98.30	98.13	98.30	97.12	98.35	98.66	98.77	98.05	98.39	98.80
		\bar{x}			S									
SiO ₂		40.7279			.339	.832								
TiO ₂		1.8107			.165	9.11								
Al ₂ O ₃		13.2200			.285	2.15								
Cr ₂ O ₃		.0071			.022	303								
FeO		16.0621			.559	3.48								
MnO		.0821			.059	71.3								
MgO		10.5193			.245	2.32								
CaO		12.1786			.153	1.26								
Na ₂ O		1.5150			.114	7.50								
K ₂ O		2.0243			.068	3.36								
Total		98.1471												

DT-177 Hornblende

	1.	2.	3.	4.	5.	6.	7.	8.	\bar{x}	S	%
SiO ₂	40.41	40.27	40.76	41.82	40.82	40.51	40.88	40.08	40.6938	.534	1.31
TiO ₂	1.99	1.98	1.57	1.63	1.55	1.50	1.71	1.86	1.7238	.196	11.4
Al ₂ O ₃	13.28	13.33	13.16	13.56	13.61	13.77	13.91	13.46	13.5100	.254	1.88
Cr ₂ O ₃	.00	.02	.01	.05	.02	.04	.07	.07	.0350	.027	76.4
FeO	17.45	17.45	16.70	17.03	16.93	17.63	16.63	17.79	17.2013	.437	2.54
MnO	.14	.11	.15	.19	.18	.23	.15	.21	.1700	.040	23.3
MgO	9.59	9.26	9.71	9.19	9.19	9.47	9.47	9.06	9.3675	.226	2.41
CaO	11.32	11.37	11.30	11.29	11.30	10.83	11.37	11.42	11.2750	.185	1.64
Na ₂ O	1.40	1.29	1.31	1.39	1.08	1.51	1.61	1.59	1.3975	.175	12.5
K ₂ O	2.34	2.12	1.95	2.05	2.09	2.15	1.97	2.28	2.1188	.137	6.48
Total	97.91	97.20	96.63	98.21	96.77	97.64	97.76	97.82	97.4927		

305

DT-178 Hornblende

	1.	2.	3.	4.	5.	6.	7.	8.	9.	10.	11.	12.	13.
SiO ₂	40.73	40.55	41.13	40.65	40.84	41.28	40.79	40.57	40.83	41.15	41.14	41.36	41.41
TiO ₂	1.05	1.05	1.05	.92	1.04	.91	.95	1.06	1.06	1.01	1.03	.91	.97
Al ₂ O ₃	13.29	13.29	13.05	13.37	13.36	13.11	12.87	12.78	12.59	12.40	12.46	12.62	12.25
Cr ₂ O ₃	.00	.04	.00	.07	.00	.00	.00	.00	.00	.00	.02	.00	.00
FeO	18.25	17.64	18.11	17.97	18.05	17.70	16.88	17.71	17.27	17.84	17.40	17.75	17.07
MnO	.21	.21	.31	.25	.29	.25	.26	.38	.18	.23	.23	.25	.23
MgO	9.52	9.55	9.41	9.37	9.40	9.75	9.85	9.84	9.55	9.63	9.90	10.00	10.03
CaO	11.70	12.02	11.94	11.86	11.87	11.91	12.19	12.01	11.97	11.86	11.84	12.03	11.73
Na ₂ O	1.55	2.07	1.45	1.65	1.55	1.71	1.45	1.49	1.46	1.68	1.51	1.71	2.00
K ₂ O	1.30	1.14	1.22	1.36	1.34	.84	1.21	1.14	1.18	1.16	1.27	.96	1.07
Total	97.62	97.57	97.68	97.45	97.75	97.47	96.46	96.98	96.10	96.97	96.79	97.59	96.76

 \bar{x}

S

%

SiO ₂	40.9562	.302	.736
TiO ₂	1.0008	.060	6.00
Al ₂ O ₃	12.8800	.393	3.05
Cr ₂ O ₃	.0100	.022	216
FeO	17.6646	.410	2.32
MnO	.2523	.051	20.3
MgO	9.6769	.231	2.39
CaO	11.9177	.131	1.10
Na ₂ O	1.6369	.201	12.3
K ₂ O	1.1685	.148	12.6
Total	97.1639		

DT-98 Hornblende

	1.	2.	3.	4.	5.	6.	7.	8.	9.	10.	11.	12.	13.	14.	15.
SiO ₂	40.43	40.27	40.98	40.60	40.86	41.02	41.63	40.79	40.66	40.77	40.90	40.41	40.09	39.04	41.57
TiO ₂	2.63	2.66	2.61	2.54	2.52	1.68	1.71	1.99	2.36	2.50	1.91	2.35	2.27	2.25	1.83
Al ₂ O ₃	12.85	11.61	12.04	12.07	12.19	12.53	12.29	12.33	12.37	12.26	12.40	12.38	12.42	12.40	12.16
Cr ₂ O ₃	.14	.07	.07	.08	.11	.08	.07	.11	.10	.10	.10	.19	.13	.09	.07
FeO	18.18	16.69	17.36	18.23	17.62	18.25	17.52	17.50	17.31	17.90	18.34	18.13	18.23	18.47	17.97
MnO	.05	.10	.04	.02	.05	.13	.04	.03	.05	.07	.08	.07	.09	.06	.10
MgO	8.71	8.93	9.06	8.79	8.88	9.34	9.38	9.50	8.91	8.68	8.93	8.41	8.55	8.53	9.02
CaO	11.64	11.62	11.57	11.59	11.29	11.37	11.18	11.38	11.47	11.38	11.48	11.80	11.10	11.40	11.46
Na ₂ O	2.10	1.61	2.08	1.87	1.88	1.84	1.87	1.86	1.82	1.98	1.79	1.72	1.87	1.96	1.71
K ₂ O	2.19	2.16	1.89	1.96	2.07	1.94	1.98	2.00	1.96	1.98	1.95	2.04	2.01	1.94	1.91
Total	98.90	95.70	97.70	97.76	97.48	98.17	97.66	97.49	97.01	97.63	97.89	97.50	96.75	96.14	97.77

	1.	2.	3.	4.	5.	6.	7.	\bar{x}	s	%
SiO ₂	39.94	40.07	40.10	39.73	39.85	39.99	39.66	39.9057	.167	.419
TiO ₂	.01	.01	.00	.04	.03	.02	.00	.0157	.015	96.2
Al ₂ O ₃	22.00	21.31	21.51	21.61	21.23	21.68	21.34	21.5257	.266	1.24
Cr ₂ O ₃										
Fe	23.01	24.21	23.67	23.37	23.17	23.46	24.20	23.5843	.473	2.00
MnO	.64	.60	.61	.58	.62	.62	.64	.6157	.022	3.49
MgO	8.52	8.27	8.76	8.66	8.53	8.23	8.05	8.4314	.255	3.02
CaO	6.70	6.62	6.27	6.38	6.29	6.54	6.52	6.4743	.165	2.55
Na ₂ O										
K ₂ O										
Total	100.83	101.09	100.93	100.37	99.73	100.54	100.41	100.5528		

306

DT-37 Garnet

	1.	2.	3.	4.	\bar{x}	s	%
SiO ₂	38.11	37.53	37.59	37.86	37.7725	.267	.706
TiO ₂	.10	.25	.21	.20	.1900	.064	33.6
Al ₂ O ₃	20.56	20.07	20.23	20.68	20.3850	.283	1.39
Cr ₂ O ₃	.04	.13	.03	.00	.0500	.56	111
FeO	28.86	28.40	30.24	30.25	29.4375	.951	3.23
MnO	1.04	1.12	1.25	1.10	1.1275	.088	7.85
MgO	3.36	2.95	3.43	3.45	3.3050	.220	6.66
CaO	8.93	9.04	7.30	7.23	8.1250	.994	12.24
Na ₂ O	.00	.00	.00	.00	.0000		
K ₂ O	.04	.00	.01	.00	.0125	.019	151
Total	101.04	99.53	100.29	100.78	100.405		

DT-32 Garnet

	1.	2.	3.	4.	5.	6.	7.	8.	9.	10.	11.	12.	13.	14.	15.	16.
SiO ₂	38.14	38.40	37.85	38.24	37.94	37.98	38.09	37.83	37.63	37.76	37.00	38.12	38.11	38.46	37.65	38.22
TiO ₂																
Al ₂ O ₃	21.33	21.09	21.16	21.37	21.37	20.89	21.14	21.23	21.19	21.61	21.38	21.17	20.92	21.37	21.45	21.22
Cr ₂ O ₃																
FeO	28.22	27.71	28.49	27.73	27.84	28.07	28.07	27.79	28.07	27.87	27.90	27.79	27.79	27.79	27.47	27.87
MnO	1.05	.94	1.03	.98	1.21	1.18	1.04	1.01	1.07	1.34	1.16	1.19	1.12	1.08	1.02	1.32
MgO	5.02	4.71	4.93	4.74	4.85	4.98	4.49	4.61	4.95	4.87	5.32	5.09	5.04	5.20	5.41	5.25
CaO	6.71	6.75	6.78	6.99	6.65	6.93	6.79	6.65	6.96	6.91	6.85	6.73	6.70	6.63	6.85	6.64
Na ₂ O																
K ₂ O																
Total	100.48	99.59	100.25	99.88	99.88	100.04	99.63	99.11	99.87	100.06	99.70	99.36	99.69	100.52	99.86	100.54

DT-32 Garnet

	17.	18.	19.	\bar{x}	s	%
SiO ₂	37.98	38.22	37.80	37.9695	.331	.87
TiO ₂						
Al ₂ O ₃	21.36	21.25	21.00	21.2368	.183	.86
Cr ₂ O ₃						
FeO	27.94	27.93	28.28	27.8895	.304	1.09
MnO	1.09	1.14	1.10	1.0932	.091	2.36
MgO	5.26	5.34	5.18	5.0126	.259	5.17
CaO	6.87	6.88	6.93	6.8005	.117	1.72
Na ₂ O						
K ₂ O						
Total	100.50	100.77	100.29	100.0021		

DT - 34 GARNET

	1.	2.	3.	4.	5.	6.	7.	8.	9.	\bar{x}	S	%
SiO ₂	36.50	36.95	37.32	37.38	37.37	37.00	37.27	37.43	37.34	37.1733	.304	.818
TiO ₂	.03	.00	.03	.03	.04	.07	.01	.02	.00	.0256	.022	85.5
Al ₂ O ₃	20.54	20.57	20.60	20.76	20.83	20.80	20.83	20.83	20.55	20.7011	.132	.637
Cr ₂ O ₃												
FeO	31.84	32.18	32.70	32.99	32.60	32.72	32.34	32.24	32.07	32.4011	.367	1.13
MnO	1.20	1.18	1.32	1.22	1.43	1.47	1.20	1.33	1.36	1.3011	.107	8.22
MgO	1.23	1.23	1.32	1.38	1.00	.99	1.34	1.31	1.17	1.2189	.142	11.68
CaO	7.76	7.55	7.20	7.24	7.97	7.83	7.92	7.83	7.86	7.6844	.2886	3.75
Na ₂ O												
K ₂ O												
Total	99.10	99.67	100.48	100.99	101.25	100.88	100.90	101.01	100.36	100.513		

DT-35 Garnet (core)

	1.	2.	3.	4.	5.	\bar{x}	S	%
SiO ₂	38.03	38.09	37.89	37.72	38.25	37.9960	.201	.530
TiO ₂	.07	.06	.05	.07	.07	.06400	.009	14.0
Al ₂ O ₃	21.04	20.86	20.95	20.72	20.63	20.8400	.167	.800
Cr ₂ O ₃								
FeO	29.45	29.62	29.40	29.91	29.23	29.5220	.258	.873
MnO	1.13	1.10	1.08	1.04	1.08	1.0860	.033	3.03
MgO	3.30	3.18	3.10	3.44	3.46	3.2960	.158	4.79
CaO	7.09	7.26	7.08	7.16	7.13	7.1440	.072	1.01
Na ₂ O								
K ₂ O								
Total	100.11	100.18	99.55	100.07	99.63	99.9480		

DT-35 Garnet (rim)

	1.	2.	3.	\bar{x}	S	%
SiO ₂	37.92	38.22	37.99	38.0433	.157	.041
TiO ₂	.02	.05	.06	.0433	.021	48.0
Al ₂ O ₃	20.77	20.59	21.46	20.9400	.459	2.19
Cr ₂ O ₃						
FeO	27.47	27.52	27.05	27.3467	.258	.944
MnO	.86	.89	.89	.8800	.017	1.97
MgO	2.61	2.91	3.02	2.8467	.212	7.46
CaO	10.05	9.83	8.61	9.4967	.776	8.17
Na ₂ O						
K ₂ O						
Total	99.69	100.00	99.07	99.5967		

DT-36 Garnet

	1.	2.	3.	4.	\bar{x}	S	%
SiO ₂	37.77	37.94	38.37	37.98	38.0156	.254	.667
TiO ₂	.09	.04	.00	.00	.0325	.043	131
Al ₂ O ₃	20.58	20.99	21.28	20.92	20.9425	.288	1.37
Cr ₂ O ₃							
FeO	29.35	29.01	28.95	29.21	29.1300	.184	.632
MnO	1.4	1.32	1.84	1.67	1.5575	.241	15.4
MgO	3.66	3.70	3.67	3.70	3.6825	.021	.560
CaO	7.52	7.39	7.09	7.14	7.2850	.204	2.81
Na ₂ O							
K ₂ O							
Total	100.38	100.38	101.20	100.61	100.645		

	1.	2.	3.	4.	5.	6.	7.		\bar{x}	S	%
SiO ₂	38.72	38.29	38.23	38.05	38.55	38.66	38.60		38.4429	.253	.657
TiO ₂	.08	.07	.07	.04	.13	.11	.09		.0843	.029	34.8
Al ₂ O ₃	21.45	21.18	21.38	21.24	21.21	21.38	21.48		21.3314	.120	.564
Cr ₂ O ₃											
FeO	25.71	25.97	26.32	26.19	26.66	26.99	26.93		26.3957	.484	1.84
MnO	1.30	.93	1.05	1.13	.91	1.00	.91		1.0329	.143	13.9
MgO	5.87	5.40	5.81	5.05	6.78	6.65	6.27		6.0900	.497	8.162
CaO	7.39	7.61	7.38	6.78	6.55	6.13	6.62		6.9229	.545	7.87
Na ₂ O											
K ₂ O											
Total	100.52	99.45	100.24	99.27	100.79	100.93	100.89		100.3001		

308

DT-178 Garnet Cores

	1.	2.	3.		\bar{x}	S	%
SiO ₂	38.38	38.86	38.51		38.5833	.248	.643
TiO ₂	.09	.09	.09		.0900	.00	.0
Al ₂ O ₃	21.11	21.43	21.00		21.1800	.223	1.05
Cr ₂ O ₃							
FeO	26.04	25.55	27.44		26.3433	.981	3.72
MnO	.61	.86	.50		.6567	.185	28.1
MgO	5.22	5.74	5.25		5.4033	.292	5.40
CaO	8.14	8.27	7.63		8.0133	.338	4.22
Na ₂ O							
K ₂ O							
total	100.04	100.79	100.42		100.2699		

DT-178 Garnet Rim

	1.	2.	3.		\bar{x}	S	%
SiO ₂	38.16	38.05	37.65	38.45	38.0775	.331	.870
TiO ₂	.07	.11	.09	.07	.0850	.019	22.5
Al ₂ O ₃	21.22	21.16	20.85	21.00	21.0575	.167	.791
Cr ₂ O ₃							
FeO	26.87	26.88	26.68	27.09	26.8800	.168	.623
MnO	2.54	2.01	3.29	2.56	2.6000	.526	20.2
MgO	3.95	4.09	3.89	4.06	3.9975	.094	2.34
CaO	7.60	7.87	7.68	7.67	7.7050	.116	1.50
Na ₂ O							
K ₂ O							
Total	100.41	100.16	100.13	100.90	100.4005		

DT-98-1 Garnet melt

	1.	2.	3.	4.	5.	6.	7.	8.	9.		\bar{x}	S	%
SiO ₂	38.40	38.62	37.86	37.84	38.04	37.69	38.04	37.79	38.16		38.0489	.304	.798
TiO ₂	.05	.04	.04	.02	.02	.06	.02	.02	.02		.0322	.016	48.5
Al ₂ O ₃	20.32	20.78	20.89	20.78	20.81	20.75	20.50	20.76	20.66		20.6944	.178	.859
FeO	28.91	28.28	27.98	28.97	27.90	28.52	27.28	28.18	28.61		28.2922	.534	1.89
MnO	.89	.86	.87	.83	.82	.84	1.16	1.07	.83		.9078	.122	13.4
MgO	3.73	3.46	3.67	3.36	3.23	3.46	3.66	3.69	2.89		3.4611	.273	7.90
CaO	7.50	7.36	7.44	7.18	7.98	8.25	8.40	7.86	7.67		7.7376	.415	5.36
Na ₂ O													
K ₂ O													
Total	99.80	99.39	98.75	99.00	98.80	99.58	99.07	99.36	98.84		99.1744		

	1.	2.	3.	4.	5.	6.	7.	8.	9.	10.	11.	12.	13.	14.	15.
SiO ₂	38.73	38.90	38.68	38.07	38.74	38.69	38.76	38.19	37.86	38.48	38.18	38.55	38.18	38.18	38.45
TiO ₂	.02	.02	.04	.04	.02	.02	.04	.04	.03	.04	.00	.03	.00	.03	.02
Al ₂ O ₃	20.94	21.00	21.02	20.93	21.30	21.66	21.49	21.31	21.49	21.34	21.47	21.14	21.06	21.13	21.18
FeO	28.28	27.94	28.20	27.69	27.98	27.48	28.71	28.55	29.07	29.07	28.26	28.10	28.45	28.51	28.70
MnO	.91	1.00	.99	.97	.90	.94	.95	.86	.66	.85	.79	.77	1.00	.99	.88
MgO	4.61	4.83	4.66	4.61	4.86	4.92	4.57	4.34	4.42	4.68	4.55	4.50	4.45	4.50	4.36
CaO	6.84	6.68	6.88	7.06	6.45	6.60	6.38	6.71	6.52	6.15	6.39	6.50	6.70	6.49	6.80
Na ₂ O															
K ₂ O															
Total	100.34	100.39	100.47	99.38	100.25	100.31	100.90	100.00	100.05	100.61	99.64	99.59	99.84	99.83	100.40

DT-98-2 & DT-98-3 Garnet (cont.)

	16.	17.	18.	19.	\bar{x}	s	%
SiO ₂	38.35	38.73	38.29	38.21	38.4326	.291	.758
TiO ₂	.00	.02	.00	.02	.0226	.015	63.9
Al ₂ O ₃	21.51	21.20	21.32	21.14	21.2437	.213	1.00
FeO	28.79	28.48	29.19	28.88	28.4374	.470	1.65
MnO	1.10	.94	.97	.95	.9168	.100	10.9
MgO	4.28	4.85	4.23	3.97	4.5363	.243	5.35
CaO	6.95	6.23	6.92	6.72	6.6300	.250	3.76
Na ₂ O							
K ₂ O							
Total	100.97	100.44	100.91	99.90	100.219		

DT-31 Garnet

	1.	2.	3.	4.	5.	6.	7.	8.	9.	10.	11.	12.	13.
SiO ₂	38.52	38.19	38.13	38.28	38.56	37.95	37.61	37.77	37.98	37.54	37.86	38.28	38.09
TiO ₂	.06	.05	.04	.07	.12	.09	.05	.08	.05	.04	.02	.06	.03
Al ₂ O ₃	21.49	21.56	20.92	21.51	21.26	21.22	21.26	21.44	20.93	21.09	21.25	21.42	21.51
Cr ₂ O ₃													
FeO	27.25	27.43	27.69	27.41	27.86	27.67	28.00	27.46	27.42	26.79	27.32	27.04	26.77
MnO	.82	.80	.83	.94	.86	.84	.94	.82	.82	.83	1.09	.85	1.07
MgO	4.73	4.52	4.73	4.80	4.79	4.95	4.43	4.69	4.65	4.63	3.94	4.79	3.92
CaO	7.95	8.16	7.86	7.60	7.65	7.73	7.93	7.87	8.02	8.38	8.77	8.12	9.46
Na ₂ O													
K ₂ O													
Total	100.83	100.72	100.19	100.62	101.10	100.45	100.21	100.13	99.87	99.30	100.25	100.55	100.66

	\bar{x}	s	%
SiO ₂	38.0585	.316	.83
TiO ₂	.0585	.027	45.64
Al ₂ O ₃	21.2969	.217	1.02
Cr ₂ O ₃			
FeO	27.3931	.372	1.36
MnO	.8854	.097	10.92
MgO	4.5823	.317	6.93
CaO	8.1154	.511	6.30
Na ₂ O			
K ₂ O			
Total	100.390		

Mineral Oxidation States Calculated
By Charge Balancing

TABLE C-1

CLINOPYROXENE

Sample No.	Fe _{CB} ³⁺	Fe _{MOSS} ³⁺	Fe _{CB} [*]	Fe _{MOSS} [*]	ΔFe^{3+} (Fe _{CB} ³⁺ - Fe _{MOSS} ³⁺)
DT-24	.093	.074	.742	.801	+.018
DT-25	.114	.079	.682	.786	+.035
DT-28	.080	.112	.842	.786	-.032
DT-30	.005	.038	.978	.832	-.033
DT-32	.102	.078	.736	nd	+.024
DT-33	.086	.057	.743	.830	+.029
DT-34	.091	.137	.867	nd	-.046
DT-35	.189	.100	.620	.800	+.089
DT-36	.036	.086	.920	.815	-.051
DT-174	.038	.073	.906	.818	-.035
DT-176	.067	.081	.802	.768	+.014
DT-177	.053	.078	.865	.807	-.026
DT-98	.054	.078	.861	.803	-.024
			\bar{X} .813	.804	
			S .103	.019	
			% 12.7	2.36	

ORTHOPYROXENE

Sample No.	Fe _{CB} ³⁺	Fe _{MOSS} ³⁺	Fe _{CB} [*]	Fe _{MOSS} [*]	ΔFe^{3+} (Fe _{CB} ³⁺ - Fe _{MOSS} ³⁺)
DT-24	.061	.036	.929	.958	+.025
DT-25	-.005*	.054	.999*	.937	-.059*
DT-30	.050	.021	.929	.971	+.029
DT-32	.030	.019	.970	.974	+.011
DT-33	.105	.005	.883	.994	+.100
DT-37	.014	.047	.986	.955	-.033
DT-174	.012	.049	.988	.950	-.038
DT-176	.084	.039	.916	.950	+.045
DT-177	.021	.047	.977	.950	-.026
DT-98	.064	.019	.934	nd	+.045
			\bar{X} .951	.960	
			S .038	.016	
			% 4.02	1.67	

TABLE C-1 (Cont'd)

HORNBLLENDE

Sample No.	Fe ³⁺ _{CB}	Fe ³⁺ _{MOSS}	Fe* _{CB}	Fe* _{MOSS}	ΔFe^{3+} (Fe ³⁺ _{CB} - Fe ³⁺ _{MOSS})
DT-24	.853	.574	.593	nd	+ .279
DT-25	.458	.567	.780	.727	-.109
DT-28	.560	.819	.799	nd	-.220
DT-30	.277	.391	.804	.722	-.114
DT-31	.727	.745	.716	.710	-.018
DT-32	.680	.668	.718	.723	+ .012
DT-33	.635	.574	.701	.730	+ .061
DT-34	.843	1.001	.767	nd	-.158
DT-35	.581	.792	.700	nd	-.111
DT-36	.591	.698	.765	.721	-.107
DT-37	.677	.630	.733	.752	+ .047
DT-174	.730	.686	.702	nd	+ .044
DT-176	.725	.581	.638	.710	+ .144
DT-177	.627	.603	.709	nd	+ .024
DT-178	.805	.667	.637	nd	+ .138
DT-98	.544	.644	.762	.717	-.100
DT-12	.779	.736	.669	.686	+ .043
			\bar{x} .717	.720	
			s .059	.017	
			% 8.27	2.36	

GARNET

Sample No.	Fe ³⁺ _{CB}	Fe ³⁺ _{MOSS}	Fe* _{CB}	Fe* _{MOSS}	ΔFe^{3+} (Fe ³⁺ _{CB} - Fe ³⁺ _{MOSS})
DT-28	.103	.297	.974	.924	-.195
DT-30	-.025*	.170	.999*	.943	-.195
DT-31	.171	.212	.952	.941	-.042
DT-32	.158	.201	.957	.946	+ .043
DT-34	.171	.301	.961	.943	-.130
DT-35	.022	.237	.994	.930	-.215
DT-36	.149	.309	.961	.939	-.161
DT-37	.211	.311	.946	nd	-.101
DT-176	.147	.202	.957	.919	-.055
DT-178	.091	.247	.973	.942	-.156
DT-98	-.003	.260	.999*	.928	-.263
			\bar{x} .963	.935	
			s .022	.008	
			% 2.21	0.90	

